13 AFD

RCC13

DOT HS 800 626

UNDERRIDE/OVERRIDE OF AUTOMOBILE FRONT STRUCTURES IN INTERVEHICULAR COLLISIONS

Volume 1
Heavy Vehicle Rear Underride

Cornell Aeronautical Laboratory, Inc.
4455 Genesee Street
Buffalo, New York 14221

Contract No. FH-11-7317
December 1971
Final Report

PREPARED FOR
U S DEPARTMENT OF TRANSPORTATION
NATIONAL HIGHWAY TRAFFIC SAFETY ADMINISTRATION
WASHINGTON, D C 20590

The opinions findings, and conclusions expressed in this publication are those of the authors and not necessarily those of the National Highway Traffic Safety Administration

TECHNICAL REPORT STANDARD TITLE PAGE

1 Report No	2 Government Accession No	3 Recipient's Catalog No
DOT/HS-800 626		

4 Title and Subtitle	5 Report Date
Underride/Override of Automobile Front Structures in Intervehicular Collisions Volumn 1 - Heavy Vehicle Rear Underride	December 1971
	6 Performing Organization Code
7 Author(s) Norman J. DeLeys and Melvin O. Ryder	8 Performing Organization Report No VJ-2844-V-3
9 Performing Organization Name and Address Cornell Aeronautical Laboratory, Inc. 4455 Genesee Street Buffalo, New York 14221	10 Work Unit No N25
	11 Contract or Grant No FH-11-7317
12 Sponsoring Agency Name and Address U. S. Department of Transportation National Highway Traffic Safety Administration Washington, D. C. 20590	13 Type of Report and Period Covered Final Report June 1969 - December 1971
	14 Sponsoring Agency Code

15 Supplementary Notes

16 Abstract

Analytical and experimental results obtained in a study of requirements and the performance of rear underride guards for heavy vehicles are presented in this report. A total of twelve full-scale tests were conducted in two phases of the experimental program. Results of the first phase, consisting of six tests using a rigid simulated underride guard mounted on an SAE barrier are reported in Reference 1. The second series of six full-scale tests, reported herein, were performed using prototype underride guard designs mounted on the rear of semi trailer trucks. The effects of impacting vehicle size and weight, impact velocity, rigid and yielding underride guards, and underride guard ground clearance height are among the parameters investigated.

Data on pertinent automobile and truck geometric characteristics and on various energy dissipating systems for possible application to truck underride guards are presented and discussed. Also, results from a computer model of vehicle collisions with an underride guard that was applied to explore the effects of various guard load-deflection properties on vehicle impact response are described.

Based on the results of the full-scale crash tests and the engineering analyses, recommendations are given for underride guard requirements and compliance test procedures.

17 Key Words	18 Distribution Statement
Truck Safety Underride Guards Automobile Front Impact Response Crash Energy Control	unlimited

19 Security Classif (of this report)	20 Security Classif (of this page)	21. No of Pages	22 Price
unclassified	unclassified	189	

Form DOT F 1700.7 (8-69)

FOREWORD

This report is one of a two-volume final report presenting findings of a program of research aimed at reducing the injury potential to occupants of automobiles that results from mismatch and underriding of the forward structure of automobiles involved in intervehicular longitudinal collisions.

The research was performed by the Cornell Aeronautical Laboratory (CAL) for the National Highway Traffic Safety Administration of the U. S. Department of Transportation under Contract No. FH-11-7317. Other reports published in connection with the investigations conducted under this contract are:

"Full-Scale Crash Tests of Rigid Simulated Heavy Vehicle Underride Guard", CAL Report No. VJ-2844-V-1, March, 1970.

"An Evaluation of the Teledyne-Geotech Model 33300 Crash Recorder", CAL Report No. VJ-2844-V-2, September, 1971.

"Underride/Override of Automobile Front Structures In Intervehicular Collisions, Volume 2 - Car-to-Car Headon Impacts", CAL Report No. VJ-2844-V-4, December, 1971.

The opinions, findings and conclusions expressed in this publication are those of the authors and not necessarily those of the National Highway Traffic Safety Administration.

This report has been reviewed and approved by

Edwin A. Kidd

Edwin A. Kidd, Head
Transportation Research Department

SUMMARY

Analytical and experimental results obtained in a study of requirements and the performance of rear underride guards for heavy vehicles are presented in this report. A total of twelve full-scale tests were conducted in two phases of the experimental program. Results of the first phase, consisting of six tests using a rigid simulated underride guard mounted on an SAE barrier are reported in Reference 1. The second series of six full-scale tests, reported herein, were performed using prototype underride guard designs mounted on the rear of semi-trailer trucks. The effects of impacting vehicle size and weight, impact velocity, rigid and yielding underride guards, and underride guard ground clearance height are among the parameters investigated.

Data on pertinent automobile and truck geometric characteristics and on various energy dissipating systems for possible application to truck underride guards are presented and discussed. Also, results from a computer model of vehicle collisions with an underride guard that was applied to explore the effects of various guard load-deflection properties on vehicle impact response are described.

Based on the results of the full-scale crash tests and the engineering analyses, recommendations are given for underride guard requirements and compliance test procedures.

TABLE OF CONTENTS

		Page No.
	FOREWORD	ii
	SUMMARY	iii
1.0	INTRODUCTION	1
2.0	CONCLUSIONS AND RECOMMENDATIONS	3
	2.1 Conclusions	3
	2.2 General Recommendations	5
	2.3 Recommendations for Compliance Test Procedures	6
3.0	TRUCK AND UNDERRIDE GUARD CONFIGURATIONS	11
	3.1 Trucks and Truck Trailers	11
	3.2 Underride Guard Configurations	14
4.0	TRAILER-MOUNTED UNDERRIDE GUARD TEST PROGRAM	25
	4.1 Methodology and Equipment	25
	4.2 Test Results	29
	4.2.1 Crash Test No. 7	31
	4.2.2 Crash Test No. 8	38
	4.2.3 Crash Test No. 9	47
	4.2.4 Crash Test No. 10	59
	4.2.5 Crash Test No. 11	72
	4.2.6 Crash Test No. 12	82
5.0	DISCUSSION OF RESULTS	94
6.0	REFERENCES	104
	APPENDIX A - SURVEY OF ENERGY ABSORBING DEVICES	105
	APPENDIX B - COMPONENT TESTS OF FRICTION TUBE ENERGY ABSORBING DEVICES	151

TABLE OF CONTENTS (continued)

	Page No.
APPENDIX C - MATHEMATICAL MODEL OF AUTOMOBILE-TRUCK UNDERRIDE COLLISION	160
APPENDIX D - STRESS ANALYSIS OF TEST TRAILERS AND RIGID UNDERRIDE GUARD DESIGNS	172

LIST OF FIGURES

Figure No	Description	Page No.
1	Typical Dimensions of Rear Area of Large Trucks and Trailers	13
2	Flatbed 18" Rigid Underride Guard Configuration	15
3	18" Rigid Underride Guard Installation on Flatbed Trailer	17
4	24" Rigid Underride Guard Installation on Flatbed Trailer	18
5	Flatbed 18" Energy Absorbing Underride Guard Configuration	19
6	18" Energy Absorbing Underride Guard Installation on Flatbed Trailer	21
7	Van Trailer 24" Rigid Underride Guard Configuration	23
8	24" Rigid Underride Guard Installation on Van Trailer	24
9	Vehicle Mounted Sensors	27
10	Sketch of Test Site Showing Location of Sensors and Cameras	30
11	Test No. 7: Passenger Compartment Longitudinal Data	32
12	Test No. 7 Engine and Frame Acceleration Data	34
13	Test No. 7 Vehicle Acceleration and Strain Data	35
14	Test No. 7: Vehicle-Guard Relative Penetration	36
15	Test No. 7: Vehicle Impact Load	37
16	Test No. 7 Test Vehicle and Underride Guard	39

LIST OF FIGURES (continued)

Figure No.	Description	Page No.
17	Test No. 8: Passenger Compartment Longitudinal Data	40
18	Test No. 8 Vehicle Acceleration Data	42
19	Test No. 8· Friction Tube Axial Strain Data	43
20	Test No. 8. Friction Tube Axial Loads	44
21	Test No. 8: Vehicle Impact Load	45
22	Test No. 8. Vehicle and Underride Guard Displacements	46
23	Test No. 8: Test Vehicle Before and After Impact	48
24	Test No. 8· Collapsible Underride Guard Before and After Impact	49
25	Test No. 9: Compartment Longitudinal Acceleration Data, Filtered at 1000 Hz	50
26	Test No. 9: Compartment Longitudinal Acceleration Data, Filtered at 50 Hz	51
27	Test No. 9: Compartment and Trunk Acceleration Data	53
28	Test No. 9: Engine and Frame Acceleration Data	54
29	Test No. 9: Longitudinal Loads at Front of Trailer	55
30	Test No. 9: Friction Tube Axial Strain Data	56
31	Test No. 9: Friction Tube Axial Loads	57
32	Test No. 9: Vehicle Impact Load	58
33	Test No. 9: Vehicle and Underride Guard Displacements	60

LIST OF FIGURES (continued)

Figure No.	Description	Page No.
34	Test No. 9 Plan View Sketch of Damaged Vehicle Outline	61
35	Test No. 9 Underride Guard and Test Vehicle After Impact	62
36	Test No. 10: Passenger Compartment Acceleration Data	64
37	Test No. 10: Compartment Rear Deck Acceleration Data	65
38	Test No. 10 Engine Acceleration Data	66
39	Test No 10 Vehicle Impact Load	68
40	Test No. 10 Vehicle Displacement	69
41	Test No. 10 Vehicle Impact Load Vs. Displacement	70
42	Test No. 10 Photographs of Test Vehicle and Underride Guard	71
43	Test No. 11 Compartment Longitudinal Acceleration Data, Filtered at 1000 Hz	73
44	Test No. 11: Compartment Longitudinal Acceleration Data, Filtered at 50 Hz	74
45	Test No. 11 Passenger Compartment Vertical Acceleration	76
46	Test No. 11: Compartment Rear Deck Acceleration Data	77
47	Test No. 11 Engine Acceleration Data	78
48	Test No. 11: Longitudinal Load at Front of Van	79
49	Test No. 11: Vehicle and Underride Guard Displacements	81

LIST OF FIGURES (continued)

Figure No.	Description	Page No.
50	Test No. 11: Automobile and Van Trailer After Impact	8[illegible]
51	Test No. 12 Compartment Longitudinal Acceleration Data, Filtered at 1000 Hz	84
52	Test No. 12 Compartment Longitudinal Acceleration Data, Filtered at 50 Hz	85
53	Test No. 12 Compartment and Engine Acceleration Data	87
54	Test No. 12: Compartment Rear Deck Acceleration Data	88
55	Test No. 12: Vehicle Impact Load	89
56	Test No. 12: Vehicle Displacement From Photographic Analysis	91
57	Test No. 12: Vehicle Impact Load Vs. Displacement	92
58	Test No. 12: Vehicle and Rigid Underride Guard	93
59	Comparison of Compartment Longitudinal Accelerations for Rigid and Yielding Underride Guard Impacts	97
60	Test No. 8: Underride Guard and Vehicle Load - Deflection Characteristics	99

LIST OF TABLES

Table No.	Description	Page No.
1	Summary of Underride Guard Test Results	95

1.0 INTRODUCTION

The consequences of automobile collisions with the aft portions of heavy trucks and tractor-trailer combinations are often severe due to the limited engagement of the frontal structure of the automobile. The safety of automobile occupants in such collisions can be greatly enhanced by mounting a structure at the rear of the truck or trailer to prevent underriding by the impacting vehicle and thereby reduce the likelihood of injuries resulting from intrusion of the passenger compartment.

Although the need for heavy vehicle underride guards is clear, research is required to establish performance requirements and to develop configurations that will assure intervehicular compatibility and effective crash energy control. For example, the location and total contact area must be such as to ensure adequate engagement of the frontal structures of automobiles of several sizes. Also, given an adequate engagement of the automobile frontal structure, there is a further need to determine the required load capacity of underride guards and how they may be designed to limit collision forces and absorb energy in a controlled manner to minimize the hazard to occupants of the striking vehicle.

This report presents results of a combined program of analytical and experimental research to determine rear underride guard requirements and to develop, demonstrate, and evaluate the dynamic performance of prototype systems that will provide intervehicular compatibility and effective crash energy control. Detailed results of an initial series of six full-scale tests of automobiles impacting a simulated rigid underride guard are reported in Reference 1. In the second phase of testing, reported herein, six additional full-scale tests of automobiles impacting specific underride guard designs mounted on the rear of two different types of trailers were conducted. The two trailers selected for these tests provide information on the feasibility of incorporating effective underride guards on both frame and frameless type heavy vehicle structures and on the weight

penalty that might be incurred in providing this safety feature on trucks.

In addition to the trailer-mounted underride test results, pertinent information generated during the performance of various tasks associated with the overall effort is included in the Appendices of this report. Appendix A contains the results of a literature survey of energy absorbing devices examined as possible candidates for an energy absorbing yielding underride guard. Appendix B contains the results of laboratory dynamic tests of a friction tube energy absorbing device conceived at CAL and incorporated in the design of a yielding underride guard that was fabricated and tested. A mathematical simulation formulated and exercised in support of the yielding guard design and experimental effort is described in Appendix C. Appendix D presents results of stress analyses of the 18 inch and 24 inch ground clearance rigid underride guard configurations tested on flatbed and van semi-trailers, respectively.

2.0 CONCLUSIONS AND RECOMMENDATIONS

2.1 Conclusions

2.1.1 To effectively prevent excessive underride by full size automobiles impacting at 40 MPH, the underride guard ground clearance above the roadway should not exceed 24 inches. This conclusion is based on the results of three crash tests of full size cars against simulated and truck-mounted rigid underride guards positioned at this height which indicate that the penetration was acceptable but approached the maximum that could be tolerated. Higher ground clearance will not permit adequate engagement with the engine or other strong frontal structures of the automobile to prevent intrusion of the passenger compartment.

2.1.2 To assure adequate underride protection for small subcompact cars, the roadway clearance height of the guard should not exceed, and preferably should be less than, 18 inches. In tests of a Volkswagen impacting a rigid guard installed on a truck at 24 inch height, the guard penetrated as far as the passenger compartment front bulkhead in a 30 MPH test and more than two feet into the compartment in a 40 MPH test. Thus, the protection afforded was marginal to completely inadequate for this speed range.

Two previous 40 MPH tests of small cars (VW and Simca) using a simulated underride guard positioned at a height of 18 inches (Reference 1) showed the guard to be effective in the case of the VW, but not for the Simca. The differences in the crash response of these two vehicles were attributed primarily to the smaller wheels of the Simca which underrode the guard so that the crush resistance of the relatively strong supporting structure for the suspensions was not fully utilized in stopping the car.

2.1.3 The average load imposed on a rigid underride guard during a 40 MPH crash of a standard full size automobile is of the order of 65,000 to 75,000 lbs. However, short-duration forces in excess of 200,000 lbs. are developed when the engine contacts the guard. Peak loads measured in the trailer-mounted underride guard tests were substantially lower than in the previous test series using a simulated rigid guard. This is believed to be a reflection of the effects of mass and small deflections of the trailer structure on the loads transmitted to the load cells which were located at the front of the trailer approximately 15 feet from the point of force application to the underride guards.

2.1.4 Lifting of the rear of heavy vehicles, from vertical force components due to wedging of the automobile, that would be conducive to greater underride penetration is indicated not to be a serious problem. No appreciable lifting of the aft end occurred in any of the tests of underride guards installed on the trailers. Indeed, the opposite effect was observed with the aft end moving downward as a result of bending of the trailer structure in reacting the eccentrically applied longitudinal loads.

2.1.5 Properly designed energy absorbing (yielding) underride guard systems can provide the advantages of reduced accelerations and crush of the impacting automobiles, better control of crash energy dissipation, and lower loadings on the truck structure. From results of computer simulations it is concluded that a square wave (constant force) characteristic of the underride guard is preferred and that, for a yielding guard having a maximum stroke of 24 inches, a constant force of 60,000 to 70,000 lbs. will produce near minimum vehicle crush and compartment deceleration level in stopping a 4,000 lb. front engine automobile impacting at 40 MPH. Results of a full-scale test of a 60,000 lb. yielding underride guard configuration were in substantial agreement with the model predictions for the automobile acceleration response, car crush and guard stroke distances, and the distribution of absorbed crash energy between the vehicle and the underride guard.

2.1.6 The guard design and testing effort of this study indicates that the strength of existing frame or monocoque truck-trailer structures is sufficient to withstand the underride guard loads generated by the conditions of these tests without major modifications. Furthermore, the weight of a rear underride guard, which might also serve as the docking bumper often provided on heavy vehicles, is deemed not excessive and would add approximately 200 to 250 lbs. to the weight of the vehicle.

2.2 General Recommendations

2.2.1 Although both rigid and energy absorbing yielding rear underride guards were tested and demonstrated to be effective in preventing excessive underride of a full size automobile, the latter type are recommended because of the improved control of the impact forces and energy dissipation process. For the same total underride penetration distance (entirely vehicle crush for a rigid guard and the sum of vehicle crush and guard displacement for the case of a yielding guard), the reduced crushing of the automobile that occurs in an impact with a yielding guard increases the safety of the occupants as a result of less possibility of compartment intrusion by rearward displacement of the engine or the steering column.

2.2.2 Further testing is recommended to obtain more information on how the dynamic load requirements of an underride guard are affected by the degree of transverse engagement with the front of an automobile. The smaller contact width of the car with increased offset between vehicle centerlines increasingly tends to produce a spinning motion of the impacting automobile, thereby reducing the loads imposed on the guard. In addition, it seems reasonable to expect that the crush resistance of automobiles decreases with reduced width of contact of the front structure so that less energy can be dissipated by the car structure without experiencing dangerous intrusion of the passenger compartment. The strength requirement of underride guards loaded near the extremities is therefore probably less than for central impacts to provide an effective minimum level of performance.

2.2.3 It is recommended that static tests be conducted on the rigid underride guard used in the full-scale dynamic impact tests reported herein. The data obtained in such tests would provide useful information for relating dynamic and static load capabilities needed as a basis for specifying realistic static loading requirements of underride guards in compliance testing.

2.3 Recommendations for Compliance Test Procedures

Test procedures and performance requirements for compliance testing of guards to provide protection against rear underride of heavy vehicles are described in Federal Docket No. 1-11 in which the establishment of a Motor Vehicle Safety Standard concerned with that subject has been proposed. In the following, recommendations are made for changes to these procedures based on the results of the experiments and analyses performed within this research program.

There are basically two factors that are of prime importance in relation to the effectiveness of an underride guard. These are (1) the location of the guard which must be such as to ensure adequate engagement of the front structures of impacting vehicles and (2) the strength of the guard must be adequate to withstand the applied dynamic loads.

The preferred location of the face of the underride guard is as far aft on the vehicle as possible. A criticism of the proposed safety standard is the possibility of losing up to 15 inches of penetration distance with little or no energy dissipation. For example, under the proposed requirements, a rigid underride guard could be located 15 inches forward of the rear of the vehicle and the total penetration or underride distance of an impacting vehicle would, therefore, be that much more than if the guard were to be located at the rear of the truck. Any such loss of potential penetration distance over which crash energy might otherwise be absorbed lowers the maximum speed for which a given impacting vehicle can be

prevented from experiencing an unacceptable amount of underride.

Two conflicting considerations affect the establishment of rear underride guard roadway clearance height requirements. To be most effective in the prevention of underride, particularly for the case of small impacting vehicles, the underride guard clearance should not exceed 18 inches. On the other hand, a guard at this height could be detrimental to normal truck operations for some truck or trailer configurations as a result of creating too low an angle of departure.

It is recommended that the maximum clearance of the underride guard be established on the basis of an allowable angle of departure, but in no case permitted to exceed 24 inches when the vehicle is at curb weight. An allowable angle of departure of 10 degrees at rated load conditions is suggested which is the minimum value recommended by the SAE for automobiles. This would permit the clearance, for some vehicles under no load conditions, to be as much as 24 inches which is a height that has been found to be acceptable in preventing excessive underride of full size automobiles impacting at speeds up to 40 MPH and a subcompact car (VW) impacting at 30 MPH. Under loaded conditions, the reduced height of the guard would increase the effectiveness in preventing underride.

However, by relating the guard height at rated load to an allowable 10 degree departure angle of the truck or trailer, the maximum clearance in many instances will be limited to less than 24 inches, depending on the amount of rear overhang of the body beyond the rear axle. Thus, for example, all vehicles with overhang of less than 8.5 feet would require that the underride guard clearance height be no greater than 18 inches at full rated load.

Measurements made during dynamic tests of underride guards installed on trailers indicate that loads in excess of 150,000 lbs. are imposed on a rigid underride guard when impacted by full size (3,500 to 4,000 lb. weight class) automobiles at 40 MPH. The brief peak loading is approximately twice the calculated load carrying capacity of the center of the guards, indicating one or more of the following

- the impact force is distributed over a considerable length of the guard bumper
- the static load calculations of the guard are conservative
- the dynamic load capacity of the structure exceeds the static capability.

From analysis of films and data from the tests it is evident that the high loads result from impact and abrupt deceleration of the mass of the engine and transmission, closely followed by contact of the relatively strong structure of the front wheel and suspension assemblies with the underride guard. Thus, the principal loading points are spaced along the width of the guard at approximately the half-tread of the wheels of the impacting vehicle or at about 30 inches for a full size automobile.

It is deemed unrealistic to require that underride guards be capable of withstanding the observed very high dynamic forces in a compliance test in which, for economic reasons, the loads must be applied statically. It therefore becomes necessary to base such specification of static test loads on rationalistic grounds. From the tests of the yielding underride guards described in this report, it may be concluded that the minimum force requirement should be approximately 60,000 lbs. However, higher forces are developed on rigid underride guards for which the average force for a 40 MPH central impact of the guard is approximately 70,000 lbs.

The test results also indicate that the loads imposed on an underride guard are reduced in off-center impacts as a result of less engagement of the full width of the striking vehicle and the tendency for the vehicle to spin out.

With the aforementioned considerations as a guide, changes in the proposed test procedures are recommended as follows

1. Through appropriate measurements, determine that the underride guard installation complies with each of the following criteria:

   (a) With the vehicle loaded to full rated load on level ground, the clearance height of the lower edge of the underride guard shall not exceed that which corresponds to a vehicle angle of departure of 10 degrees.

   (b) With the vehicle at curb weight on level ground, the clearance height of the lower edge of the underride guard shall not exceed 24 inches.

2. Restrain the vehicle to prevent motion. The means used to restrain the vehicle must not inhibit forward movement of the portions tested relative to the rest of the vehicle.

3. Prepare a load applicator comprised of two test blocks of rigid material, each with a plane surface in the form of a rectangle 4 inches high and 12 inches wide (the "test surfaces"), suitably connected by a strong rigid member so as to prevent relative movement. The distance between the vertical center-lines of the test surfaces shall be 30 inches and the axis of force application (the "force axis") shall be

midway between these centerlines.

4 Position the load applicator so that

(a) the test surfaces are vertical and facing in the direction of forward travel of the vehicle,

(b) the lower edge (12 inch side) of each test surface is in the horizontal plane through the lower edge of the underrine guard

5. Apply a forward static force to the load applicator along the force axis as prescribed below

(a) 80,000 lbs. with the force axis at any point within 18 inches of the vehicle centerline,

(b) 60,000 lbs. with the force axis at any point greater than 18 inches from the centerline of the vehicle and equal to or greater than 21 inches inboard from either end of the underride guard.

6. Required Result:

The guard must support the specified test loads without yielding or, if it yields, the test surfaces shall not move forward more than 20 inches and the average force during yielding shall equal or exceed two-thirds of the specified test load. Each vehicle must be capable of meeting the test requirements at any point of loading as specified above, but it is not required that a given vehicle that is successfully tested at one loading condition be capable of withstanding subsequent loading at any other condition.

3.0 TRUCK AND UNDERRIDE GUARD CONFIGURATIONS

3.1 Trucks and Truck Trailers

A brief literature search was conducted to obtain data on truck configurations, dimensions and construction relevant to the design and development of underride guards. For this investigation, consideration was given only to heavy vehicles with gross vehicle weights greater than 10,000 lbs. which, from truck registration data obtained from Reference 2, comprised about 20 percent of new truck registrations in 1968.

There are many and varied geometries and configurations of heavy vehicles in the GVW > 10,000 lb. weight class. Some of these vehicles, because of special purpose bodies or equipment, present unique problems of underride guard installation. However, the most common configurations of large trucks, which because of the height of the cargo bed structure are easily underriden by automobiles, are van or flatbed type tractor semi-trailers or single unit chassis-cabs with van, flatbed, or dump bodies attached. In general, most of these trucks are similar in configuration in the region from ground level to the bottom of the cargo body floor. Specifically, the cargo body has a flat floor located above the tires and which oftentimes extends a considerable distance aft of the rear axle. Some exceptions are, for example, furniture vans and drop-frame heavy equipment haulers which have the cargo body floor below tire height. Such vehicles comprise only a small percentage of the total population of trailers in use and, because of their smaller ground clearance, do not usually present an underride problem.

The overall maximum dimensions of large trucks are set by state laws (Reference 3). Widths are limited to 96 inches in all states except two which allow 102 inches. Overall height is limited to 13'6" in most states with several requiring a 12'6" maximum. Two states have no restriction on height, and one allows 14'. Overall lengths allowed for

single unit trucks [illegible] aries from 35' to 50' with about one half the states requiring 35' [illegible] 'ple unit trucks are limited to 50'-55' for [illegible] states.

Truck underside [illegible] determined by the necessity to [illegible] components. The 10.00 x 20 tire size [illegible] large trucks which, combined with 6 to 8 [illegible] sections, results in a cargo bed ground clear[illegible] hes. Most dimensions such as w[illegible] rail width, cargo bed height, wheel [illegible] rious types of trucks. Many trucks are [illegible] comprised of longitudinal rails and cross [illegible] support [illegible]. These frame rails are typically channel sections [illegible] inches and spaced 33 to 35 inches apart [illegible] type of construction is [illegible] the strength to carry the loads is developed by stressing the [illegible] sides and roof. Such vehicles usually have [illegible] attachment of axle suspension components [illegible] frame type units.

Typical dimensions [illegible] the [illegible] position of large trucks and trailers are shown in Figure [illegible] (dimension L in Figure 1) varies from [illegible] 10 feet. Some trailers have provisions [illegible] the [illegible] position of the rear axle to change the [illegible] with permissible axle loads specified in state regulations.

Two used [illegible] axle [illegible] 1950 Fruehauf 33 ft. flatbed and a 1959 [illegible] ft. [illegible], were obtained for installation and testing [illegible] configurations. These vehicles were selected be[illegible] mechanical and representative of the [illegible] types of construction, respectively, commonly used. [illegible] afforded [illegible]

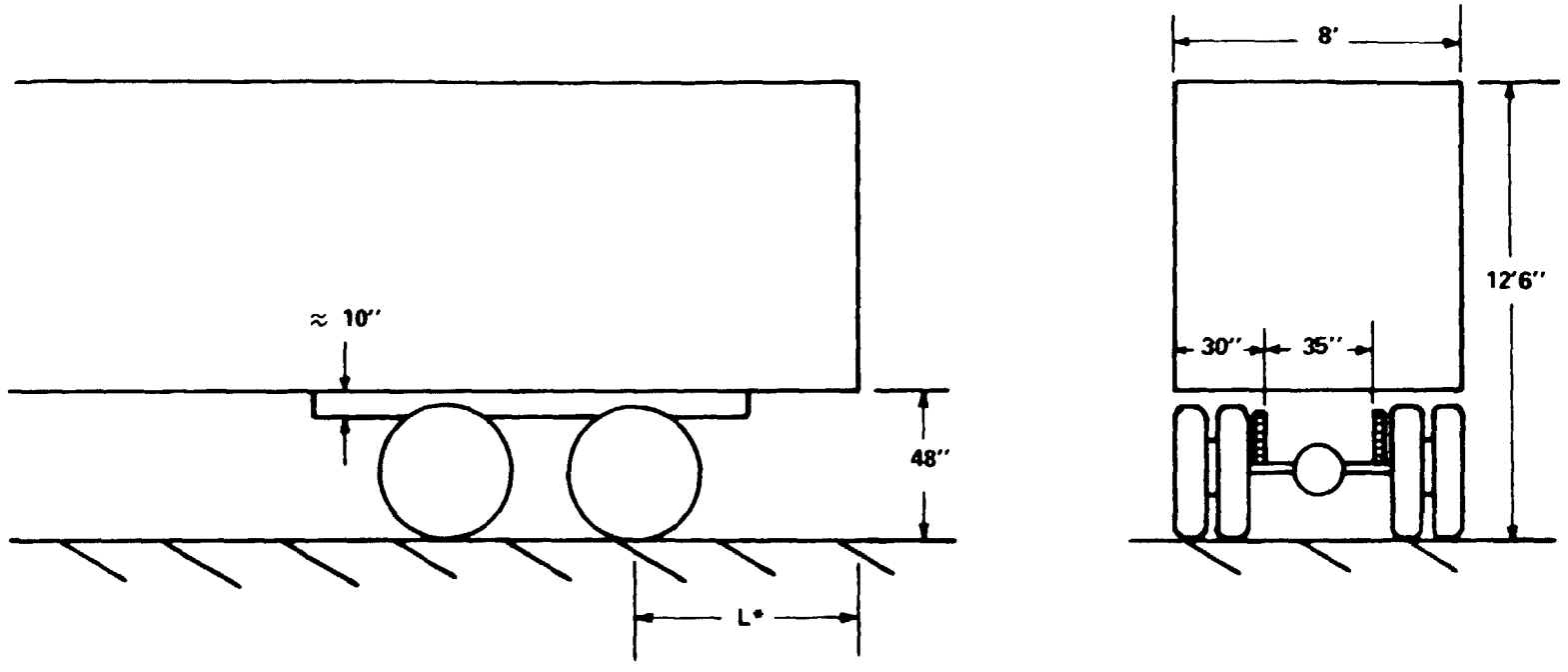

*VARIES FROM APPROXIMATELY ONE TIRE RADIUS (APPROX. 21") TO ABOUT 10'

Figure 1 TYPICAL DIMENSIONS OF REAR AREA OF LARGE TRUCKS AND TRAILERS

advantages of ease of mounting of the underride guards and the likelihood of minimum damage which would permit its reuse for several tests.

3.2 Underride Guard Configurations

Four rear underride guard configurations were designed and tested in the trailer-mounted underride guard test program. These included three guards designed to be rigid structures and one energy absorbing guard designed to yield at a nearly constant force level. The guard configurations and design loads were based on results from the initial series of tests of simulated underride guards (Reference 1) and from a computer simulation model (see Appendix C). Brief descriptions of each of these configurations are presented in the following paragraphs.

Flatbed 18" Rigid Underride Guard

This underride guard, which was the first design tested, was designed as a rigid structure of sufficient strength to insure against failure of the structure under the high impact loadings indicated by the simulated underride guard tests. The guard was purposely overdesigned with the intention that, should yielding occur, it would result from failure of the truck structure rather than from collapse of the underride guard itself.

A sketch of the underride guard showing principal dimensions and components is presented in Figure 2. The guard bumper face member is a 4" x 3" x 1/4" wall structural steel tube extending the full width of the trailer and with the lower edge located 18 inches above the roadway. Supporting structure for the bumper includes five 3" x 2" x 1/4" vertical tubes welded to the aft surface of the cargo platform and eight 3" - 5.7" #I beams angled forward and welded to the trailer frame and cargo bed side rails. Plates and gussets were added at various places on the truck structure for local reinforcement.

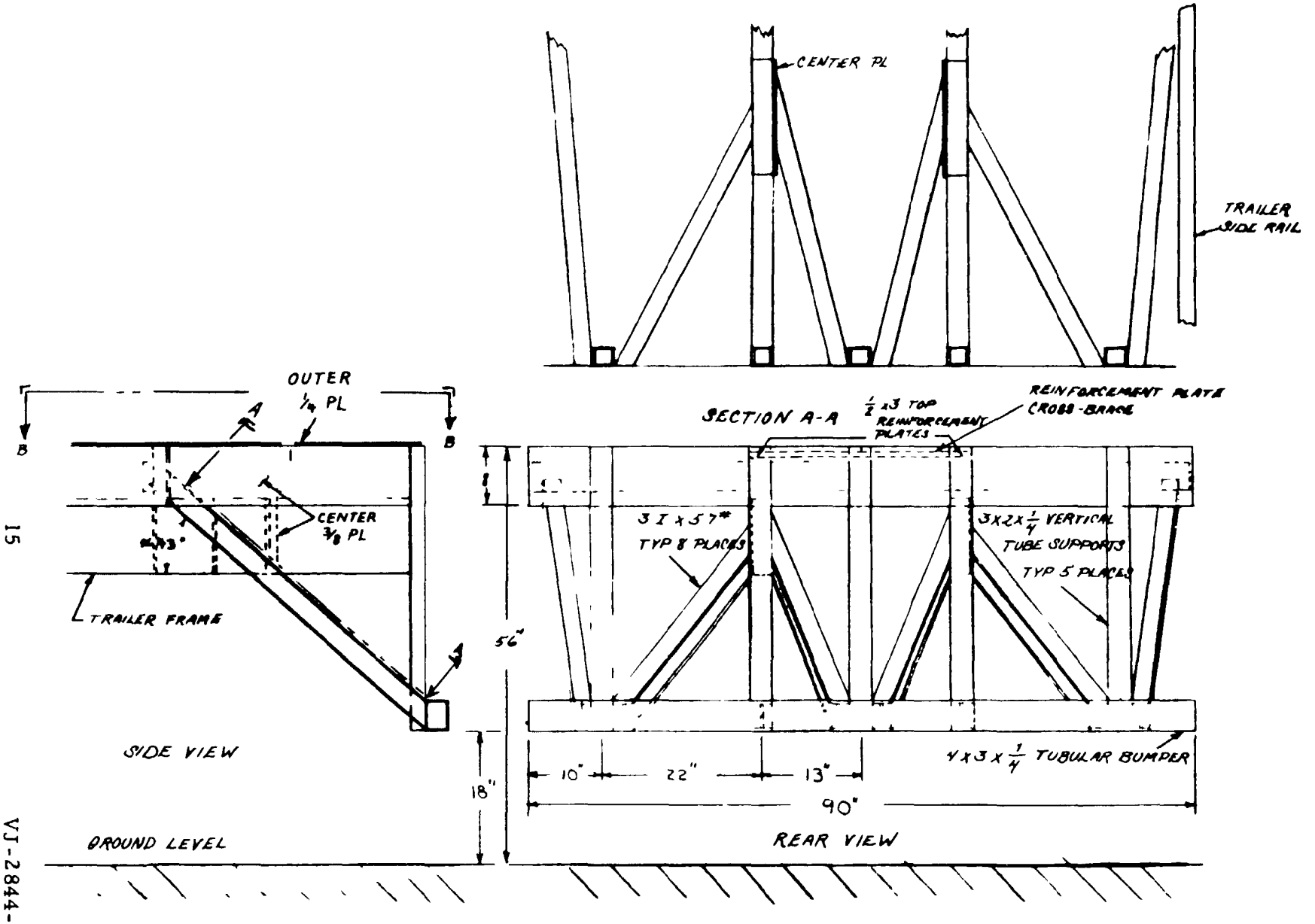

Figure 2 FLATBED 18" RIGID UNDERRIDE GUARD CONFIGURATION

Photographs of the underride guard installed on the flatbed trailer are shown in Figure 3. The calculated weight of this guard and support structure is 340 lbs.

Flatbed 24" Rigid Underride Guard

The 18 inch rigid underride guard described above was modified and converted into one having a clearance of 24 inches above the roadway by shortening the support members. In addition, six supports (two vertical members at the face of the guard and four angled rear I beam supports) were eliminated which reduced the installed weight of the guard to approximately 208 lbs. The underride guard mounted on the trailer is shown in the photographs of Figure 4.

Flatbed 18" Energy Absorbing Underride Guard

The 18" ground clearance yielding underride guard configuration is depicted in Figure 5 and was designed to provide a nearly constant force level of approximately 60,000 to 70,000 lbs. throughout a bumper displacement of two feet. Selection of the force-deflection characteristics was based on the results of computer simulations which indicated that the guard would displace about 20 inches and absorb approximately 60 percent of the kinetic energy of a 3,500 lb. automobile impacting at 40 MPH.

Energy dissipation is accomplished primarily by two friction tube energy absorption devices developed by CAL. These units consist of two close-fitting, telescoping cylindrical tubes with the inner one having two milled slots along its length. A hardened steel pin slightly larger in diameter than the width of the slots is inserted through holes drilled through the wall of the outer tube and the slots of the inner tube. Thus, energy dissipation is accomplished by cold working of the metal at the edges of the slots by the oversize pin which also expands the inner

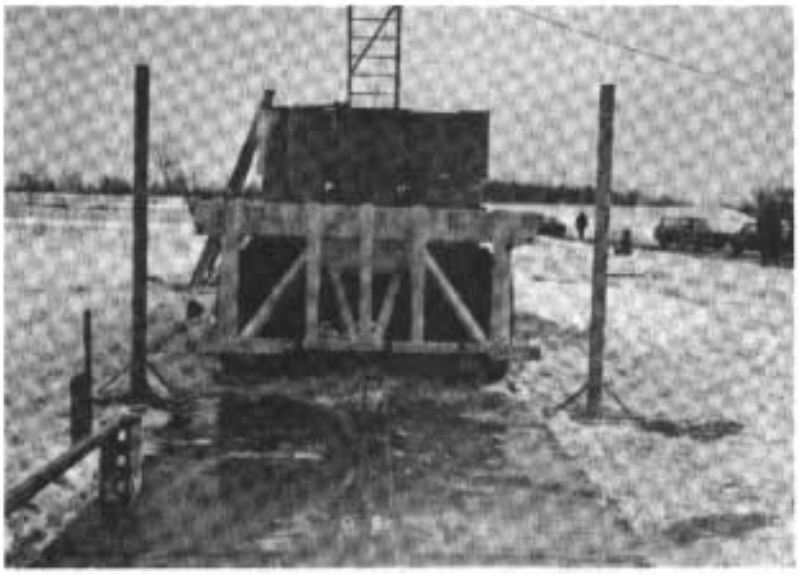

Figure 3 18" RIGID UNDERRIDE GUARD INSTALLATION ON FLATBED TRAILER

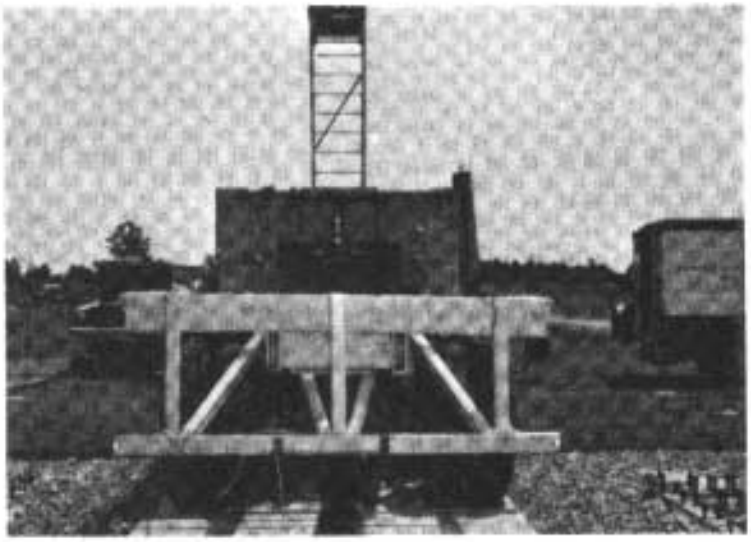

Figure 4 24" RIGID UNDERRIDE GUARD INSTALLATION ON FLATBED TRAILER

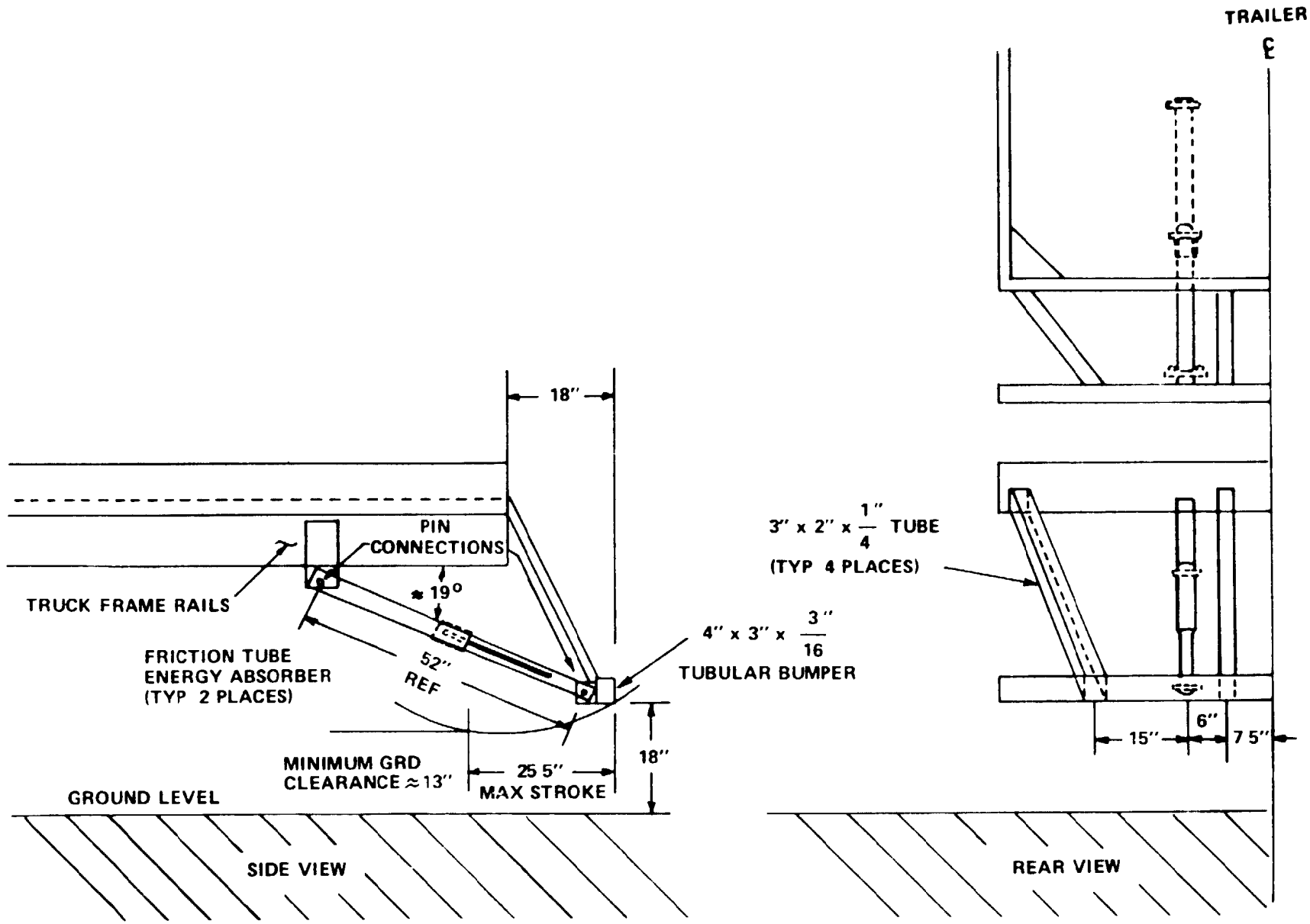

Figure 5 FLATBED 18" ENERGY ABSORBING UNDERRIDE GUARD CONFIGURATION

tube to create friction between the mating surfaces of the two cylinders as they telescope together. (See Appendix B for description and results of laboratory tests performed in the development of the friction tube energy absorber.)

Approximately 15 percent of the total energy absorbed by the underride guard is accomplished through the formation of plastic hinges at the upper end of the four 5" x 2" x 1/4" tubular bumper support members where they attach to the trailer bed. The two outboard support members are angled, as may be seen in Figure 5, to provide increased lateral stability to the system. Ground clearance of the guard is initially 18 inches and decreases to approximately 13 inches as the guard is displaced longitudinally.

It is recognized that the test arrangement, in which the underride guard projects 18 inches beyond the end of the trailer, is not necessarily the best location of the underride guard on this particular truck from an operational point of view since there is adequate space behind the rear axle for the installation. The reason for locating the underride guard as shown was primarily one of expendiency. The construction of the end of the trailer bed allowed direct attachment of the underride guard support members with little or no need for additional structure or reinforcement to provide the required strength and hence saved time and reduced the expense of the test installation.

However, for added realism and to aid in the interpretation of the results, a mock-up extension of the trailer bed was provided to simulate an installation in which the guard and the rear of the truck are in the same plane.

Photographs of the energy absorbing underride guard mounted on the flatbed trailer are presented in Figure 6. The weight of this guard configuration was approximately 200 lbs

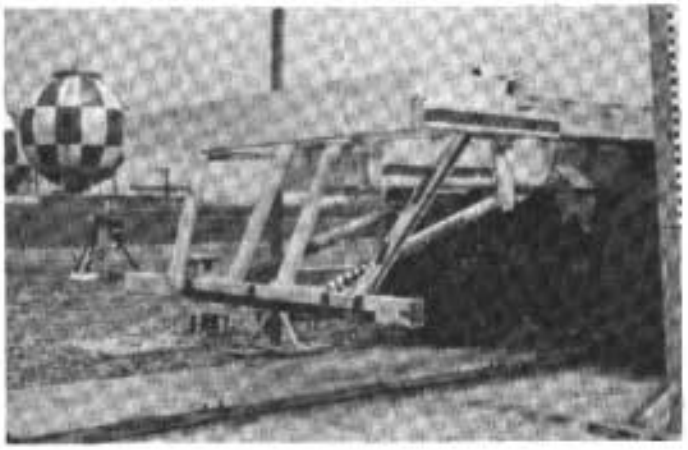

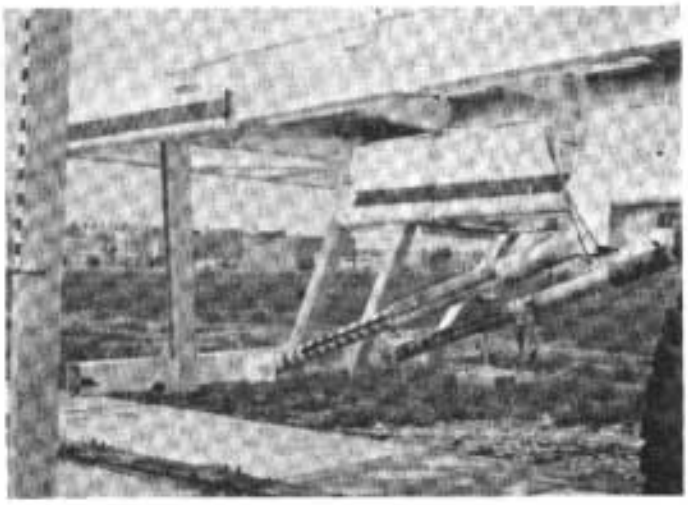

Figure 6 18" ENERGY ABSORBING UNDERRIDE GUARD INSTALLATION ON FLATBED TRAILER

Van Trailer 24" Rigid Underride Guard

Construction of the 24" ground clearance rigid underride guard designed for installation on the van trailer is depicted in Figure 7 The guard bumper is a 4" x 3" x 3/16" wall structural steel tube extending the full 96" width of the trailer. The bumper is supported by four 3" x 2" x 3/16" wall vertical tubular members and four similar supports attached to the underside structure of the trailer. The existing short frame in the vicinity of the axles was extended to the rear of the trailer using 3" x 2" x 3/16" wall steel tubing. In this manner, the underride guard loads are distributed over many cross members of the trailer floor support structure and also taken directly into the existing trailer stub frame. Plates and gussets were used as required to provide reinforcement at the local points of guard attachment.

The calculated installed weight of the underride guard and trailer reinforcements is 237 lbs. However, since approximately 95 lbs were removed as a result of elimination of the existing dock bumper, the net weight increase of the trailer due to addition of the underride guard was less than 150 lbs.

Photographs of the underride guard installed on the van trailer are shown in Figure 8.

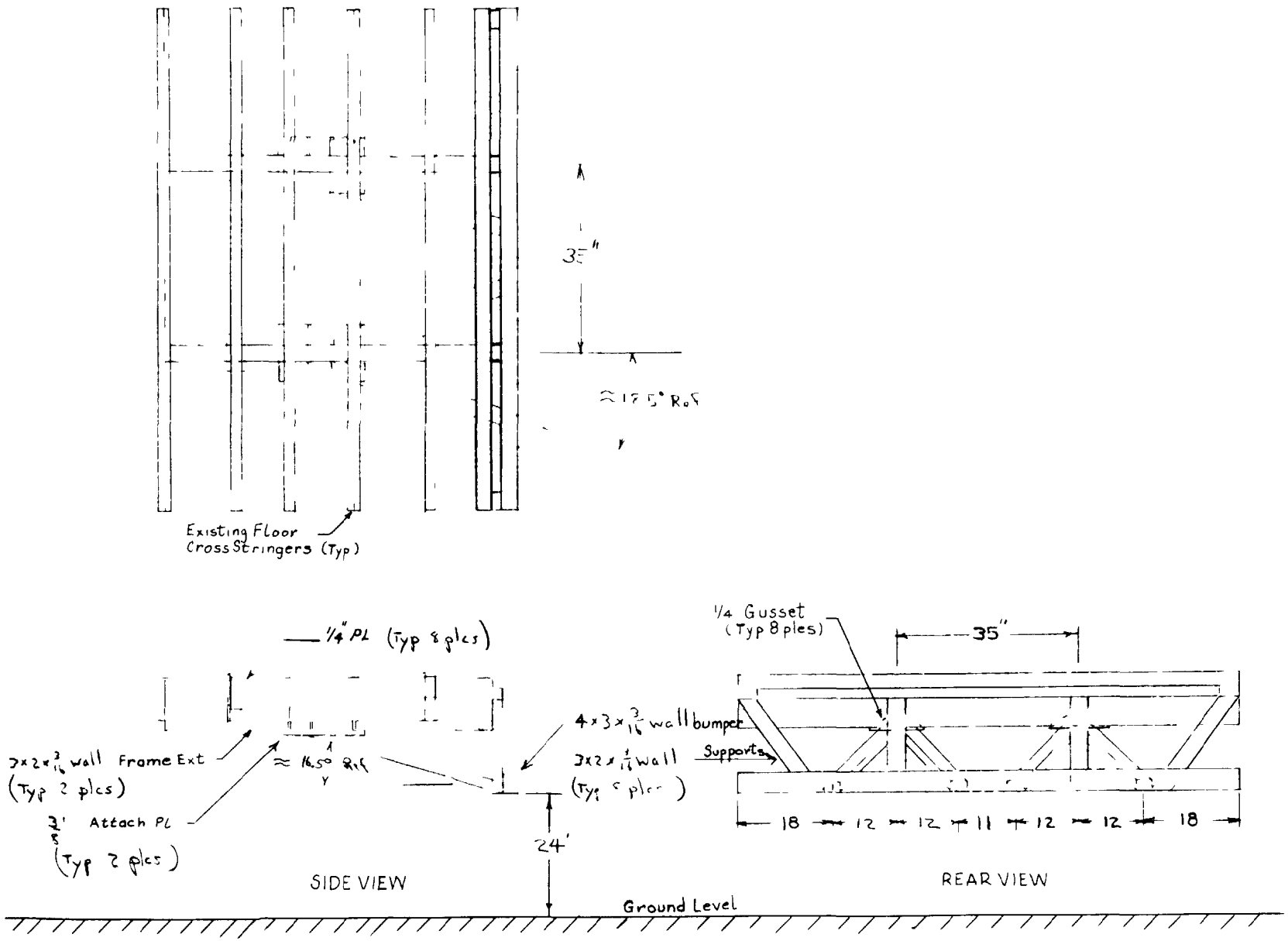

Figure 7 VAN TRAILER 24" RIGID UNDERRIDE GUARD CONFIGURATION

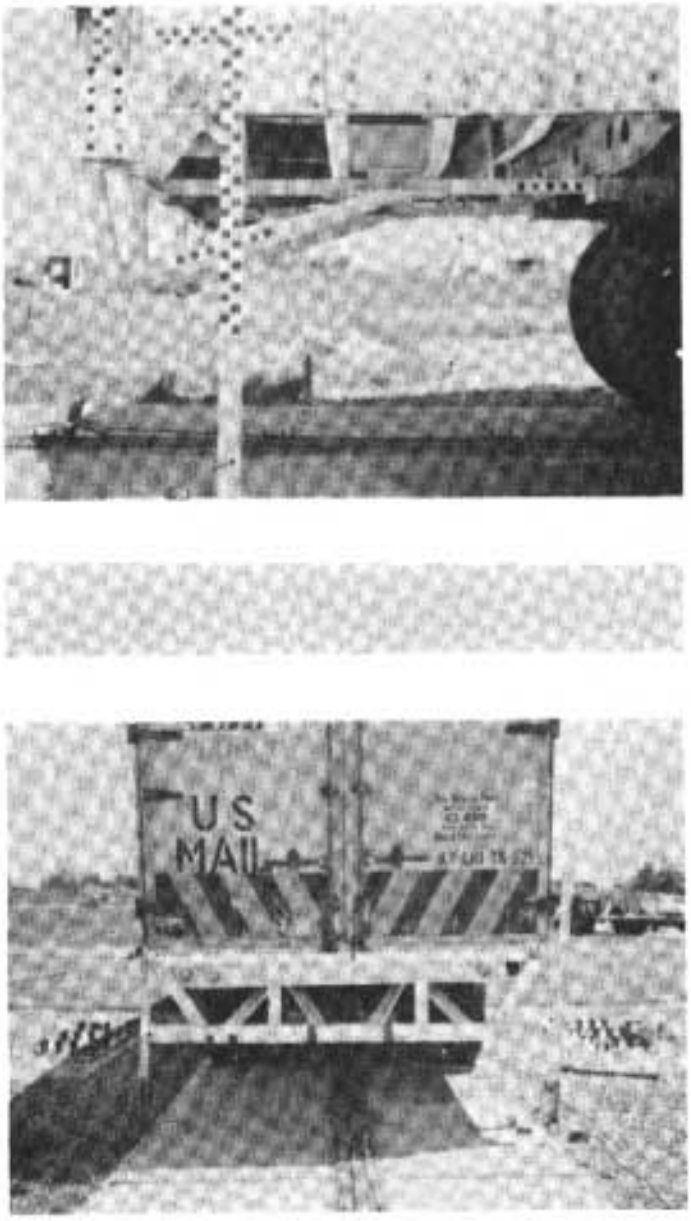

Figure 8 24" RIGID UNDERRIDE GUARD INSTALLATION ON VAN TRAILER

4.0 TRAILER-MOUNTED UNDERRIDE GUARD TEST PROGRAM

4.1 Methodology and Equipment

Six full-scale impact tests of automobiles striking the rear of trailers equipped with the underride guards described in the preceding section were conducted. The trailers were positioned in front of an SAE barrier with two 200,000 lb capacity BLH Electronics, Inc. compression type load cells interposed between the front of the trailer and the barrier for measurement of longitudinal impact loads.

All tests were conducted with the trailers unloaded. The combination of an unloaded trailer and restraint of longitudinal motion represented an aggravated condition as regards the effects of vehicle mass on underride guard performance. Thus, the possibility of lifting of the rear of the trailer, which is conducive to increased underride, is increased with the trailer unloaded. At the same time, however, preventing the trailer from rolling forward upon impact by the automobile simulated, in effect, a trailer of infinite mass which results in maximum crash forces and dissipation of energy. Actually, the momentum transfer to a truck with a mass only 10 times that of an impacting automobile, which is not an unusually high mass ratio for loaded trucks, would reduce the collision energy to be dissipated by only 9%. Hence, the setup represented stringent but realistic and easily controlled conditions for testing of underride guard performance.

The automobiles for this series of tests were 1966 Ford sedans used in four of the tests and 1966 Volkswagen "beetle" sedans used in two tests. The test cars, guided by small wheels running on a guide rail, were propelled by a tow cable and winch arrangement located behind the SAE barrier and driven by a stationary power unit equipped with a semiautomatic speed control system. The guide rail terminated a short distance upstream from the rear of the trailers where the tow cable was also released so the test cars were completely free of artificial restraints immediately before and during the impact.

In preparing a vehicle for test, the front half of the car was painted with highly reflective paint for improved visibility and contrast in the high speed color films of the impacts if the original color of the car did not provide sufficient contrast. Reference targets and photo tape were also applied to the vehicles to facilitate reduction of the photographic data.

Because in some instances portions of the vehicle could underride before actual contact with the guards was made, a small vertical bracket was attached to the front bumper that closed a switch on the underride guard to indicate "time zero" when the leading edge of the bumper was initially in the face plane of the guard.

Instrumentation mounted in the test vehicles consisted primarily of triaxial accelerometers to measure the dynamic response of the automobiles during the impact. The accelerometers were Statham Laboratories bidirectional strain gauge type with ranges up to 350 G. Three accelerometers mounted on a rigid plate attached to the drive line tunnel at the approximate location of the front seat belt anchorage measured accelerations of the passenger compartment along orthogonal vehicle axes. A similar triaxial accelerometer package was attached to the flat deck behind the rear seat in the trunk area above the rear axle. Two accelerometers with sensitive axes in the longitudinal and vertical directions were also mounted on the engine block. In three of the tests with the Ford cars, an additional longitudinal accelerometer was attached to the engine support frame on the left side of the vehicle. The general locations of the various accelerometers are shown in the sketch of Figure 9.

Signals from the various instrumentation transducers were amplified by Nexus USL-1 solid state operational amplifiers which, for the accelerometers, were mounted aboard the test cars along with the necessary power supplies and associated electronic circuitry. The amplified signals were transmitted via an umbilical cable and recorded on Sangamo 14 channel FM magnetic tape recorders and/or Consolidated

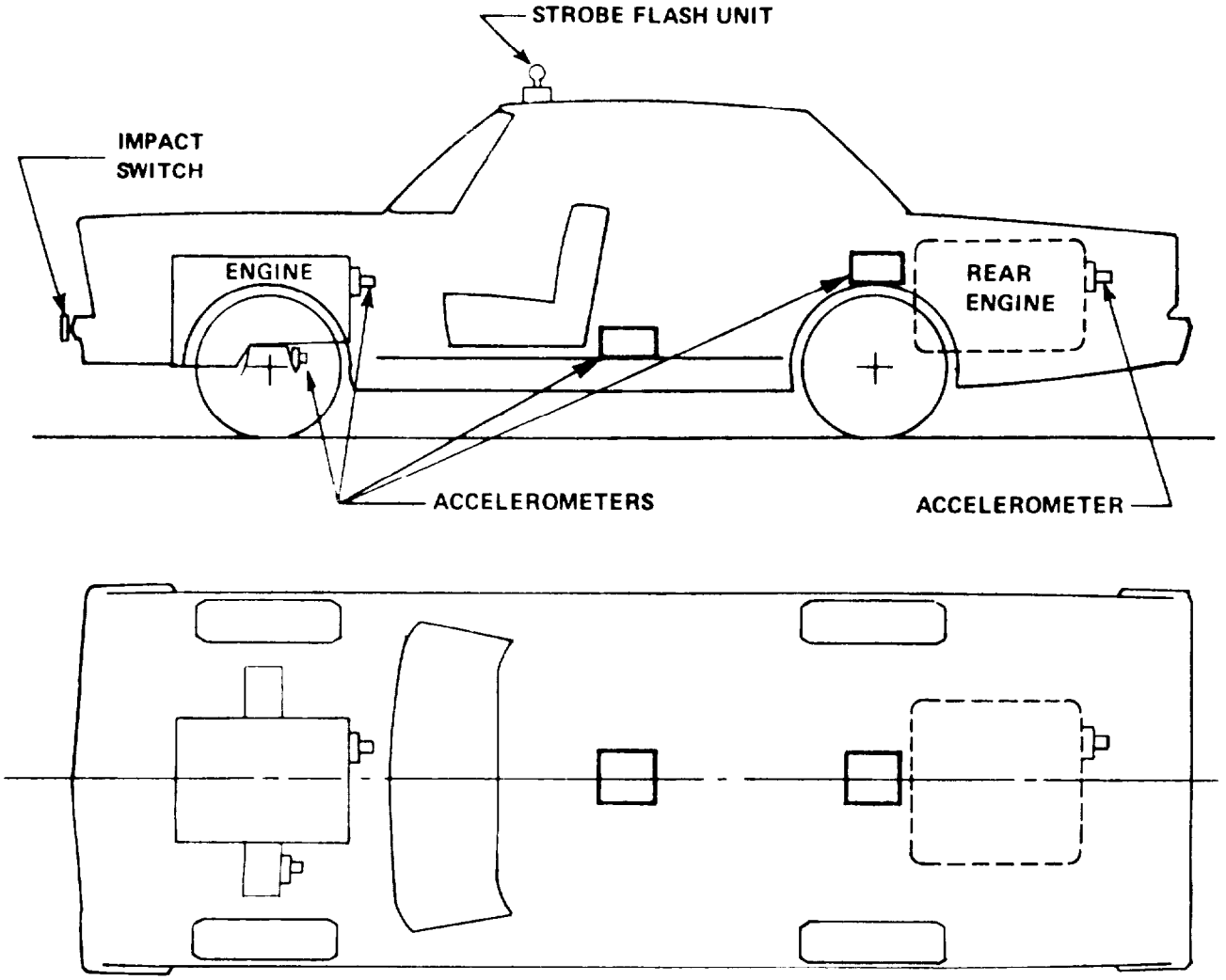

Figure 9 VEHICLE MOUNTED SENSORS

Electrodynamic Corporation light beam oscillographs quipped with Series 7-300 galvanometers magnetically damped to 64 percent of critical.

Two strip switches were placed across the approach roadway a short distance ahead of the underride guard. Closure of the switches upon traversal by the wheels of the test car produced pulses which were recorded along with a 100 Hz timing signal for determination of impact speed. The redundancy provided by this system, which allowed two independent calculations of the speed based either on the known spacing between the switches or on the wheelbase of the test vehicle, was a safeguard against possible malfunction of one of the switches. For most of the tests, a time interval counter, actuated by light beams at an accurately known spacing and interrupted by passage of the car, was also used for computation of impact velocity.

Other strip switches attached to the front of the test vehicle and on the face of the underride guard closed circuits to fire flashbulbs strategically located in the field of view of all data cameras for correlation of "time zero" at initial contact in the film and data records.

Several high speed movie cameras using 16 mm color film and operating at frame speeds between 1000 and 1500 frames per second were used to obtain a visual record of the details of the impacts for post-collision analysis. Cameras with different fields of view provided side view coverage of the crashes from both sides of the cars. For some of the tests, a camera was also located underneath the rear axle of the trailer to provide a rearward view toward the impacting car. All high speed data cameras were equipped with neon lamps that were triggered by a Red Lake Laboratory timing light generator for recording timing pulses on the films at 0.01 second intervals.

Documentary photographic coverage was obtained with a movie camera operated at a nominal speed of 50 frames per second and by still photos of the vehicles both before and after each crash test.

A sketch showing the general layout of the test setup for the trailer-mounted underride guard tests is presented in Figure 10.

4.2 Test Results

The test results presented here were obtained in six tests (Nos. 7-12) performed on the prototype underride guard configurations described in Section 3.2. Detailed results of the preceding series of six tests using a simulated rigid underride guard can be found in Reference 1. In the following subsections, time history plots of the reduced data are presented along with brief descriptions of the test condition, vehicle response and damage as observed from the films and post-crash inspection. Passenger compartment longitudinal deceleration data are shown both in "raw" form, i.e., the analogue signal as recorded, and also as processed by a computer. The computer data reduction program performs two functions (1) applies a Martin-Graham numerical filtering technique as described extensively in Reference 5 to provide filtered acceleration responses, and (2) integration of the acceleration data to yield passenger compartment velocity and displacement as functions of time.

The reason for filtering the acceleration data is, of course, to attenuate unwanted high frequencies which tend to obscure the significant characteristics of the gross vehicle response. The filtered responses shown are with a 50 Hz cutoff frequency, a roll-off length of 100 Hz and using a weighted average of 20 data points on either side of the data point being filtered. Experience has indicated that these filter characteristics are appropriate for evaluation of gross vehicle collision responses because the velocity and displacements obtained by integration of the acceleration data are only slightly affected by filtering at the 50 Hz cutoff level.

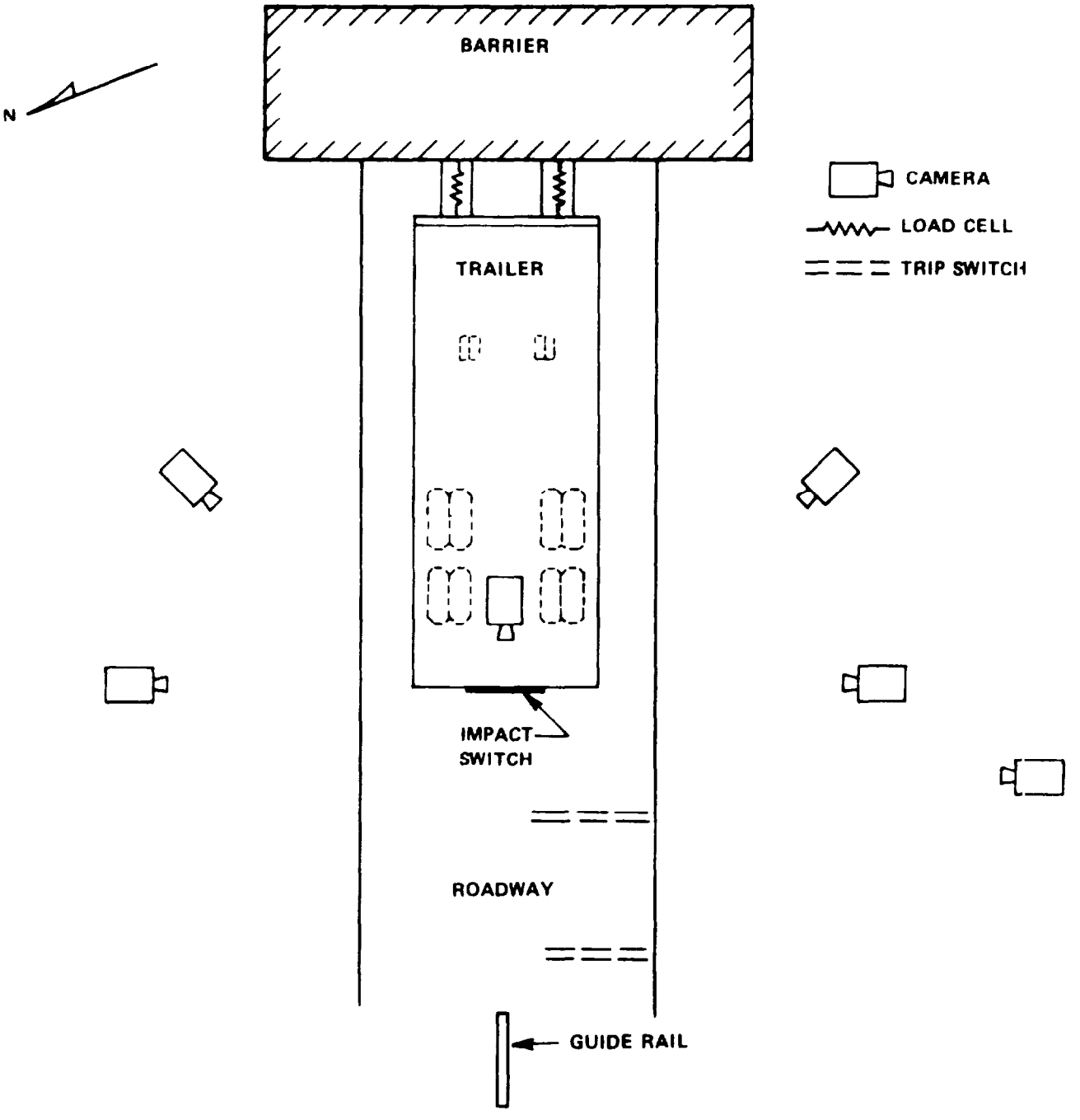

Figure 10 SKETCH OF TEST SITE SHOWING LOCATION OF SENSORS AND CAMERAS

4.2.1 Crash Test No. 7

In this test, a standard 1966 Ford four-door sedan weighing 3,750 lbs. was impacted head-on against the 18" rigid underride guard installed on the flatbed trailer (see Figure 3) at a speed of 39.6 MPH.

Passenger compartment filtered and unfiltered longitudinal acceleration data (numerical filtering with 50 Hz cutoff and 100 Hz roll-off frequency) are shown in Figure 11 along with the velocity and displacement curves. The unfiltered data were reduced from an oscillograph record read at one millisecond time intervals. The velocity and displacement curves were obtained by integration of the acceleration data. The maximum filtered acceleration is approximately 35 g's occurring at .069 seconds. The measured frontal crush distance, following the test, was 31 inches compared with a dynamic maximum of 41 inches obtained from integration of the acceleration data. Post-crash measurements of vehicle deformation are usually less than the maximum that occurs during impact because of partial elastic recovery of vehicle structural components.

Times of significant events, which were noted in the analysis of high speed movie films, are marked along the abscissa at the top of the figure. The films showed that the underride guard and aft end of the trailer deflected downward a maximum of approximately two inches at .066 seconds. The bumper member of the guard also moved forward approximately 1.5 inches at the same time due to bending of the trailer structure. Inspection of the guard, following the test, however, revealed no permanent set in the structure. The vehicle came to rest against the guard at approximately .105 seconds and exhibited very little rebound.

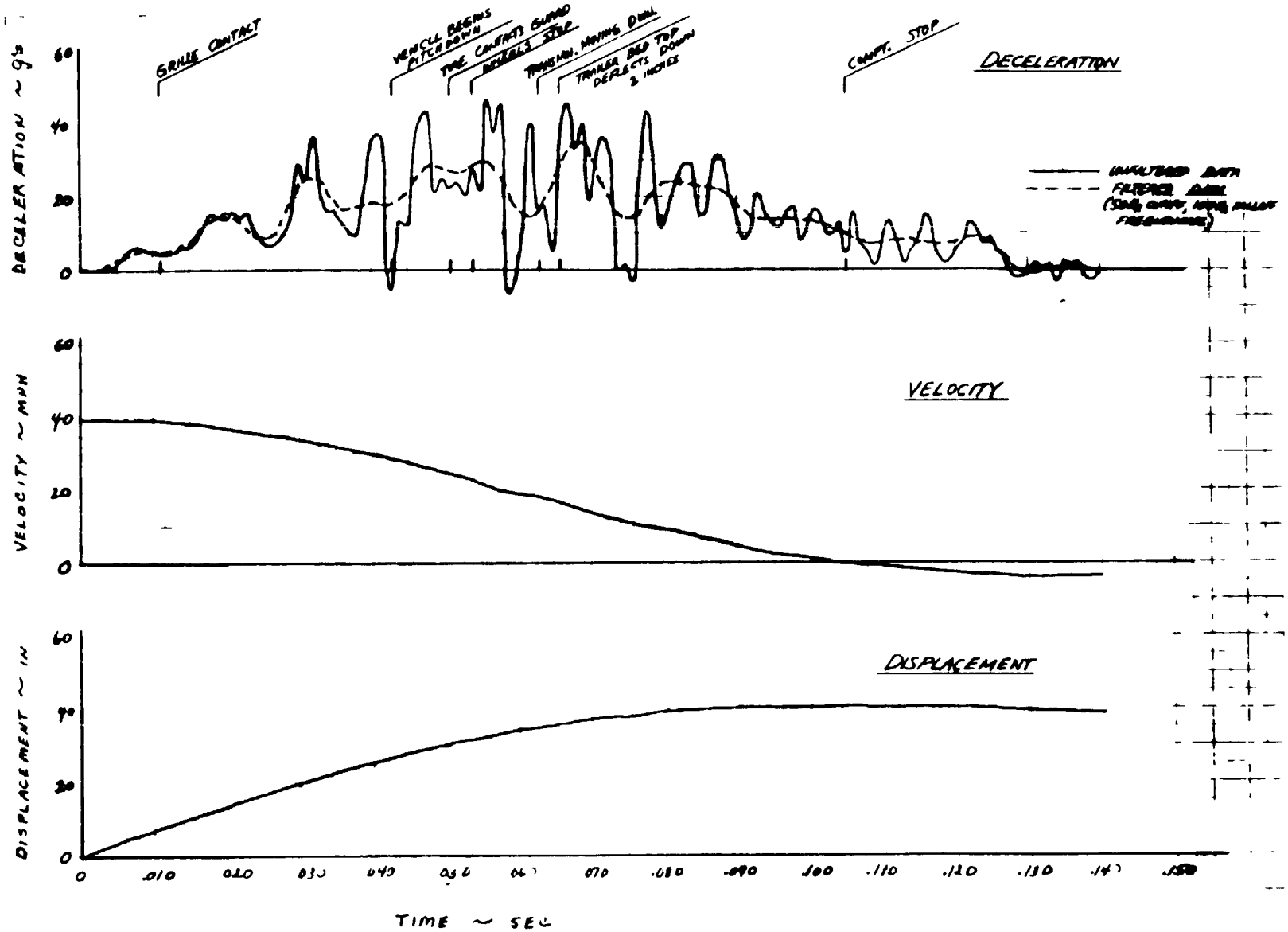

Figure 11 TEST NO. 7: PASSENGER COMPARTMENT LONGITUDINAL DATA

Data from the other on-board sensors are shown in Figures 12 and 13. The engine frame acceleration data and drive shaft strain data were both lost following approximately .060 seconds when electrical connections were severed during the impact.

The drive shaft showed a peak axial load, before data loss, of approximately 37,600 lbs at .042 seconds. It is not known if larger loads were sustained by the shaft before it failed near the differential housing because of the data interruption.

Penetration distance of the guard into the vehicle was also obtained from analysis of high speed movie film. These data, presented as a function of time in Figure 14, show a maximum penetration of 41 inches and a stopping time of .105 seconds which are nearly identical with the integrated accelerometer results.

The time history of longitudinal impact force, as measured by load cells at the forward end of the trailer bed, is presented in Figure 15. The maximum load was approximately 168,000 lbs. occurring at .045 seconds. This maximum load is undoubtedly due to engine contact with the guard. Note from Figure 12 that peak acceleration of the engine occurred at approximately .035 seconds after impact. The difference between this time and the time of maximum load measured by the load cells is probably due to mass effects since the forces had to be transmitted throughout the entire length of the trailer before being reacted by the load cells. The average force computed for the .105 second time interval was 69,500 lbs.

Integration of the area under the longitudinal force curve (Figure 15) over the .105 second stopping time interval yields a measured impulse of 7,300 lbs-sec compared to the 6,780 lbs-sec change of linear momentum represented by the product of the automobile mass and initial velocity.

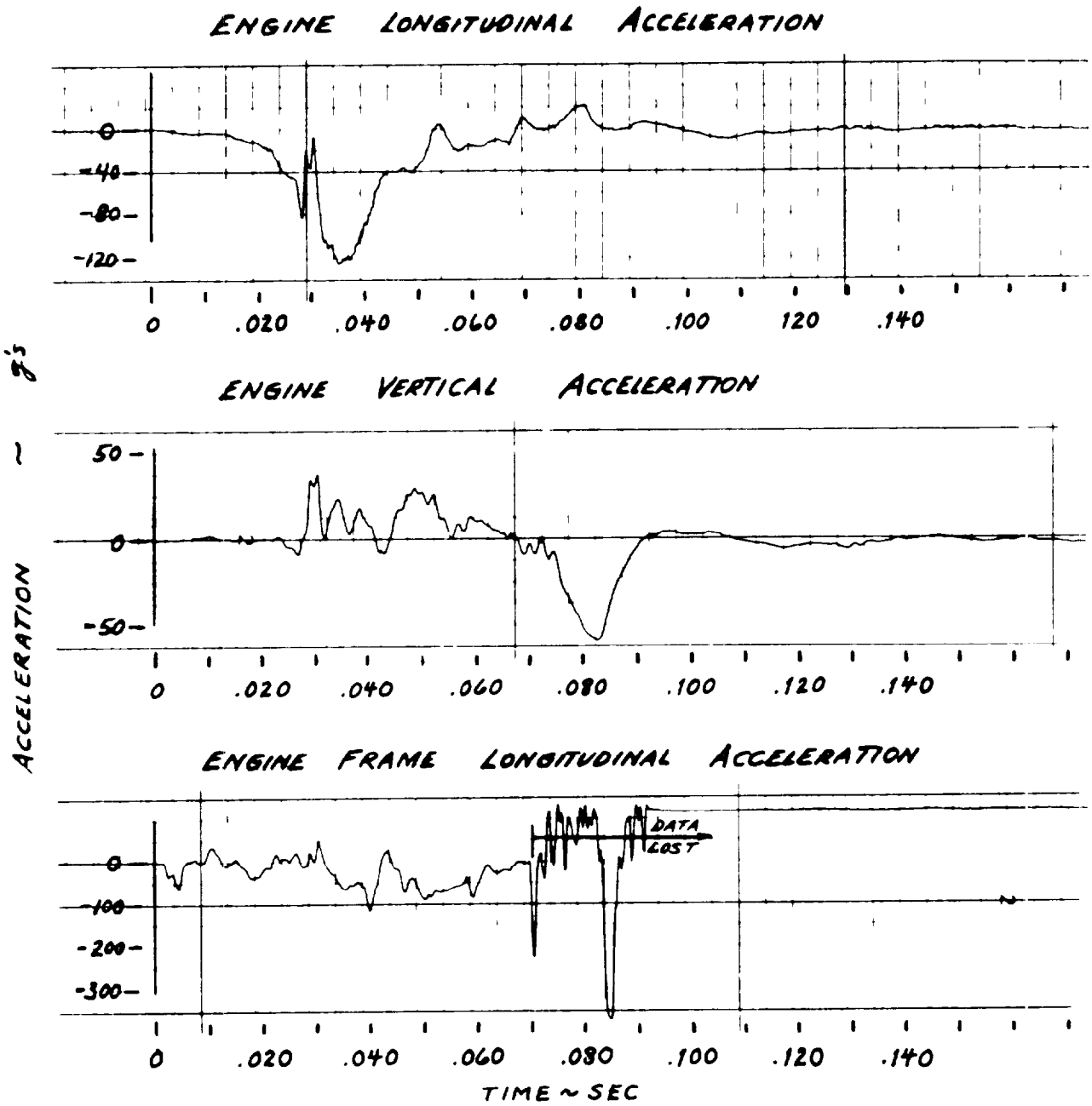

Figure 12 TEST NO. 7: ENGINE AND FRAME ACCELERATION DATA

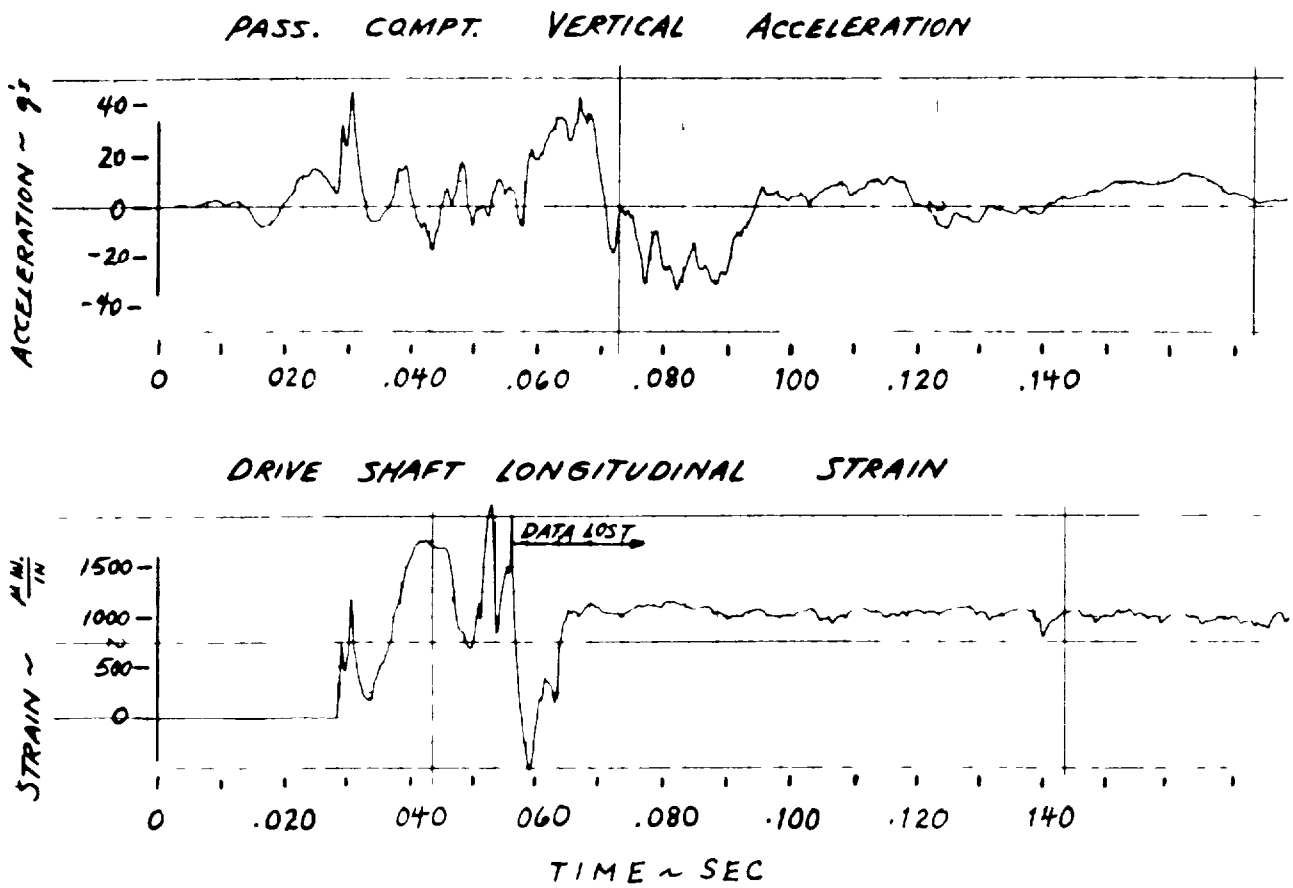

Figure 13 TEST NO. 7: VEHICLE VERTICAL ACCELERATION AND DRIVE SHAFT STRAIN

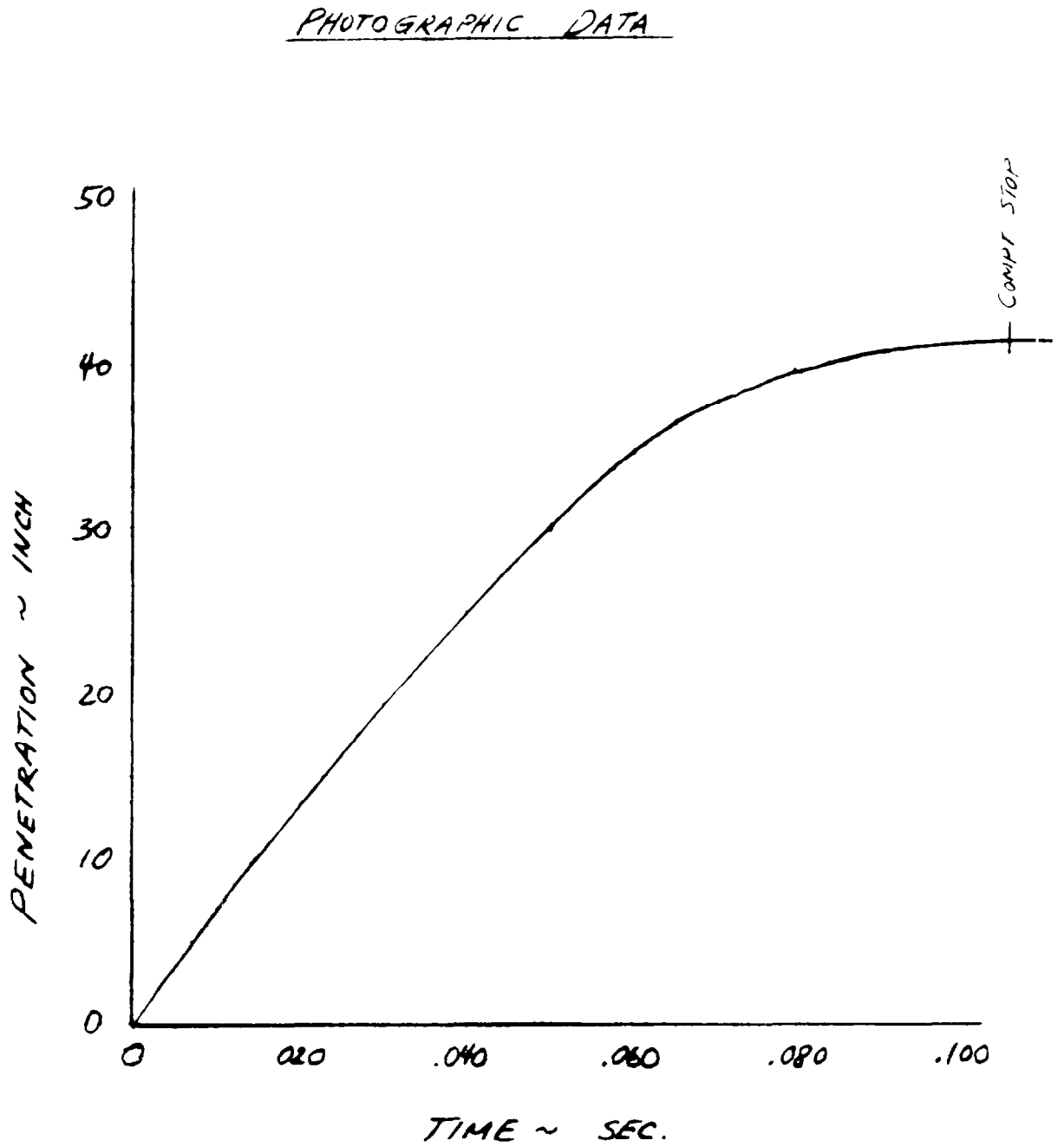

Figure 14 TEST NO 7: VEHICLE-GUARD RELATIVE PENETRATION

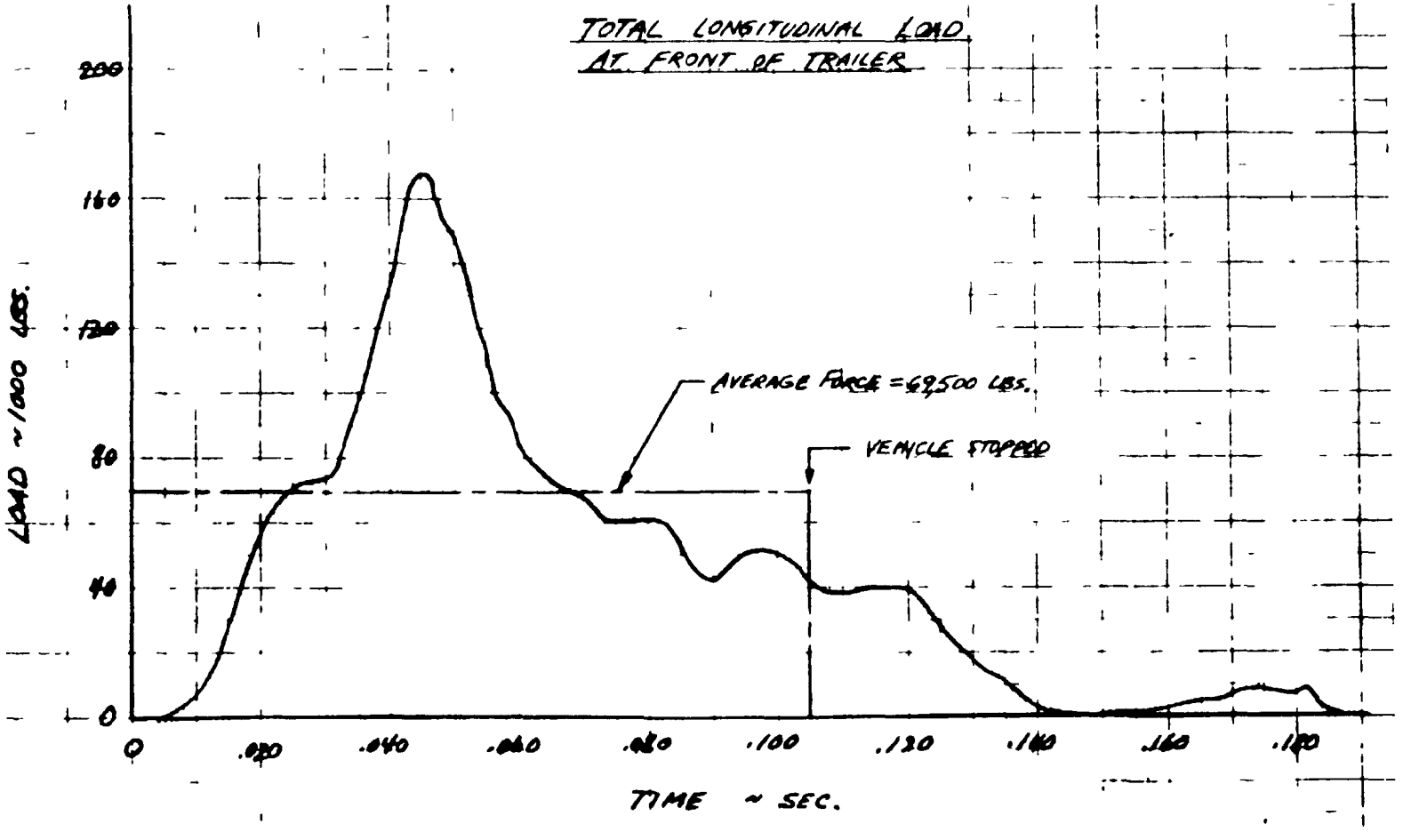

Figure 15 TEST NO. 7: VEHICLE IMPACT LOAD

Photographs of the vehicle before and after the test are presented in Figure 16. Post-crash inspection revealed that the bumper remained in contact with the underride guard during impact but was sheared off of its supports as it moved aft. The fire wall was pushed back into the passenger compartment area a slight amount due to rearward displacement of the engine, and the steering column rotated upward toward the vertical along with the dashpanel.

4.2.2 Crash Test No. 8

The performance of the 18" energy absorbing underride guard installed on the flatbed trailer (Figure 6) was investigated in this test. The test automobile was a standard 1966 Ford four-door sedan weighing 3,840 lbs. that impacted the guard at a speed of 39.0 MPH.

Reduced data from the oscillograph record of the acceleration of the passenger compartment are shown in Figure 17. Also shown in the figure are plots of filtered acceleration and of the velocity and displacement of the car obtained by integration of the acceleration data. Peak acceleration (filtered) was approximately 34 G, which occurred .042 seconds after impact. The maximum dynamic longitudinal displacement of the car obtained from the accelerometer data was 46 inches compared to 41 inches from post-crash measurements of the vehicle crush and displacement of the underride guard which were 19 and 22 inches respectively.

Times of significant events, which were noted in the analysis of high speed movie films, are marked along the abscissa at the top of the figure The films showed that the underride guard started to collapse at approximately .020 seconds and that the forward velocity of the passenger compartment was zero at approximately .126 seconds and rebounded only slightly.

(a)

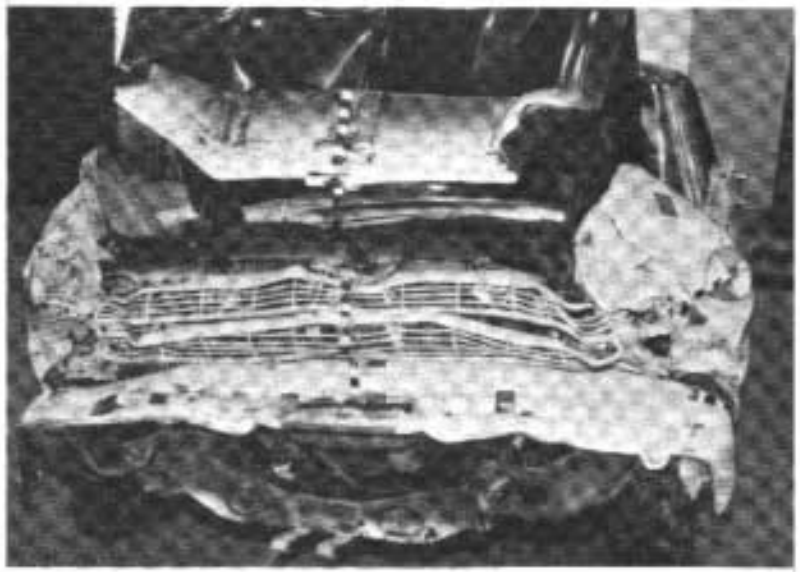

(b)

(c)

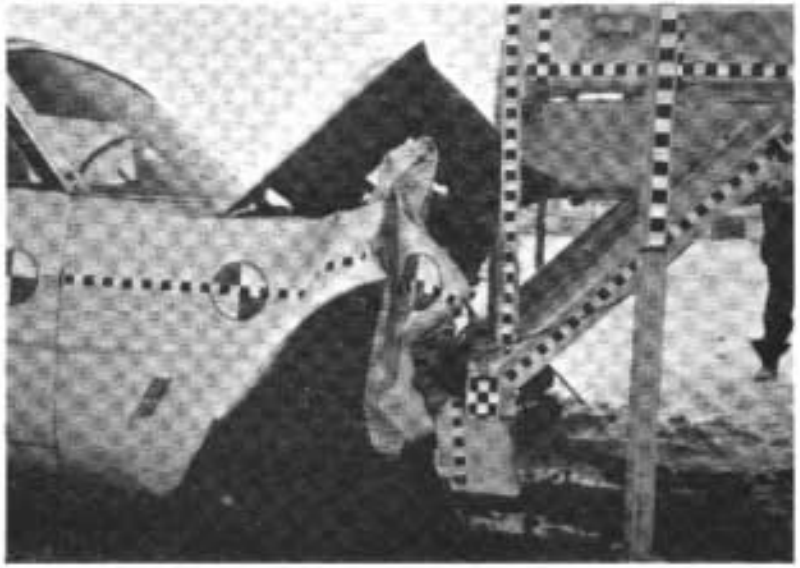

(d)

Figure 16 TEST NO. 7: TEST VEHICLE AND RIGID UNDERRIDE GUARD

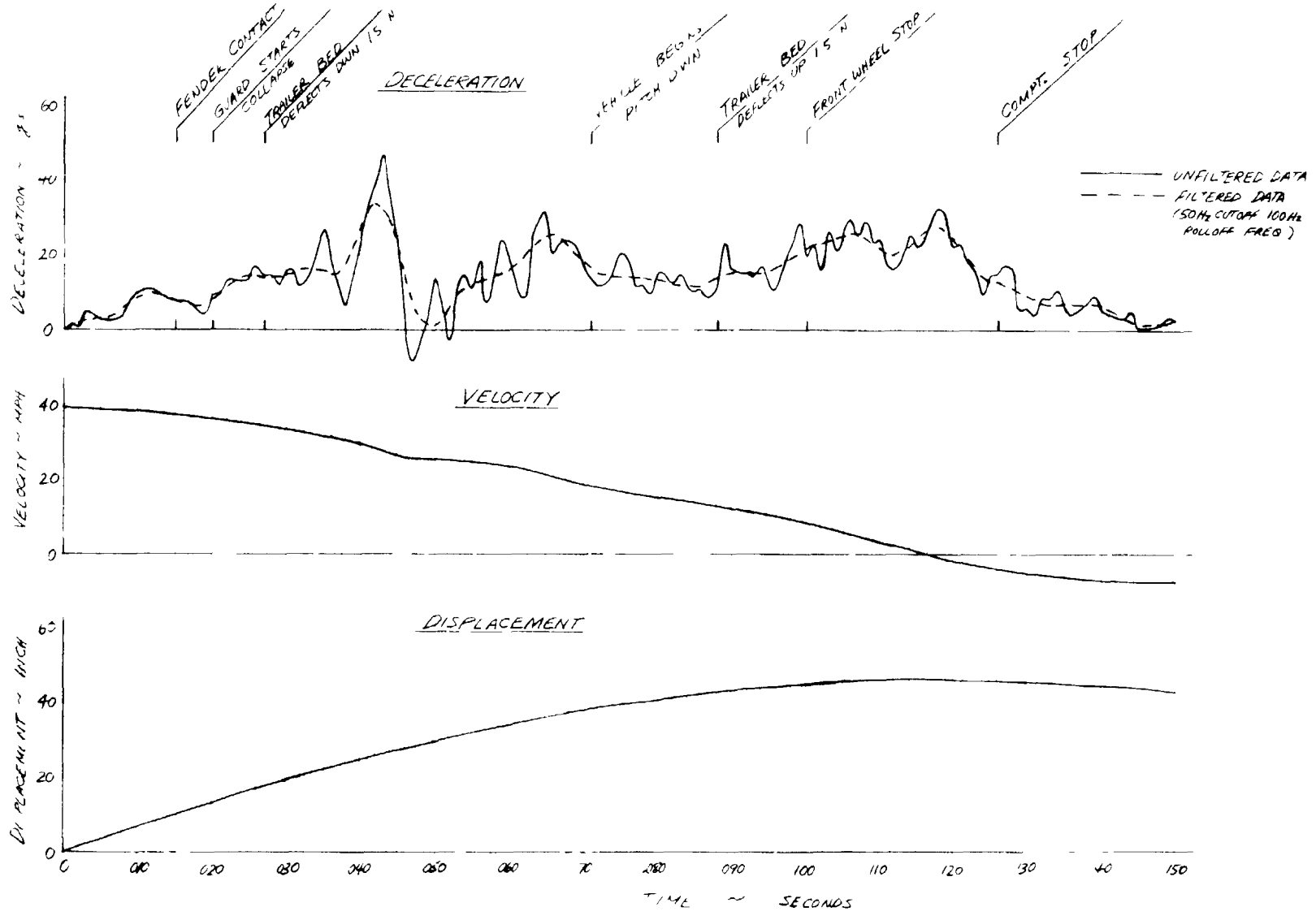

Figure 17 TEST No. 8: PASSENGER COMPARTMENT LONGITUDINAL DATA

Data from the other v hicle mounted sensors are shown in Figure 18. The engine peak longitudinal decel ration of approximately 60 g's occurred at .034 seconds.

Time histories of axial strains measured in each of the collapsible energy absorbers are shown in Figure 19. Two strain gauges were mounted on each unit, on opposite sides, approximately 7 inches from the upper pivot point. The strain measurements were converted to axial loads and are presented versus time in Figure 20. These data indicate peak compressive loads of approximately 28,000 lbs. and 34,000 lbs. in the right and left side struts, respectively, but the overall force levels were quite constant throughout the impact.

A time history of the total longitudinal impact force, as measured by load cells at the forward end of the trailer is presented in Figure 21. The maximum load was approximately 90,000 lbs. occurring at .045 seconds. The average force determined from these data over the .126 second stopping time interval was 52,600 lbs. Integration of the area under the force curve over the .126 second stopping time interval yields a measured impulse of 6,620 lbs-sec compared to the 6,830 lbs-sec change of linear momentum represented by the product of the vehicle mass and initial velocity. The close agreement between the momentum and measured impulse attests for the accuracy and validity of the measured data.

Total displacements of both the vehicle and underride guard during impact as determined from analysis of high speed movie film are shown in Figure 22. The displacement of the guard was subtracted from total vehicle displacement to obtain the vehicle crush data which indicate a maximum crush of approximately 24 inches. The total vehicle displacement of 45.5 inches compares favorably with the integrated accelerometer results.

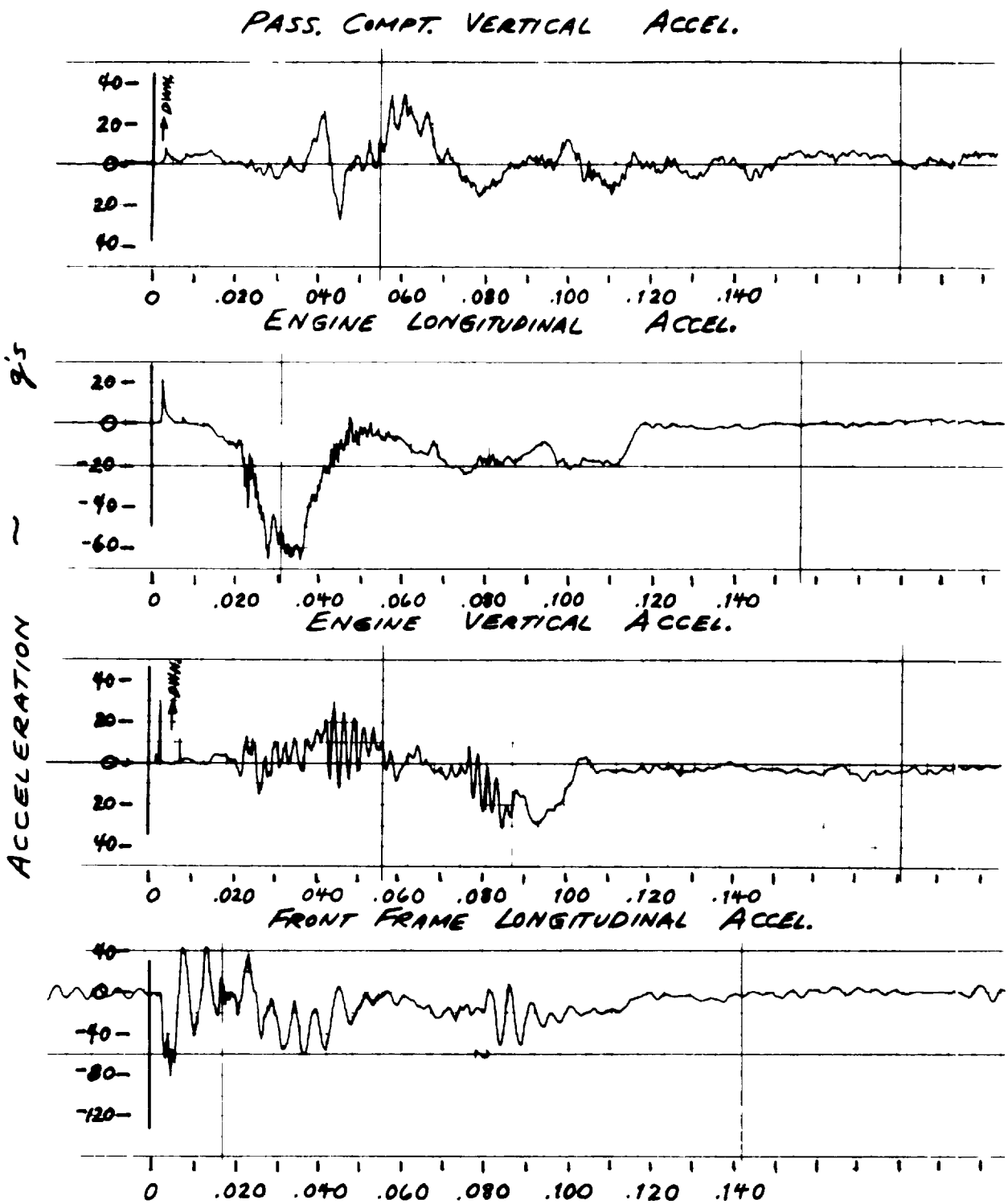

Figure 18 TEST No. 8: VEHICLE ACCELERATION DATA

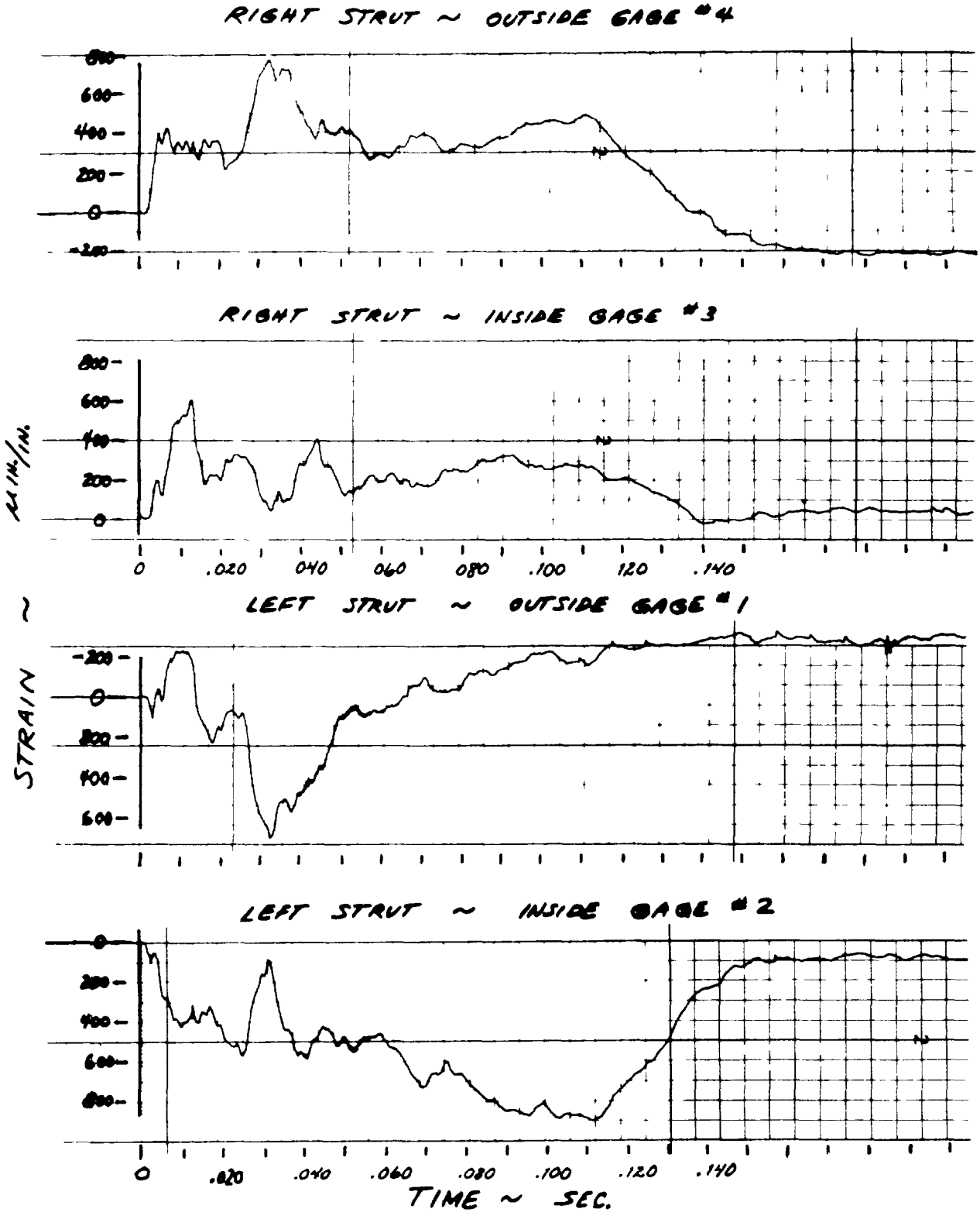

Figure 19 TEST No. 8: FRICTION TUBE AXIAL STRAIN DATA

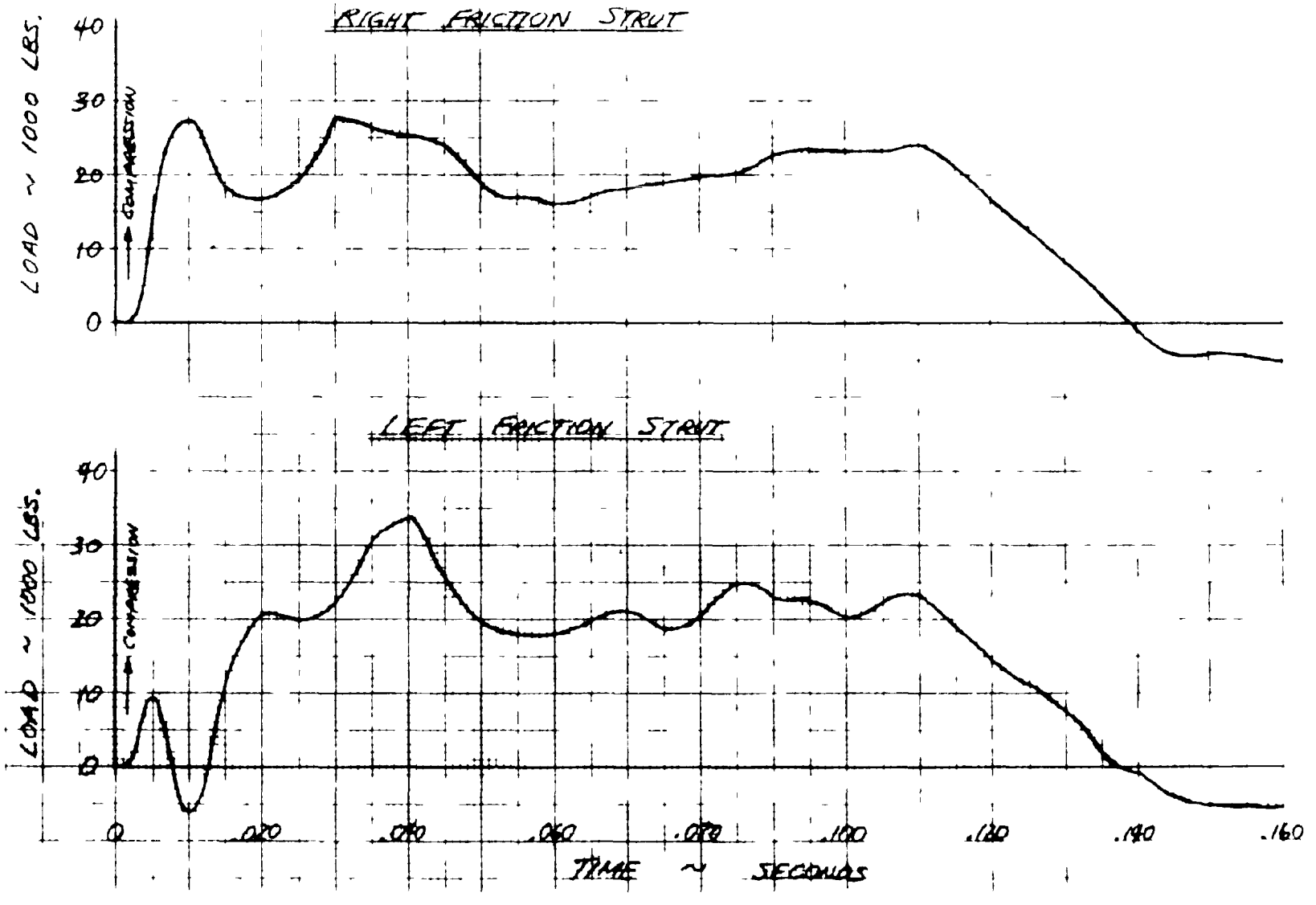

Figure 20 TEST No 8 FRICTION TUBE AXIAL LOADS

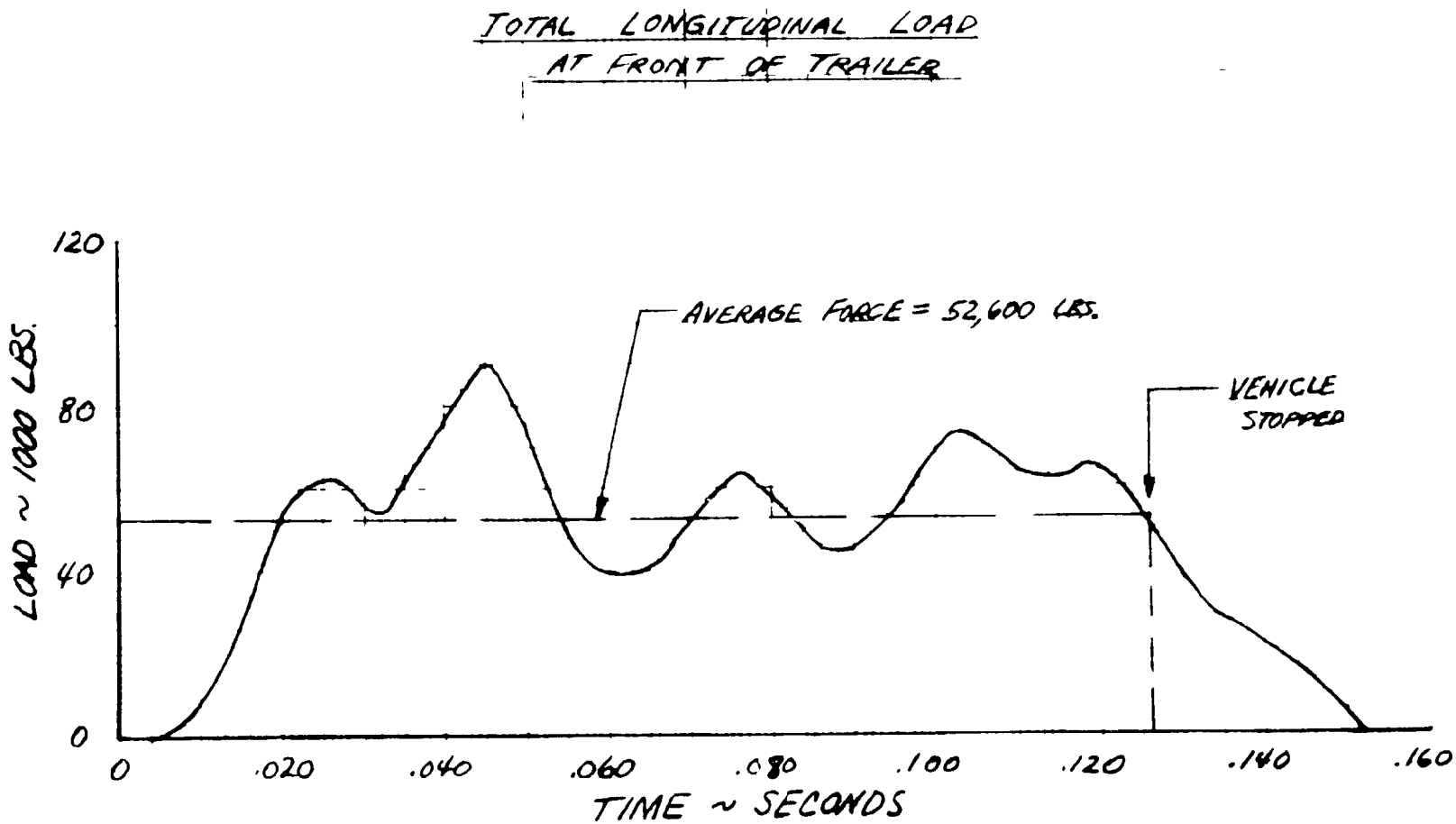

Figure 21 TEST N . 8: VEHICLE IMPACT LOAD

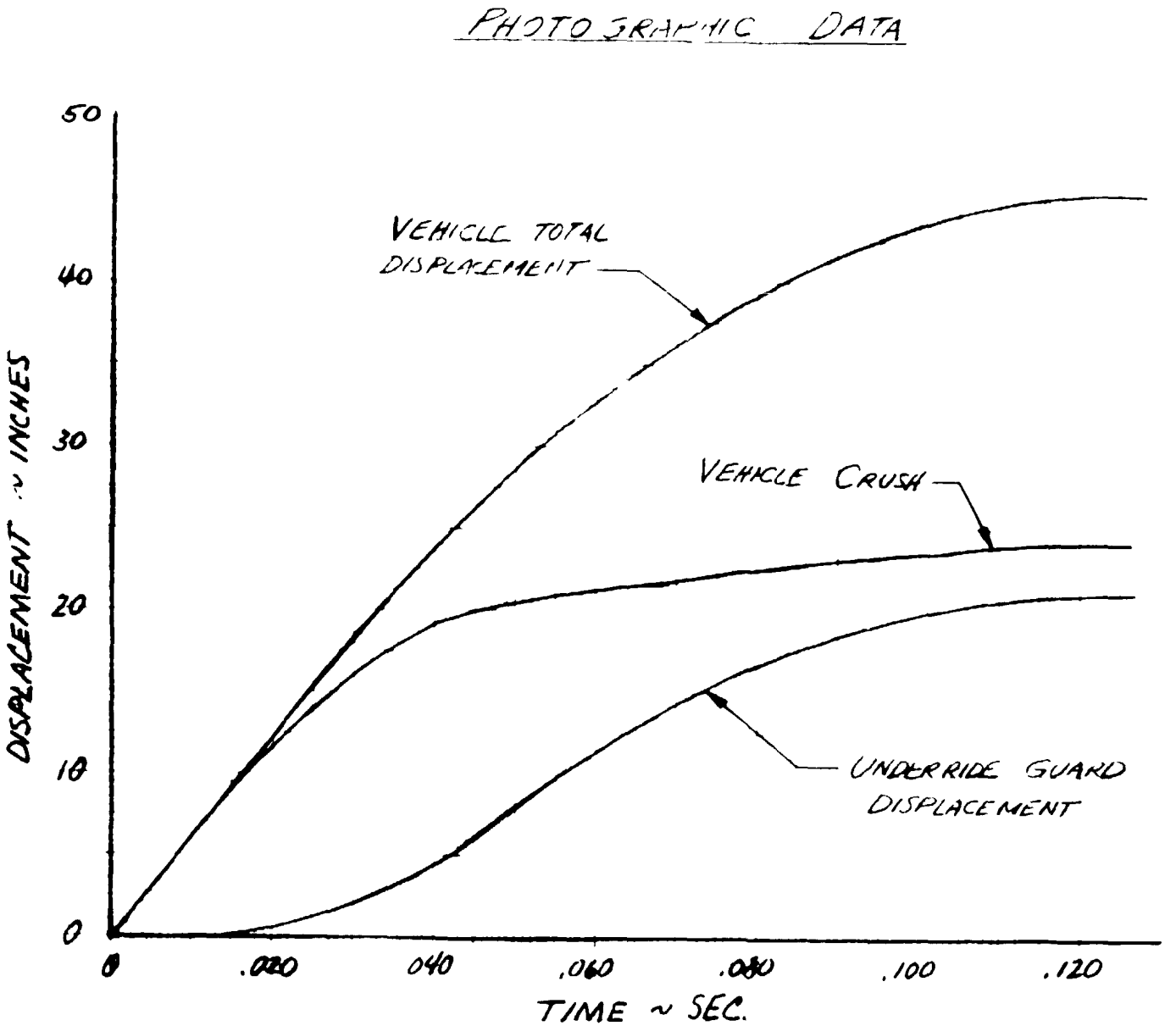

Figure 22 TEST No 8: VEHICLE AND UNDERRIDE GUARD DISPLACEMENTS

Photographs of the vehicle before and after the test are presented in Figure 23. Post-crash inspection revealed that the bumper remained in contact with the underride guard during impact but sheared off at the supports as it moved aft. The interior of the passenger compartment was virtually undamaged as may be seen in Figure 23 (d). Steering column aft movement appeared to be approximately one-half inch.

Several views of the trailer and underride guard are presented in Figure 24. Both energy absorber struts telescoped approximately 17.25 inches and did not bottom out.

4.2.3 Crash Test No. 9

The objective of this test was to determine the performance of the energy absorbing underride guard (Figure 6) in an off-center head-on impact by a full size car. The test vehicle was a 1966 Ford four-door sedan weighing 3,760 lbs. that impacted the underride guard at a speed of 38.2 MPH. The lateral off-set between the longitudinal center lines of the car and the trailer was 22.5 inches.

Passenger compartment longitudinal acceleration "raw" data are presented in Figure 25 along with vehicle velocity and displacement curves. These plots were obtained by first filtering the acceleration data recorded on FM magnetic tape with a 1000 Hz cutoff filter and then digitizing the results at .0002 second sampling time intervals. These data were then plotted, along with the two integrated curves, on a Houston Omnigraphic Recorder.

The compartment acceleration data filtered at a frequency of 50 Hz are shown in Figure 26. Times of events noted in the analysis of the high speed movie film are marked along the abscissa at the top of the figure. The maximum acceleration for the 50 Hz filtered data is 17 g's.

(a)

(b)

(c)

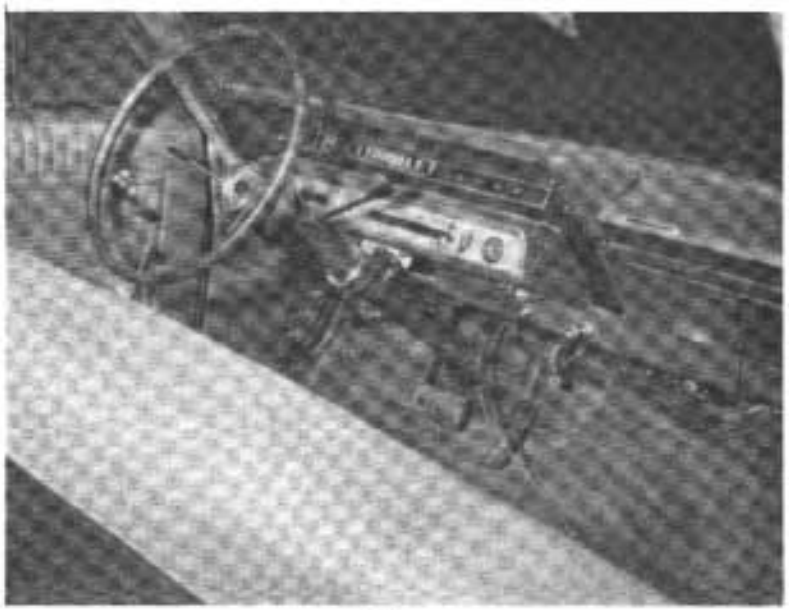

(d)

Figure 23 TEST No. 8: TEST VEHICLE BEFORE AND AFTER IMPACT

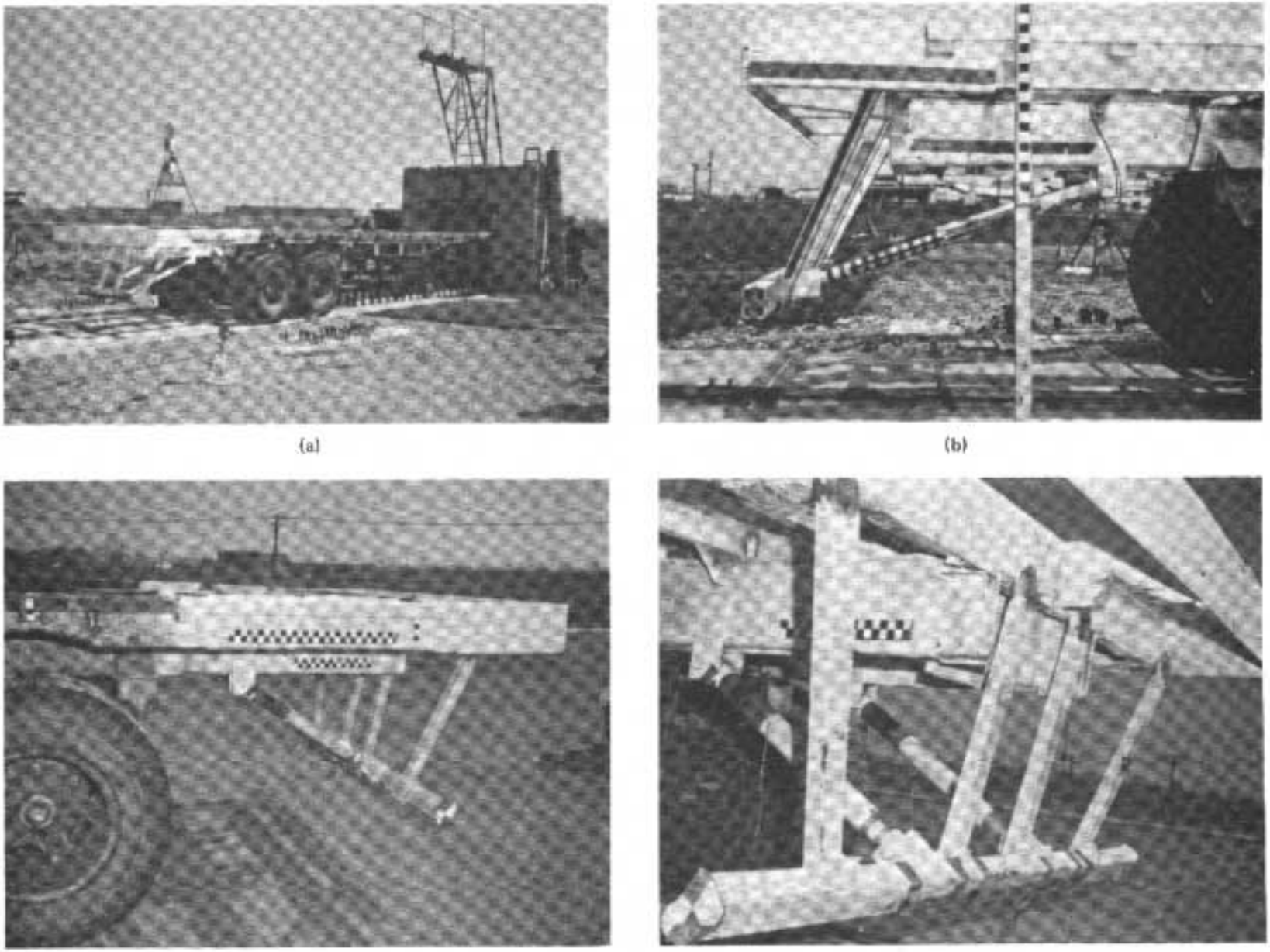

(a) (b) (c) (d)

Figure 24 TEST No. 8: COLLAPSIBLE UNDERRIDE GUARD BEFORE AND AFTER IMPACT

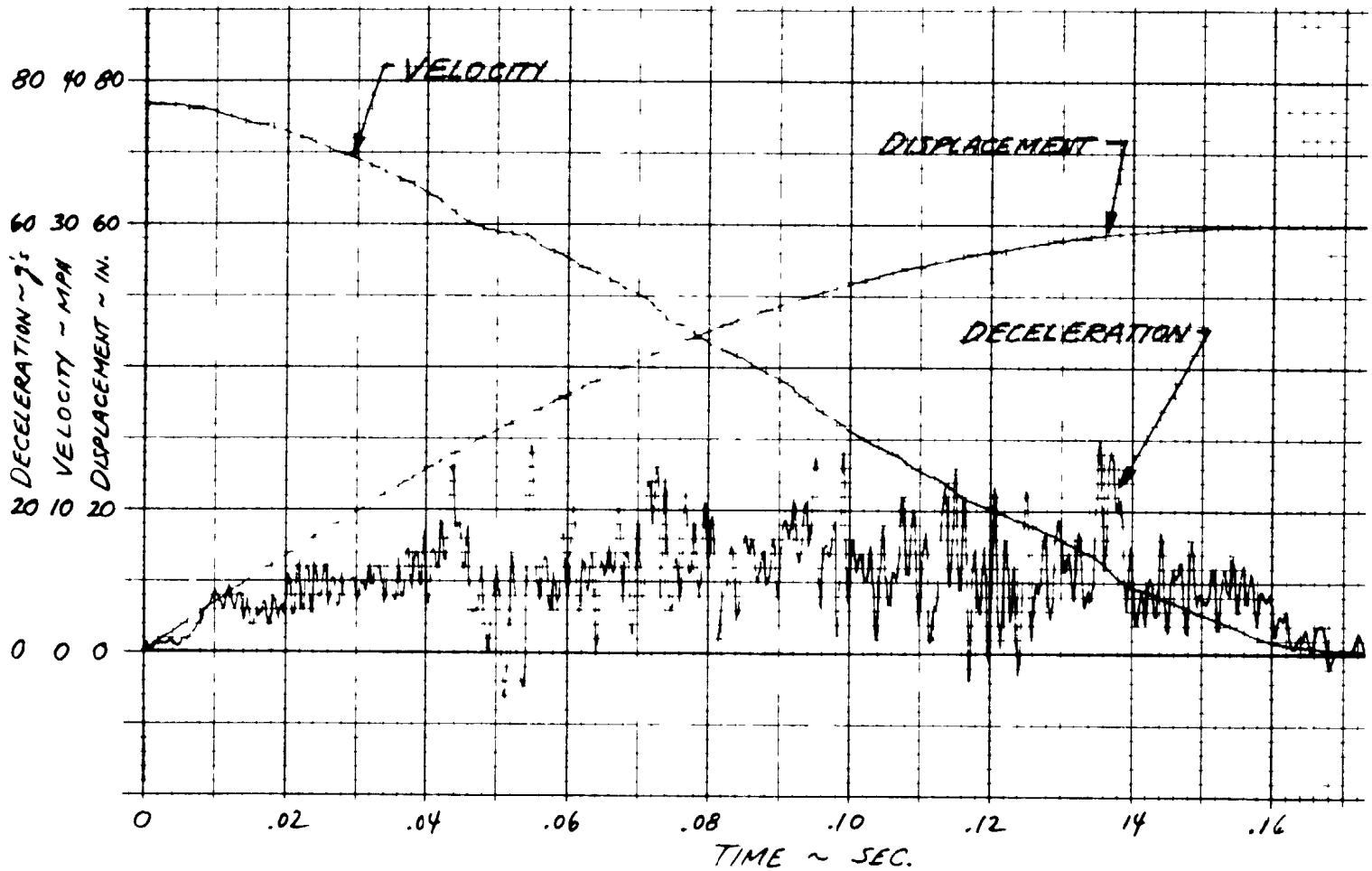

Figure 25 TEST NO. 9. COMPARTMENT LONGITUDINAL ACCELERATION DATA, FILTERED AT 1000 Hz

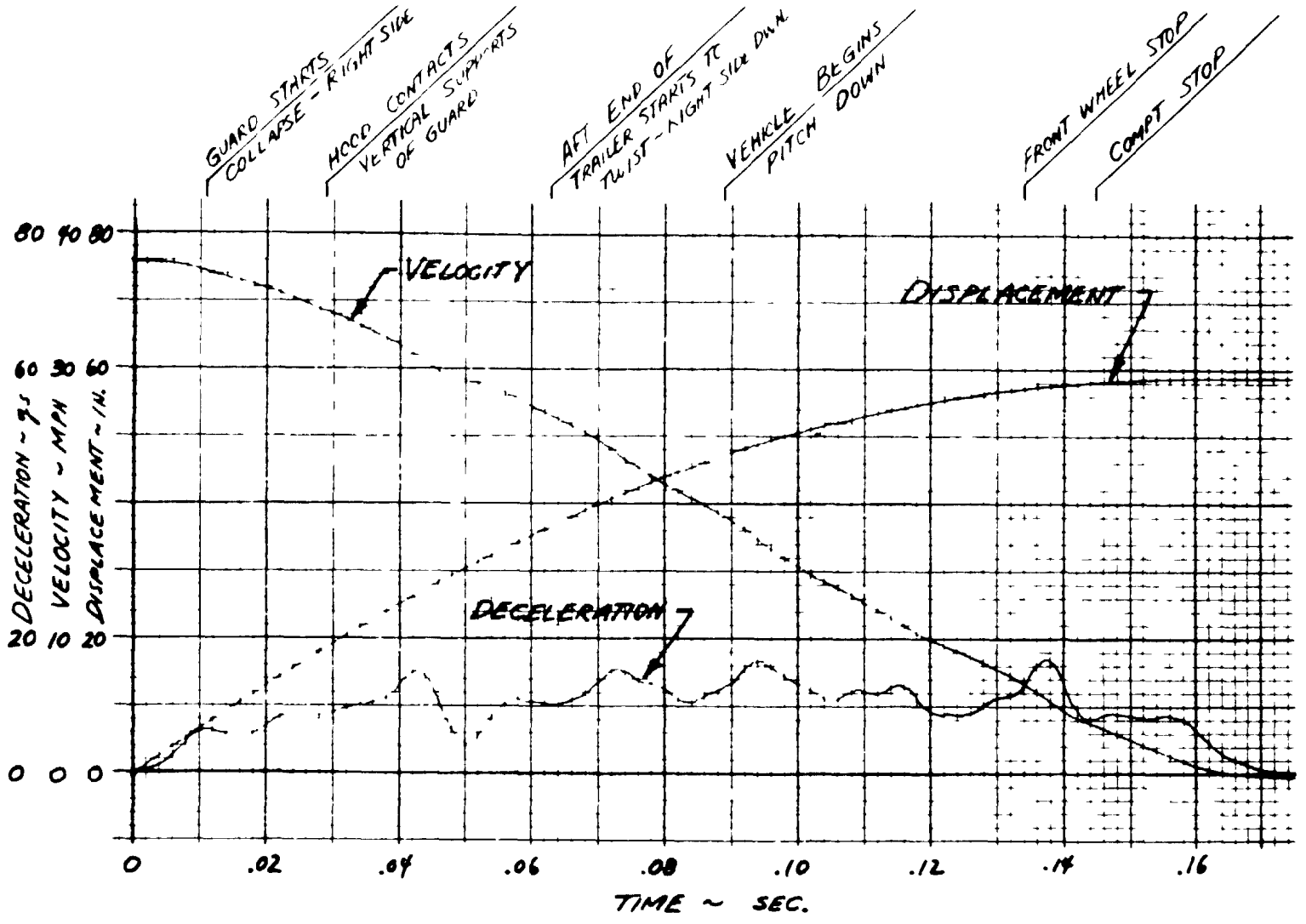

Figure 26 TEST NO. 9: COMPARTMENT LONGITUDINAL ACCELERATION DATA, FILTERED AT 50 Hz

Data from the other accelerometers aboard the vehicle are presented in Figures 27 and 28. The maximum engine longitudinal deceleration recorded was 28 g's occurring at .056 seconds.

Longitudinal loads, measured by two load cells at the forward end of the trailer, are presented in Figure 29.

Time histories of axial strains measured in each of the collapsible friction tubes are shown in Figure 30. Two strain gauges were mounted on each tube, on opposite sides, approximately 7 inches from the upper pin connections to the trailer. The strain gauge on the right side of each tube indicated tension strains because of bending moments produced by the assymmetrical loading of the underride guard.

The strain measurements from both friction tubes were converted to axial loads and are presented versus time in Figure 31. These data show maximum axial compressive loads of approximately 25,000 lbs. and 22,000 lbs. in the right and left side friction tubes, respectively. Both energy absorbers failed by buckling of the inside slotted tube before the vehicle was completely stopped. The films indicate that the absorber on the right side of the trailer, where the impact loads were mostly concentrated, failed first and is believed to account for the rapid decrease in the measured load shown in Figure 31 at approximately 0.100 seconds.

A time history of the total longitudinal impact force as measured by load cells at the forward end of the trailer (Figure 29 shows individual cell data) is presented in Figure 32. The maximum recorded load was approximately 70,000 lbs. occurring at .086 seconds after impact. The average force determined from these data over the .145 second stopping time interval was 44,000 lbs. Integration of the area under the force curve over the .145 second stopping time interval yields a measured impulse of 6,380 lbs-sec compared to the 6,550 lbs-sec change of linear momentum represented by the product of the vehicle mass and initial velocity.

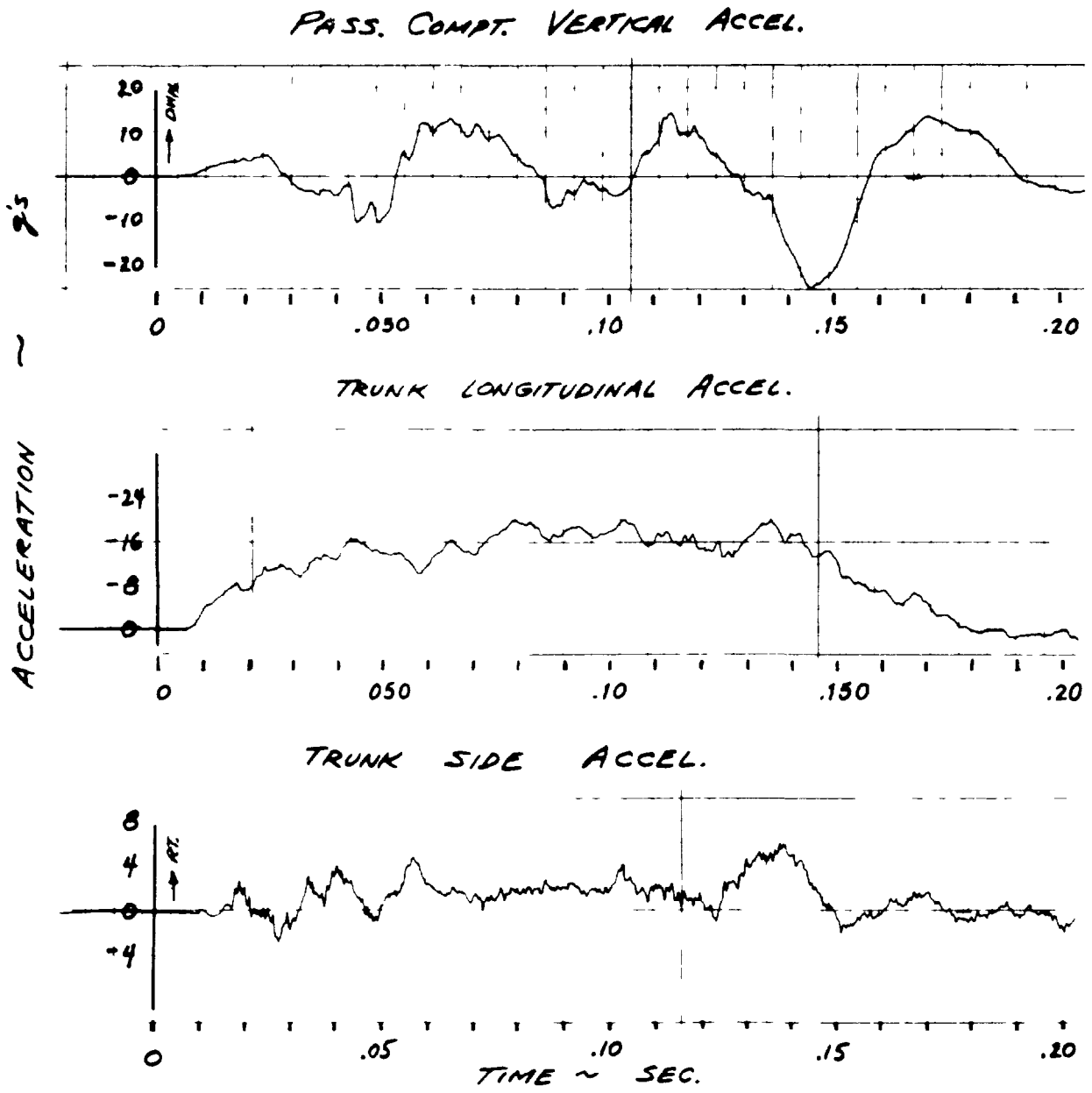

Figure 27 TEST NO. 9: COMPARTMENT AND TRUNK ACCELERATION DATA

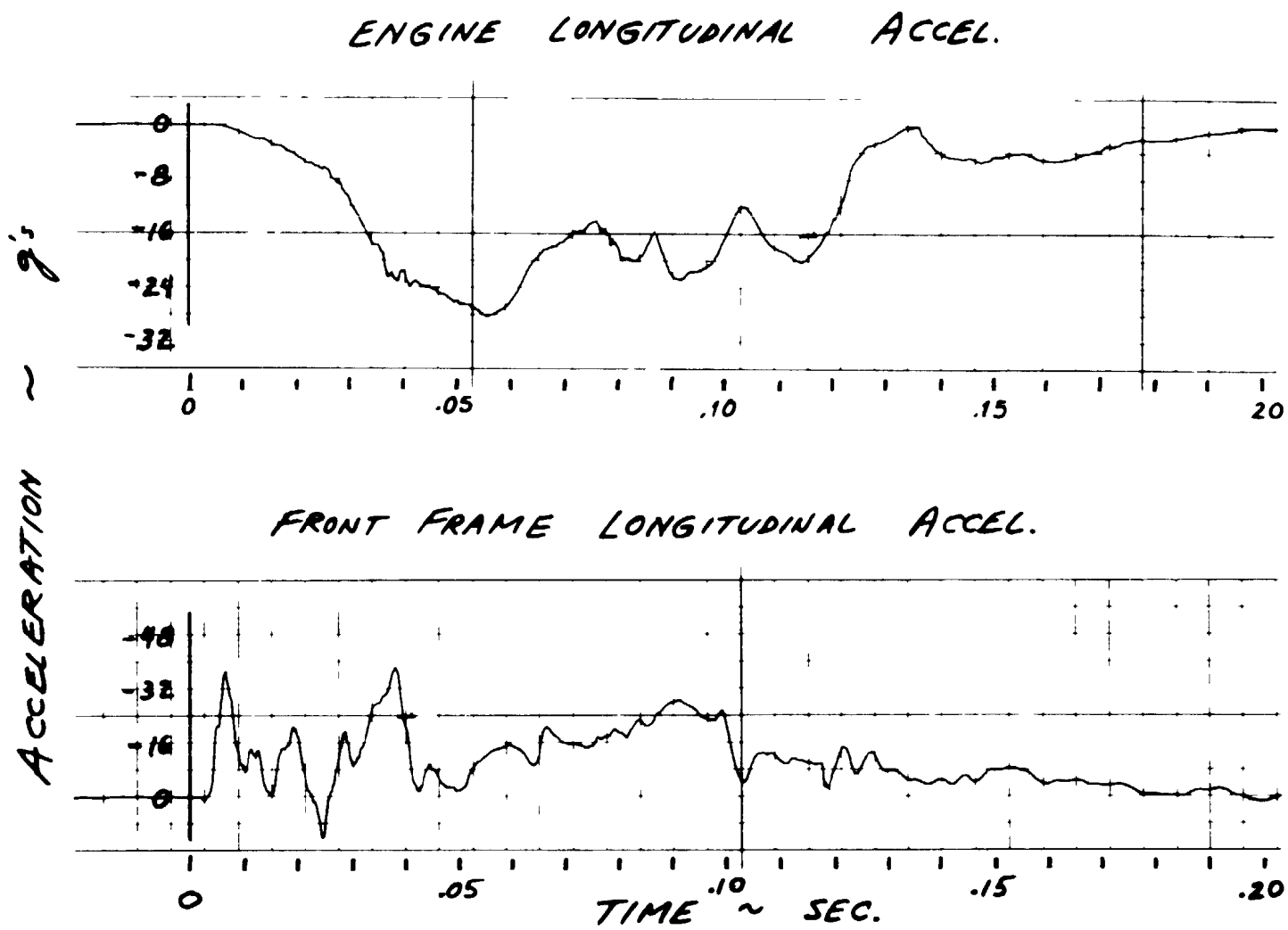

Figure 28 TEST NO. 9: ENGINE AND FRAME ACCELERATION DATA

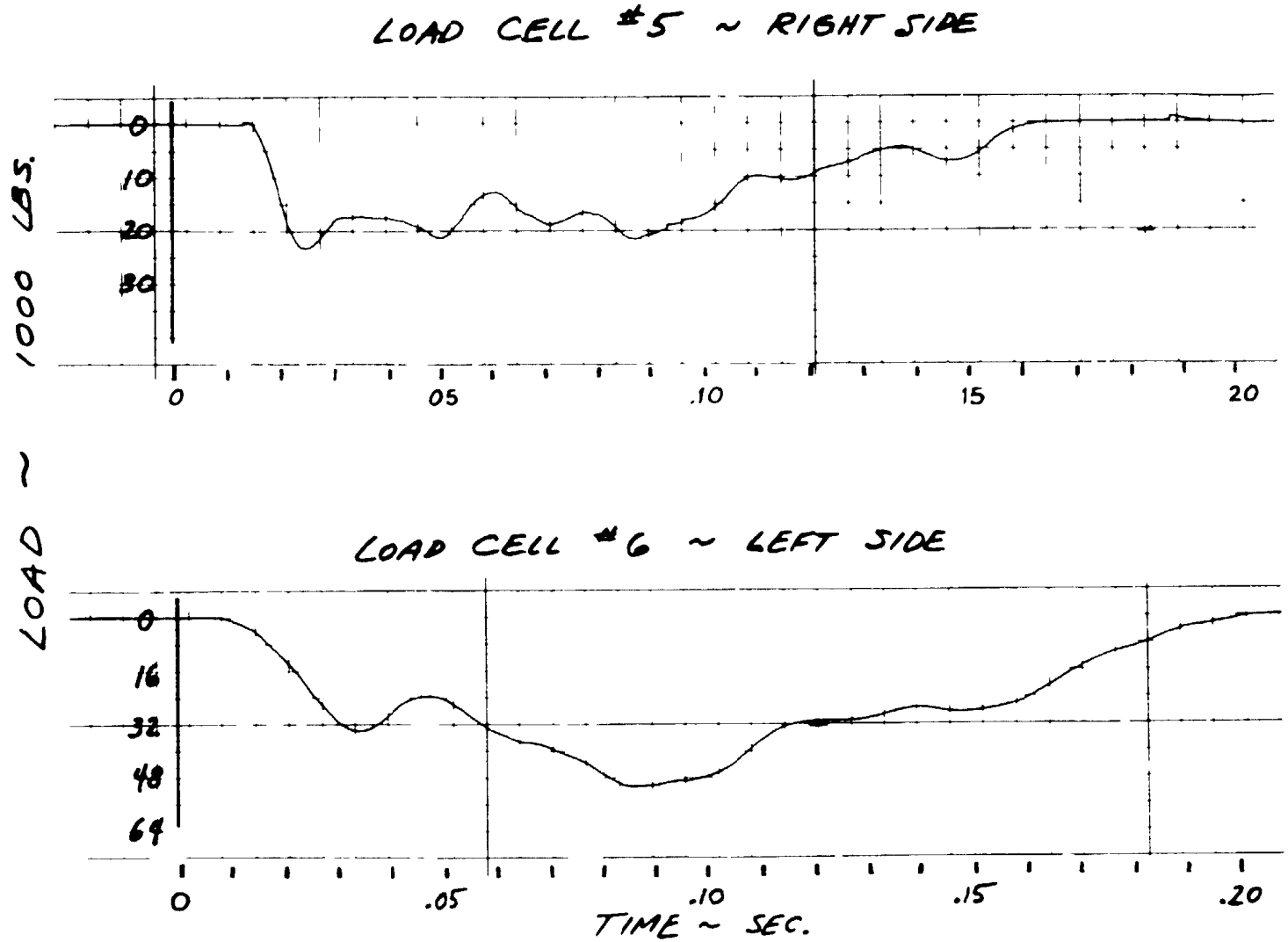

Figure 29 TEST NO. 9: LONGITUDINAL LOADS AT FRONT OF TRAILER

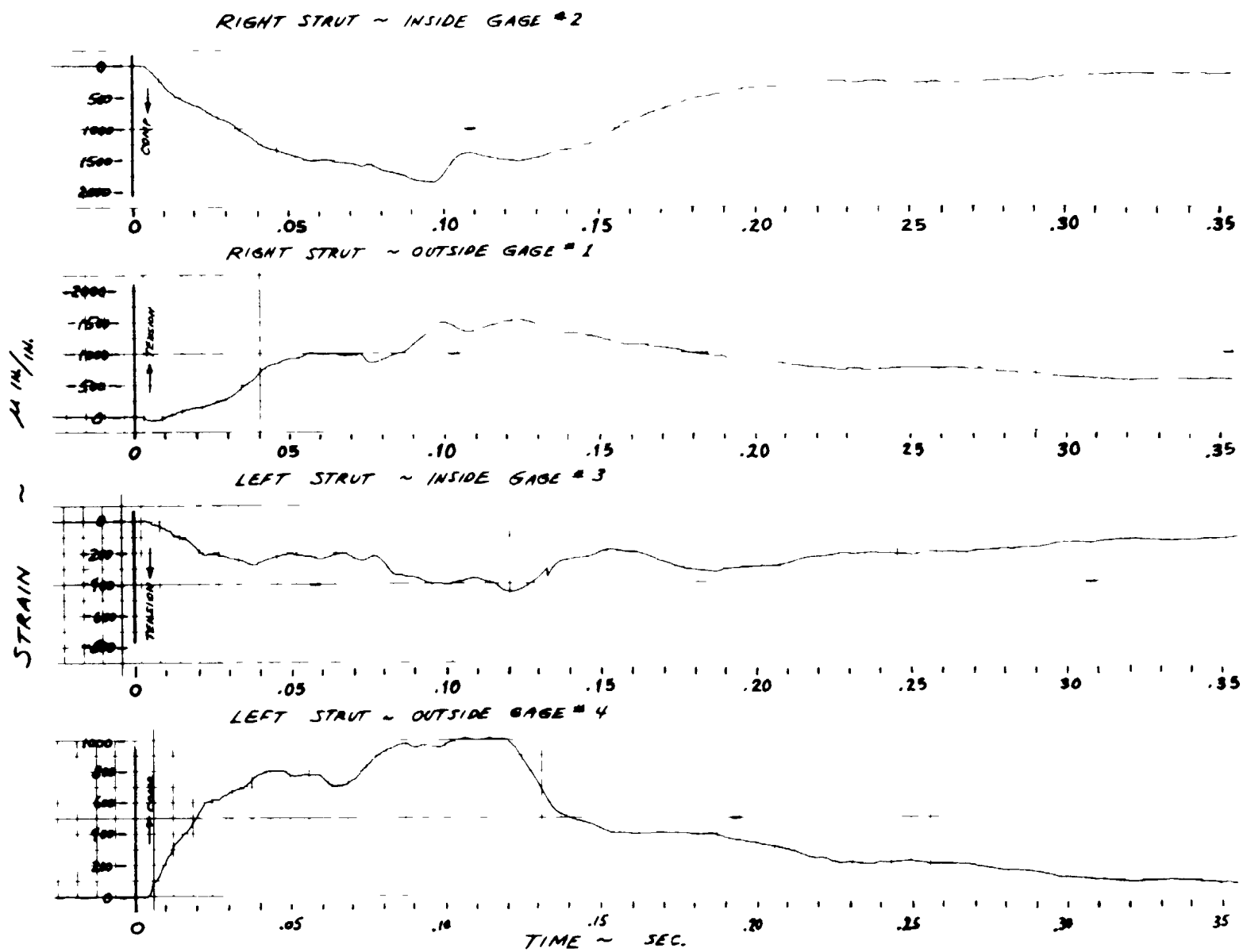

Figure 30 TEST NO. 9: FRICTION TUBE AXIAL STRAIN DATA

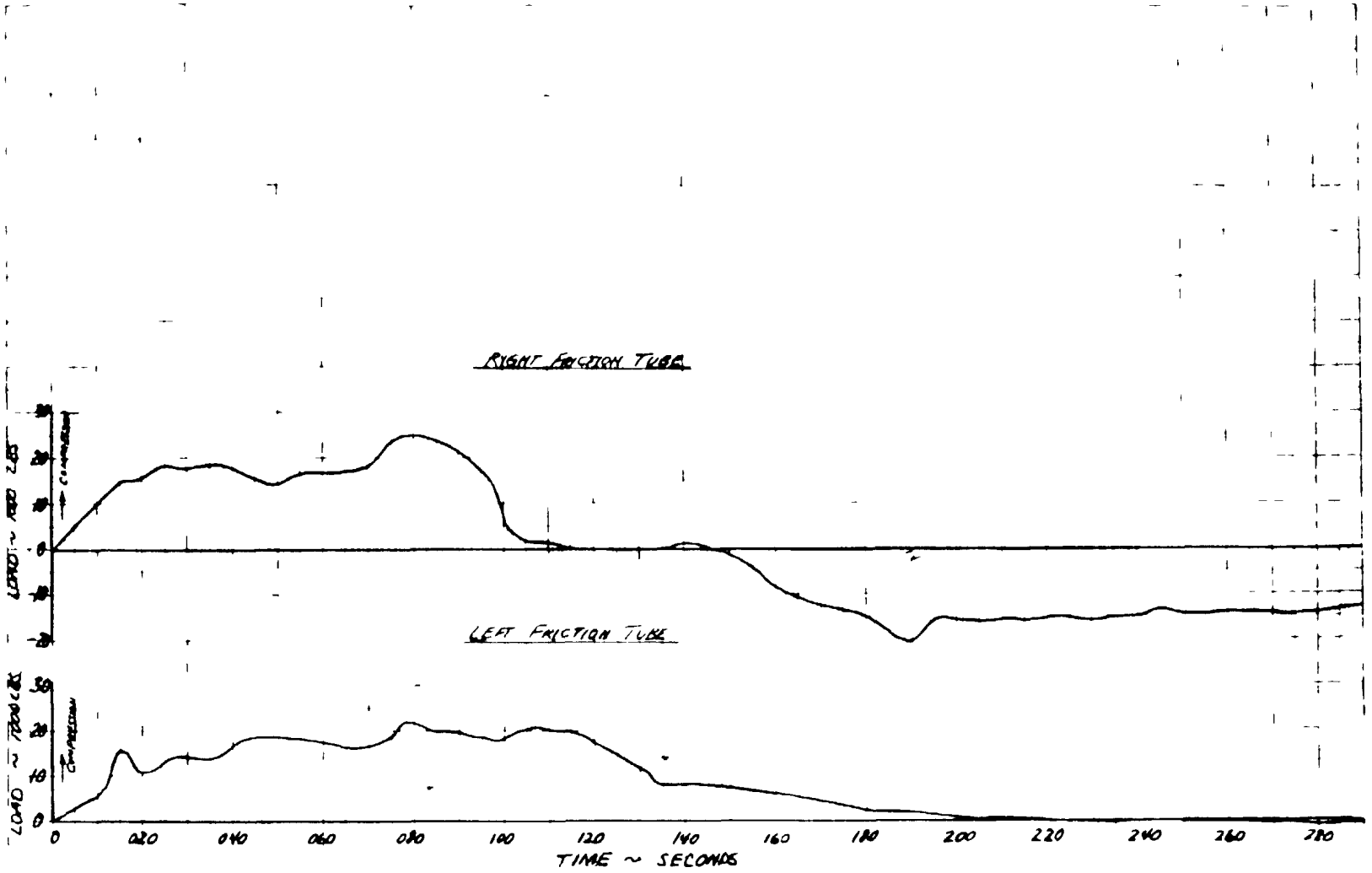

Figure 31 TEST NO. 9: FRICTION TUBE AXIAL LOADS

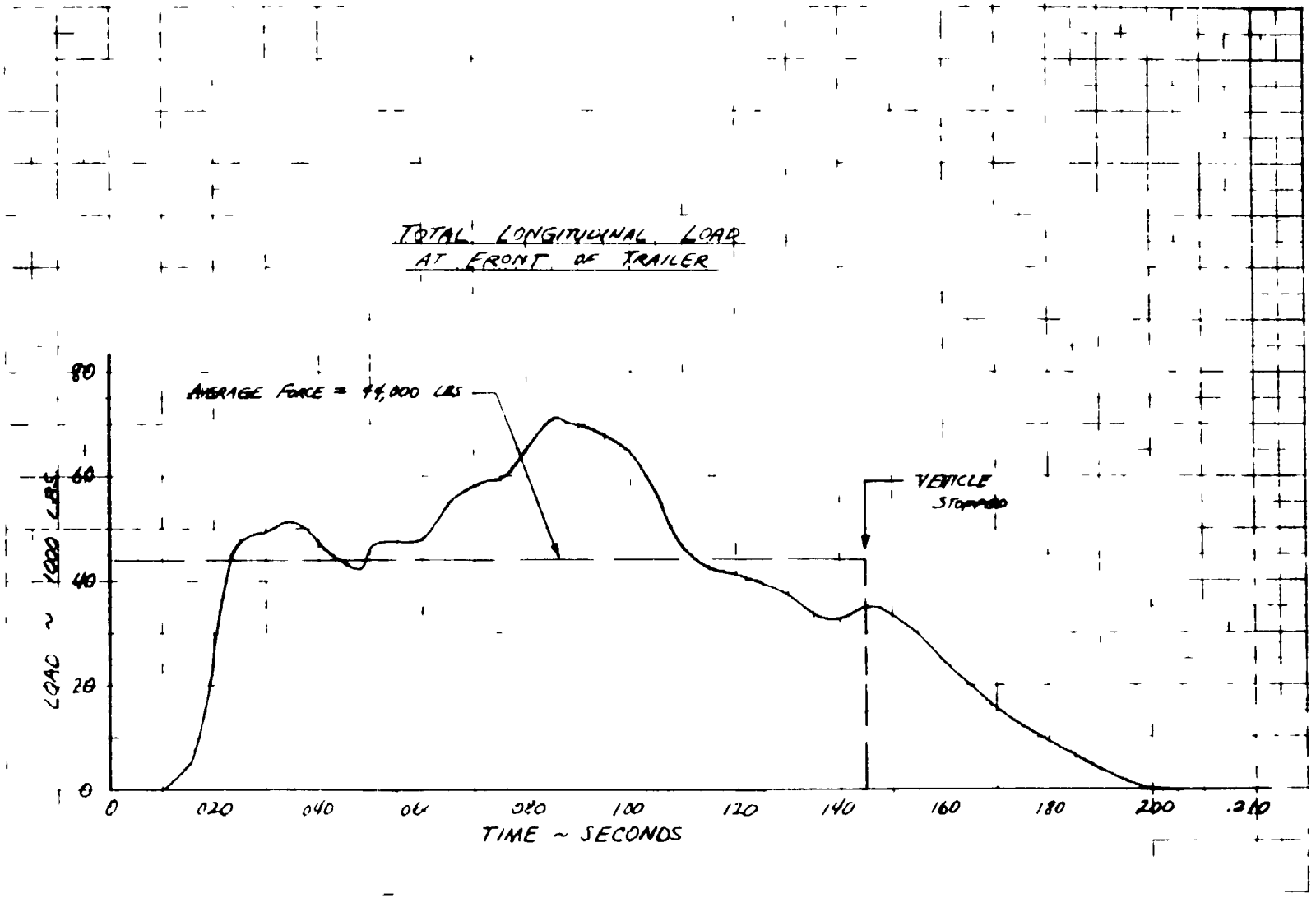

Figure 32 TEST NO. 9: VEHICLE IMPACT LOAD

Horizontal displacements of both the v hicle and underride guard during impact as determined from analysis of high speed movie film are shown in Figure 33. The two displacement curves of the underride guard are for points on the guard directly forward of the friction tube connections. The plot for the left tube was estimated based on the post-crash measurement of displacement since timing marks were not recorded by the camera located to view this component. The axial strokes of the telescoping tube energy absorbers were 8 and 16 inches for the left and right side, respectively.

Figure 34 presents a top view sketch of the test vehicle following impact for comparison with the outline of the undeformed vehicle. Front end crush measured approximately 19 inches at the center and approximately 27 inches at the left side. The pre-impact position of the underride guard relative to the car is also shown.

Photographs of the vehicles after the test are presented in Figure 35. Rearward intrusion of the fire wall and floorboard into the passenger compartment on the driver side was very slight, as may be seen from the photograph of the vehicle interior.

4.2.4 Crash Test No. 10

The response of a small compact automobile in a frontal collision with a rigid truck underride guard installed at a height 24 inches was determined in test No. 10. The objective of the test was to substantiate, or refute, the conclusion based on earlier tests that small cars would not be adequately protected against excessive underride in 40 MPH impacts for a 24 inch clearance height of the guard above the roadway.

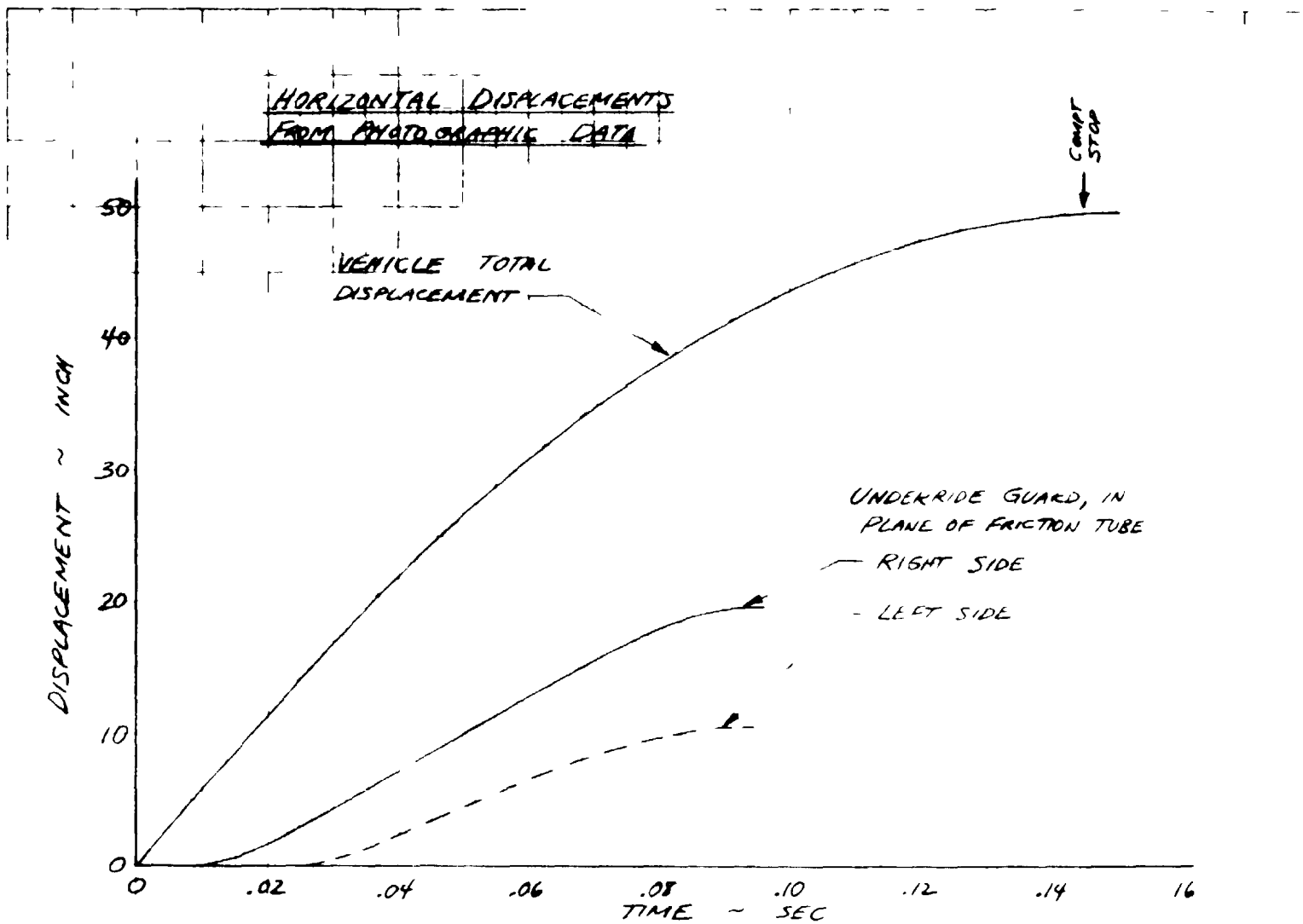

Figure 33 TEST NO. 9: VEHICLE AND UNDERRIDE GUARD DISPLACEMENTS

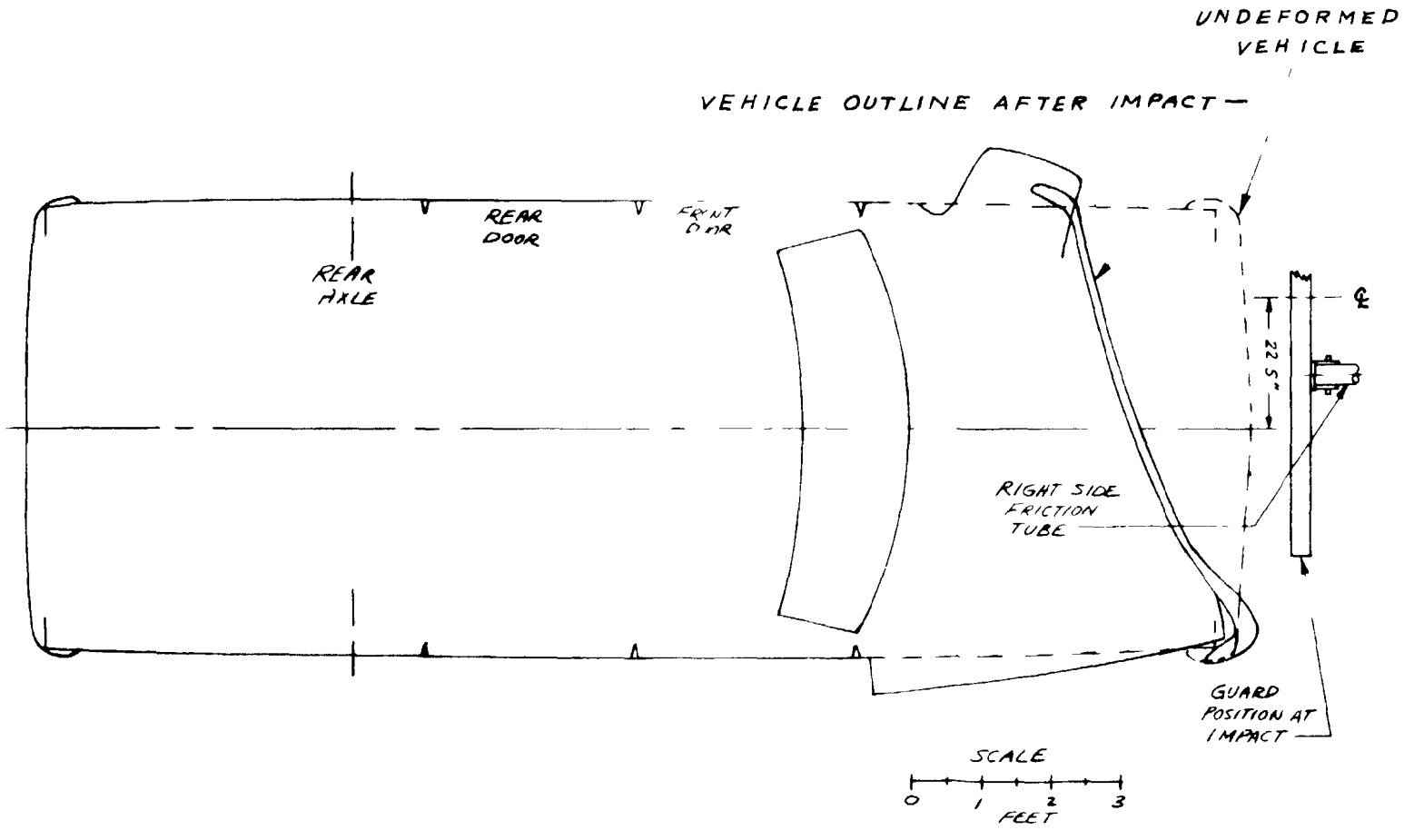

Figure 34 TEST No. 9: PLAN VIEW SKETCH OF DAMAGED VEHICLE OUTLINE

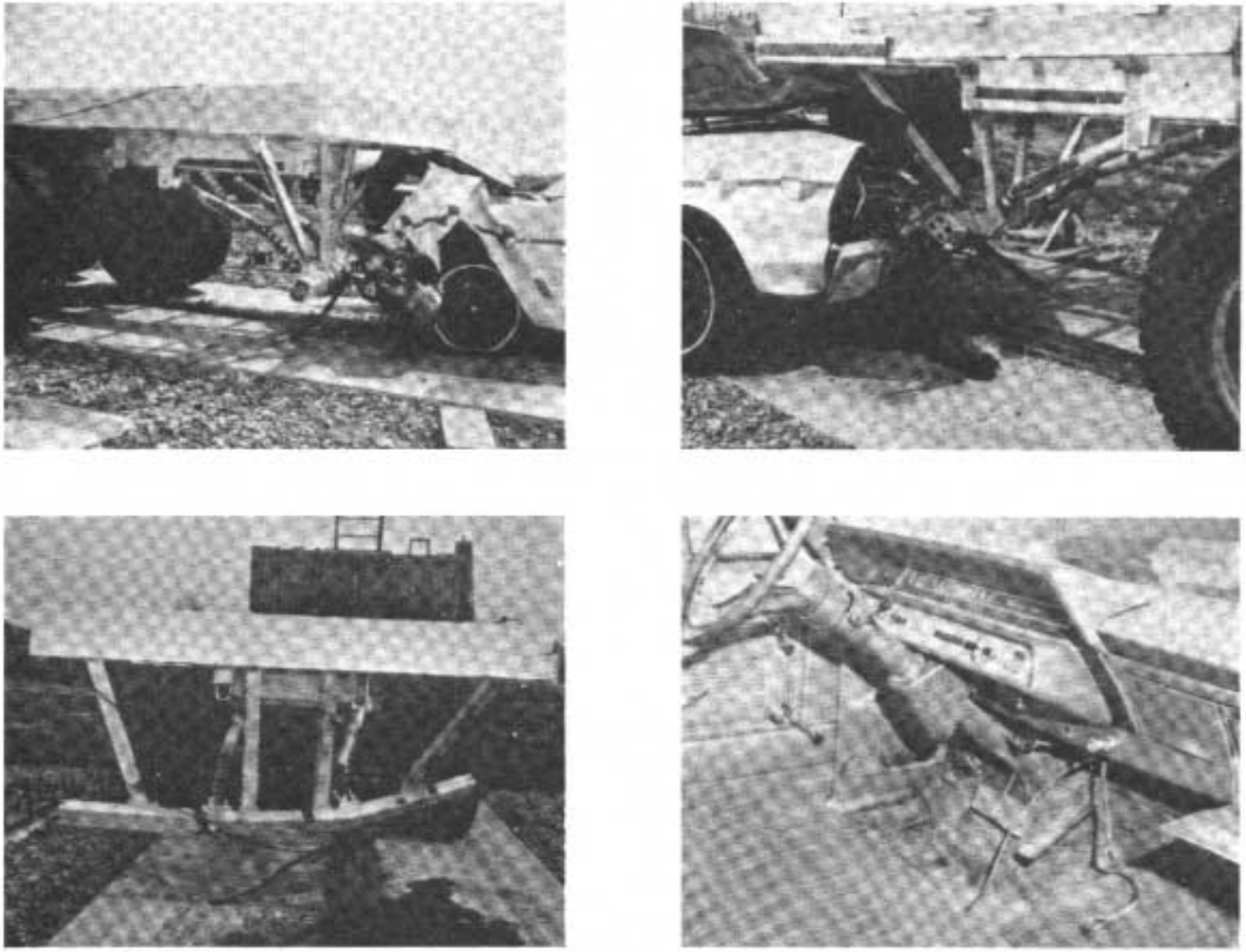

Figure 35 TEST No. 9: UNDERRIDE GUARD AND TEST VEHICLE AFTER IMPACT

The test vehicle was a 1966 Volkswagen 1300 two-door sedan weighing 1,680 lbs. that impacted the underride guard shown in Figure 4 at a speed of 42.1 MPH. The test vehicle was equipped with a spare tire and wheel in the forward baggage compartment, and the fuel tank was also approximately half full of liquid (Stoddard solvent) to provide realistic in-service conditions.

Data recorded from accelerometers located in the passenger compartment, on the compartment storage deck above the rear axle, and on the engine are presented in Figures 36, 37 and 38, respectively. The displayed records are filtered responses obtained by filtering of the raw data with an electronic filter having a corner frequency of approximately 50 Hz. In view of the catastrophic results of the test from the standpoint of passenger compartment intrusion, the passenger compartment longitudinal accelerations were not processed to provide velocity and displacement time histories. The measured peak passenger compartment longitudinal acceleration was approximately 28 g's which occurred 0.030 seconds after impact. Similar longitudinal accelerations were recorded at the rear deck location. The cause of the accelerations that may be noted in all accelerometer records beginning approximately 0.05 seconds prior to impact is unknown but may be associated with the release of the towing cable from the test vehicle since the cable clamp was activated by the release mechanism at approximately that same time. Another possibility is that the abort system might in some way have induced a preimpact braking transient to the test vehicle although no evidence of this was seen in the films of the test.

Another anomaly is evident in the displayed record for the engine which indicates an acceleration pulse of about 20 g's prior to the onset of deceleration. However, integration of the acceleration trace for the engine shows fair agreement with the measured impact velocity of the vehicle.

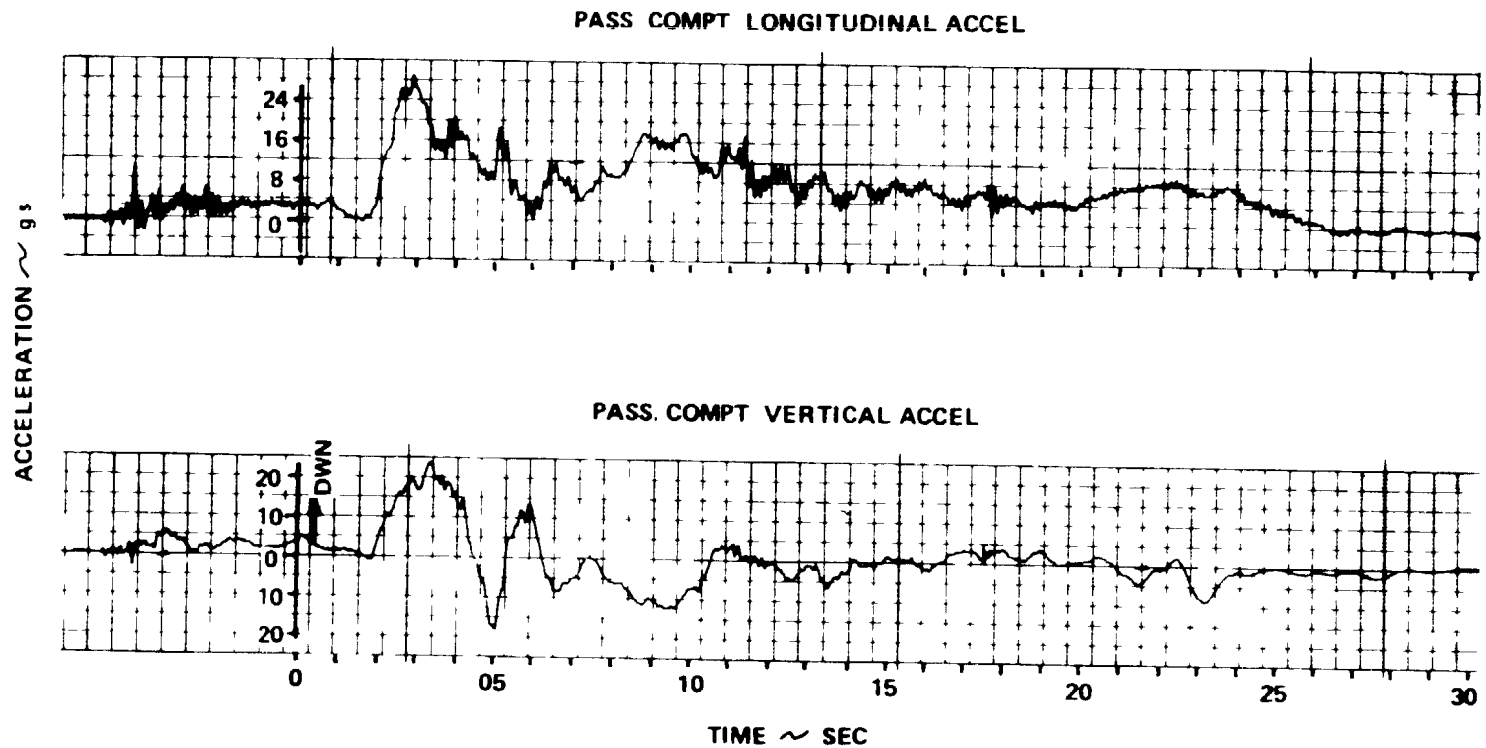

Figure 36 TEST NO 10: PASSENGER COMPARTMENT ACCELERATION DATA

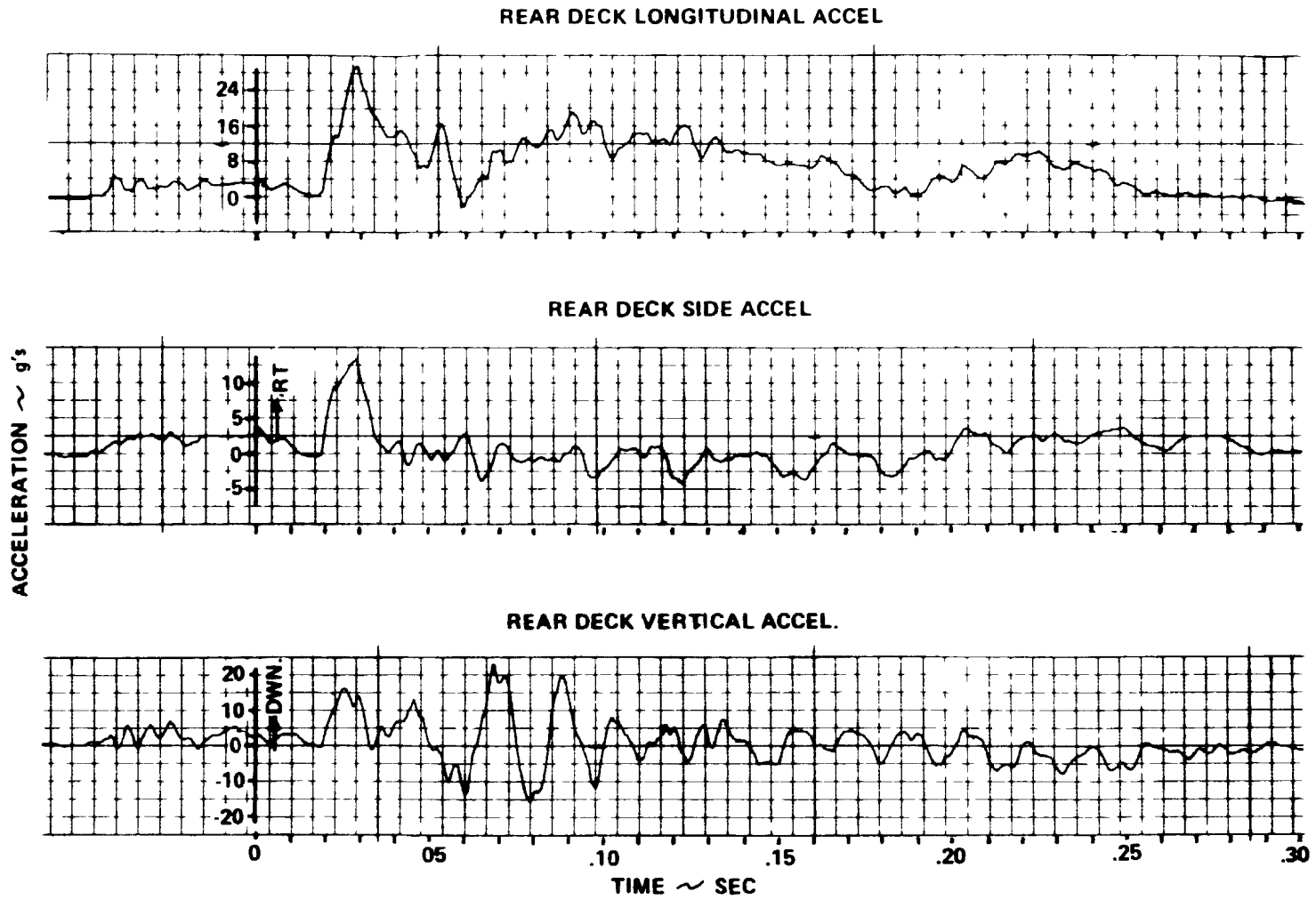

Figure 37 TEST NO. 10: COMPARTMENT REAR DECK ACCELERATION DATA

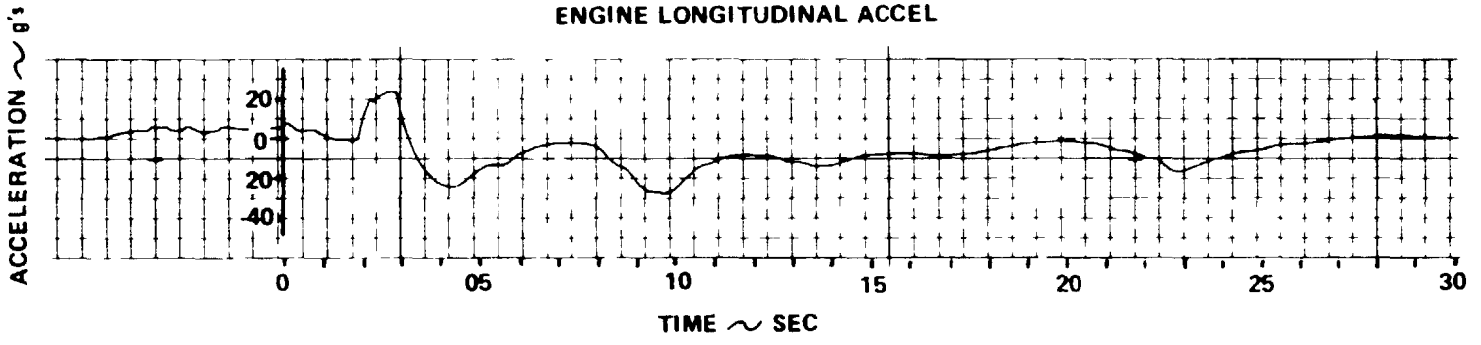

Figure 38 TEST NO. 10: ENGINE ACCELERATION DATA

The time history of total longitudinal impact force as measured by load cells at the front of the trailer is presented in Figure 39. The maximum recorded load was 55,000 lbs. occurring .043 seconds after impact. The average force over the 0.230 second stopping time interval as determined from this plot was 13,480 lbs. The 3,100 lb-sec measured impulse is in close agreement with the 3,220 lb-sec change of linear momentum obtained from the product of the vehicle mass and initial velocity.

Horizontal displacement of the vehicle during impact as determined from analysis of high speed movie film is displayed in Figure 40. The maximum displacement and the time to stop the vehicle was 79.5 inches and 0.230 seconds, respectively.

The data from Figures 39 and 40 were combined to produce the load-displacement plot displayed in Figure 41. It may be noted that the vehicle underrode the guard about 16 inches before loads started to develop when the hood and front baggage compartment contacted the underride guard. The second load peak between 50 and 60 inches of displacement is attributed to contact of the guard with the "A" pillar and front bulkhead structure. The energy represented by the area under the curve is 96,900 ft-lbs which compares favorably with the 99,800 ft-lbs initial kinetic energy of the vehicle at impact.

Photographs of the test vehicle and underride guard installation before and after the test are presented in Figure 42. As may be seen from the photographs, the bumper and front wheels passed beneath the underride guard and the guard penetrated deeply into the passenger compartment. The front tires of the test vehicle actually contacted the rear wheels of the truck as evidenced by scuff marks on the truck tire found during post-crash inspection and also as may be seen in the high speed films.

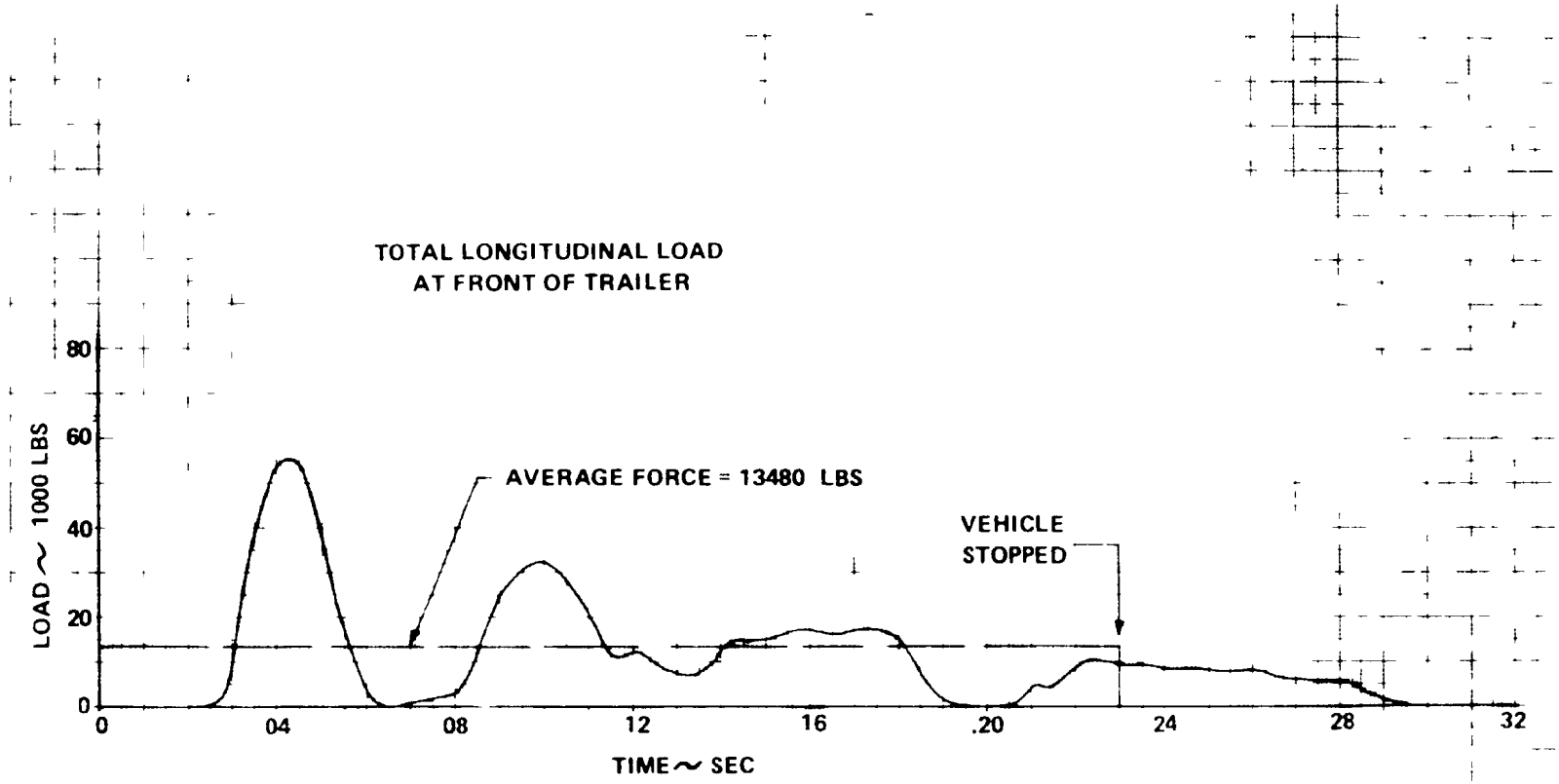

Figure 39 TEST NO. 10. VEHICLE IMPACT LOAD

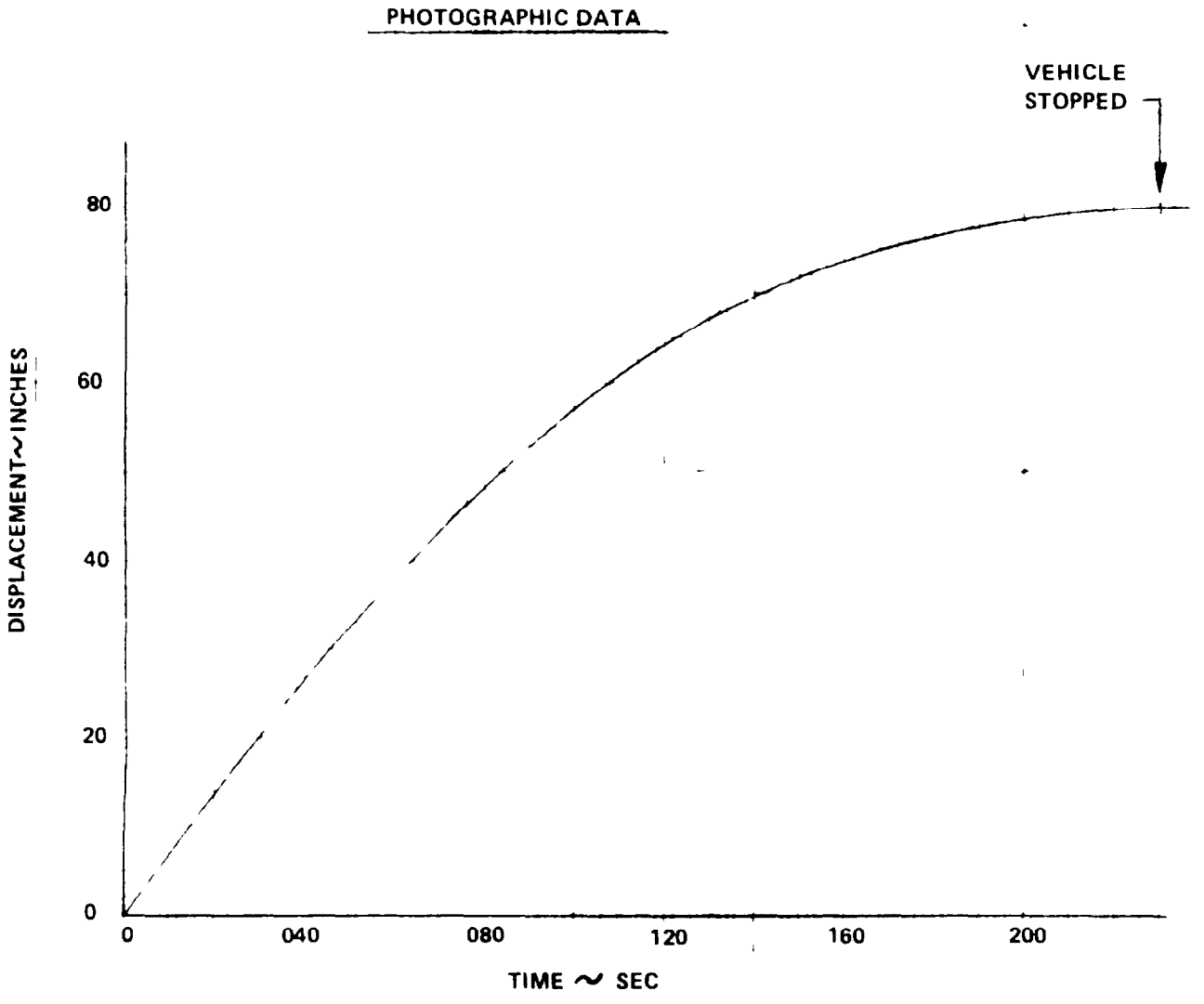

Figure 40 TEST NO. 10: VEHICLE DISPLACEMENT

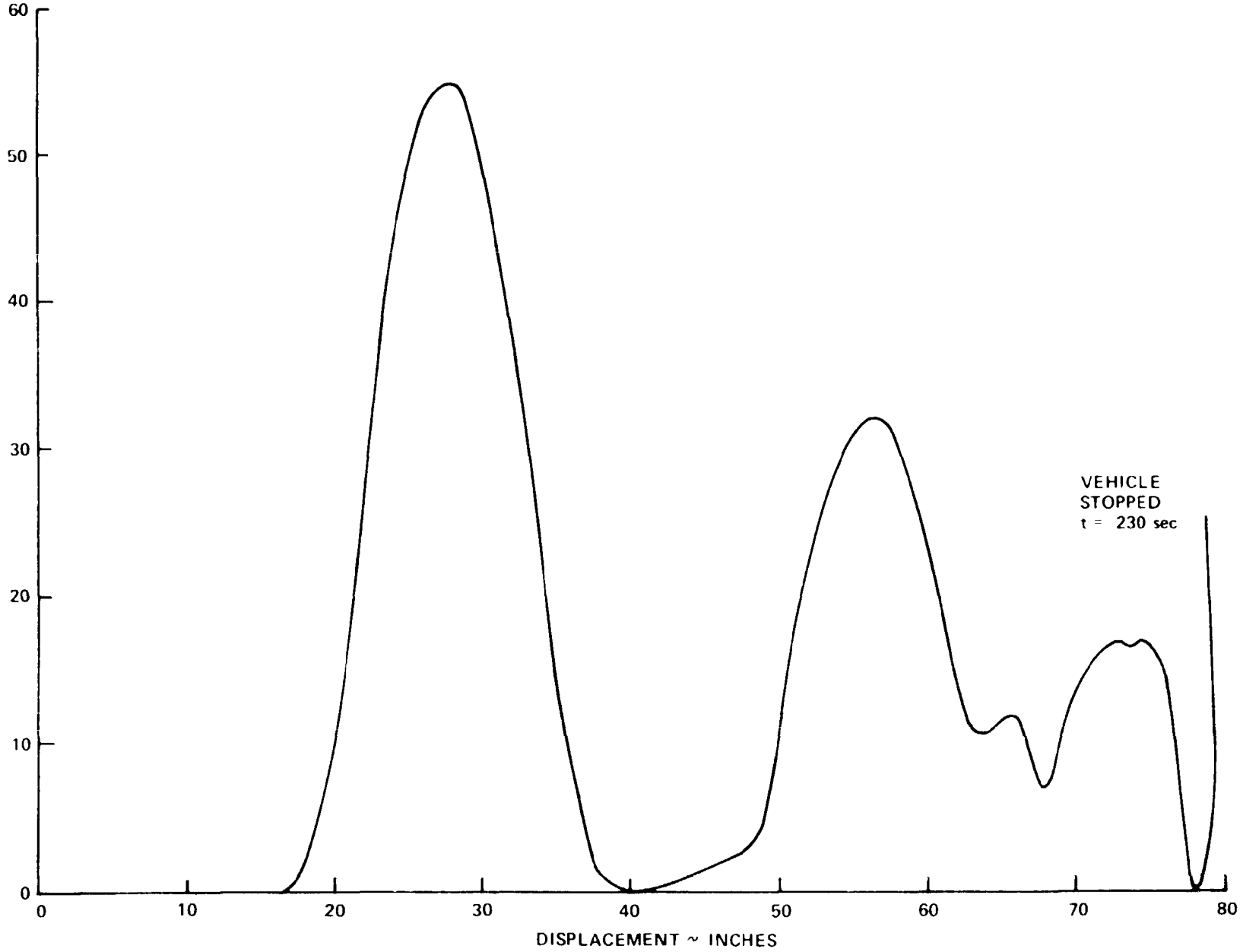

Figure 41 TEST NO 10 VEHICLE IMPACT LOAD VS DISPLACEMENT

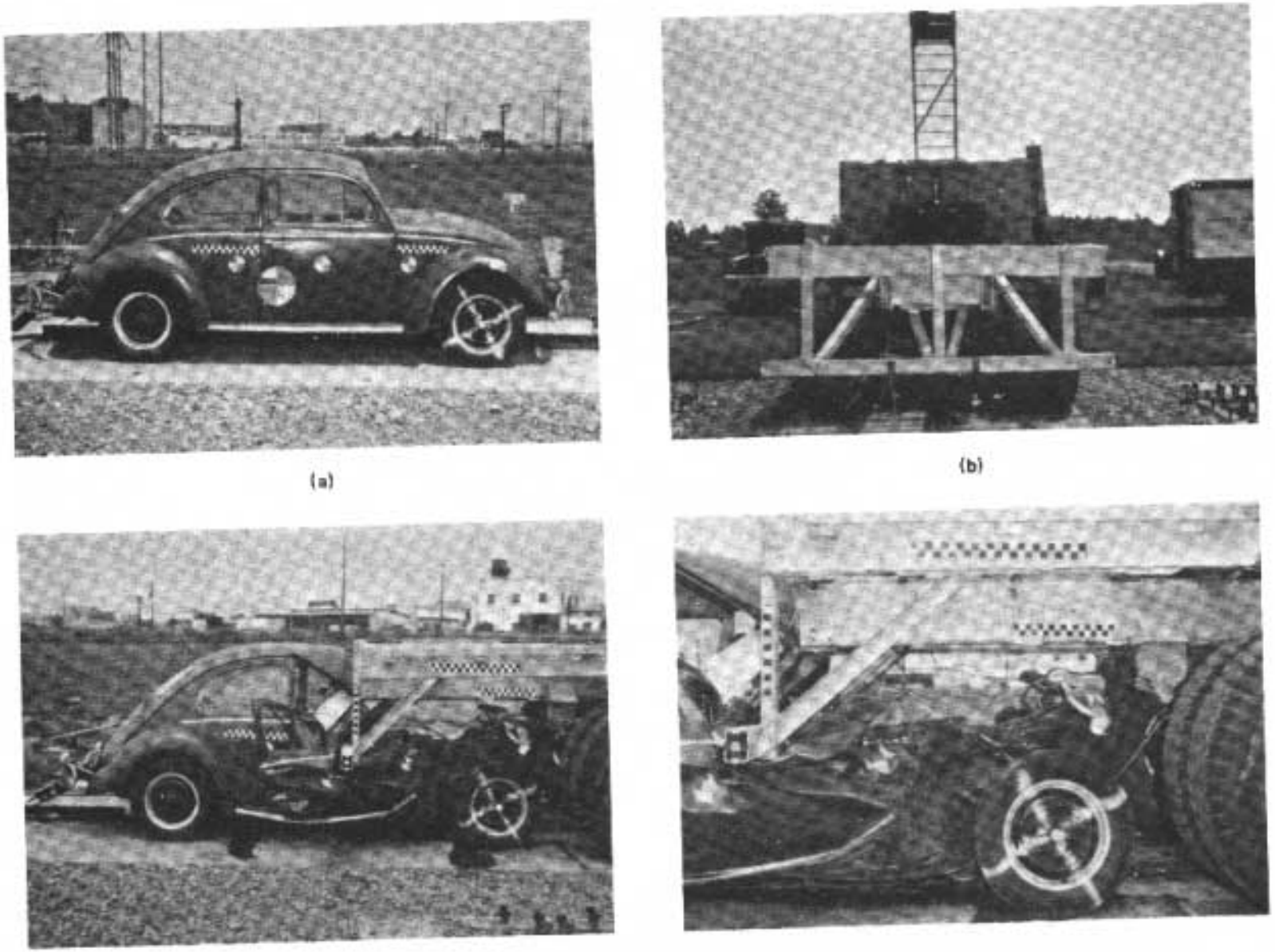

Figure 42 TEST NO. 10: PHOTOGRAPHS OF TEST VEHICLE AND UNDERRIDE GUARD

4.2.5 Crash Test No. 11

The objective of this test was to determine the performance of a 24 inch high rigid underride guard mounted at the rear of a van trailer (Figures 7 and 8). The test vehicle was a 1966 Ford four-door sedan weighing 3,460 lbs., which impacted the guard at a speed of 43.1 MPH. The trailer was a 40 ft. Copco tandem axle aluminum van weighing approximately 11,690 lbs.

Data recorded from accelerometers located in the passenger compartment on the drive shaft tunnel behind the front seat are presented in Figures 43 and 44. The data in Figure 43 are the results of filtering the raw signals with an electronic filter having a corner frequency of approximately 1000 Hz. Integration of the acceleration data produced the velocity and displacement curves.

Figure 44 is similar to Figure 43 except that the accelerometer data are filtered with a digital filter having a corner frequency of 50 Hz. The measured peak longitudinal deceleration (50 Hz filter) was approximately 44 g's which occurred .047 seconds after impac . The occurrence of several events as noted from the high speed films of the impact is indicated at the top of the figure.

Integration of the passenger compartment longitudinal deceleration yields results for velocity and displacement that do not correlate well with data obtained from the films. The accelerometer data indicates the vehicle stopped in .104 seconds while displacing a maximum of 47.5 inches compared with a stopping time of .184 seconds and a total displacement of 53.5 inches as determined from the films. It is believed tha the measured decelerations shown in Figures 43 and 44 are somewhat in error (too high) since a reduction in overall level would yield values for the time to stop and for the maximum dynamic displacement that are both more in keeping with the photographically observed results. However, the final

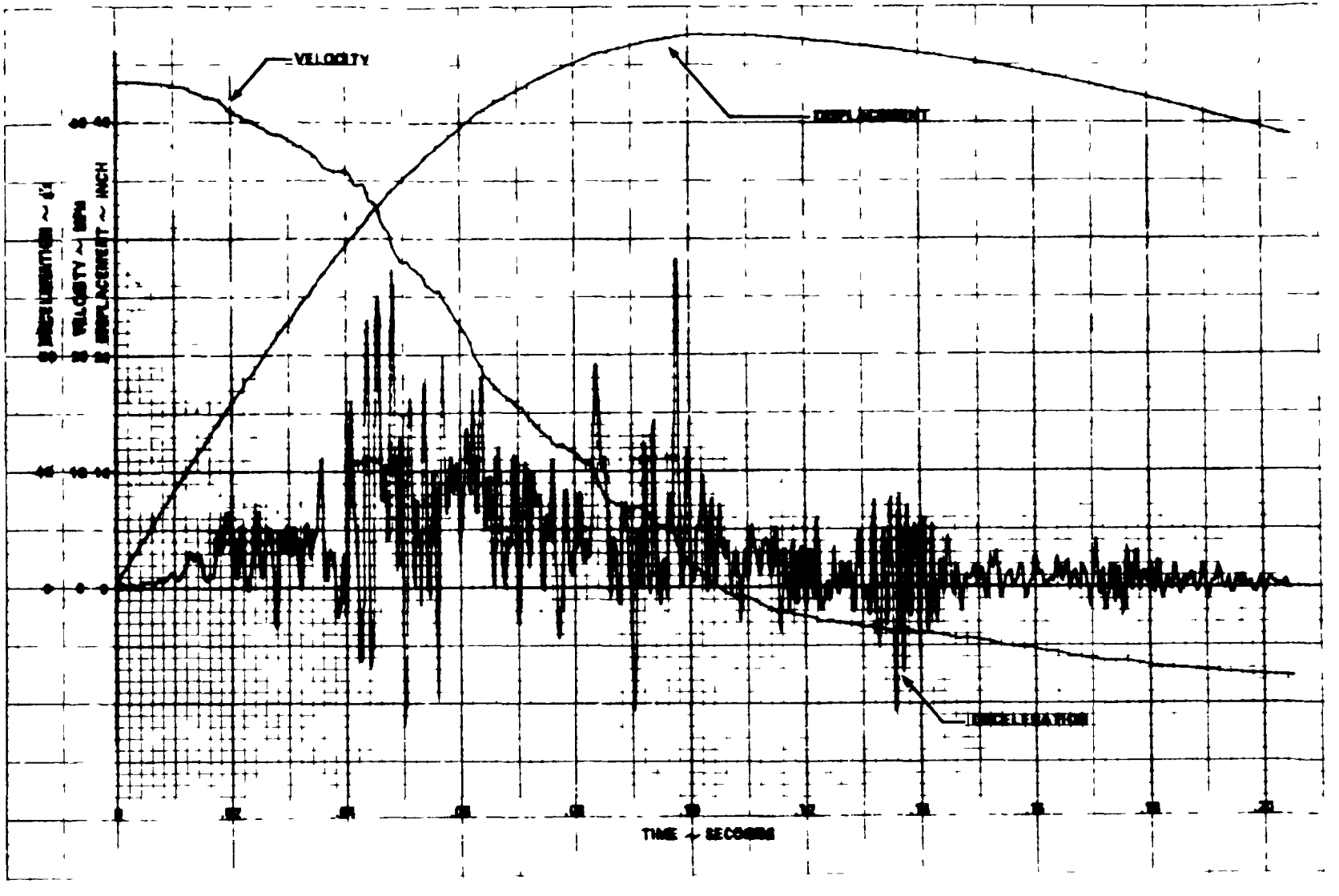

Figure 43 TEST NO. 11: COMPARTMENT LONGITUDINAL ACCELERATION DATA, FILTERED AT 1000 Hz

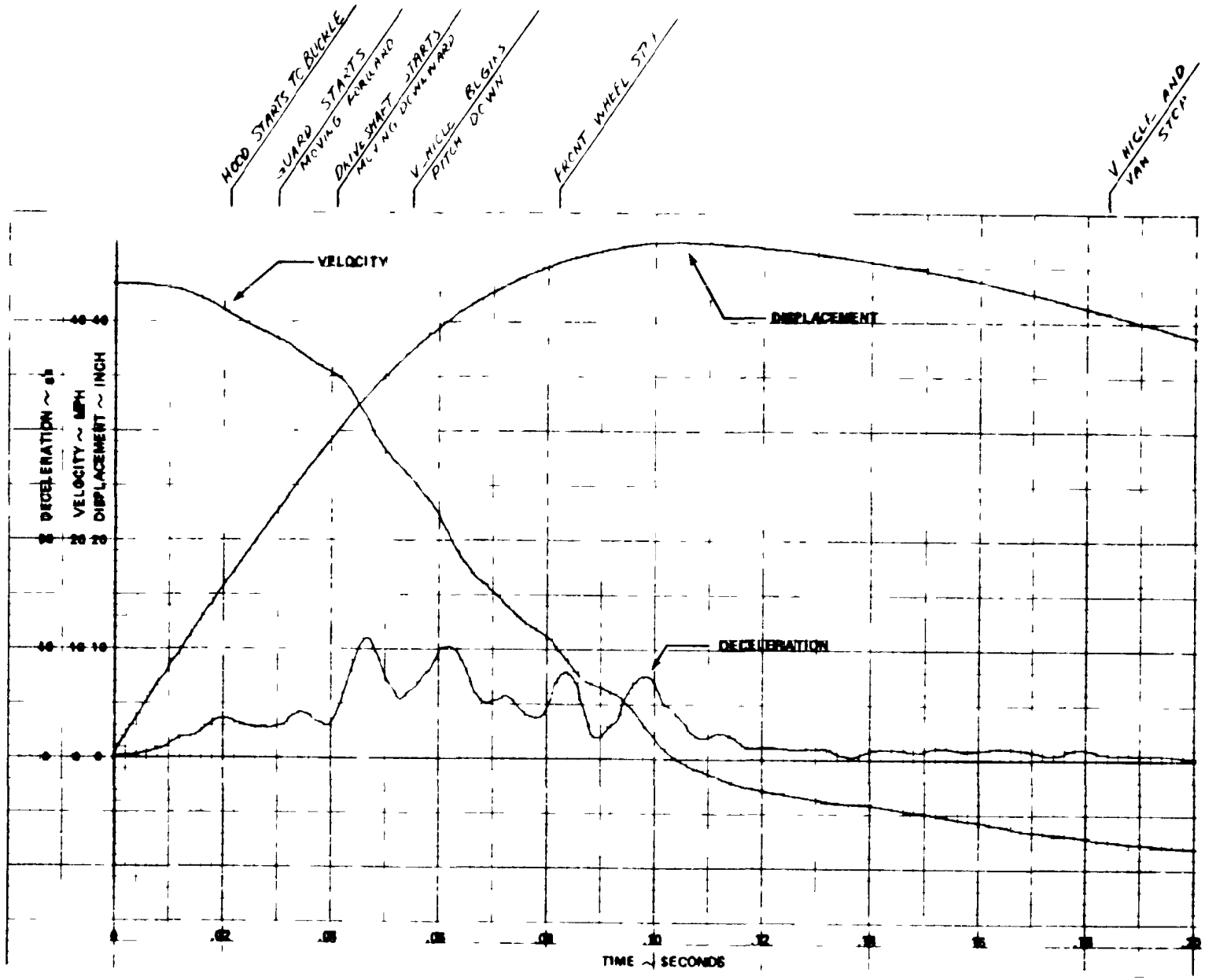

Figure 44 TEST NO. 11: COMPARTMENT LONGITUDINAL ACCELERATION DATA, FILTERED AT 50 Hz

six inches of displac ment occurred aft r maximum crush of the automobile (approximately .110 seconds fter impact) and r sulted from collapse of the trailer structure in the vicinity of the landing gear.

Other accelerometer data measured in the passenger compartment, on the flat deck over the rear axle, and on the engine ar displayed in Figures 45, 46 and 47. Peak engine longitudinal deceleration of about 113 G's occurred .031 seconds after impact. It may be noted that the longitudinal accelerations measured at the rear deck location are generally at a lower level than those recorded on the drive line tunnel in the passenger compartment.

The time history of longitudinal impact force as measured by load cells at the front of the van is presented in Figure 48. The maximum load recorded was 61,500 lbs. occurring at .040 seconds after impact and resulted primarily from engine contact with the underride guard. The measured impulse, represented by the area under the curve, is only 4,600 lbs-sec compared to the change in linear momentum of the automobile of 6,800 lbs-sec. As a result, the measured average force of 24,950 lbs. is lower than the computed value of 37,000 lbs. based on a stopping time of .184 seconds.

The low levels of force and impulse measured at the front of the van undoubtedly result from the nonrigid behavior of the trailer and the loads shown in Figure 48 do not represent the actual longitudinal forces applied to the impacting automobile. Because a major part of the mass of the trailer was accelerated as the van collapsed, large inertia forces were developed which were applied to the car but are not totally reflected in the measured load cell data.

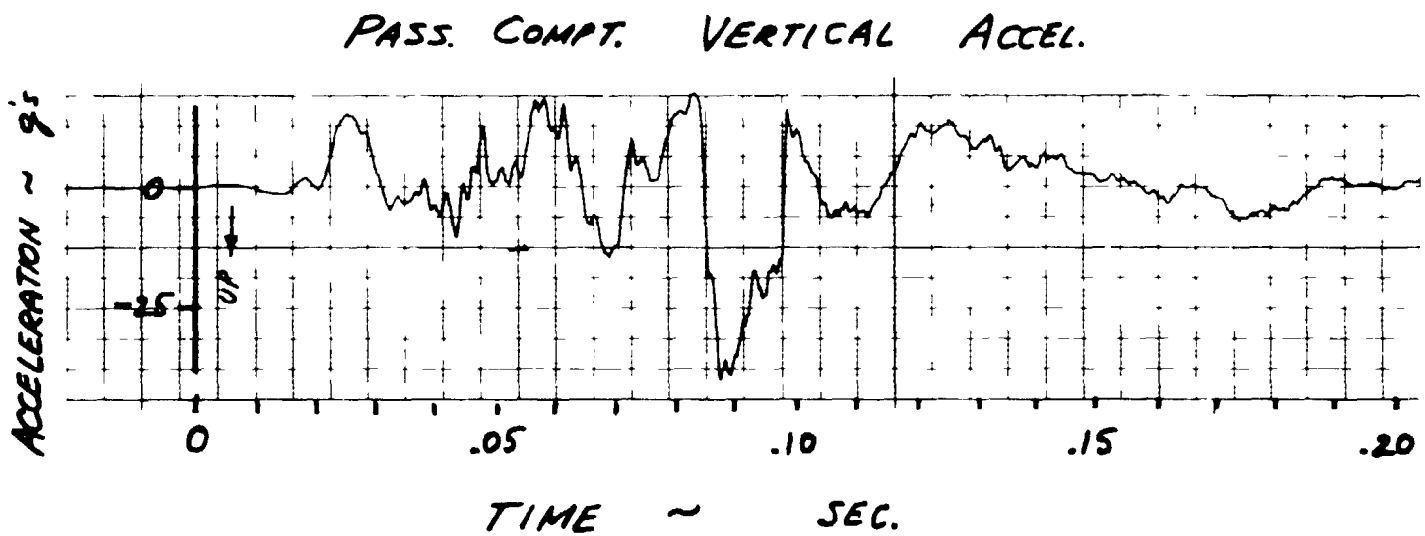

Figure 45 TEST NO. 11: PASSENGER COMPARTMENT VERTICAL ACCELERATION

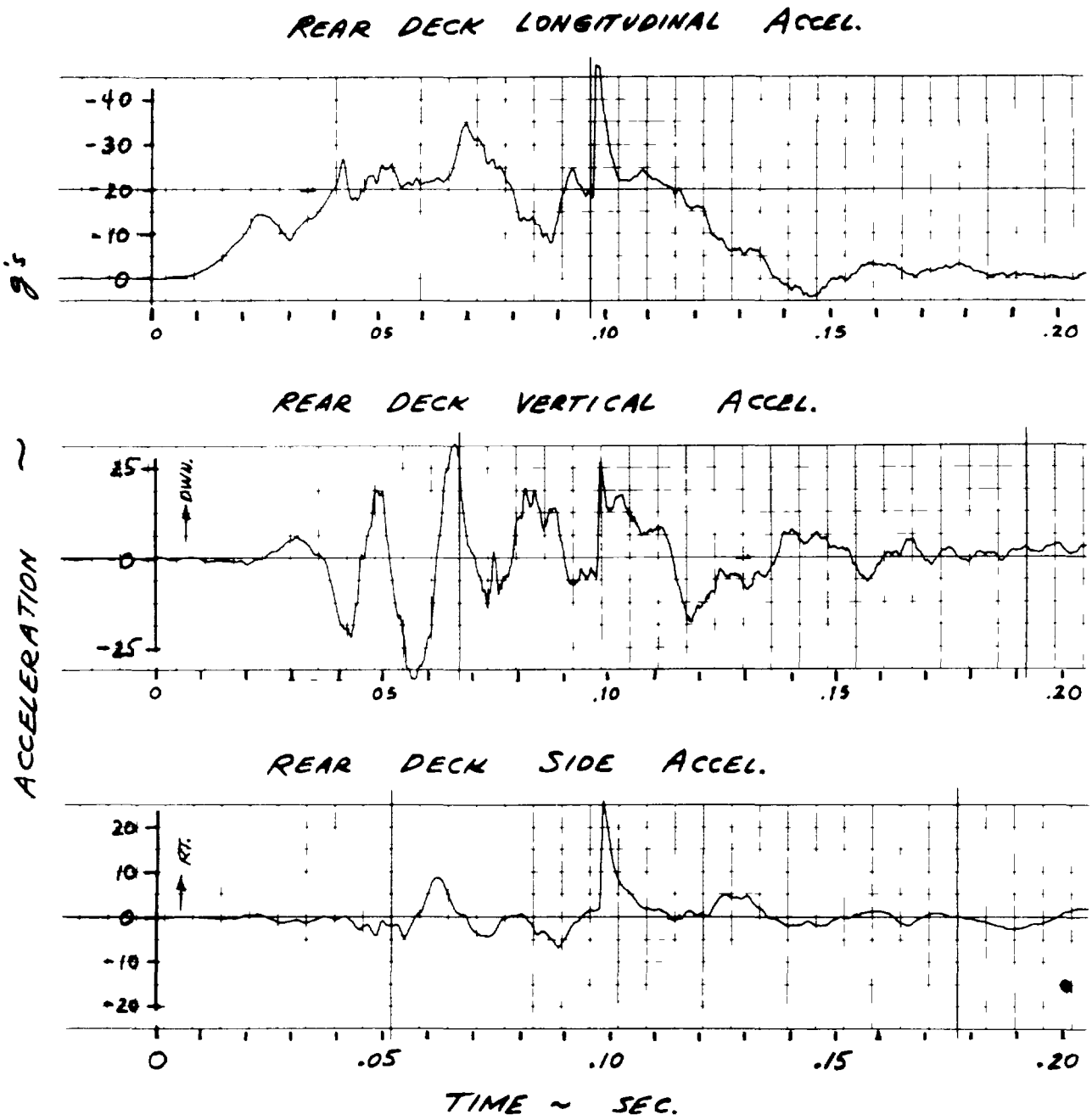

Figure 46 TEST NO 11 COMPARTMENT REAR DECK ACCELERATION DATA

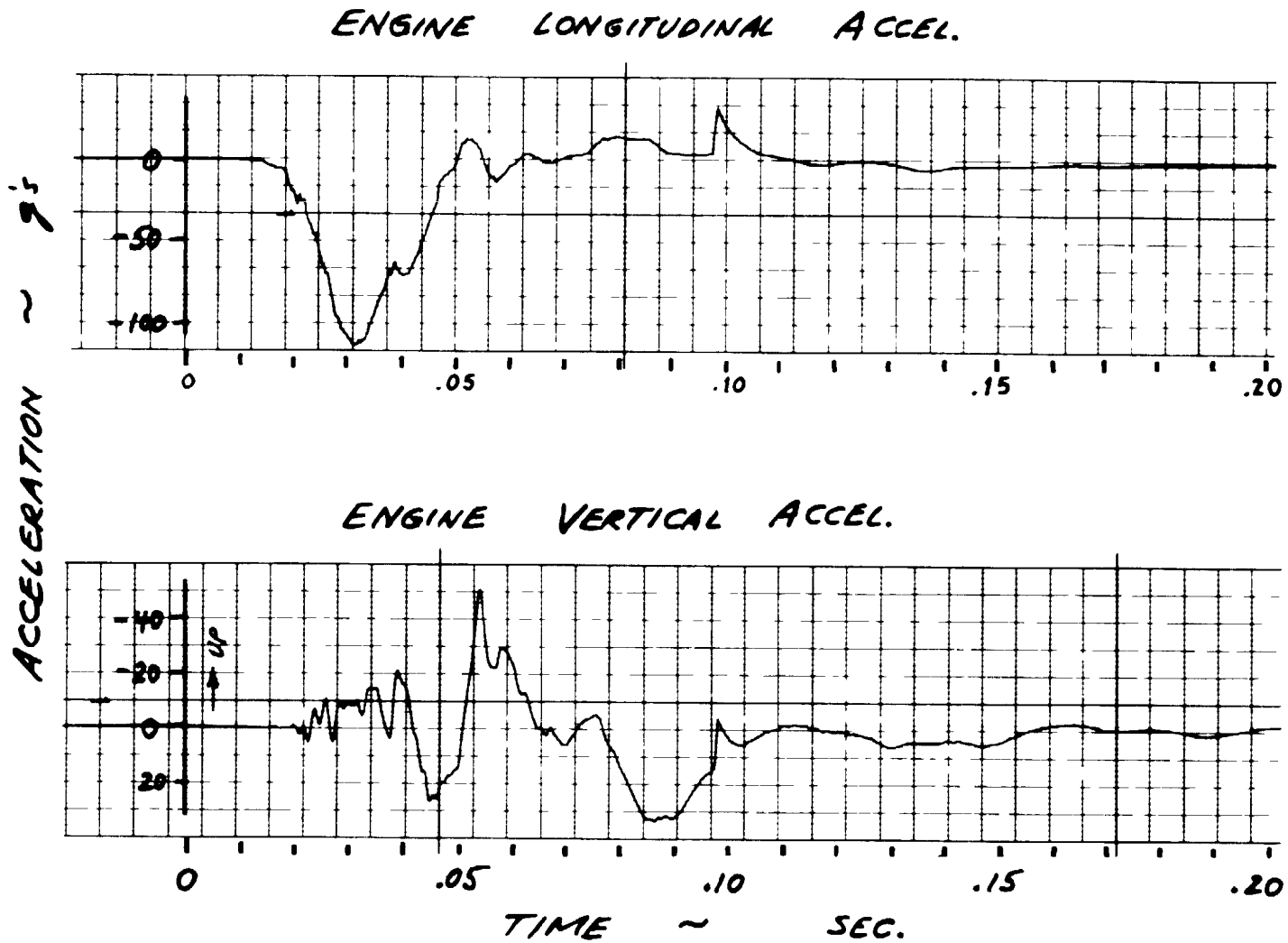

Figure 47 TEST NO 11· ENGINE ACCELERATION DATA

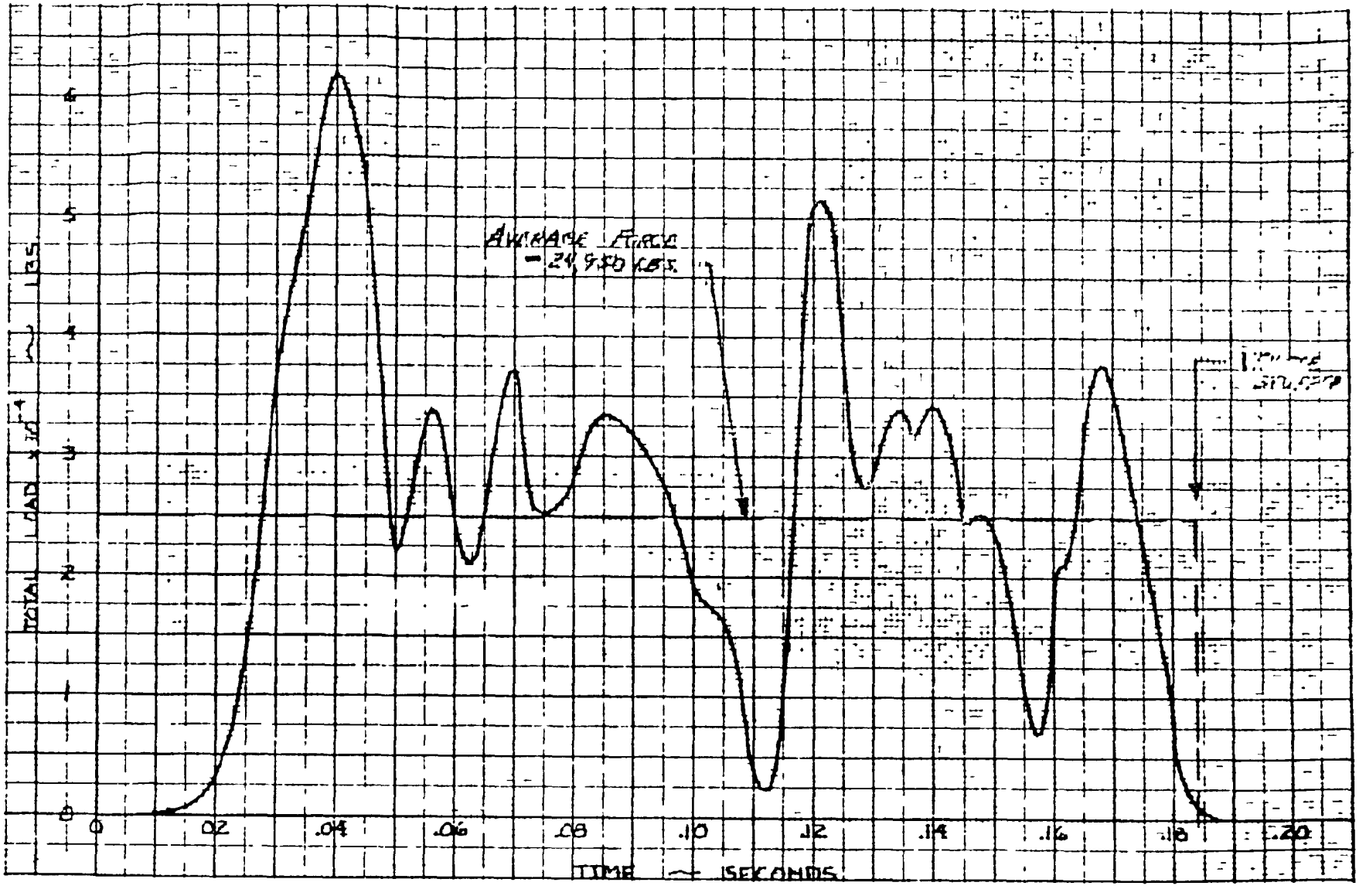

Figure 48 TEST NO. 11: LONGITUDINAL LOAD AT FRONT OF VAN

The high speed movies of the test show that, in addition to translating, the van pitched so that the landing wheels raised off the ground at least 4 inches. Inasmuch as the front end of the van was restrained by cables to prevent vertical motion, large cable forces probably were developed which caused the van to buckle in an inverted vee-shape. Hence, unknown external forces were applied to the system which could account for not having measured all of the change in linear momentum of the car. Post-crash inspection also revealed that the front of the trailer was no longer in contact with the load cells. However, as may be noted from Figure 48, separation of the van from the load cells probably did not occur until after the test automobile was already stopped.

Horizontal displacements of the vehicle and of the underride guard due to van collapse as determined from analysis of high speed movie film are displayed in Figure 49. The guard displacement was subtracted from the measured total displacement of the automobile to obtain the vehicle crush curve. Maximum dynamic displacement of the automobile was approximately 43 inches as compared with 38 inches obtained from a post-crash static measurement of the vehicle crush. It may be noted that the automobile crushed to the maximum value of 43 inches in about .110 seconds. After that time, the car and rear of the van, traveling together at a low velocity, moved a short distance before stopping completely at .184 seconds after impact.

The rigid underride guard and aft portion of the trailer moved forward about 12 inches due to deformation of the van structure. Approximately 9 inches of collapse of the trailer lower side panels was measured after the test. The front of the trailer also was displaced forward slightly as the buckling action caused the member bearing on the load cells to slide downward and under the load cells.

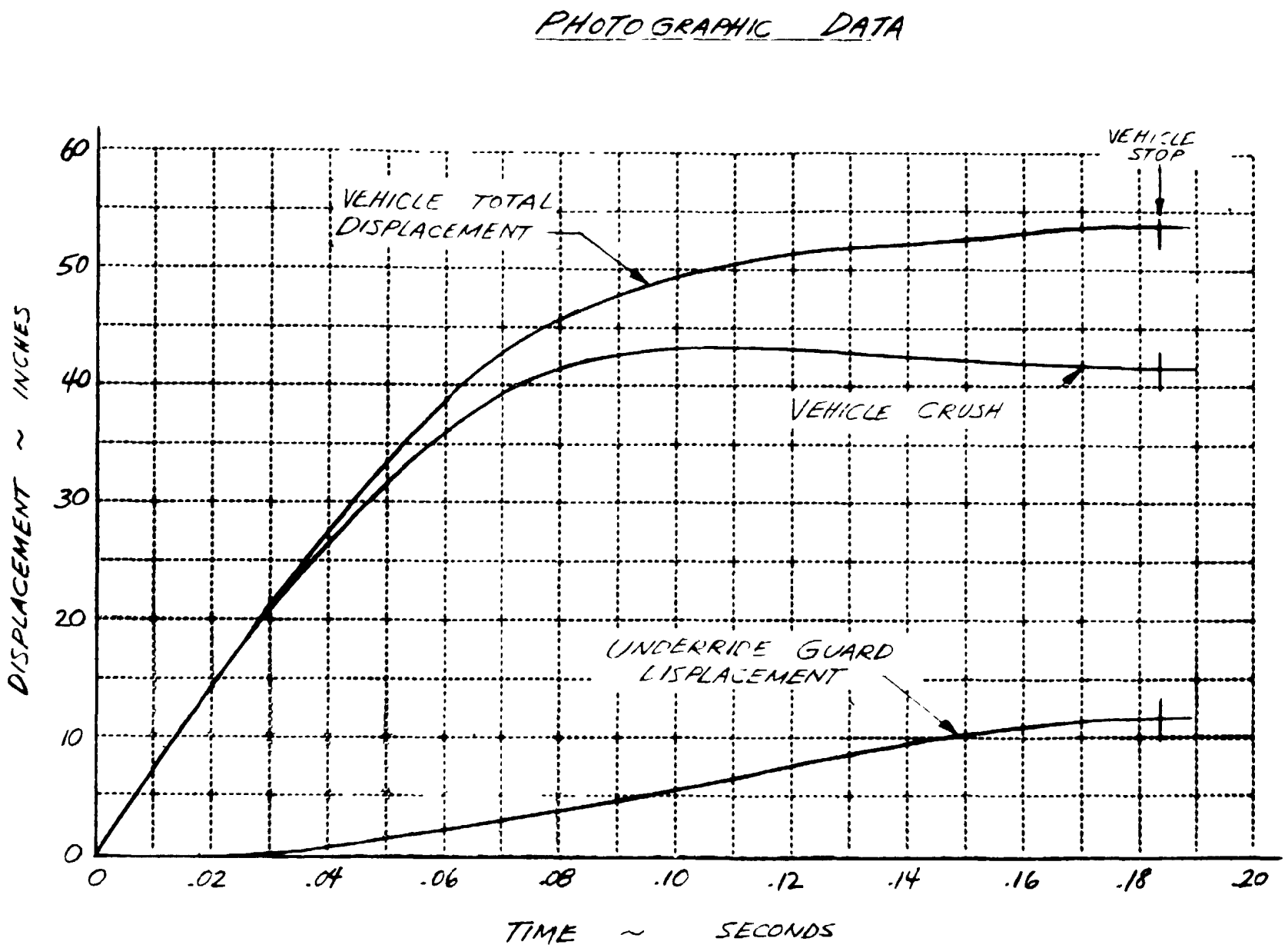

Figure 49 TEST NO. 11: VEHICLE AND UNDERRIDE GUARD DISPLACEMENTS

Photographs of the test vehicle and van trailer after the test are presented in Figure 50. Except for a dent in the underride guard caused by impact of a protruding shaft of the engine, no damage to the underride guard or the aft part of the trailer was evident. The front bumper and support members of the automobile were undamaged because they passed beneath the 24" high underride guard. The steering column and dashpanel were forced back and rotated upward to the extent that the steering wheel contacted the windshield. The frame of the car was buckled at the forward torque box location on both sides of the vehicle. The fire wall and floorboard were deformed back into the passenger compartment as a result of rearward displacement of the engine which had rotated and broken loose from the transmission housing.

4.2.6 Crash Test No. 12

The objective of this test was to determine the 30 MPH crash performance of a small car into a 24 inch high rigid underride guard mounted at the rear of a flat bed trailer. The test vehicle, a 1966 Volkswagen 1500 two-door sedan weighing 1,660 lbs., impacted the underride guard at a speed of 31.5 MPH. The test vehicle was equipped with a spare tire and wheel in the forward luggage compartment and the fuel tank was also approximately half full of Stoddard solvent to provide realistic in-service conditions.

The underride guard (Figure 4) was the same structure that was tested with the VW sedan in test No. 10.

Passenger compartment longitudinal accelerations measured on the tunnel behind the front seat are presented in Figures 51 and 52. The plot shown in Figure 51 was obtained by filtering the raw data signal with an electronic filter having a corner frequency of 1000 Hz. Integration of the acceleration data produced the velocity and displacement curves. Figure 52 shows the same compartment acceleration data after

(a)

(b)

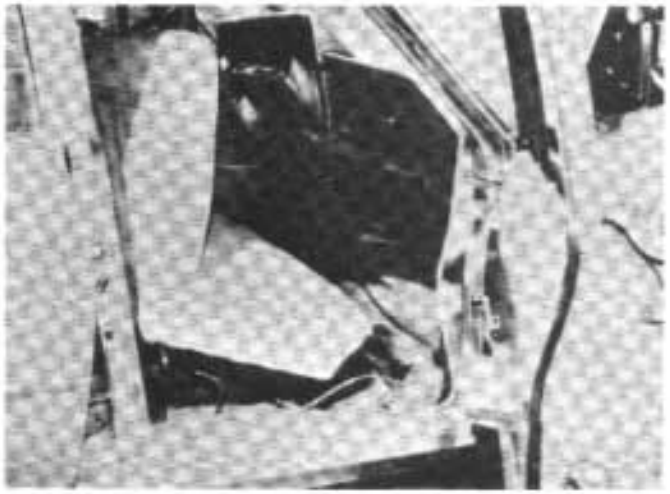

(c)

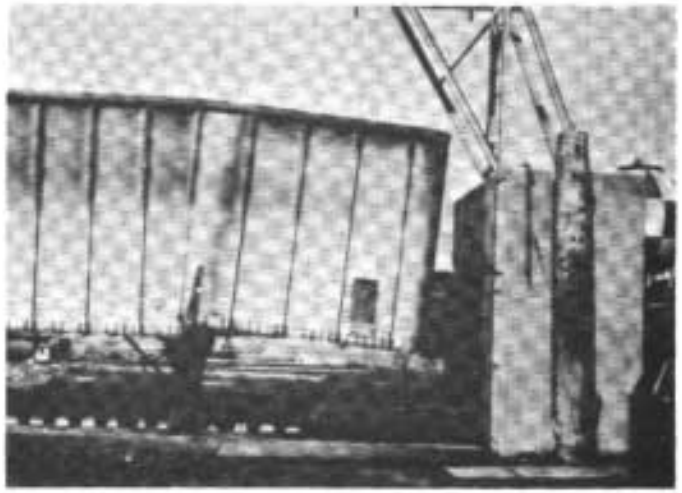

(d)

Figure 50 TEST NO. 11: AUTOMOBILE AND VAN TRAILER AFTER IMPACT

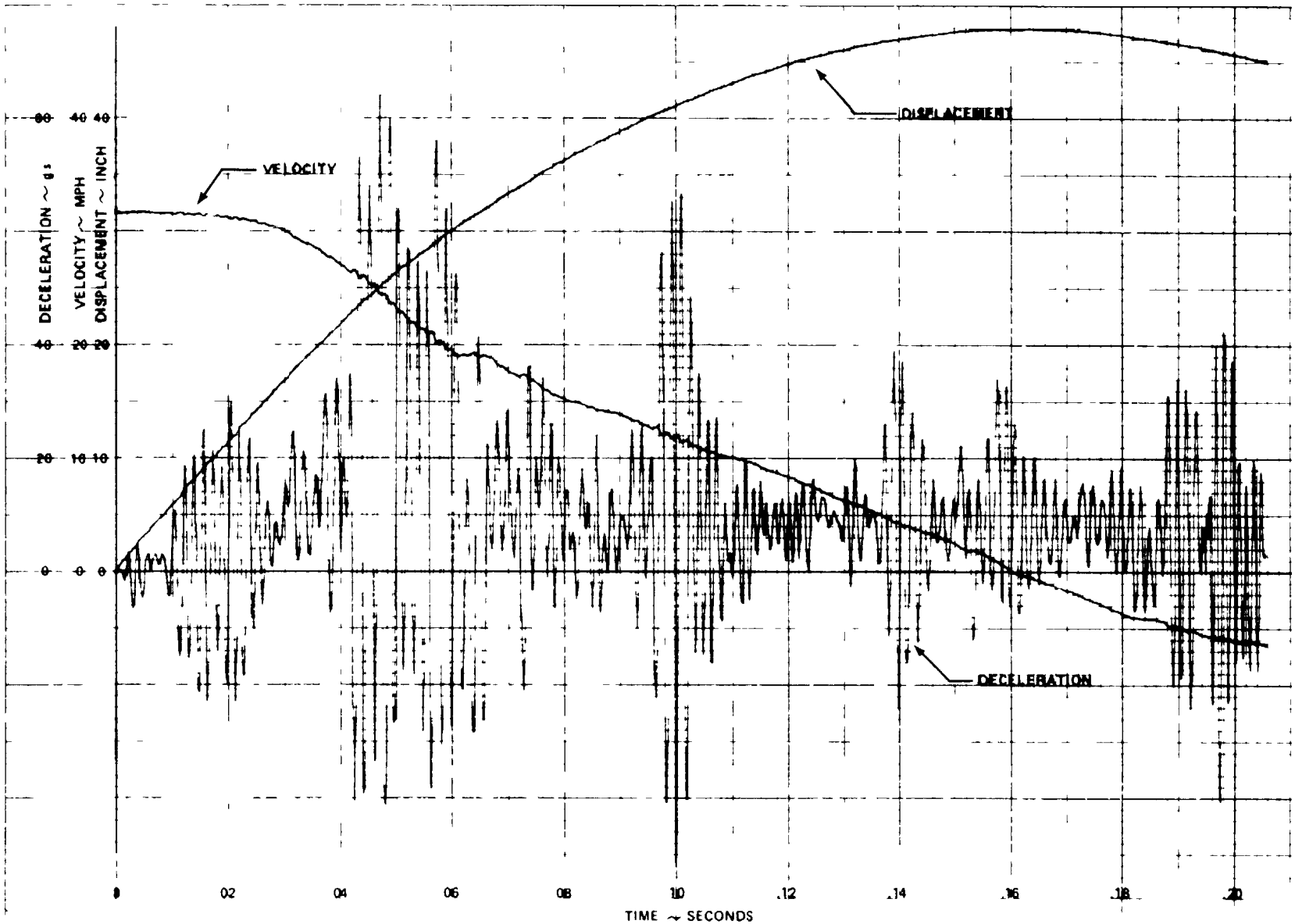

Figure 51 TEST NO. 12. COMPARTMENT LONGITUDINAL ACCELERATION DATA, FILTERED AT 1000 Hz

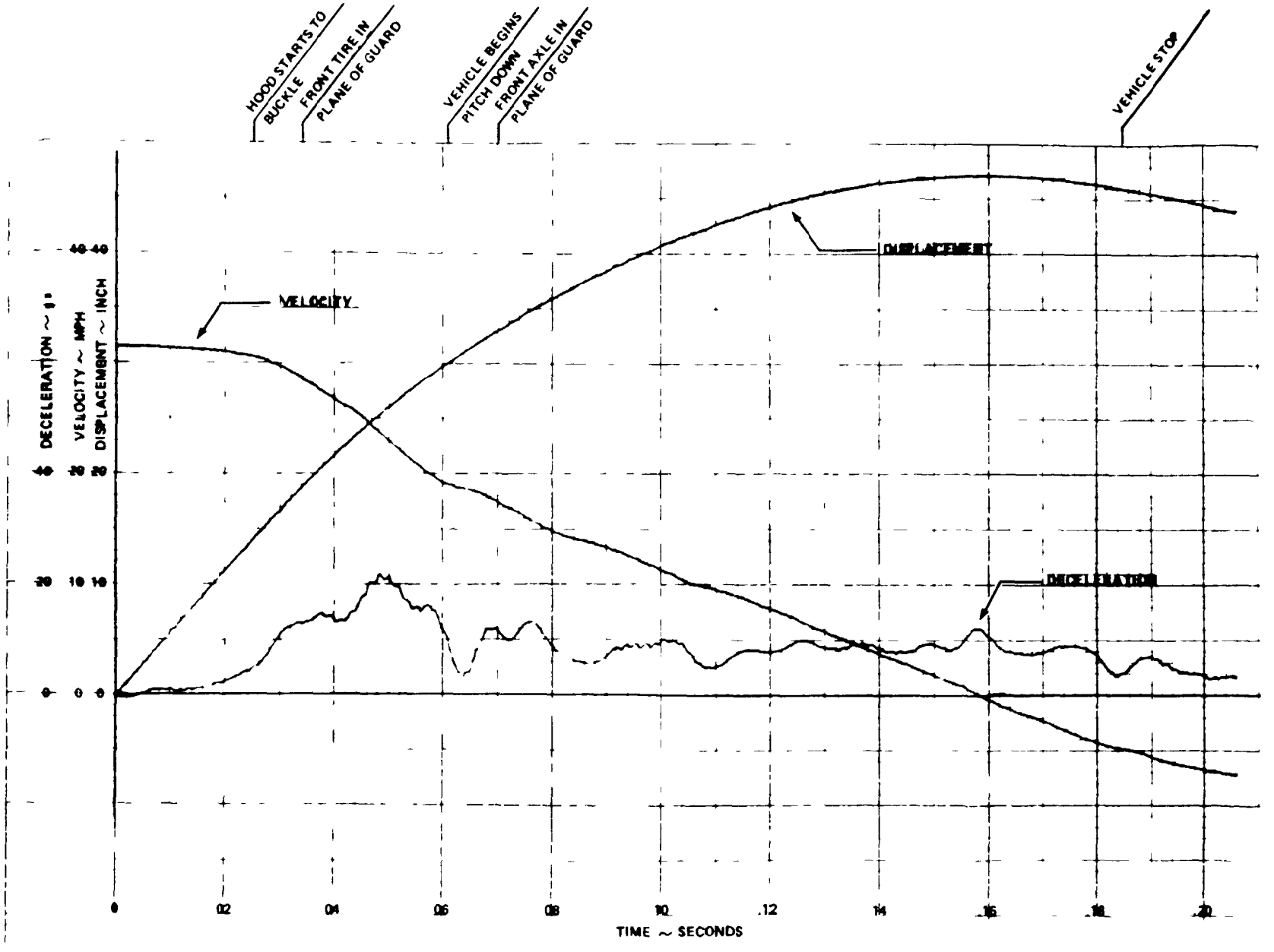

Figure 52 TEST NO. 12: COMPARTMENT LONGITUDINAL ACCELERATION DATA, FILTERED AT 50 Hz

filtering with a digital filt r having a corner frequency of 50 Hz. The measured peak longitudinal deceleration (50 Hz filter) was approximately 22 g's which occurred .048 seconds after impact.

The times of several events during the impact sequence, obtained from the high speed movie films, are marked along the top of the figure. Analysis of the films showed that the vehicle forward motion stopped at a time of .185 seconds after impact or about .025 seconds later than that indicated by the accelerometer data.

The measured frontal crush distance of the vehicle, following the test, was 48 inches which is about the maximum dynamic displacement obtained from integration of the acceleration data.

Passenger compartment vertical acceleration and engine longitudinal acceleration data are presented in Figure 53. A maximum longitudinal acceleration of approximately 20 g's was recorded on the engine .052 seconds after impact.

Compartment rear deck accelerations are shown in Figure 54. These data, as well as the data presented in Figure 53, were el ctronically filtered at a cutoff frequency of 50 Hz. A peak deceleration of approximately 19 g's was recorded by the longitudinal sensor at a time of .060 seconds. It may be noted that the time histories of longitudinal acc lerations measured in the compartment, on the engine, and at the rear deck location are generally very similar as regards wave shape and magnitude.

A time history of the total longitudinal impact force as measured by two load cells at the front of the trailer is displayed in Figure 55. The maximum recorded load was 40,000 lbs. occurring .052 seconds after impact. The average force over the .185 second stopping time interval as d termined from this plot was 12,380 lbs. The 2,290 lb-sec measured

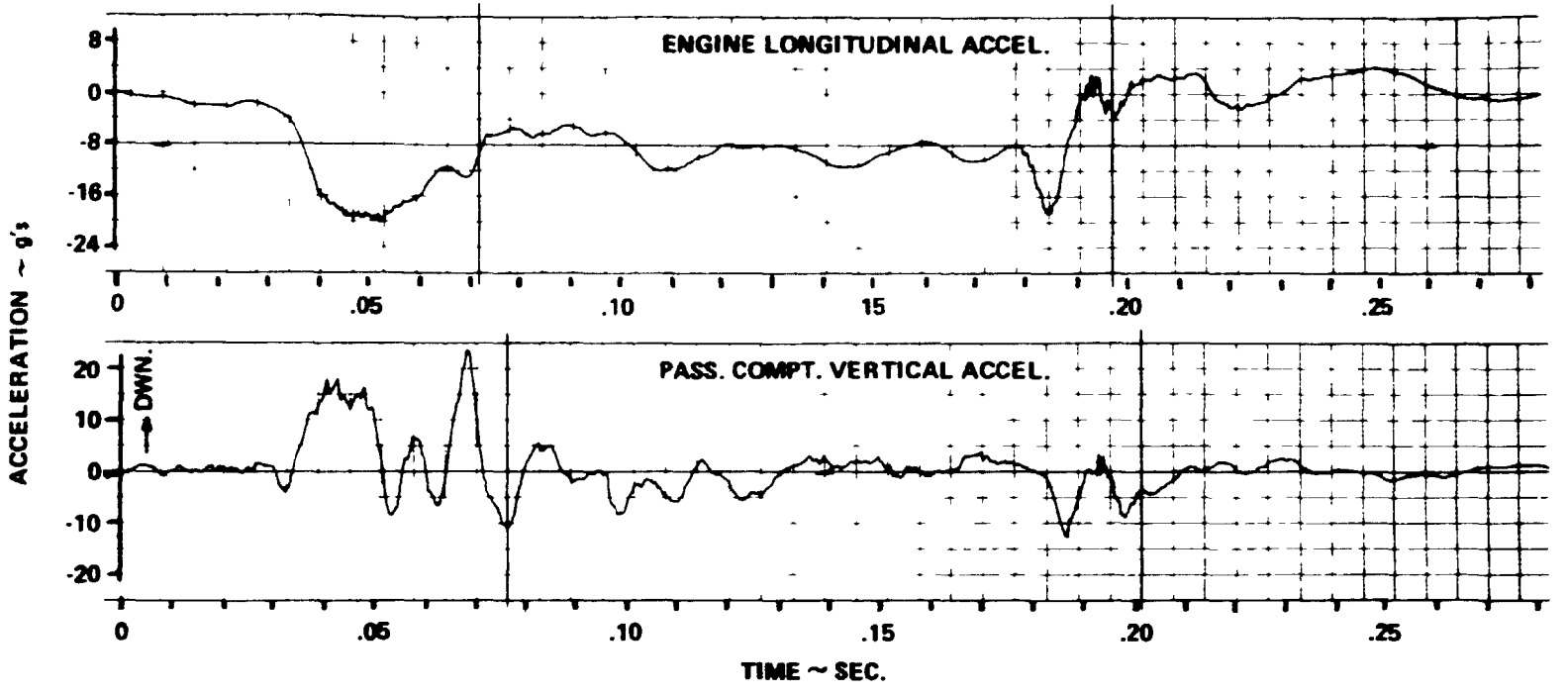

Figure 53 TEST NO. 12: COMPARTMENT AND ENGINE ACCELERATION DATA

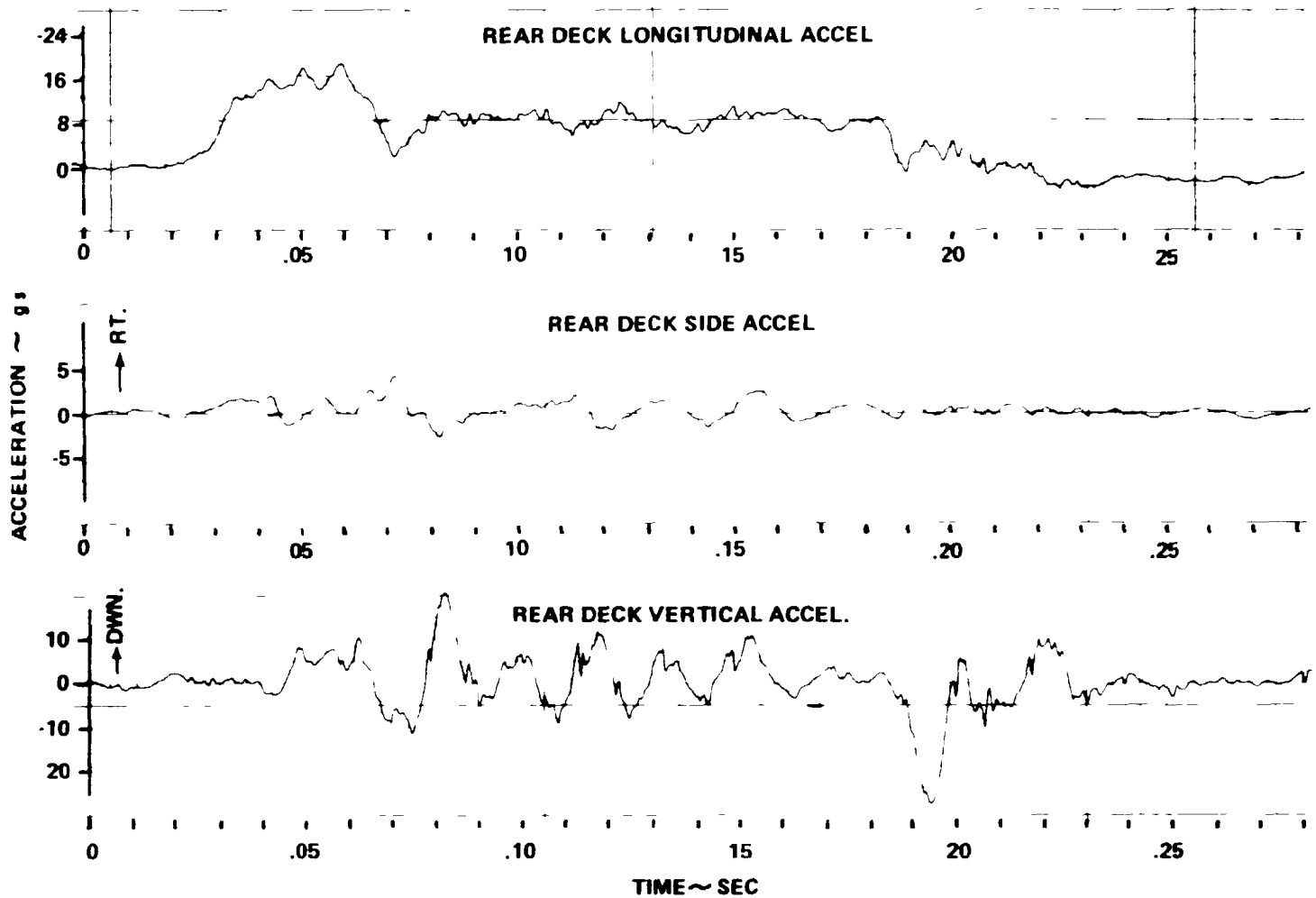

Figure 54 TEST NO. 12: COMPARTMENT REAR DECK ACCELERATION DATA

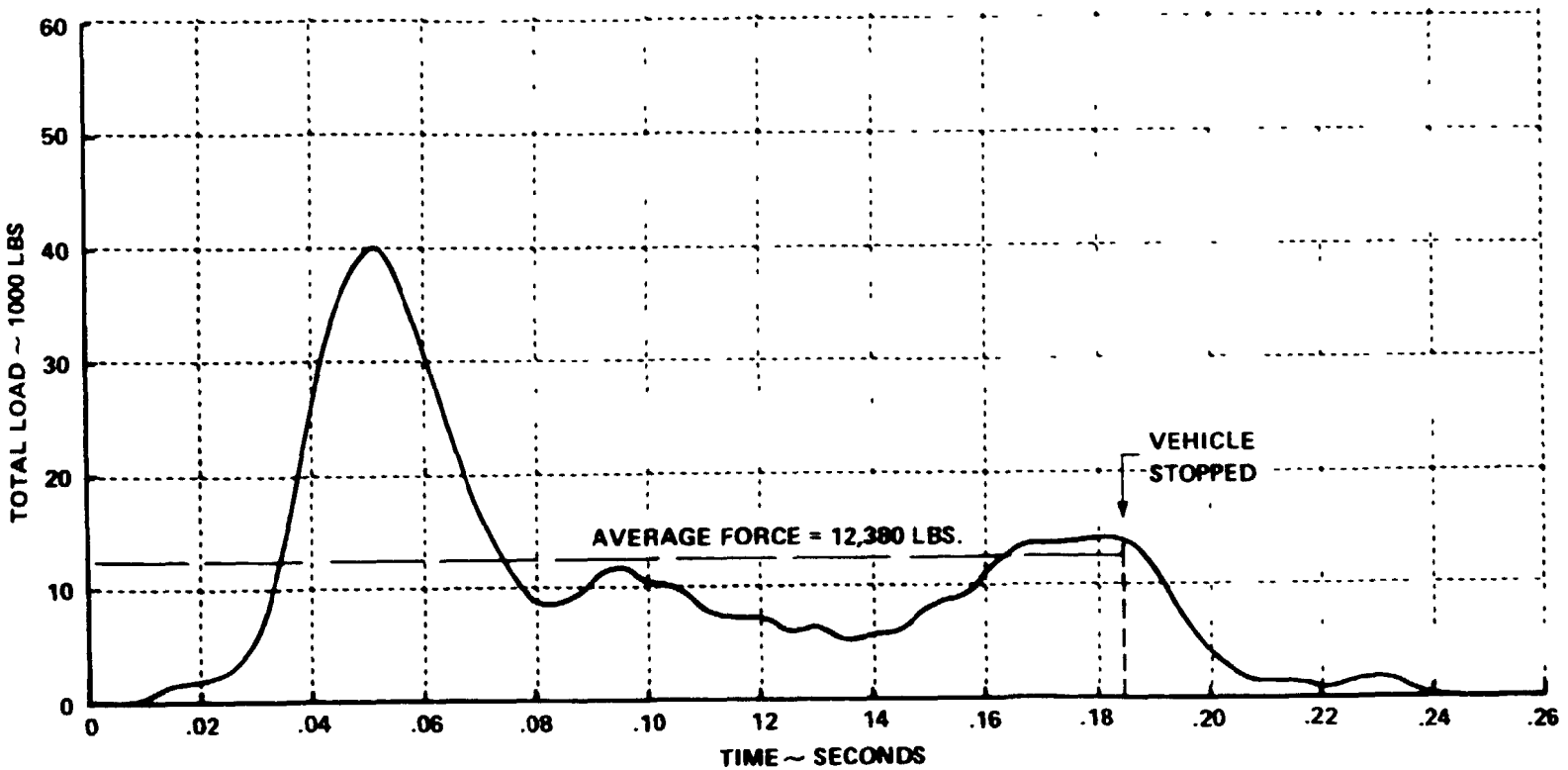

Figure 55 TEST NO. 12: VEHICLE IMPACT LOAD

impulse agrees closely with the 2,380 lb-sec change of linear momentum obtained from the product of the automobile mass and initial velocity.

Horizontal displacement of the vehicle during impact as determined from analysis of high speed movie film is displayed in Figure 56. The maximum displacement and the time to stop the vehicle was 52 inches and .185 seconds, respectively.

The data from Figures 55 and 56 were combined to obtain the load-displacement plot presented in Figure 57. The rapid increase in loading beginning at a displacement of about 13 inches is attributed principally to guard contact with the spare tire which distributed the loads to the fuel tank and other sheet metal structure in the luggage compartment. The resistance offered by the vehicle then reduced as these components collapsed and the guard penetrated the otherwise empty luggage compartment. When the guard contacted the forward bulkhead and lower "A" pillar region, the crush resistance again increased, and the automobile was finally stopped. The maximum load of 40,000 lbs. occurred at 26 inches of guard penetration. The 56,200 ft-lbs of energy represented by the area under the curve compares favorably with the 55,100 ft-lbs initial kinetic energy of the vehicle at impact.

Photographs of the test vehicle and underride guard installation before and after the test are presented in Figure 58. As may be seen from the photographs, the bumper, tires and front suspension passed completely under the guard.

The front bulkhead and dashpanel were pushed back into the passenger compartment slightly, and the steering column was also moved aft and rotated upward a small amount. However, except for the possibility of contributing to injuries to the lower limbs, the intrusion of the passenger compartment was deemed not so extensive as to create a serious hazard to occupants of the front seats.

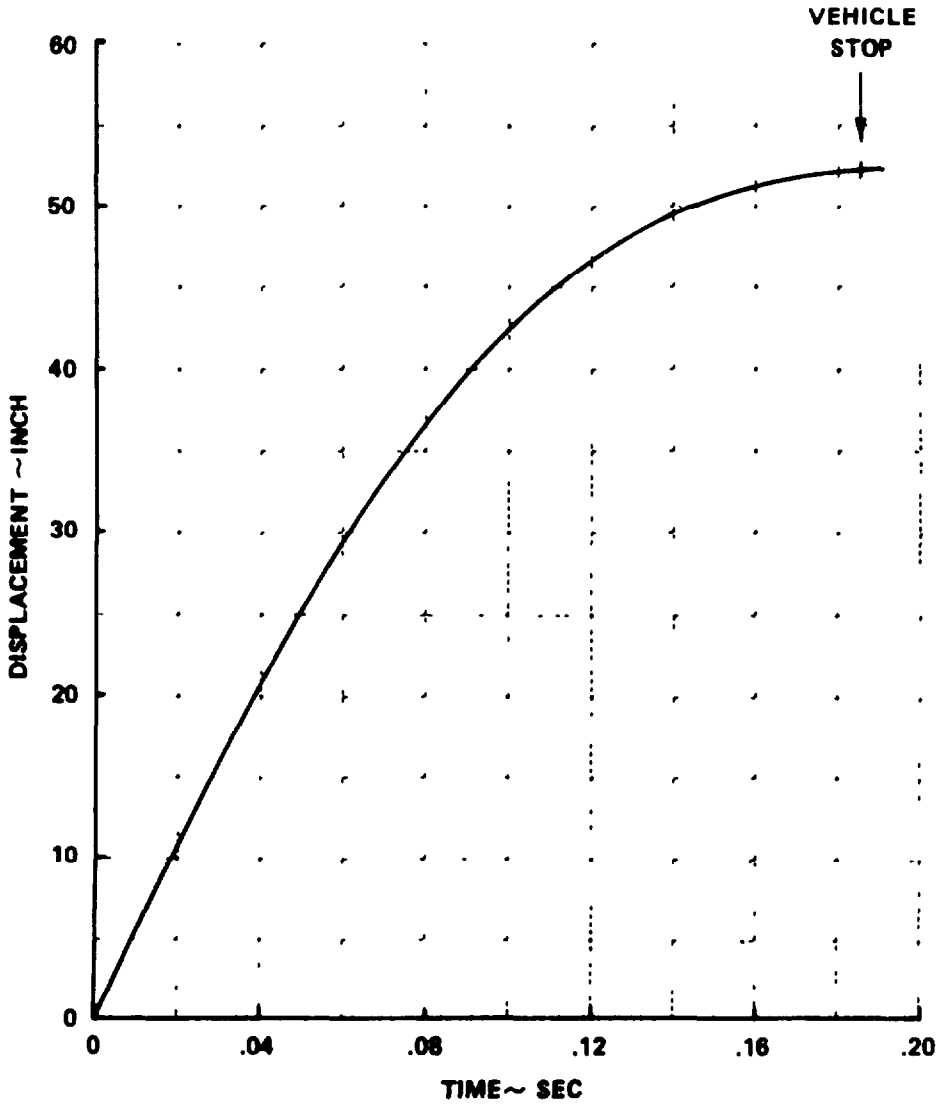

Figure 56 TEST NO. 12: VEHICLE DISPLACEMENT FROM PHOTOGRAPHIC ANALYSIS

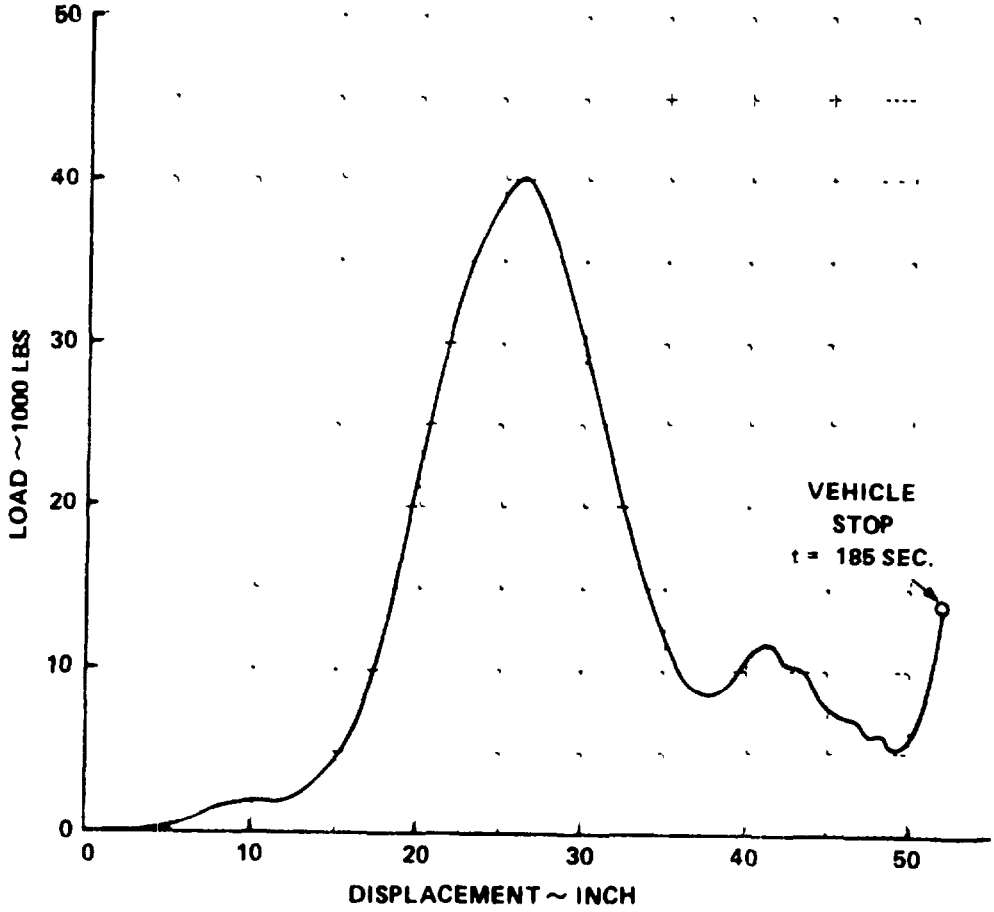

Figure 57 TEST NO 12 VEHICLE IMPACT LOAD VS DISPLACEMENT

(a)

(b)

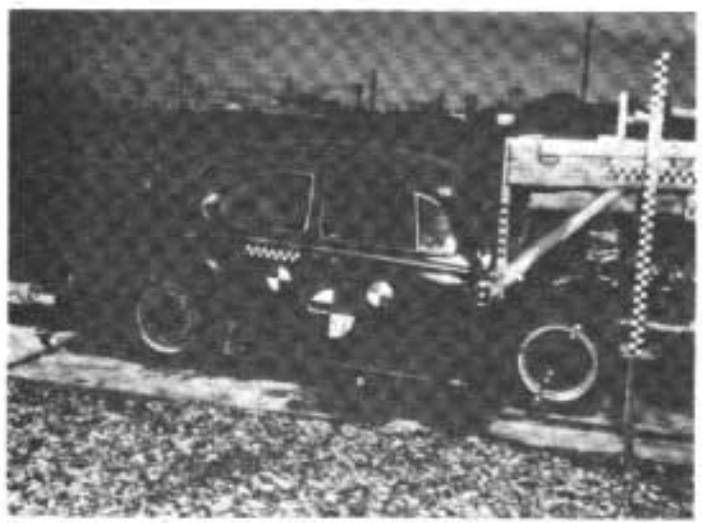

(c)

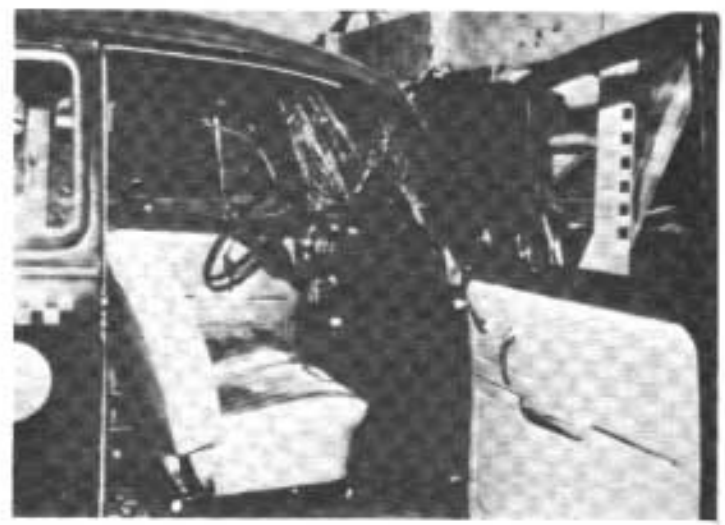

(d)

Figure 58 TEST NO. 12: VEHICLE AND RIGID UNDERRIDE GUARD

5.0 DISCUSSION OF RESULTS

Results from the six crash tests of underride guards installed on trailers described in the preceding section are summarized in Table 1. For convenience in comparing with results obtained in the initial series of six tests using the simulated rigid underride guard, data from these tests are also included in the table.

The responses of the automobile in the test of the 18 inch rigid underride guard mounted on the flatbed trailer (Test No. 7) are quite similar to those measured in Test No. 1 with the simulated guard in which the ground clearance was also 18 inches. The maximum crush of the car was about 5 inches greater than in Test No. 1 which is believed to be largely due to two factors:

(1) The slightly higher impact speed which was 39.6 MPH in Test No. 7 compared with 37.9 MPH in Test No. 1.

(2) A lesser contribution of the forward sheet metal in decelerating the car. This is reflected in a comparison of the passenger compartment longitudinal decelerations and was caused by the fact that the face of the guard in Test No. 7 had large openings, whereas the face of the simulated guard was a flat plate surface that provided more contact area with the front of the automobile.

Perhaps the most significant difference between the two tests is the maximum longitudinal load applied to the guard which occurs when the engine contacts it. In the trailer test the peak load recorded was 168,000 lbs. compared to 247,000 lbs. in the impact of an identical automobile with the rigid simulated underride guard. The reduction in peak load is attributed to the smaller contact area between the engine and the guard and correlates with the engine longitudinal acceleration data of the two tests

Table 1

SUMMARY OF UNDERRIDE GUARD TEST RESULTS

	TEST NO	1966 TEST VEHICLE	VEHICLE WEIGHT LB	GUARD HEIGHT IN	IMPACT VELOCITY MPH	MAX * DECEL G	TIME OF MAX DECEL SEC	MAX ** PENETRATION DISTANCE IN	TIME OF** VEHICLE STOP SEC	MAX GUARD LONGIT FORCE LB	AVE LONGIT FORCE DURING TIME TO VEHICLE STOP LB
RIGID SIMULATED UNDERRIDE GUARD	1	FORD	3872	18	37 9	46	052	36	093	247 000	68,200
	2	FORD	3790	24	40 4	32	052	44	112	295 000	63,200
	3	FORD (BRAKING ATTITUDE)	3880	24	39 9	63	086	51	126	–	56 000
	4	VW 1300	1680	18	41 8	–	–	38	103	177 000	30 700
	5	SIMCA 1000	1600	18	41 0	34	066	51	135	–	22,100
	6	LINCOLN	5150	18	33 1	40	054	26	081	158 000	95,200
TRIALER-MOUNTED UNDERRIDE GUARD	7	FORD	3750	18 (RIGID)	39 6	35	069	41	105	168,000	69,500
	8	FORD	3840	18 (YIELDING)	39 0	34	042	45 5 (24 CAR CRUSH 21 5 GUARD DISP)	126	90 000	52,000
	9	FORD (22' OFFSET IMPACT)	3760	18 (YIELDING)	38 2	17	090	50 (≅30 CAR CRUSH 20 GUARD DISP)	145	70 000	44,000
	10	VW 1300	1680	24 (RIGID)	42 1	28	030	79 5	230	55 000	13 400
	11	FORD	3460	24 (RIGID) VAN TRAILER	43 1	44	047	43 (12' VAN COLLAPSE)	184	61 500***	24 950***
	12	VW 1300	1660	24 (RIGID)	31 5	22	048	52	185	40 000	12,380

* PASSENGER COMPARTMENT FILTERED DATA (50 Hz)
** HIGH SPEED PHOTOGRAPHIC DATA
*** NOT ACTUAL LOAD ON TRUCK DUE TO INERTIA EFFECTS DURING COLLAPSE OF TRAILER STRUCTURE

which shows that the peak deceleration of the engine was reduced from more than 200 G in Test No. 1 to about 120 G measured in Test No. 7. However, the average [illegible]e during the time to stop the passenger compartment was nearly the sa[illegible]e for both tests.

The damage to the impacting automobiles was also essentially identical in the two tests. In both instances the damages to the vehicle interior were relatively minor and probably would not significantly affect occupant injury potential.

The benefits that can be derived from use of an energy absorbing underride guard may be seen from a comparison of the results for Test No. 7 and 8. The time histories of passenger compartment deceleration measured in the two tests are presented in Figure 59 for comparison. At first glance there appears to be little clear evidence to favor either of the two types of underride guard from these data. However, the large excursions in the decelerations plots tend to obscure the fact that the general level of decelerations experienced in the rigid guard test is indeed substantially higher.

The maximum dynamic crush of the automobile structure was reduced by 17 inches through use of the yielding underride guard. Although the 41 inches of vehicle crush experienced in the rigid guard test was not deemed hazardous in terms of compartment intrusion from rearward displacement of the engine, the energy absorbing underride guard system provides a greater margin of safety and would allow a higher speed of impact. Note that although there was less crushing of the automobile in the case of the yielding underride guard, the total forward displacement of the car toward the rear of the truck was slightly greater due to the 21 inches of deflection of the guard.

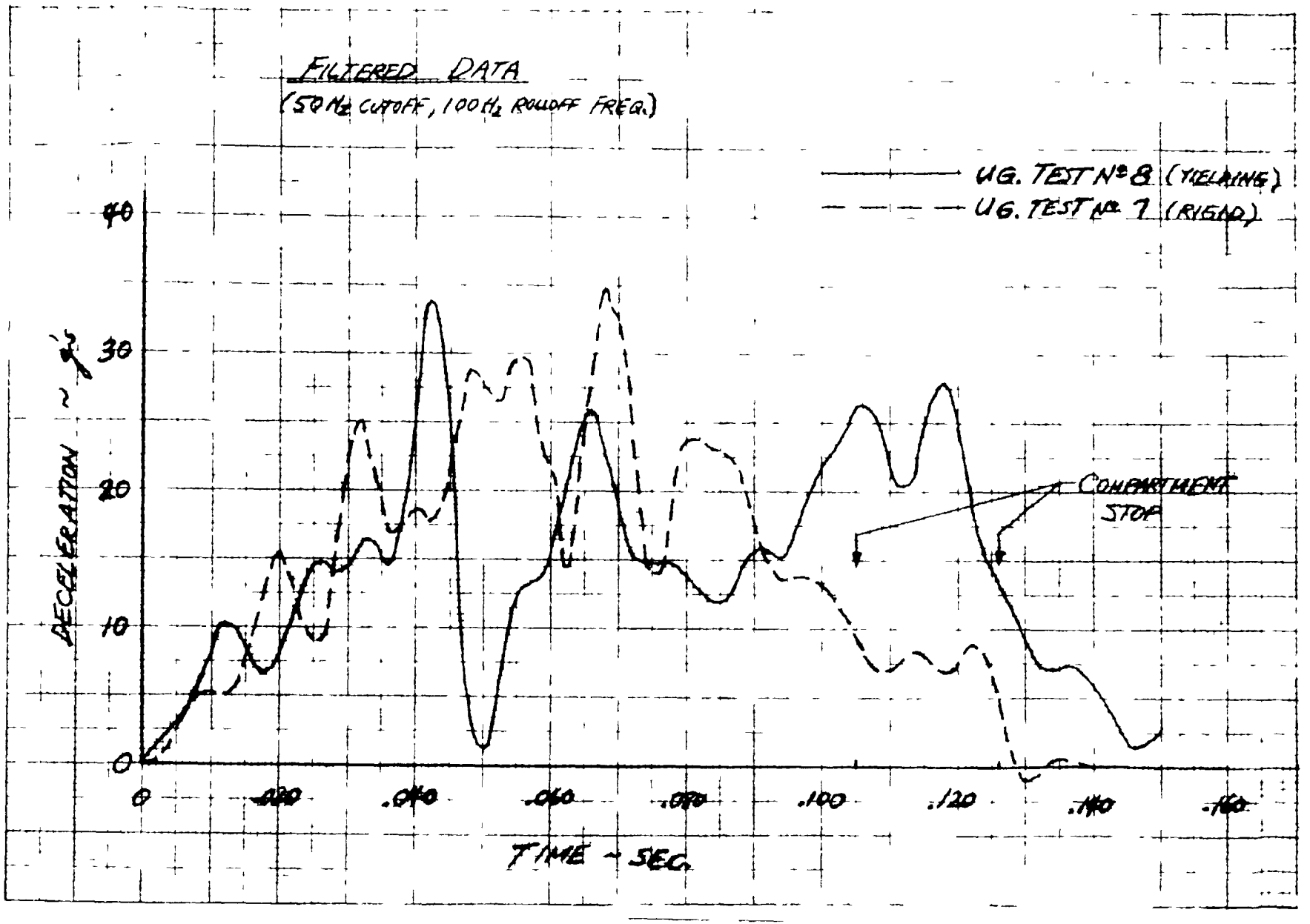

Figure 59 COMPARISON OF COMPARTMENT LONGITUDINAL ACCELERATIONS FOR RIGID AND YIELDING UNDERRIDE GUARD IMPACTS

Figure 60 is a plot showing the force-deflection characteristics of the energy absorbing underride guard and the vehicle in Test No. 8 as constructed from the data presented in Figures 21 and 22. The areas under these curves represent the energy absorbed by the guard and by deformation of the automobile structure. The average longitudinal force of the underride guard is 59,300 lbs. and the absorbed energy is 103,800 ft-lb. The energy dissipated in crushing the vehicle was only 79,200 ft-lb. The total measured dissipated energy is therefore 183,000 ft-lb compared to 195,200 ft-lb initial kinetic energy of the automobile. The discrepancy (approximately 6%) is attributed to small inaccuracies of the instrumentation and in reducing the photographic data. Also, some energy was dissipated as a result pitching of the car and slight vertical movement of the aft end of the truck, and local deformations of other parts of the vehicle. These results show that the underride guard dissipated approximately 57 percent of the total measured kinetic energy which is very close to that expected based on results from the mathematical model used to establish the design load requirements for the guard.

From the plots shown in Figure 60, it may be seen that the underride guard did not begin to yield until the load had reached a value of approximately 60,000 lbs. which was developed after the car had crushed about 14 inches. The increase of the load to 90,000 lbs. after the guard began to displace is probably due to inertial effects in accelerating the mass of the guard structure. During the remainder of the guard displacement, the energy absorbing friction tubes effectively limited and maintained the crash loads to a relatively constant level. Comparison of the loads measured in Test Nos. 7 and 8 shows that the yielding underride guard resulted in substantially lower loads imposed on the truck structure with consequent reduced likelihood of damaging the truck.

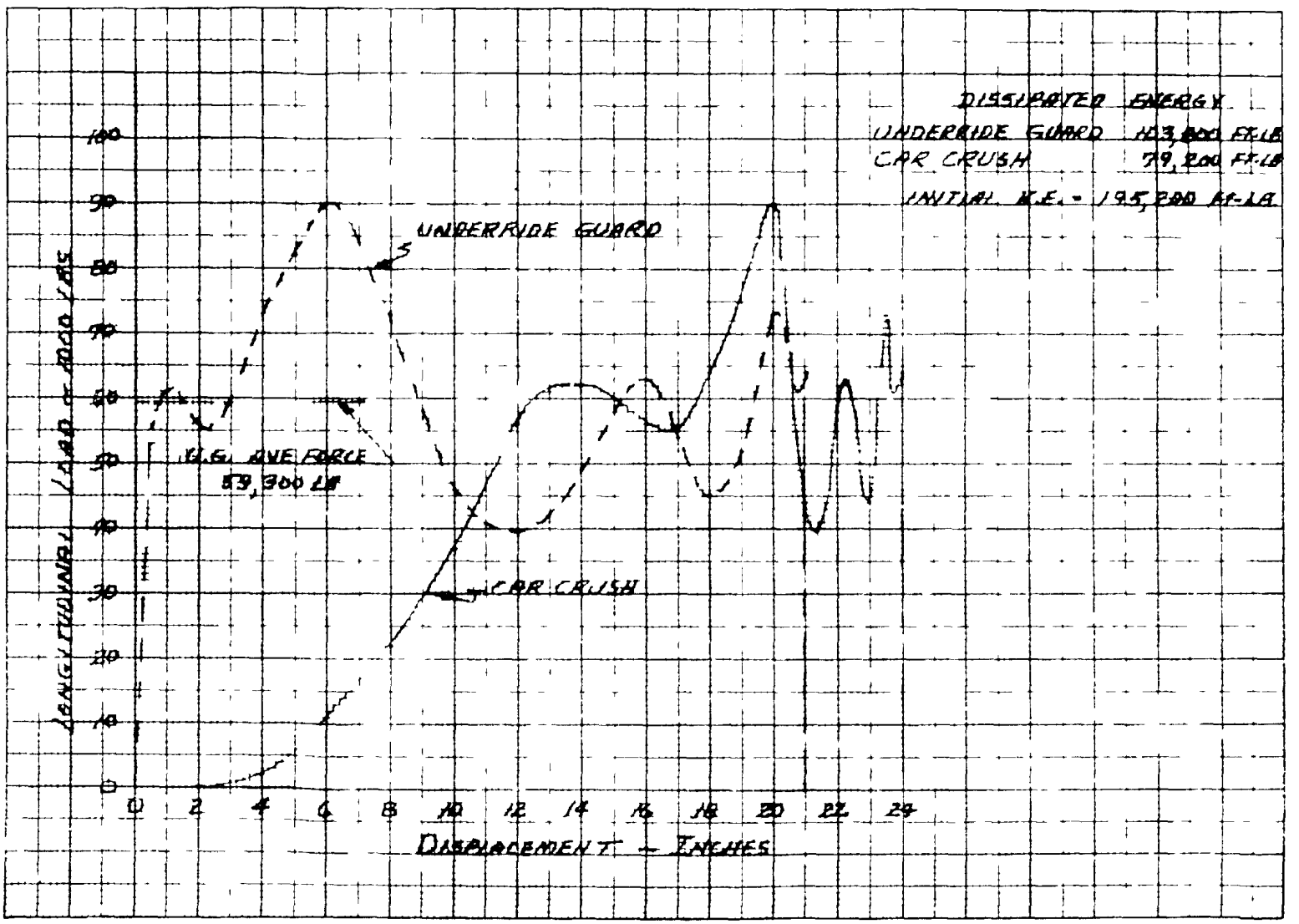

Figure 60 TEST NO. 8 – UNDERRIDE GUARD AND VEHICLE LOAD-DEFLECTION CHARACTERISTICS

The performance of the yielding underride guard in the off-center impact (Test No. 9) was satisfactory inasmuch as excessive underride of the truck was prevented, the passenger compartment was not intruded, and the deceleration of the car was low. The impact to the right of center of the rear of the trailer resulted in unequal strokes of the energy absorbers and the distortion of the guard ultimately caused buckling of the inner slotted tubes. The axial strokes of the right and left energy absorbers were 16 inches and 8 inches, respectively, as compared with the 17.5 inch stroke of each device in the central impact of Test No. 8.

The high speed films show that the absorber on the right side failed first but later than .090 seconds after impact. The rapid decrease in measured load that occurred between .090 and .100 seconds (see Figure 31) is believed indicative of the occurrence of buckling. The general level of axial loads developed in both friction tubes prior to buckling was slightly less than was measured in Test No. 8.

A comparison of other data measured for Test Nos. 8 and 9 shows that the duration of the impact was longer (.145 sec vs. .126 sec) in the off-center impact and that the total vehicle displacement was somewhat greater (49.5" vs. 45.5"). The longer time to stop is reflected in the generally lower decelerations throughout the impact and the measured peak deceleration was also lower (17 g vs. 34 g). Both the maximum force and the average force imposed on the truck were smaller for the off-center impact. These values were 71,000 lbs. and 44,000 lbs., respectively, for Test No. 9 as contrasted with loads of 90,000 lbs. (maximum) and 52,600 lbs. (average) measured in Test No. 8. Because the collapse distance of the forward structure of the vehicle was nonuniform and the underride guard deflection was variable from one side to the other, a comparison of the distribution of energy dissipated by the guard and through crushing of the vehicle is not possible for the two tests.

The results of the tests of rigid underride guards installed on the trailers at a 24 inch ground clearance (Test Nos. 10, 11 and 12) substantiate the findings and conclusions of the first series of tests conducted with the simulated underride guard concerning the relationship between guard height and size of the impacting vehicle. The test of the guard on the van trailer demonstrated that a 24 inch guard would adequately protect against excessive underride of a full size automobile and that the guard and attachment could be designed to withstand and distribute the impact loads into the trailer structure without a severe weight penalty. The response of the car in this test was very similar to that observed in Test No. 2 in which the height of the simulated guard was also 24 inches. Note that the maximum dynamic crush of the vehicle structure was nearly identical in the two tests but the peak deceleration of the passenger compartment was noticeably higher in the trailer-mounted test.

As discussed in the previous section, the measured loads shown in Table 1 for Test No. 11 are not the true loads imposed on the underride guard because the trailer structure yielded in the vicinity of the landing wheels. However, based on the measured longitudinal accelerations of the engine, the maximum load in Test No. 11 was probably much less than the value of 295,000 lbs. measured in Test No. 2. Except for a dent in the bumper of the underride guard caused by the impact of a protruding shaft of the engine, no damage to the underride guard or to the aft part of the trailer was evident.

In the tests with the simulated rigid underride guard, relatively large vertical loads due to wedging of the car beneath the underride guard were measured and it was thought that lifting of the rear of the truck, which would be conducive to increased underride penetration, might constitute a potential problem. However, the results of the series of tests with trailer-mounted guards indicated that such was not the case. In fact, the tendency in each of the tests was for the rear of the truck to move downward as a result of the eccentricity of the load applied through the guard to the trailer structure. Note that the trailers were purposely tested without

cargo load to favor any tendency for the rear of the truck to move upward.

The two tests with the Volkswagen (Test No. 10 and 12) were conducted for the purpose of demonstrating the consequences of small cars impacting underride guards having greater than 18 inches of ground clearance. The results were not unexpected since the simulated underride guard tests (Test Nos. 4 and 5) indicated that excessive underride would surely occur for guard heights greater than 18 inches when impacted at a velocity of 40 MPH.

The test of the Volkswagen impacting the 24 inch underride guard at 40 MPH resulted in extreme penetration of the guard into the passenger compartment and would clearly have been unsurvivable for occupants of the front seats. In contrast with the result of the test with the simulated underride guard with 18 inch ground clearance, the front wheels passed beneath the 24 inch guard so that it did not engage the stronger portions of the vehicle structure.

It is of interest to note the similarity of the plots of vehicle load versus displacement for Test Nos. 10 and 12 which are presented in Figures 41 and 57, respectively. In each case, the load did not start to incr ase appreciably until the vehicles had underriden the guard approximately 15 to 18 inches. The rapid increase in loading occurred when the guard contacted the spare tire in the front luggage compartment which assisted in distributing the load to the partially filled fuel tank and other portions of the forward structure. Peak loads were developed at approximately 28 inches of displacement after which the loads diminished rapidly due to collapse of the luggage compartment and fender sheet metal structures. Very little energy was then dissipated until, at approximately 50 inches of displacement, the underride guard contacted the front bulkhead of the passenger compartment and the load again started to increase.

The energy represented by the area under each curve is nearly the same for the two tests up to the value of 52 inch s of displacement measured in the 31.5 MPH test (Test No. 12). The additional 44,200 ft-lb of kinetic energy in Test No. 10 (42.1 MPH) was dissipated by further crushing of the vehicle for more than 2 feet into the passenger compartment. The nearly 80 inches of penetration experienced in this test contrasts with the 38 inches that resulted with the underride guard at 18 inches ground clearance (Test No. 4) for the same impact speed, and dramatically demonstrates the desirability of placing the underride guard as low as possible to ensure an adequate engagement with the stronger portions of the vehicle forward structure.

6.0 REFERENCES

1. DeLeys, Norman J. and Naab, Kenneth N., "Full-Scale Crash Tests of Rigid Simulated Heavy Vehicle Underride Guard", Technical Report, Cornell Aeronautical Laboratory, Inc. Report No. VJ-2844-V-1, March, 1970.

2. Automotive Industries, March 15, 1969, Volume 140, No. 6.

3. "Maximum Desirable Dimensions and Weights of Vehicles Operated on the Federal-Aid Systems", Commerce Department, Bureau of Public Roads, 88th Congress, Second Session, House Doc. No. 354.

4. Sidelko, William J., "An Objective Approach to Highway Truck Frame Design", SAE SP276, December, 1965.

5. Anders, E. B., et al, "Digital Filters", Auburn Research Foundation, Inc., Report No. NASA CR-136, December, 1964.

APPENDIX A

SURVEY OF ENERGY ABSORBING DEVICES

As a preliminary to selecting and designing prototype energy dissipating devices or systems for automobile bumpers and truck underride guards, a literature search was conducted to determine the state of the art in energy management techniques. Although similar studies exist in the open literature, the intent here is to present quantitative experimental data as opposed to studies which mainly give qualitative and/or idealized performance data.

Energy dissipation devices have been classified as one of three types, mechanical, hydraulic or low density crushable materials. Each device is briefly described, pertinent references are given, and various operating characteristics such as force-stroke response, impact velocity sensitivity and other pertinent performance characteristics are presented. Table A-1 is a summary of the more significant performance parameters for the various energy management devices examined in this effort.

Some of the important characteristics of energy dissipators are:

specific energy absorbed (SEA);
velocity sensitivity;
force-stroke characteristic,
stroke efficiency,
directional sensitivity;
energy dissipation density, and
cost effectiveness.

Table A1

SUMMARY OF ENERGY DISSIPATOR CHARACTERISTICS

DEVICE	SPECIFIC ENERGY ABSORPTION $\frac{ft\text{-}lb}{lb}$	VELOCITY SENSITIVITY	MAX VELOCITY TESTED mph	FORCE STROKE CHARACTERISTICS	STROKE EFFICIENCY	DIRECTION SENSITIVITY	ENERGY DISSIPATION DENSITY	REFERENCES
FRANGIBLE TUBE	31 000 2024-T3 AL 39 000 A151 4130 56 600 THEO MAX	INSENSITIVE 0-5 mph & SENSITIVITY > 5 mph	12 (FOR 2024-T3 ONLY)	RECTANGULAR FOR AVERAGE FORCE HIGH FREQUENCY FLUCTUATIONS ABOUT AVERAGE	0 9	HIGH	HIGH	1 2
INVERTUBE	6500 3003-H14 AL	INSENSITIVE BELOW 0 7 mph & SENSITIVITY ABOVE 0 7 mph	20 5	RECTANGULAR	1 8-2	HIGH	HIGH	3
TUBE SHREDDER	6000 2024-T3 AL (11 000 USING TUBE WT ONLY)	INSENSITIVE	11 (REF 4 INDICATES METHOD HAS BEEN DEMONSTRATED TO 51)	RECTANGULAR	1 0	HIGH	HIGH	4
FRICTION TUBE	1600 COLD DRAWN STEEL 2300 (PROB MAX)	INSENSITIVE	STATIC	RECTANGULAR	0 5-1*	LOW	MEDIUM	5
A R L (AUSTRALIA) ENERGY ABSORBER	900 STEEL	INSENSITIVE	N/A	RECTANGULAR	1 8-2	HIGH	HIGH	6
TOR-SHOK	1100	SLIGHTLY NEGATIVE	35	RECTANGULAR	0 4-0 8*	MEDIUM	MEDIUM	7 8
SOLID MEDIA SHOCK ABSORBER	820-1250*	HIGH POSITIVE SENSITIVITY	11 2	RECTANGULAR	0 7	MEDIUM	HIGH TO LOW	9
KNEE STRUT STATIC DYNAMIC	1000 STEEL 1700 STEEL	INSENSITIVE	STATIC 25	DECREASING RAMP	NOT APPLICABLE	LOW	HIGH	10
PLASTIC HINGE	N/A	INSENSITIVE	N/A	RECTANGULAR – TORQUE VS ANGULAR DISPL	NOT APPLICABLE	LOW	HIGH	11
ALUMINUM HONEYCOMB	10 000	INSENSITIVE	16	RECTANGULAR	0 8	LOW	LOW	12 15
BALSA	9000† 24000††	INSENSITIVE	N/A	RECTANGULAR	0 8	LOW	LOW	15 16
FOAMED PLASTICS	1000 FOR 40% STRAIN	INSENSITIVE	45	RECTANGULAR < 48% STRAIN INCREASING FORCE > 40%	0 4 FOR CONSTANT FORCE	LOW	LOW	17
HYDRAULIC SHOCK ABSORBERS	500	POSITIVE SENSITIVITY ($F \propto V^2$)	29	VARIABLE DEPENDENT UPON DESIGN	0 5-1*	HIGH	MEDIUM	18 19

N/A - NOT AVAILABLE
* - LOW VALUE FOR COMPRESSION HIGH FOR TENSION
† - TO GRAIN
†† - TO GRAIN
* - BASED ON MENASCO SPEC

Since an understanding of each of the above parameters is helpful in the evaluation of energy absorbers, a brief definition of each parameter is presented.

Specific energy absorbed is the energy dissipated per unit weight of the energy absorbing material or device.

Velocity sensitivity is the tendency of the force-stroke characteristic of the energy absorber to vary as a function of the rate at which the stroking (deflection) takes place. (Positive sensitivity denotes increasing force with increasing velocity.)

Force-stroke characteristics is the variation of absorber force as a function of absorber stroke (deflection). Usually a rectangular force-stroke characteristic is desired, i.e., force constant with stroke, as this allows a maximum of energy dissipation within the restraints of a fixed stroking distance and maximum allowable force level as determined by the maximum allowable deceleration of the impacting object.

Stroke efficiency is, for linear extension or compression devices or materials, the ratio of the maximum usable length of the device in energy absorption to the original total length of the device.

Directional sensitivity is the tendency of an energy absorption device or material to change energy absorption characteristics (usually a decrease in energy absorption capacity) as the direction of the applied force varies from the normal.

Energy dissipation density is the maximum energy dissipated per unit volume. Compact energy dissipators require a high value of energy dissipation density.

Cost effectiveness can be defined in terms of dollars saved versus dollars spent in a specific energy absorption application

(e.g., lower insurance costs to truck and automobile owners due to less severe accidents as th result of the installation of energy absorbing bumpers and underride guards) or by identifying the lowest cost energy absorbing method which will satisfy the requirements of a specific application.

I. Mechanical Energy Absorbers

Frangible Tube

The frangible tube consumes energy in the process of fragmenting a hollow metal tube which is forced against a die as shown in Figure A-1. A high stroke efficiency is possible with this device as nearly the entire tube length can be fragmented if the die pilot shaft length is minimized. High stroke efficiency also implies high directional sensitivity as the limited engagement of the tube with the die prohibits the device from withstanding bending loads of any consequence.

Figure A-2 is a typical force-stroke response for fragmenting tubes. The average force remains essentially constant with displacement, however, the instantaneous force exhibits undesirable fluctuations about the average. The data of Reference A-1 indicate that the fluctuating force can be reduced considerably by increasing the ratio of tube inside diameter to die bend radius.

Figure A-3, taken from Reference A-2, shows the experimentally observed rate dependency for a 2024-T3 aluminum tube. The dotted fairing in Figure A-3 indicating no rate dependency below a d formation rate of 5,000 inches per minute is based on experimental data indicating no increase in tensile yield or tensile ultimate strength of aluminum alloys for rates of displacement below approximately 5,000 inches per minute. A positive rate dependency is observed for tube deformation rates of about 12 MPH, the highest velocity tested.

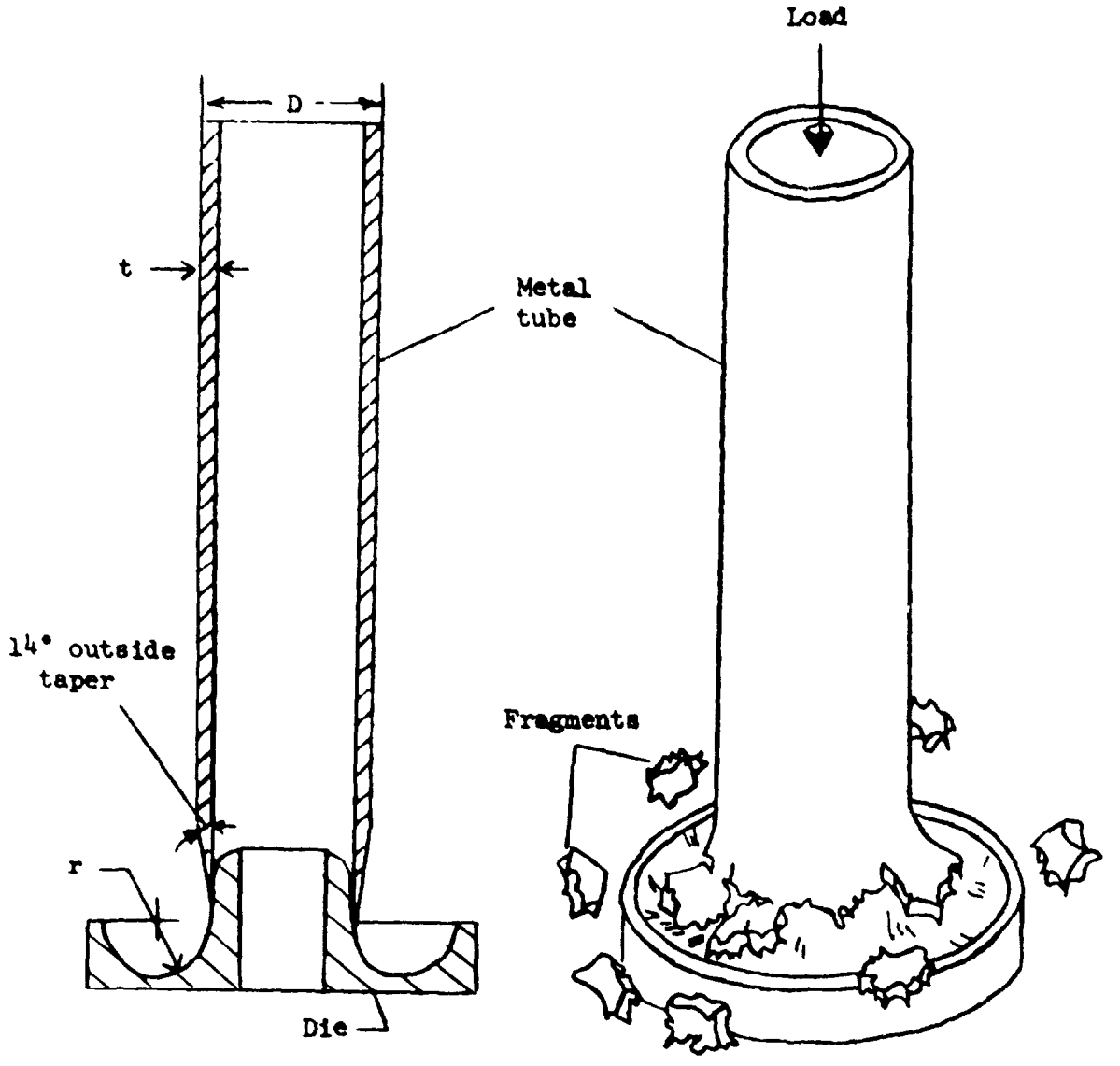

Figure A-1 SKETCH ILLUSTRATING FRAGMENTING PROCESS OF FRANGIBLE TUBE

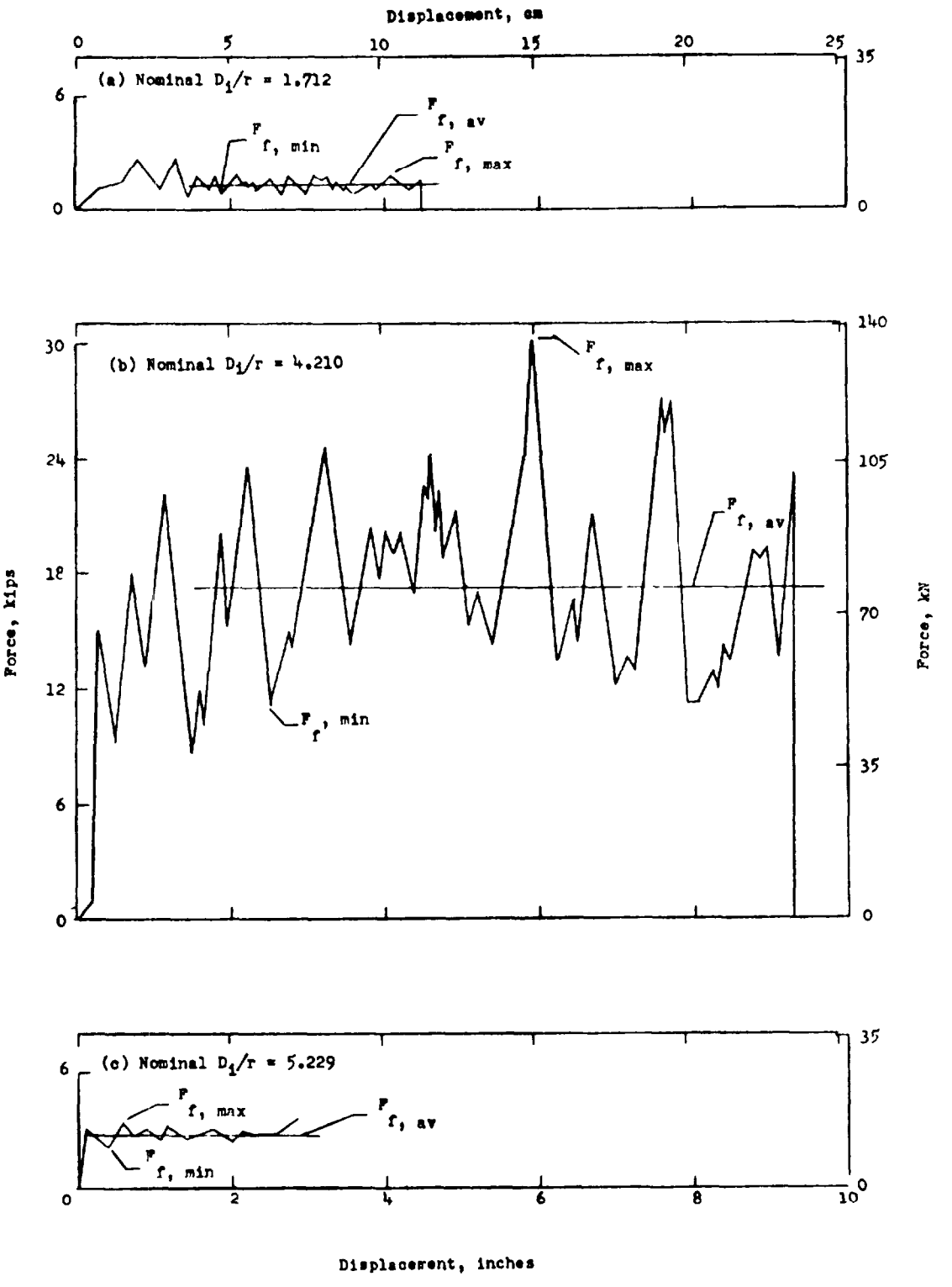

Figure A-2 TYPICAL FRAGMENTING TUBE AXIAL-FORCE VARIATIONS WITH DISPLACEMENT FOR 2024-T3 ALUMINUM ALLOY – NOMINAL t/r = 0.300

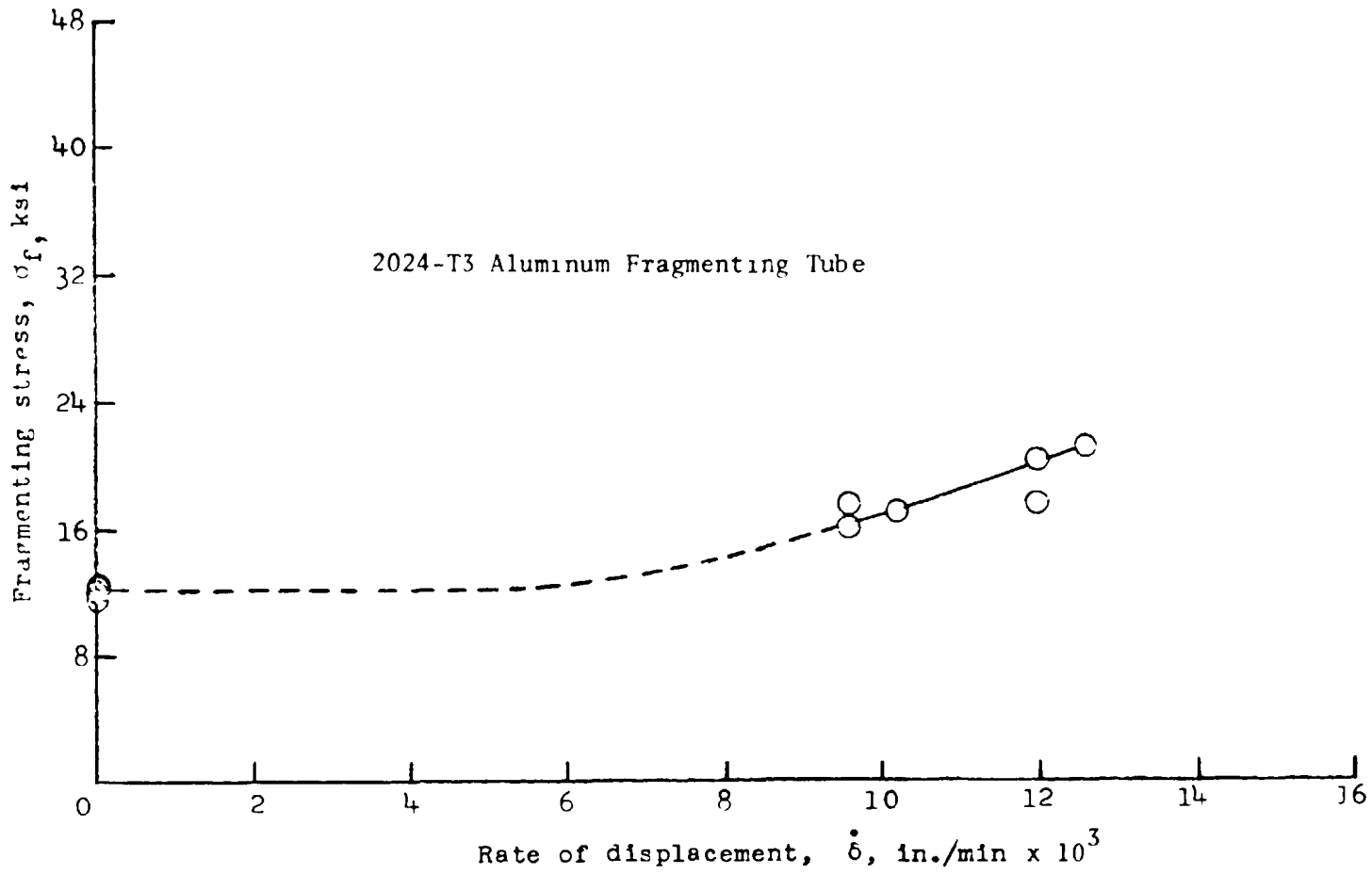

Figure A-3 VARIATION OF FRAGMENTING STRESS WITH RATE OF DISPLACEMENT. D = 1.0 INCH; t = 0.065 INCH; t/r = 0.43

Figure A-4 compares the specific energy absorbed for frangible tubes of various metals and for aluminum-alloy honeycomb. The values of specific energy absorbed given for the frangible tubes do not include the die weight and assume essentially 100 percent stroke efficiency. These experimentally observed specific energies do not represent ultimate values but rather the values obtained in the particular experiments conducted. The maximum specific energy absorption capability may be as high as 55,000 $\frac{\text{ft-lb}}{\text{lb}}$ based on an average fragmenting stress of 90 percent of the yield stress for AISI 4130 steel.

Invertube

The invertube, illustrated in Figure A-5, absorbs energy in the process of turning a tube inside-out or outside-in. This device has a very high stroke efficiency since the total displacement is approximately twice the length of the working tube.

Reference A-3 gives an analytical derivation of the expression for inversion load (P) as a function of tube material plastic yield stress (σ_P), tube wall thickness (t) and tube mean diameter (D):

$$P = 4.44 \ \sigma_P t^{3/2} D^{1/2} \qquad (1)$$

Some results using this equation are compared with experimental data in Figure A-6. Use of the load equation for tubing material other than 3003-H14 aluminum alloy would require experimental verification since certain assumptions used in the derivation of the equation may be satisfied to differing degrees with various materials.

Figure A-7 contains rate sensitivity data for aluminum invertubes tested in the experiments reported in Reference A-3. A small percentage increase in load is observed for increasing deformation speeds. The highest velocity for which data were obtained is about 20 MPH.

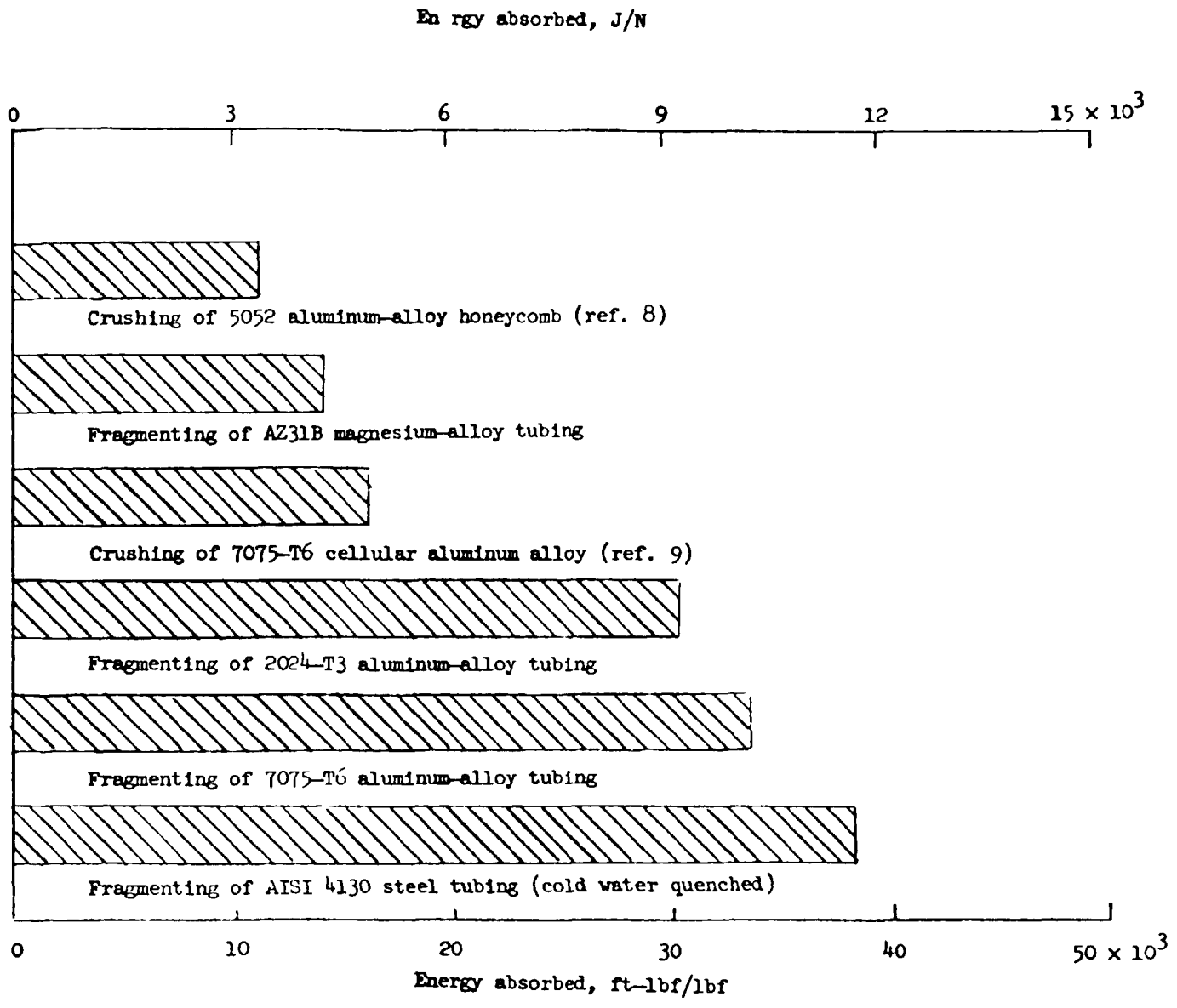

Figure A-4 ENERGY ABSORPTION CAPABILITIES OF VARIOUS MATERIALS AND PROCESSES

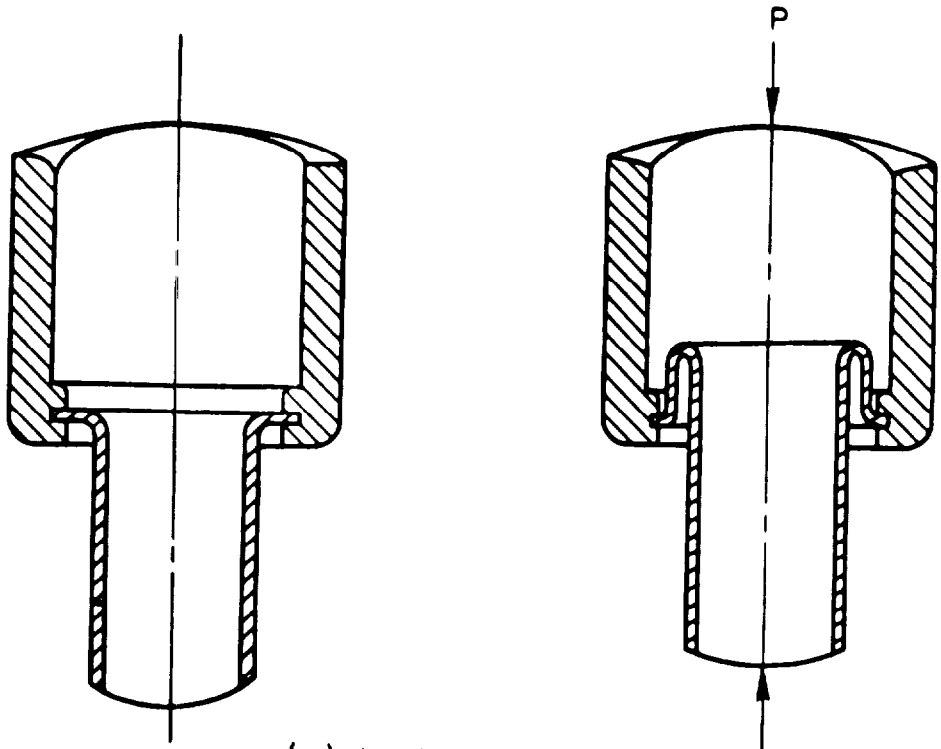

(a) Inside - out inversion

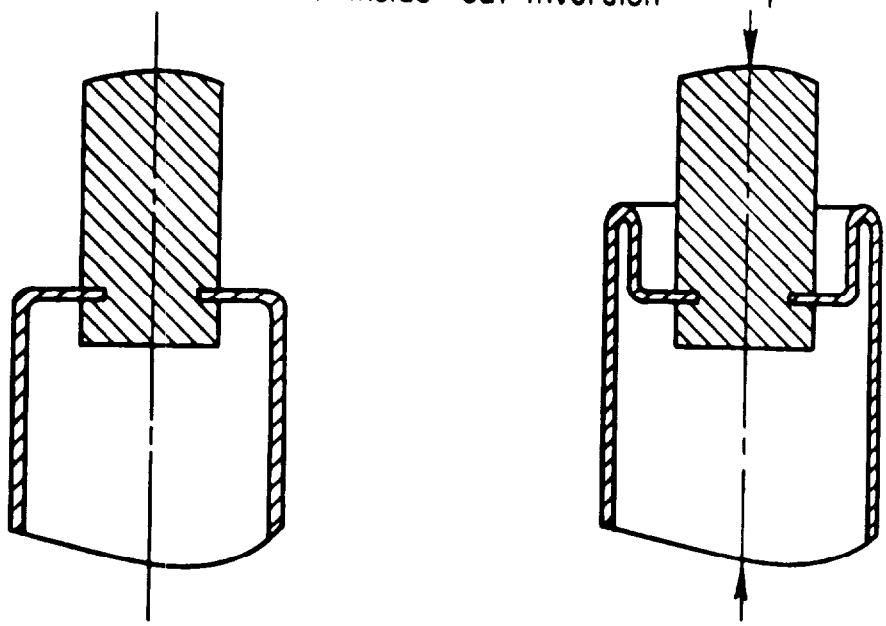

(b) Outside - in inversion

Figure A-5 INVERTUBE ENERGY ABSORBER

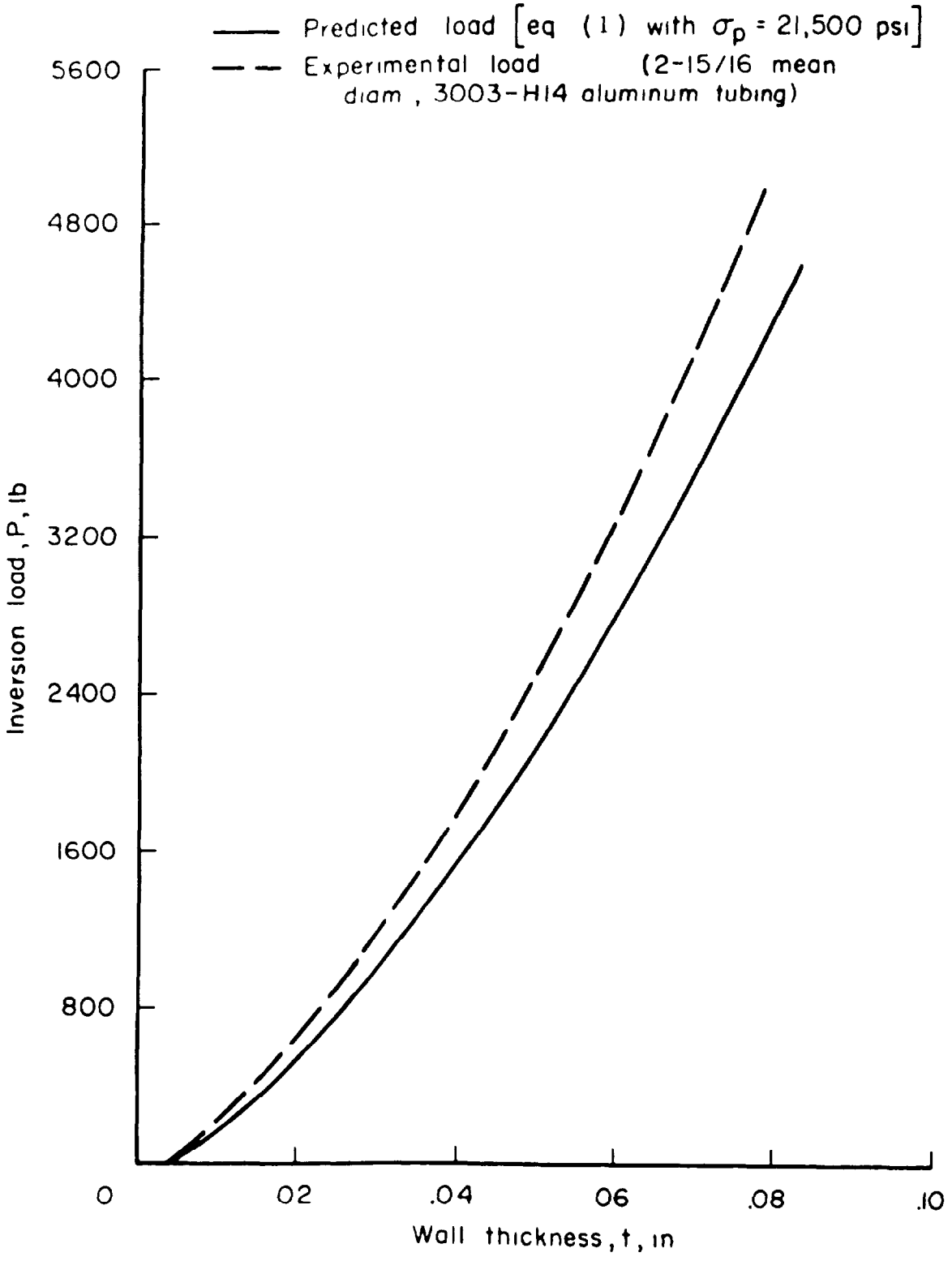

Figure A 6 COMPARISON OF PREDICTED AND EXPERIMENTAL INVERSION LOADS

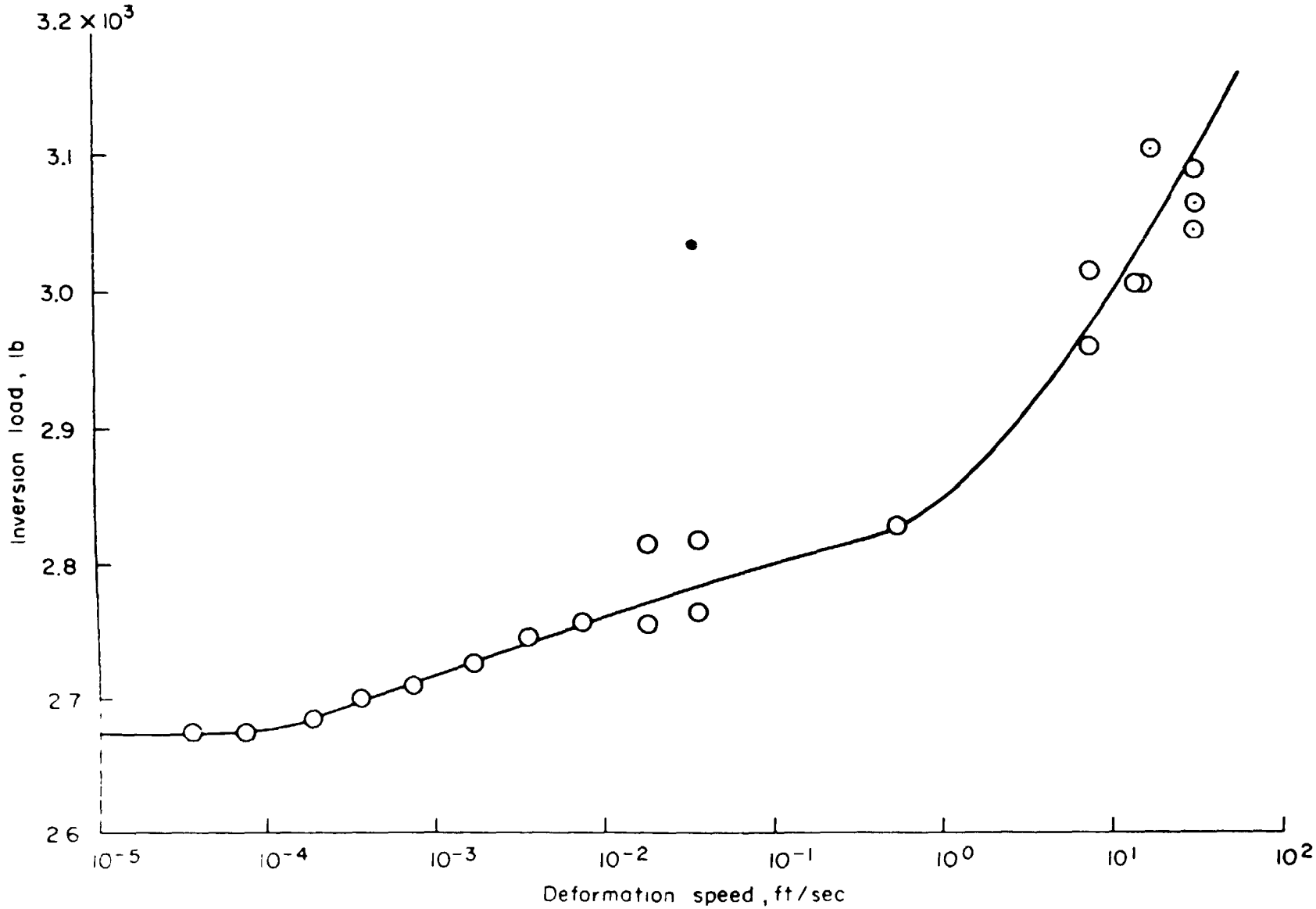

Figure A-7 EFFECT OF INVERTUBE DEFORMATION RATE

Figure A-8 indicates the computed specific energy absorption using the computed inversion load. Since the computed inversion load is conservative, i.e., less than experimental, the computed value of SEA will also be conservative. The maximum value of SEA for 3003-H14 aluminum tubing is greater than 7,500 $\frac{\text{ft-lb}}{\text{lb}}$. Steel tubing should give a higher SEA based on yield stress and density considerations, however, since ductility is also a necessary consideration for successful operation of the device, experimental verification of the satisfactory performance of high strength steels in invertube applications is necessary before conclusions can be drawn concerning the relative merits of steel and aluminum.

Tube Shredder

The tube shredder (Figure A-9) dissipates energy by cutting a hollow tube into strips in the longitudinal direction using a gear shaped multi-toothed cutting tool applied to one open end of the tube. Figure A-10 shows a typical force-displacement curve for the tube shredder. Limited test results using 2024-T3 aluminum tubes (Reference A-4) indicated no variation in mean cutting force with impact velocity variation from 3-12 feet per second and impact weight variation from 600-1000 pounds.

Specific energy absorption values obtained, assuming 100 percent stroke efficiency, were 11,000 $\frac{\text{ft-lb}}{\text{lb}}$ based on tube weight only and 6,000 $\frac{\text{ft-lb}}{\text{lb}}$ based on weight of tube and fittings.

The above results were obtained using a square cutter tooth geometry. Preliminary development tests showed that a sharp cutter geometry produced larger oscillations in cutting force and a high rate dependence.

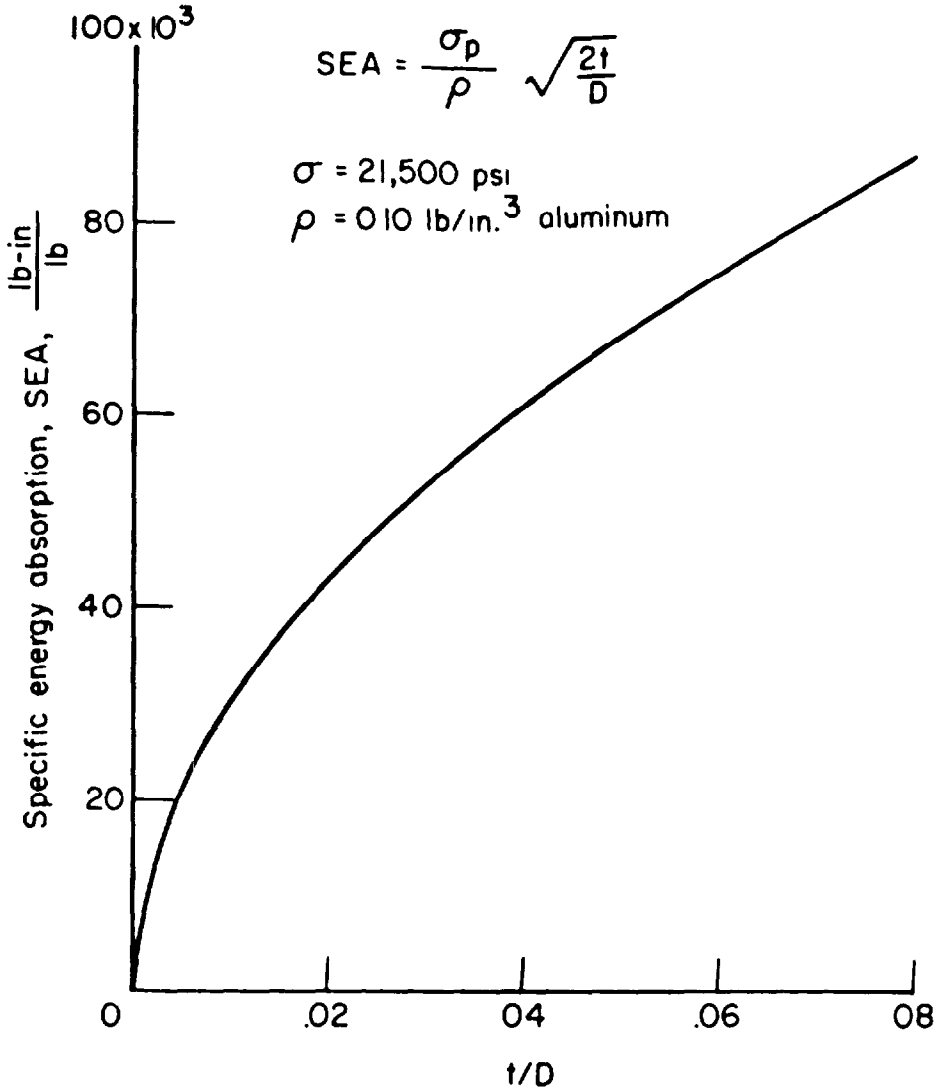

Figure A-8 INVERTUBE ENERGY ABSORPTION EFFICIENCY

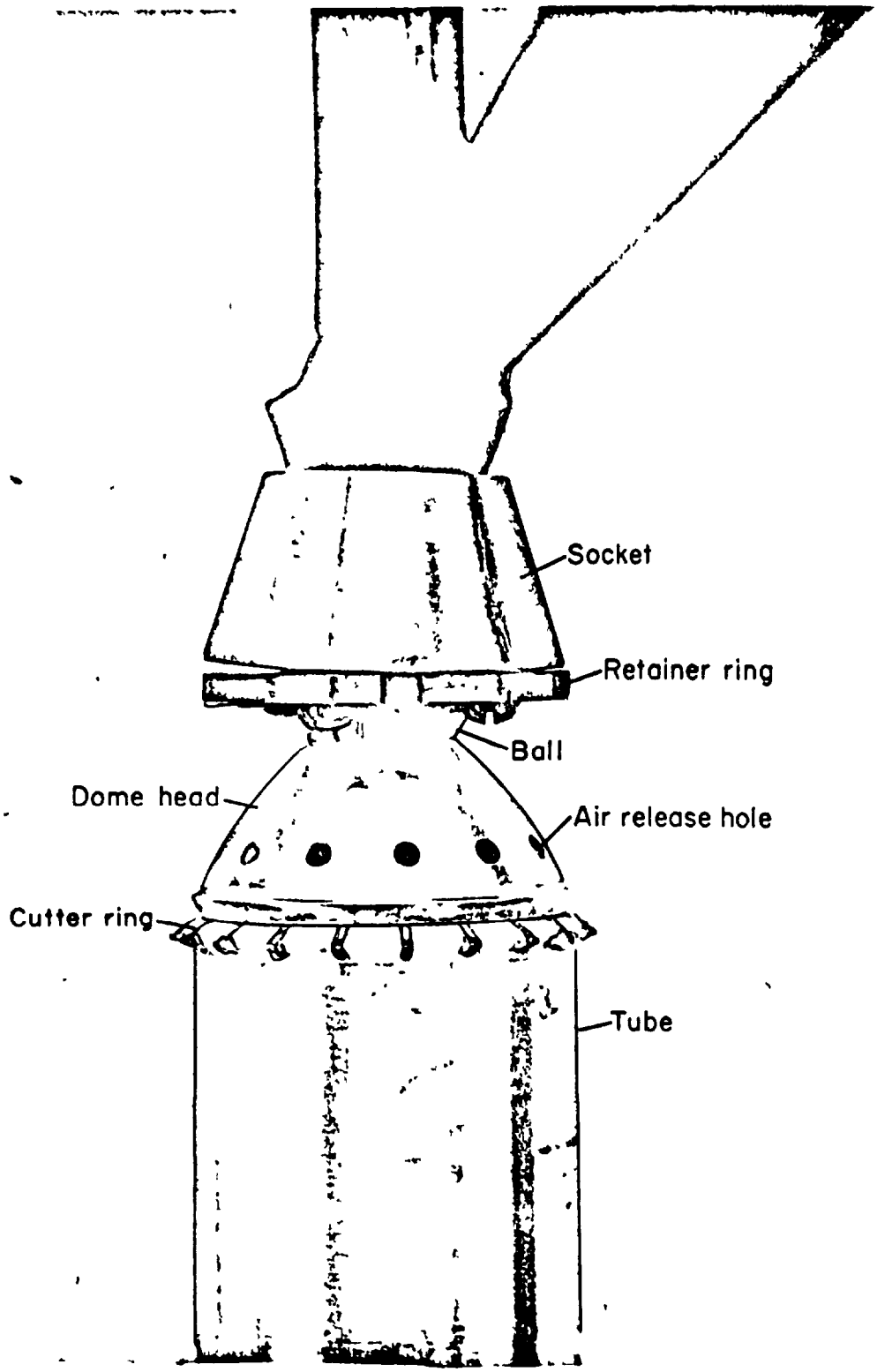

Figure A-9 CUTTING END OF FINAL ASSEMBLED MODEL TUBE SHREDDER

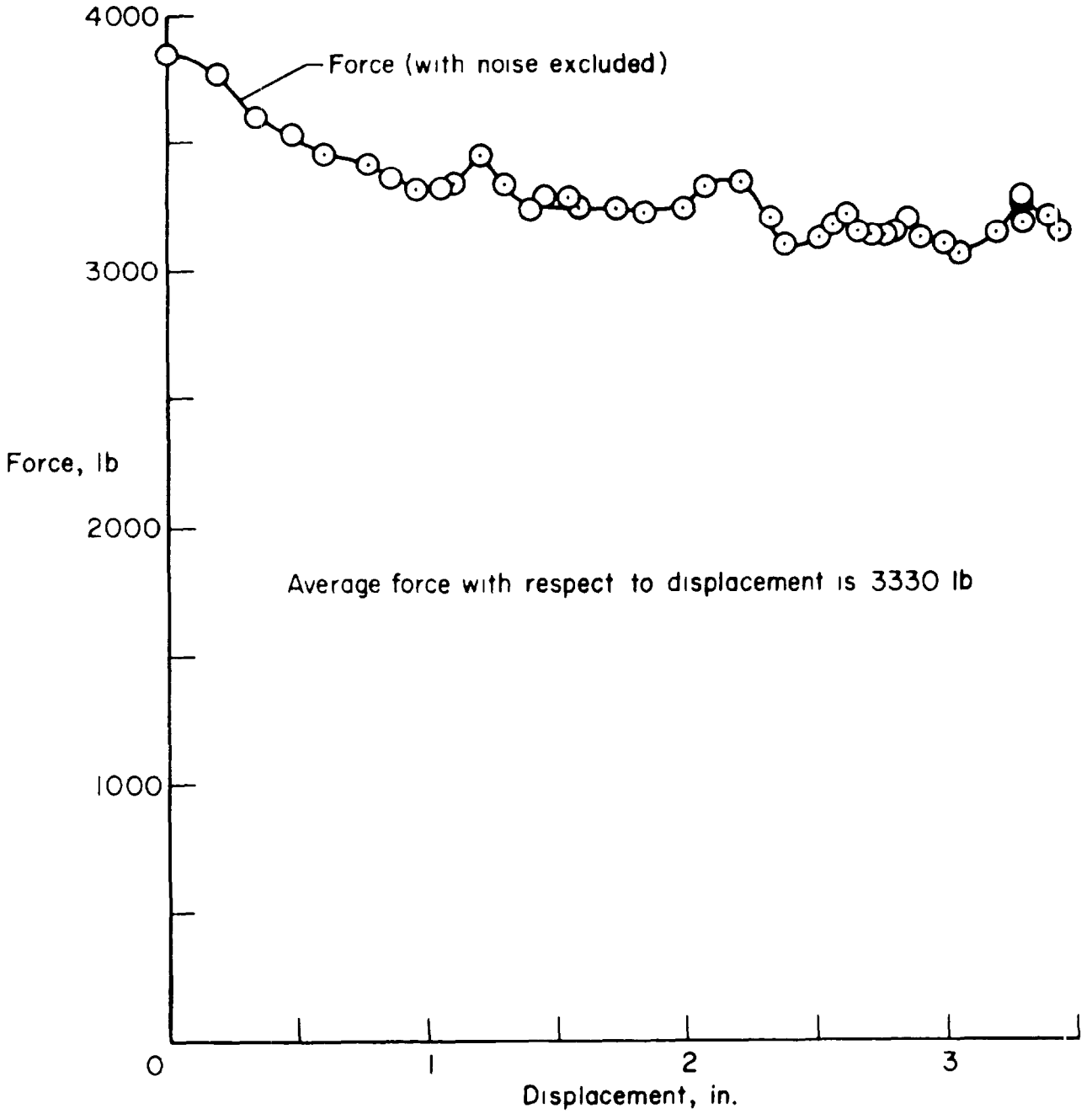

Figure A-10 TUBE SHREDDER FORCE vs DISPLACEMENT FOR ESTIMATED IMPACT VELOCITY OF 7.5 FT/SEC, MEAN WALL THICKNESS OF 0.0355 IN. WITH PRECUT

Friction Tube

The "friction tube" is shown in Figure A-11, both disassembled and mounted in a testing machine. The concentric tubes are connected by a high strength steel (4130) pin which, when the tubes are displaced, travels through a slot which is narrower than the diameter of the pin. This causes the inner tube to expand until the adjoining surfaces mate. Energy is thus dissipated by a combination of metal working and friction, the relative effectiveness depending on the amount of clearance between the tubes, size of slot, pin size and friction coefficient.

Figure A-12 is a plot of the static load-deflection data for a friction tube fabricated from 12 inch lengths of 3" O.D. x 9/32" wall and 2-3/8" x 3/16" cold-drawn seamless steel pipe. The mating surfaces were sandblasted to increase the friction coefficient and to improve the surface uniformity. A compressive static test was performed, although the concept has the advantage of being applicable in both tension and compression. It is apparent from the results shown in Figure A-12 that the device generates a very uniform and substantial force once the pin is fully engaged in the slot. The specific energy absorption is about 1,600 $\frac{\text{ft-lb}}{\text{lb}}$ for the particular tube tested, however, this value does not necessarily represent an optimum performance. Further tests using other materials would be necessary to define the maximum specific energy absorption capabilities of this device.

Results from dynamic drop tower tests of the friction tube energy absorber described in Appendix B indicate that the average dynamic force produced is about 50 to 60 percent greater than that measured in static tests.

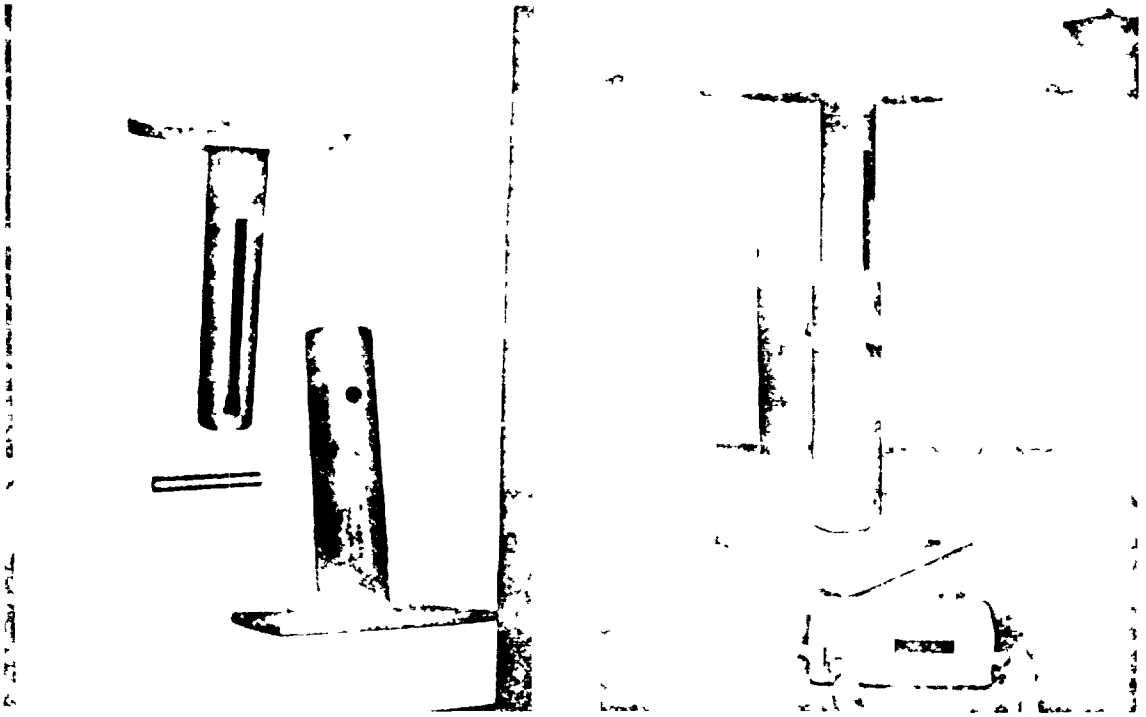

BEFORE TEST

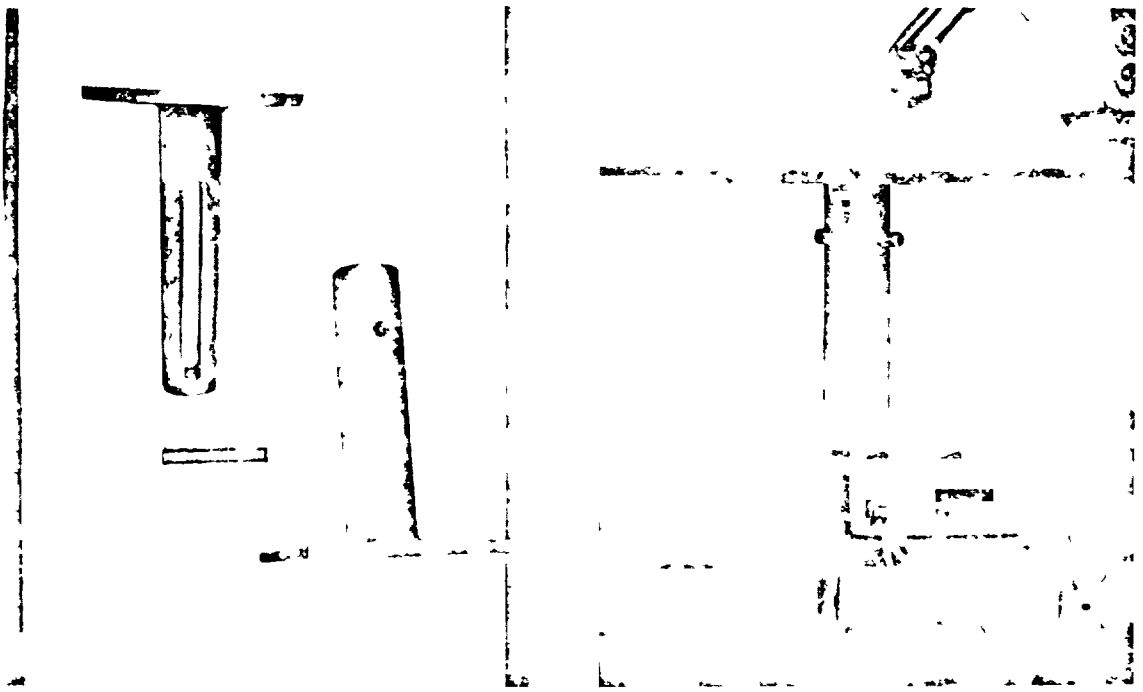

AFTER TEST

Figure A 11 FRICTION TUBE ENERGY ABSORBER

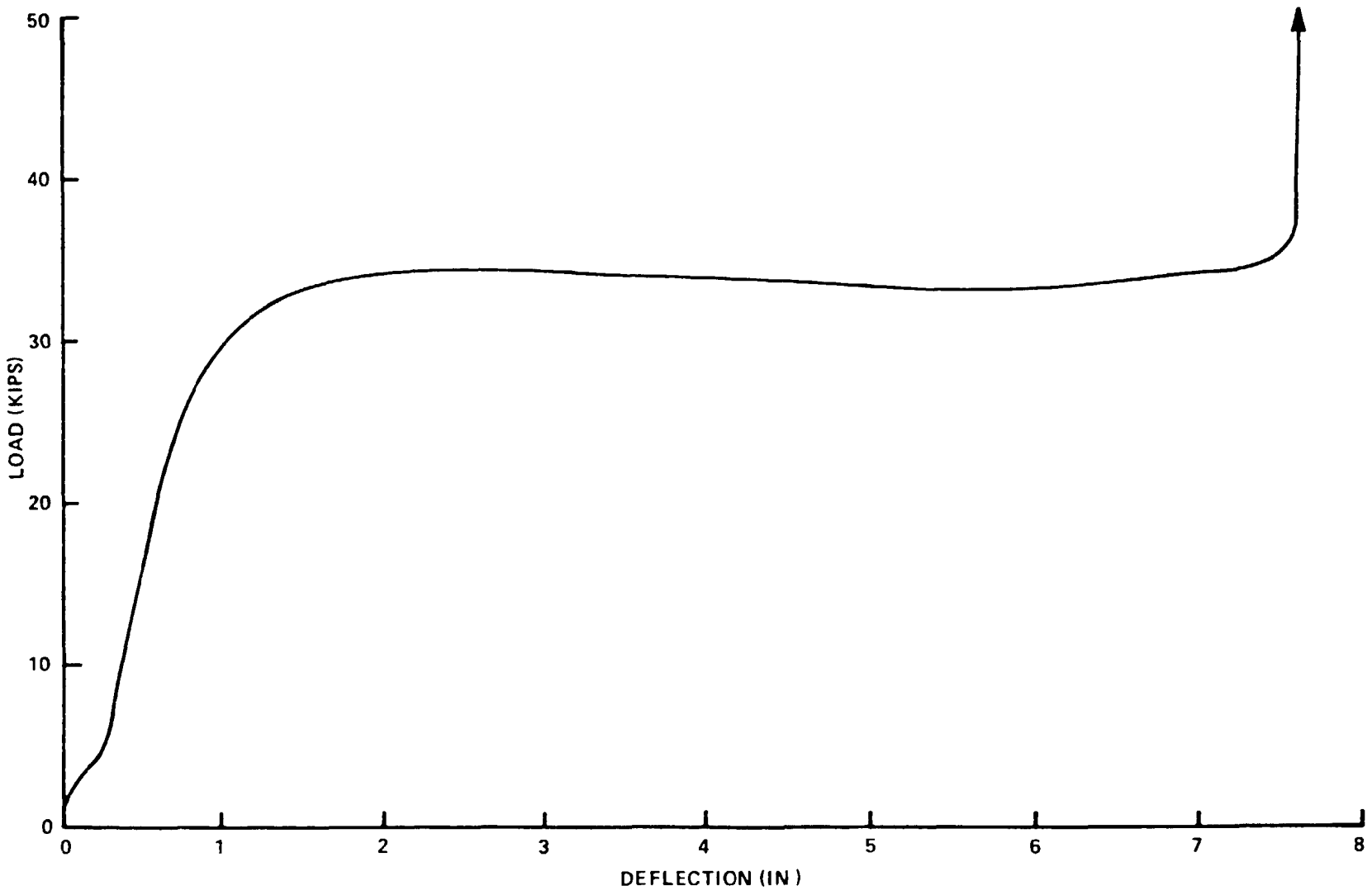

Figure A-12 LOAD-DEFLECTION BEHAVIOR OF FRICTION TUBE

Aeronautical Research Laboratory (Australia) Energy Absorber

This device absorbs energy by plastic bending of two metal strips. The principle is shown in Figure A-13. Two strips -- ABCD and $A_1B_1C_1D_1$ -- each initially bent to a U-shape fit in a case EH, E_1H_1 and are fixed to the case at A and A_1 (Figure A-13(a)). When the device is extended by tension, applied between the case and the inner arms of the strips CD, C_1D_1, the part of the strip adjacent to B and between A and B is bent to a radius and that adjacent to C is bent straight. The force F required to extend the absorber is a function of the resistance to bending at these points.

Straightening of the bend at C and C_1 may cause the inner and outer strips to contact one another (as shown in Figure A-13 (b)). The contact forces at these points are small (compared to F) and as they are the only places at which rubbing occurs, the friction forces opposing extension are small, thus the extension force is not sensitive to the degree of lubrication and/or surface finish.

The total extension is approximately equal to the length of the strip and thus nearly twice the length of the case. Figure A-13 shows that for an extension X the bend radii move along the case by an amount X/2.

A simple theory of operation developed in Reference A-6 for this device yields the result that the extension force (P) is proportional to the strip width (W), the second power of strip thickness (t) and inversely proportional to the distance (d) between the inner and outer parts of the strip.

$$P = K\frac{wt^2}{d} \quad . \qquad (2)$$

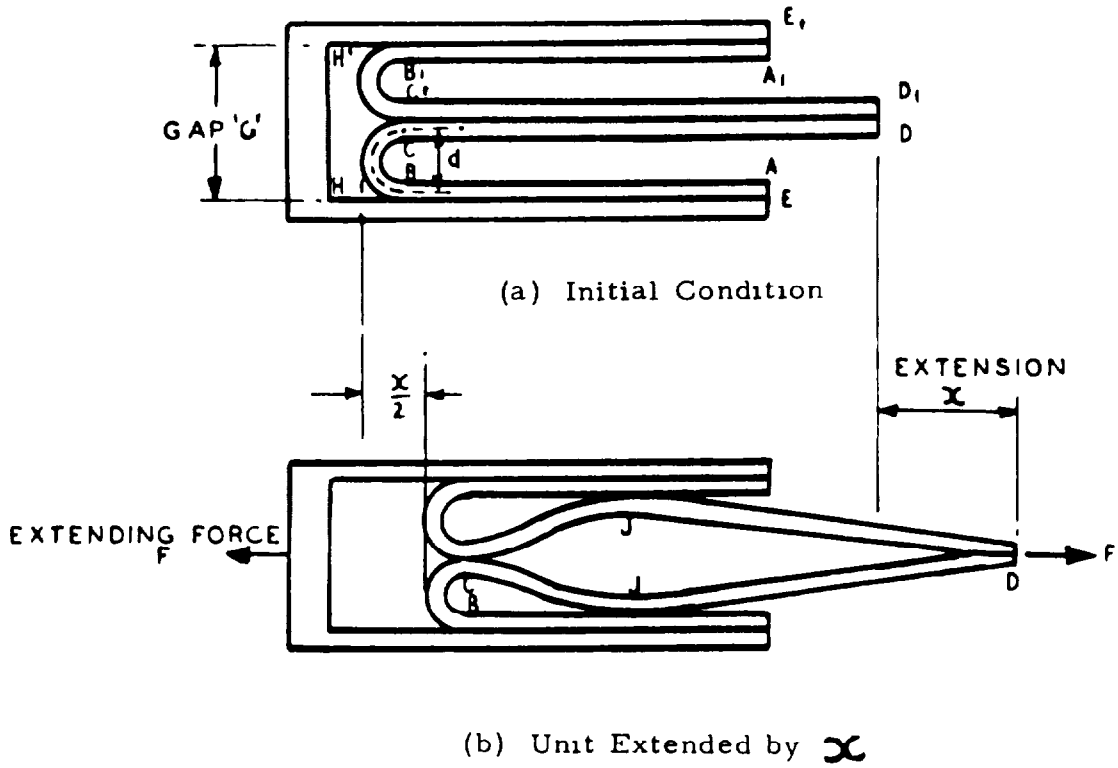

Figure A-13 ARL (AUSTRALIA) ENERGY ABSORBER

Experimental results from the work reported in Reference A-6 indicate that $K \approx 70,000$ for steel strips and $K \approx 25,000$ for aluminum strips.

This device produces a constant force which is insensitive to the rate of deformation. The specific energy absorbed was approximately 900 $\frac{\text{ft-lb}}{\text{lb}}$ for the device tested. Tension loads only can be absorbed with this device. A rotary version applying the same operating principle is described in Reference A-6.

Tor-Shok

The "Tor-Shok" or Rolling Ring Cyclic Energy Absorber shown in Figure A-14 and described in detail in Reference A-7 and A-8 consists of two concentric tubes of different outside diameters to allow one tube to fit loosely inside the other. The clearance space between the two tubes contains one or more toroidal retainer rings, each of which hold a family of small working ring elements. The diameter of the working rings is greater than the clearance gap between the two concentric tubes producing an interference fit. A force applied to either of the tubes causes a relative displacement of the tube. The resultant shearing action between the two tubes rolls the working rings and thereby, plastically deforms each of them in a cyclic process.

The main advantages of the Tor-Shok are its ability to function in either tension or compression, high specific energy absorption attributable to multi-stroke capability before fatigue failure, and low maintenance and ability to check-out before use as a result of its multi-stroke capability.

Tor-Shok devices are relatively velocity insensitive with only a very slight negative sensitivity, and they produce a very repeatable constant force response. Figure A-15 shows the force, velocity and acceleration characteristics of a Tor-Shok weighing 13.6

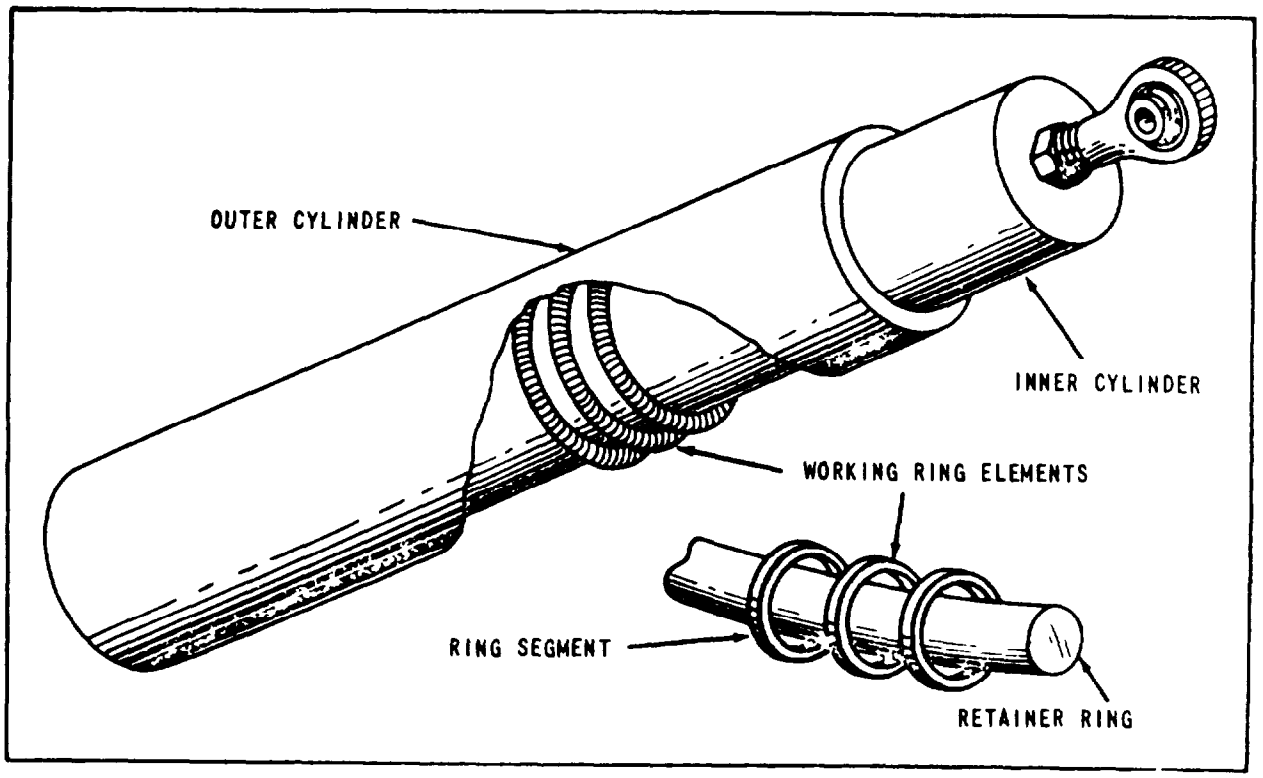

Figure A-14 TOR-SHOK DEVICE

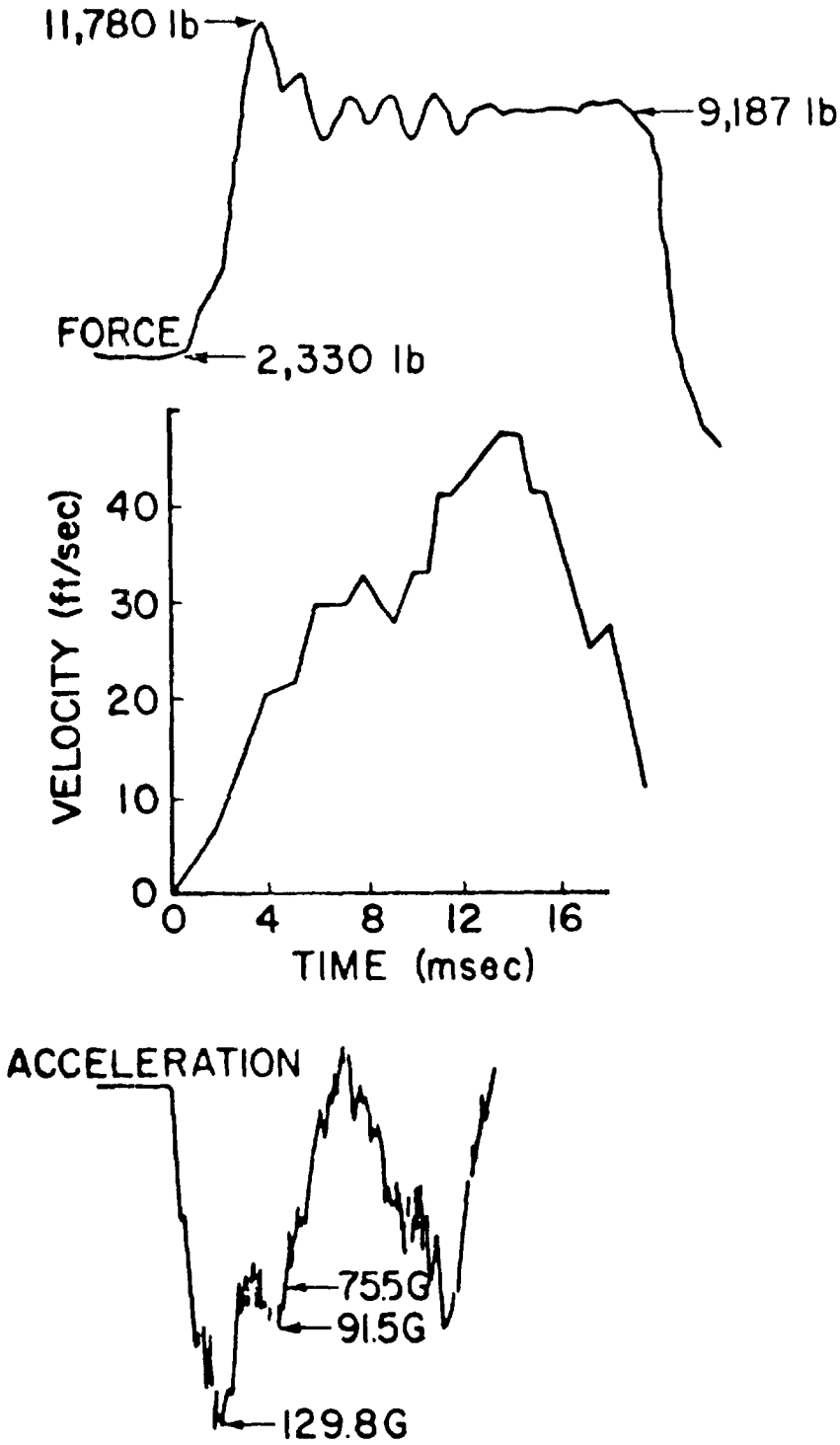

Figure A-15 TYPICAL HIGH VELOCITY DATA FOR TOR-SHOK DEVICE

pounds. The specific energy absorption for the device of Figure A-15, based on a maximum stroke length of 20 inch s (comput d from drawing in Reference A-8) is approximately 1,100 $\frac{\text{ft-lb}}{\text{lb}}$.

Solid Media Shock Absorber

Solid media energy absorbers dissipate impact energy by employing the viscoelastic properties at extremely high pressures of certain newly developed silicone elastomers. As the energy absorber shortens under an impact load, elastomeric material contained therein is simultaneously reduced in volume and forced through small orifices and passages. The volume reduction phenomena produces the equivalent effect of a powerful mechanical spring, while the material flow causes the unit to perform as though it were a hydraulic damper.

The spring effect serves two useful functions: (1) prevention of the shock absorber from shortening under sustained loads such as are encountered when one vehicle is pushing another, and (2) to reposition the device (elongate) after an impact.

The hydraulic effect of the device produces a positive impact velocity sensitivity. Figure A-16 shows the force-stroke and velocity sensitivity characteristics of a bumper system employing solid media shock absorbers.

The specific energy absorption capability of solid media shock absorbers is about 500 $\frac{\text{ft-lb}}{\text{lb}}$.

Viscoelastic materials are those in which stress depends on strain and strain rate.

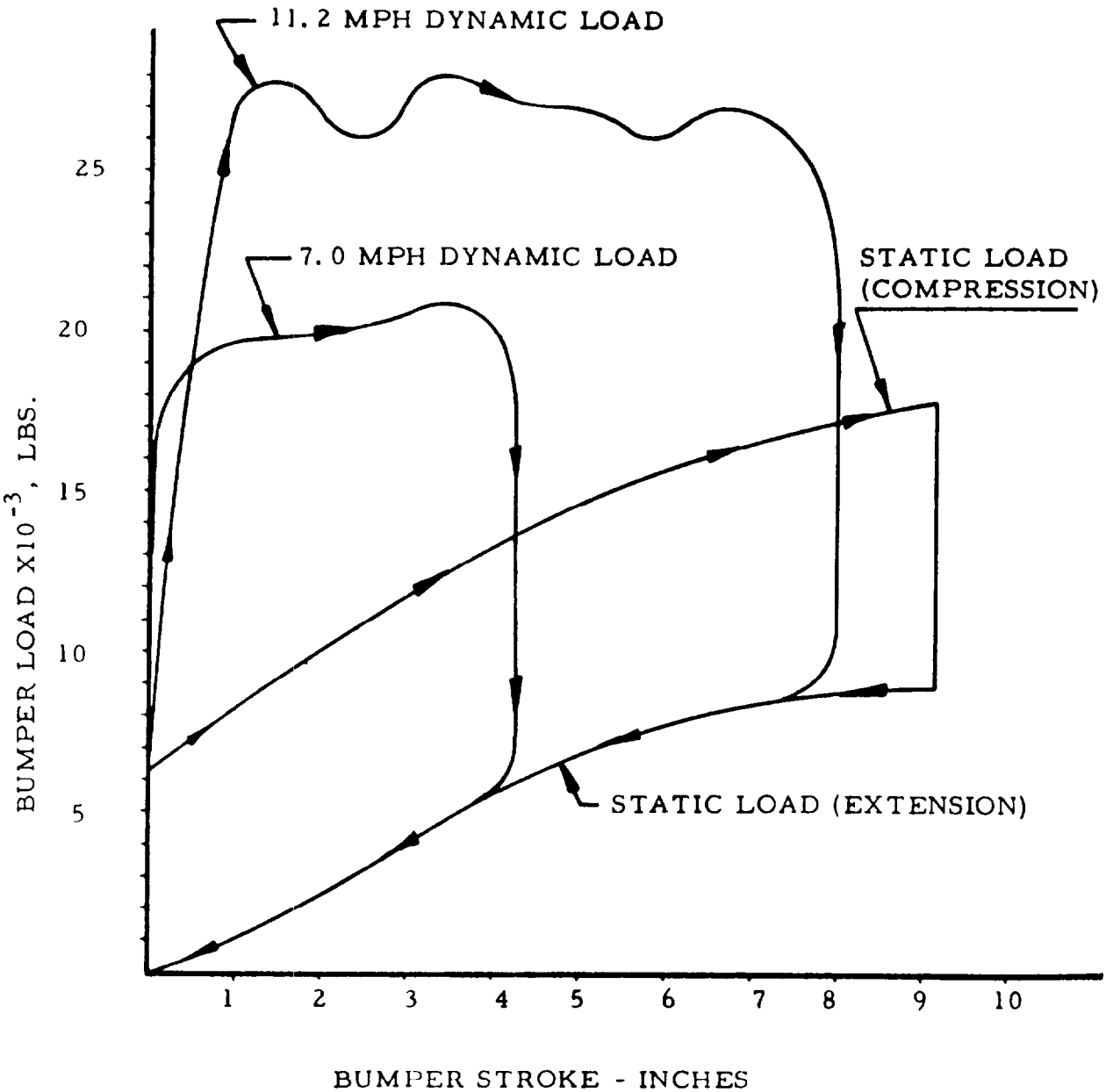

Figure A-16 FORCE-STROKE CHARACTERISTICS OF A SOLID MEDIA SHOCK ABSORBER BUMPER SYSTEM

Plastic Hinges

A simple concept for absorbing energy is the plastic deformation of metal at the hinge point of two structural arms which undergo a relative angular displacement. One such device, shown in Figure A-17, is a "knee strut" consisting of two sections of rectangular tubing welded together. Experimental data from Reference A-10 for a knee strut is shown in Figure A-18. The specific energy absorption calculated for the data given in Figure A-18 is about 1,000 $\frac{\text{ft-lb}}{\text{lb}}$.

A more sophisticated plastic hinge is shown in Figure A-19. For this device, all the energy is absorbed in plastic deformation of the hinge pin which is subjected to torsional loading. This plastic hinge device would be expected to have higher specific energy absorption and a more uniform force-deflection characteristic than the knee strut. Unfortunately, no experimental data are available for this type of plastic hinge.

II. Crashable Materials

Three basic types of crushable materials which may be considered as possible energy dissipators for truck underride guards or automobile bumpers are honeycomb, balsa and foamed plastic. A brief description of a representative material from each basic group will serve to indicate the prominent energy dissipation characteristics.

Honeycomb

Honeycomb structures can be made from a variety of materials including paper and metal. However, only metal honeycomb, specifically aluminum, will be discussed here since it appears that lighter materials, such as paper, have too low an energy dissipation density for application to underride guard on automobile bumper systems. Aluminum

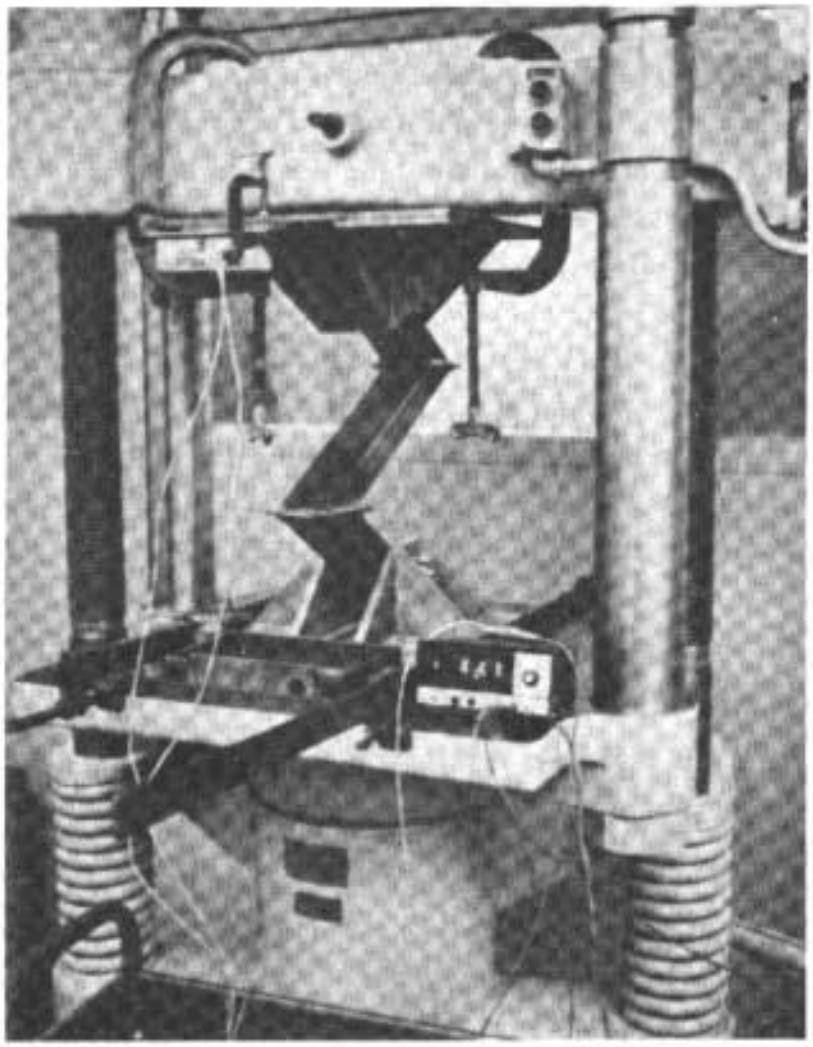

Figure A-17 STATIC TEST OF TUBULAR KNEE

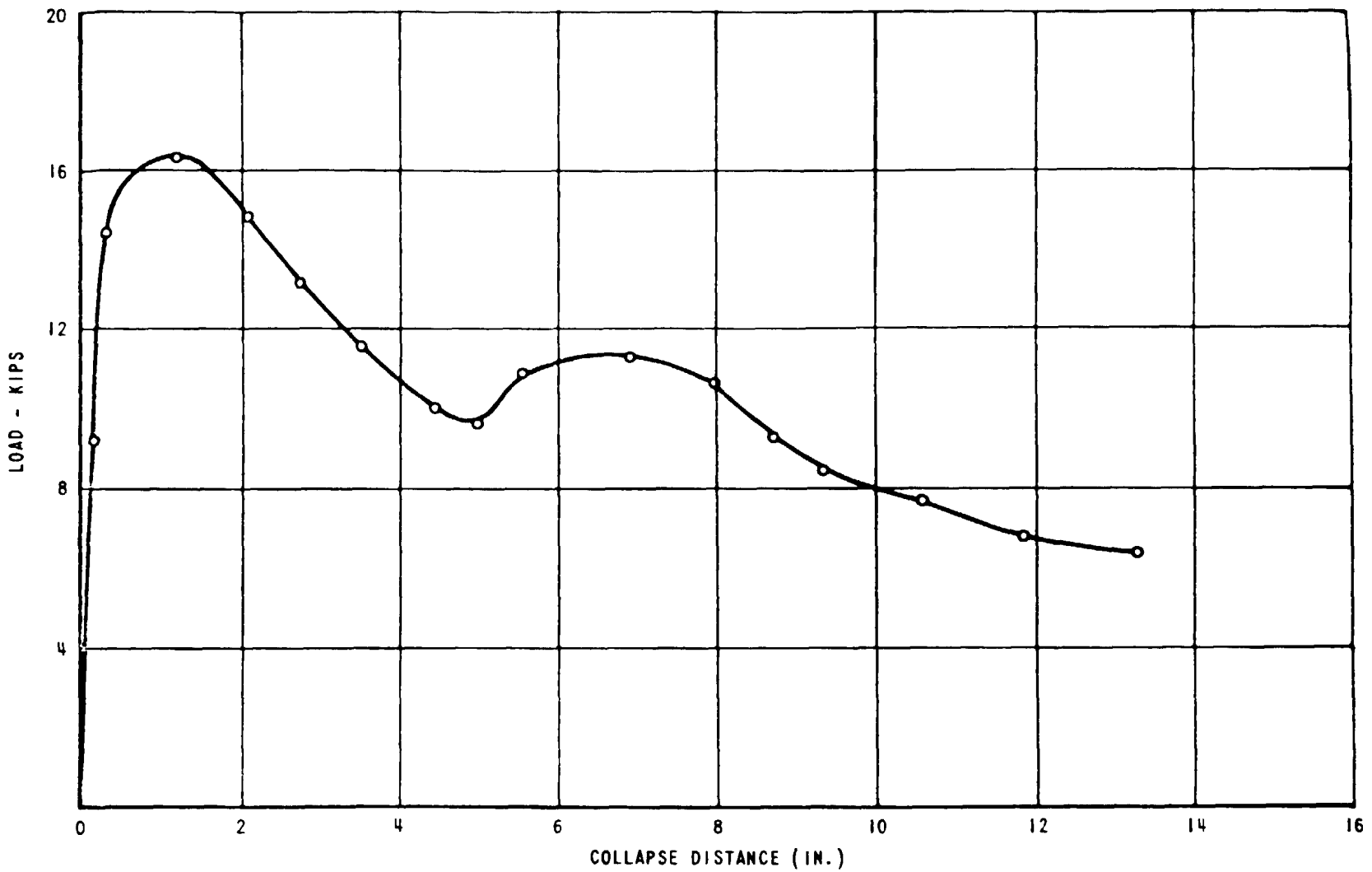

Figure A-18 STATIC TEST RESULTS FOR KNEE STRUT

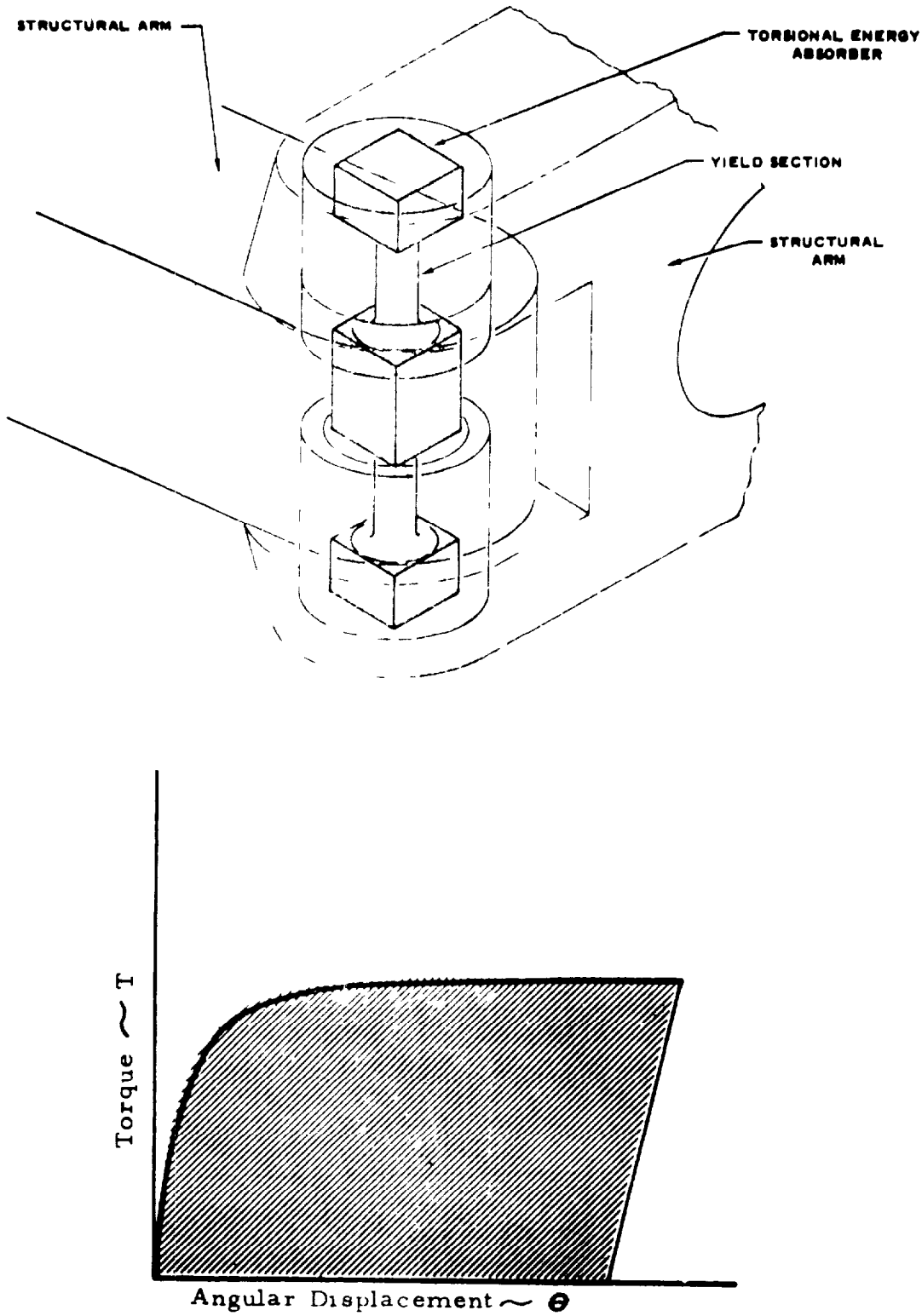

Figure A 19 TORSIONAL PLASTIC HINGE

honeycomb performance in crush is reported in References A-12 through A-15. The material responds to impact with an essentially constant force and is velocity insensitive. Figure A-20 is a force-stroke diagram, and Figure A-21 is a plot of average crush load as a function of impact velocity. The maximum experimentally observed specific energy absorption for aluminum honeycomb was 10,000 $\frac{\text{ft-lb}}{\text{lb}}$ as reported in References A-12 and A-13.

Balsa Wood

Balsa wood is a very efficient energy absorber having a value of specific energy absorption ranging from 10,000 to 30,000 $\frac{\text{ft-lb}}{\text{lb}}$ for static crushing depending upon moisture content, temperature and grain orientation relative to the crushing force (Reference A-16). Crushing parallel to the grain gives about a factor of 2.5 increase in specific energy absorbed compared to crushing perpendicular to the grain. Dynamic crushing of balsa wood (Reference A-15) shows approximately the same maximum specific energy absorption values as static crushing, however, dynamic crushing parallel to the grain is accompanied by a violent rebound which is undesirable for many applications. Dynamic crushing perpendicular to the grain exhibits some rebound. The rebound problem can be minimized by using all the energy absorbing capability of the balsa wood, i.e., complete crushing, but a given specimen is then limited to a specific impact velocity. Velocities higher than the "correct" velocity would cause bottoming of the absorbing device with attendant high force levels and velocities lower than the correct value would result in rebound. Consequently, this rebound characteristic would seem to limit the usefulness of balsa wood as an energy absorber for those applications which require satisfactory performance over a range of impact velocities.

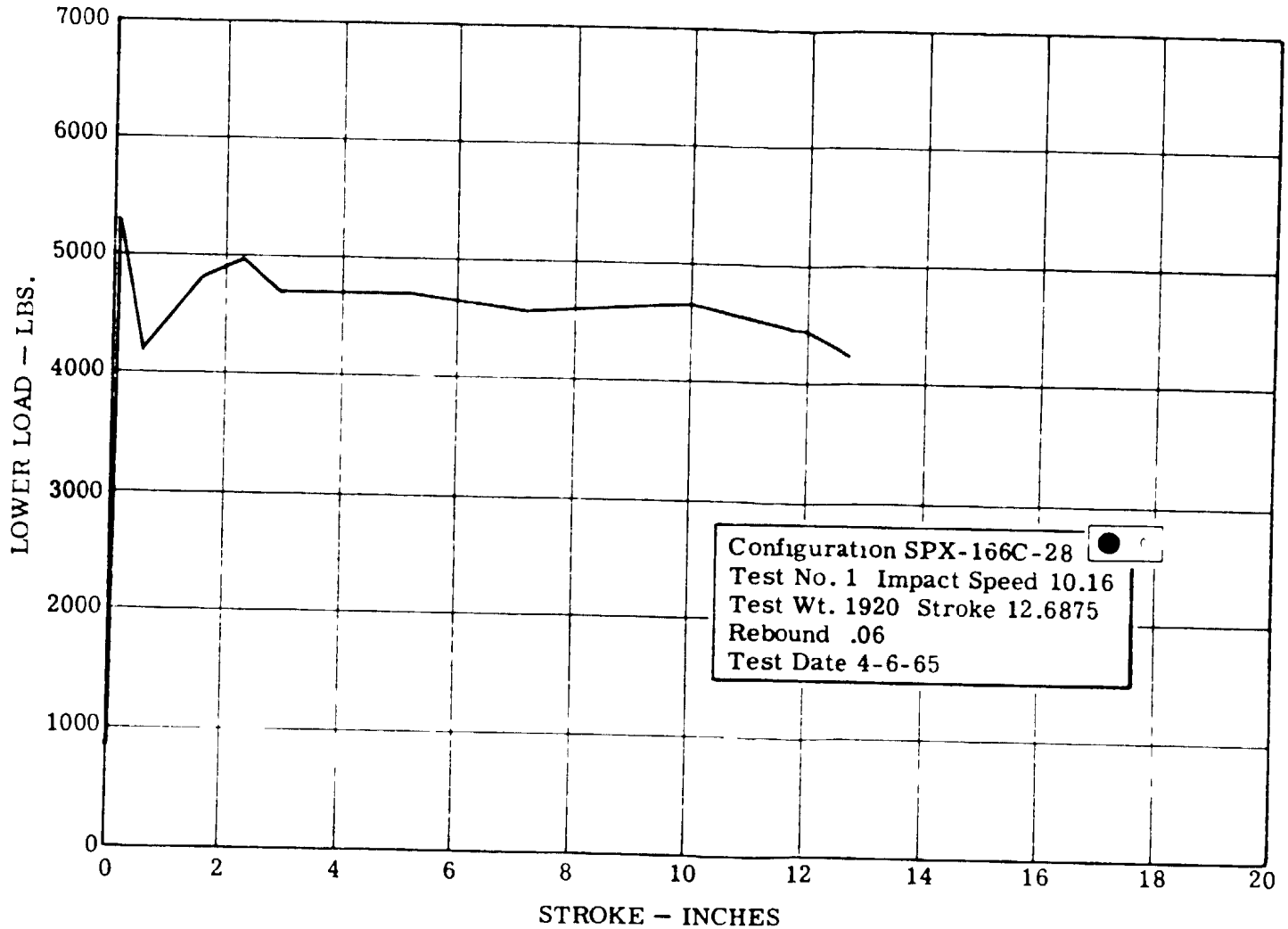

Figure A-20 LOAD vs STROKE FOR ALUMINUM HONEYCOMB

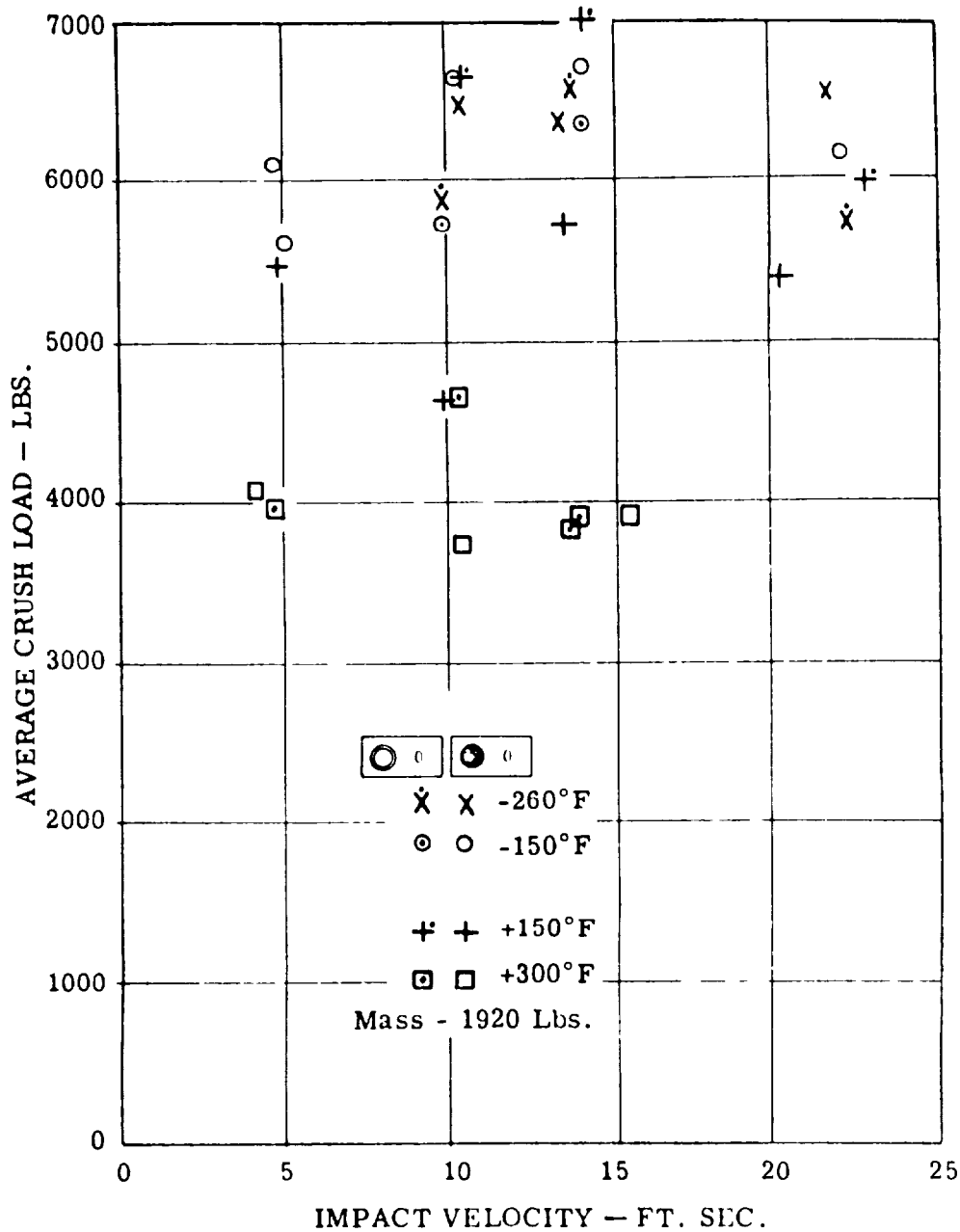

Figure A-21 HONEYCOMB CRUSH LOAD vs IMPACT VELOCITY

Foamed Plastics

Foamed plastics are similar to balsa wood in their crush characteristics for low strains but are different for high strains. Figure A-22 shows the stress-strain characteristics for five different foamed plastic densities and four different impact velocities. It can be seen that the departure from an approximately rectangular force deflection characteristic occurs at about a 40 percent strain beyond which stress increases with strain in a rather smooth manner.

The data shown in Figure A-23 indicate that crushing force is independent of impact velocity. Specific energy absorption based on 40 percent strain for the two types of foamed plastic studied in the work of Reference A-17 is about 1,000 $\frac{\text{ft-lb}}{\text{lb}}$. SEA based on higher strain rates is much higher due to the rapidly rising crushing force as strain increases beyond 40 percent.

III. Hydraulic Shock Absorbers

Hydraulic energy absorbers are velocity sensitive devices which can be designed to provide essentially any load-displacement characteristic desired. Basically, a hydraulic device consists of a piston, fluid-filled cylinder and an orifice through which fluid is forced by the action of the piston. Load-displacement curves are shown in Figure A-24, A-25 and A-26 for three idealized hydraulic devices discussed in Reference A-18. Figure A-24 shows a simple fixed orifice device. The equation for the resisting force produced by this device is

$$F = \frac{1}{2} \frac{V^2 A_p^3 \quad d}{C^2 A_o^2} \tag{3}$$

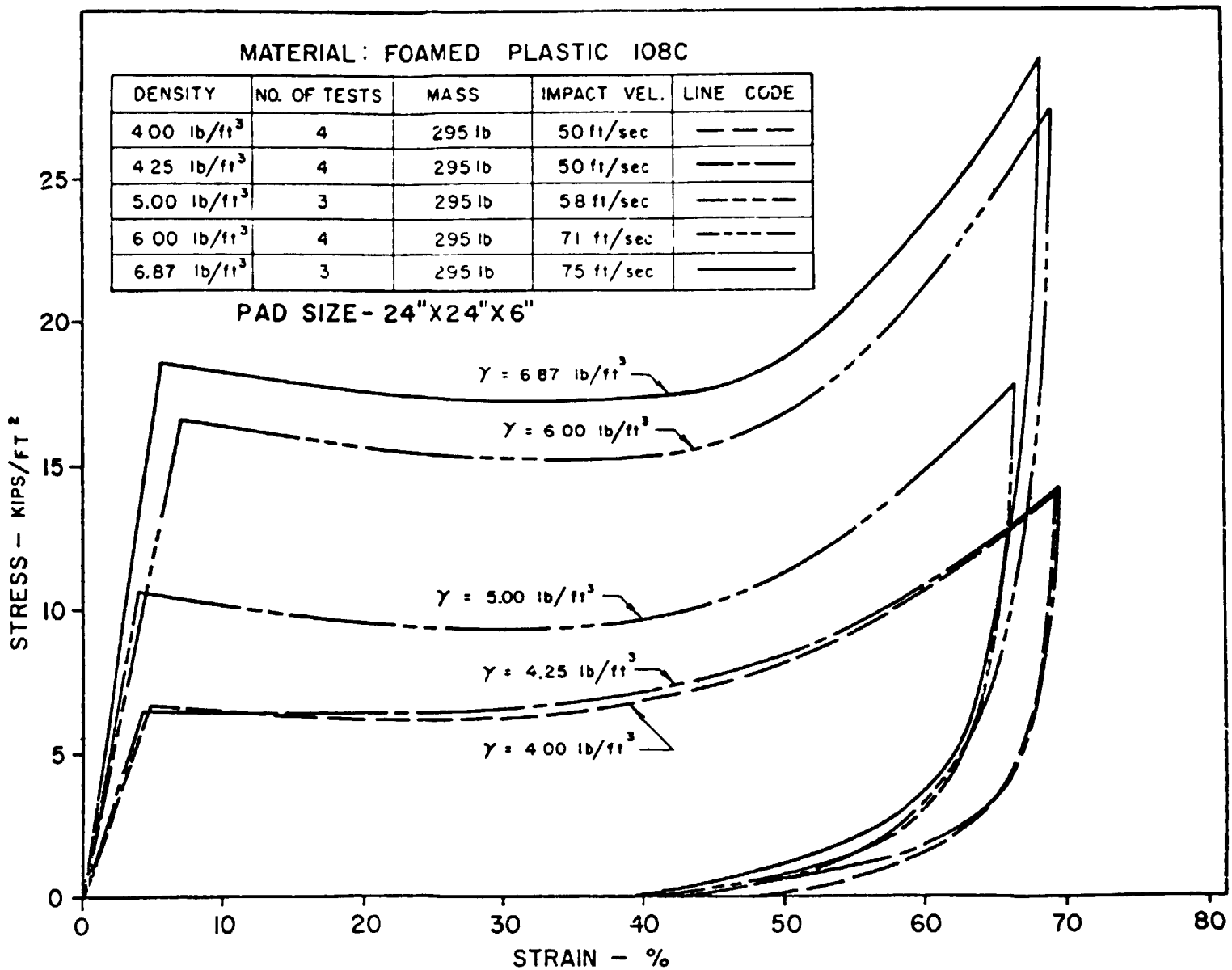

DENSITY	NO. OF TESTS	MASS	IMPACT VEL.	LINE CODE
4.00 lb/ft³	4	295 lb	50 ft/sec	— — —
4.25 lb/ft³	4	295 lb	50 ft/sec	— - —
5.00 lb/ft³	3	295 lb	58 ft/sec	— - - —
6.00 lb/ft³	4	295 lb	71 ft/sec	— - - - —
6.87 lb/ft³	3	295 lb	75 ft/sec	———

Figure A-22 EFFECT OF DENSITY ON THE STRESS-STRAIN CURVE FOR FOAMED PLASTIC 108C

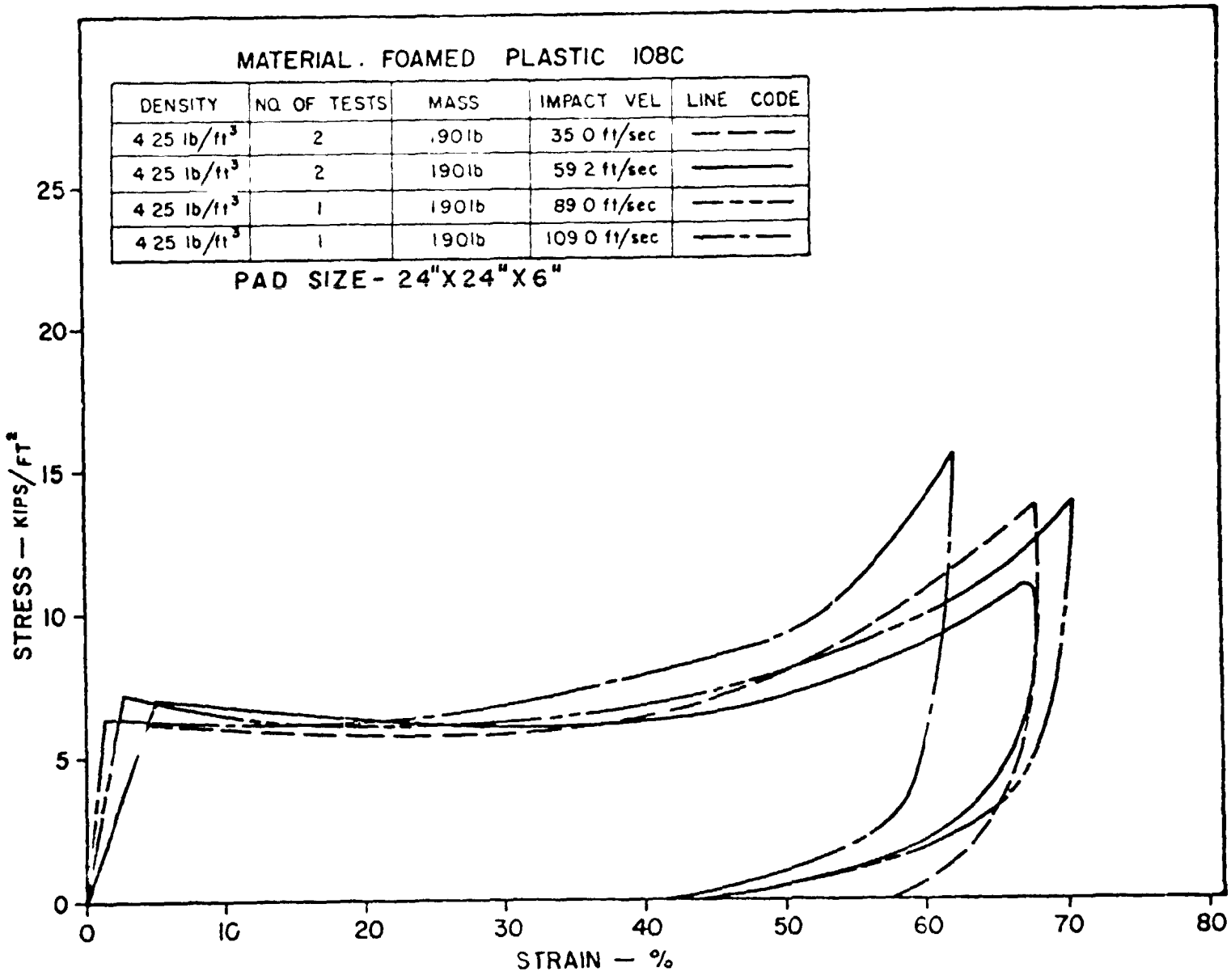

DENSITY	NO. OF TESTS	MASS	IMPACT VEL	LINE CODE
4 25 lb/ft³	2	190 lb	35 0 ft/sec	— — —
4 25 lb/ft³	2	190 lb	59 2 ft/sec	———
4 25 lb/ft³	1	190 lb	89 0 ft/sec	— - - —
4 25 lb/ft³	1	190 lb	109 0 ft/sec	—— - —

Figure A-23 EFFECT OF IMPACT VELOCITY ON THE STRESS-STRAIN CURVE FOR FOAMED PLASTIC 108C

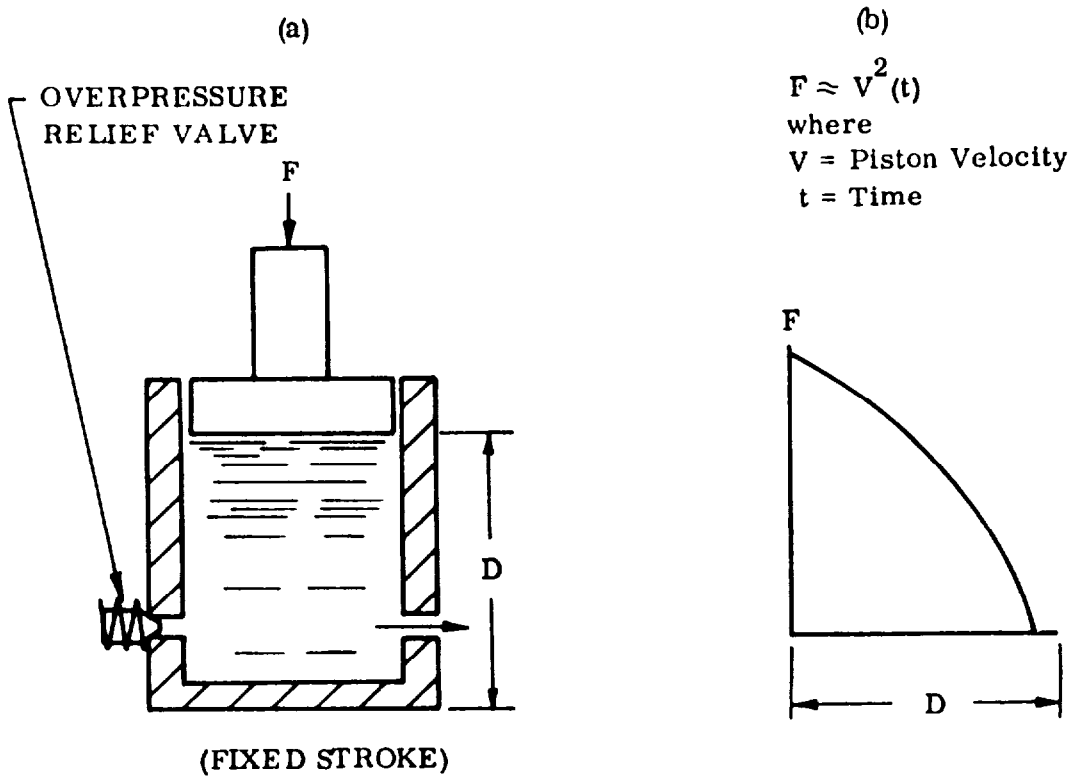

Figure A-24 FIXED ORIFICE CYLINDER CONCEPT

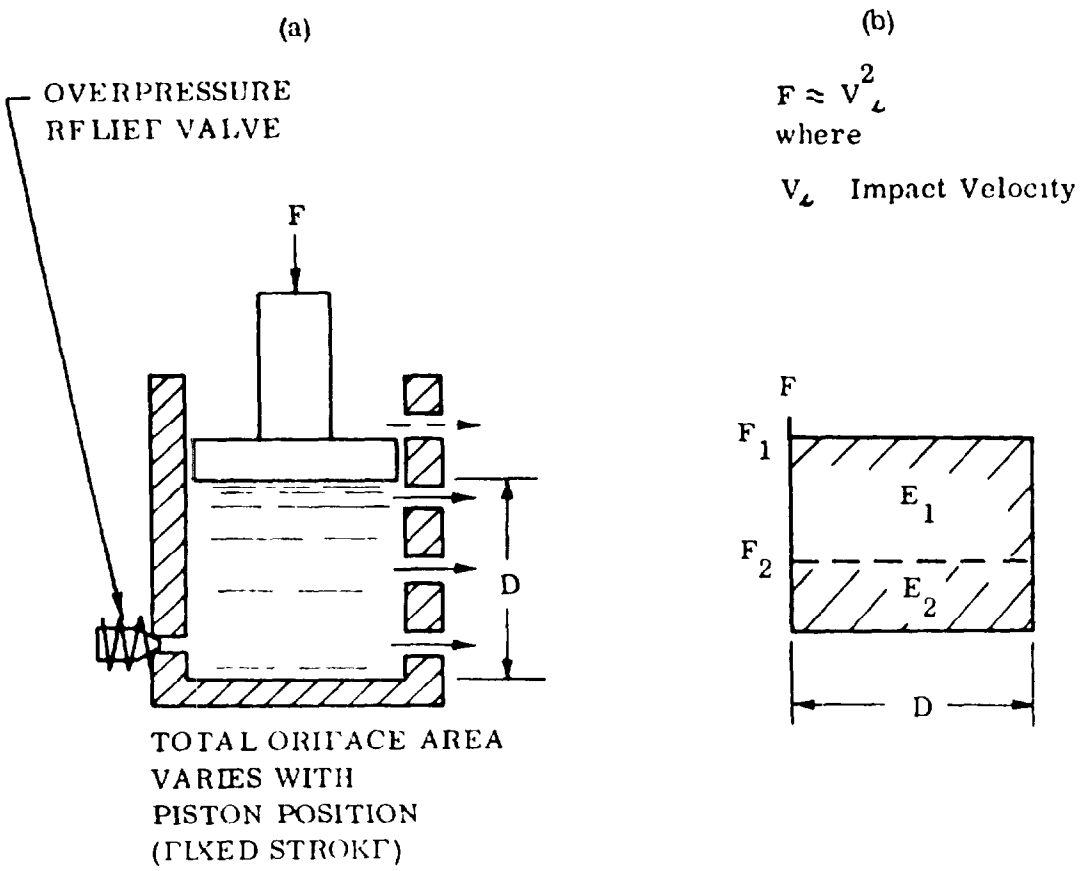

Figure A-25 VARIABLE ORIFICE CYLINDER CONCEPT

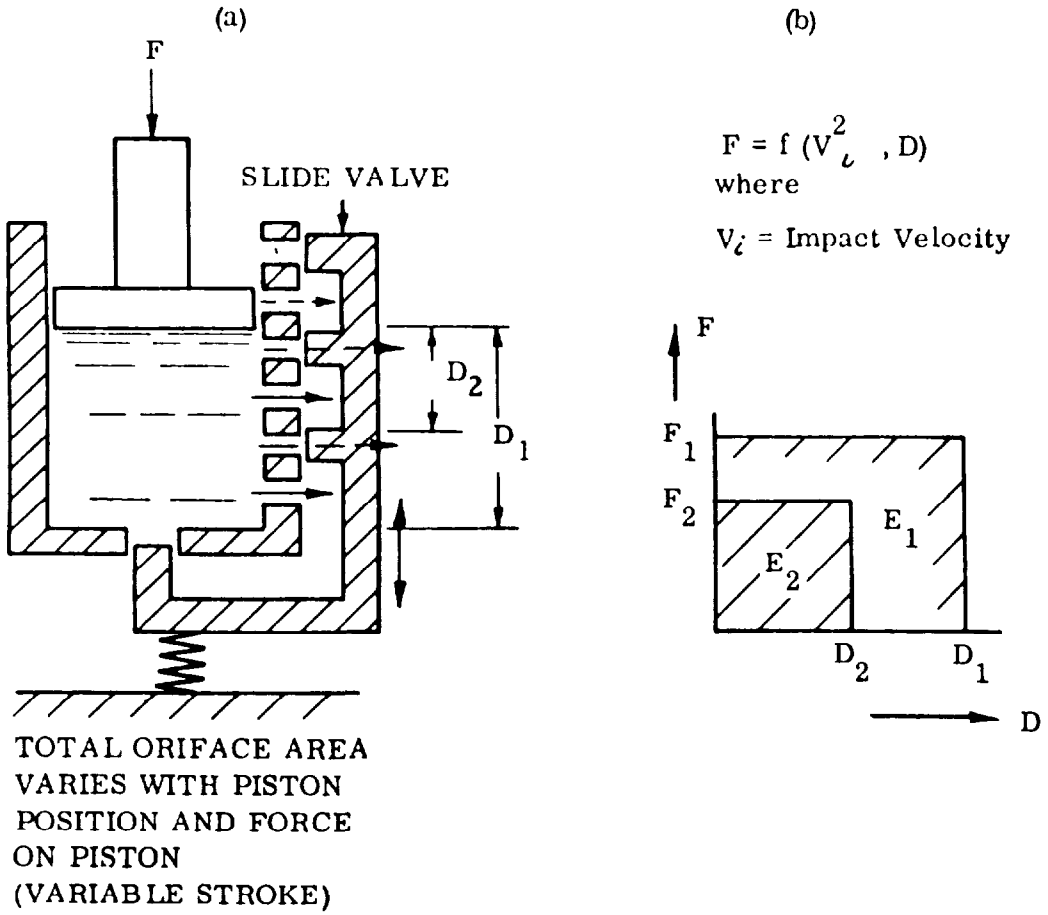

Figure A-26 FORCE PROPORTIONING HYDRAULIC CYLINDER

where

F	=	resisting force
V	=	piston velocity
C	=	orifice coefficient
A_p	=	piston area
A_o	=	orifice area
d	=	fluid density

From the above equation it is readily apparent that, for a given device geometry and fluid density, the force is directly proportional to the square of the piston velocity.

The variable orifice device shown in Figure A-25 produces a constant force throughout the stroke length by reducing the orifice area as the piston moves. The equation for the fixed orifice device also describes the performance of the variable orifice device at the instant of impact. However, in the variable orifice design, as the piston velocity decreases so also does the orifice area such that the ratio of V^2/A_o^2 remains constant. Hence, the device shown in Figure A-25 produces a constant resisting force which is proportional to the square of the impact velocity.

A third type of hydraulic device, shown in Figure A-26, employs a pressure sensitive slide valve in addition to variable orifice area to obtain a force which is proportional to the square of the impact velocity and the first power of the stroke length. The stroke control is achieved by the slide valve which opens more orifices near the bottom end of the device as the fluid pressure (impacting force) increases. The stroke control feature of this device would be advantageous for an automotive bumper design since at low impact velocities the smaller stroke could result in less damage to the automobile than would be sustained with a constant stroke device.

The actual characteristics of hydraulic devices differ somewhat from the idealized performances indicated. Some experimental data are shown in Figures A-27 and A-28. These data, obtained from Reference A-19, show deceleration versus displacement of a mass impacting at three different velocities (Figure A-27) and deceleration versus time and displacement (Figure A-28) for three different weights impacting at the same velocity. An expected deviation from the idealized performance is the finite rise time needed for the resistive force to build up. However, as expected from theory, the average forces (decelerations), based on equal strokes, are approximately in the ratios of the velocity ratios squared for the data of Figure A-27 Figure A-28 indicates a slightly higher average deceleration for the lighter mass than for the heavier masses. This result is not expected, based on hydraulic effects only, however, mechanical friction effects could account for the discrepancy.

Concluding Discussion

The energy dissipation methods examined in this literature survey represent a variety of possible techniques for crash energy management and control. However, selection of techniques or devices for application to truck underride guard and/or automobile bumper systems requires consideration of many factors including performance, weight, cost, and the ability to implement without adversely affecting the primary utility of the vehicle. Differences in the basic requirements for underride guards and automobile bumpers can bear on the choice of energy management systems for the two types of vehicles.

The relative infrequency of truck rear underride accidents and practical considerations would appear to rule out all but the most simple, rugged, and easily maintained underride guard systems. The technique best suited for an underride guard is probably a guard design that absorbs crash energy via the mechanism of plastic deformation of structural material as typified by the knee strut. Thus, the guard could be essentially a rigid

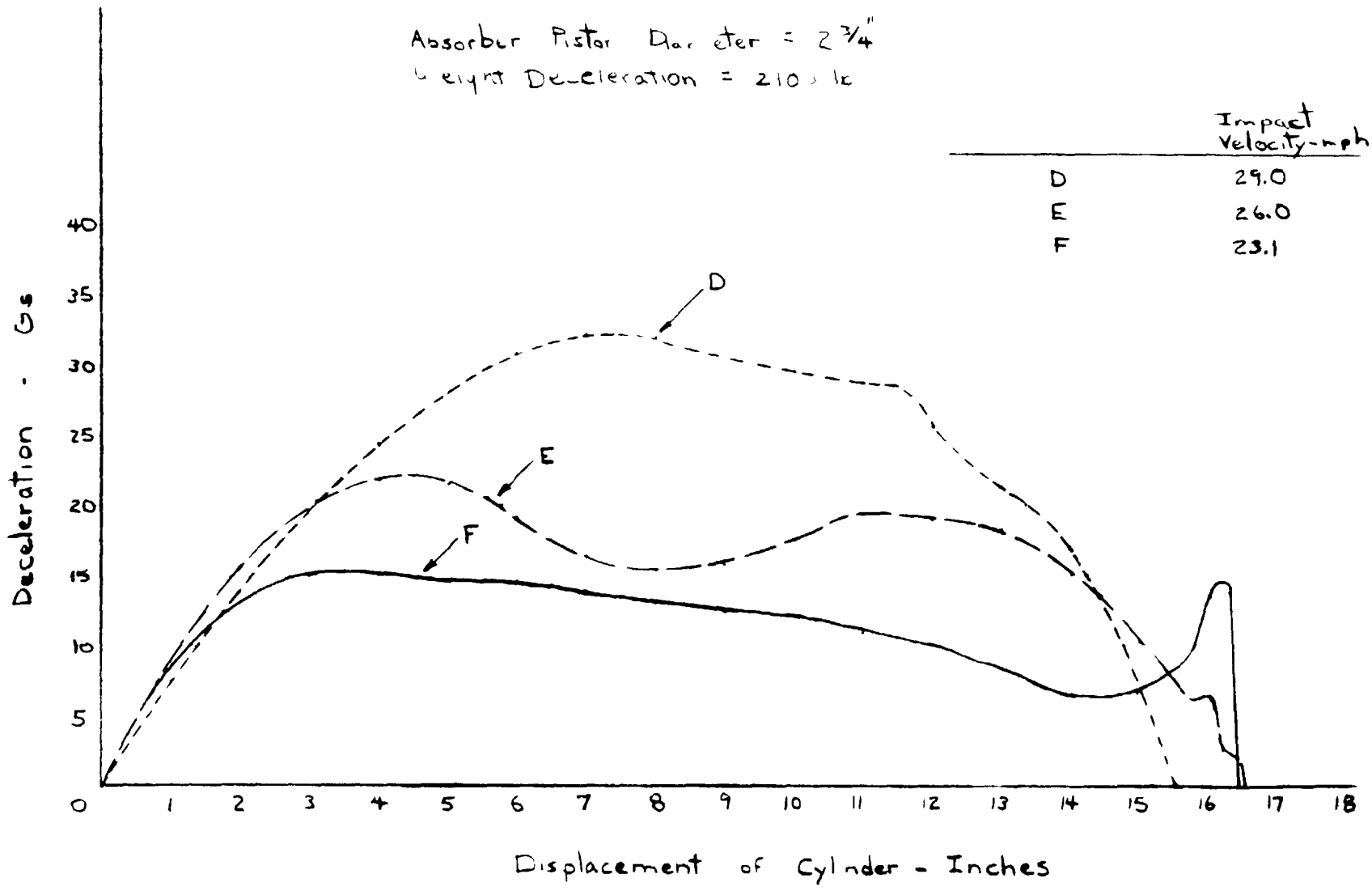

Figure A-27 VARIABLE ORIFICE HYDRAULIC SHOCK ABSORBER PERFORMANCE AT VARIOUS IMPACT VELOCITIES

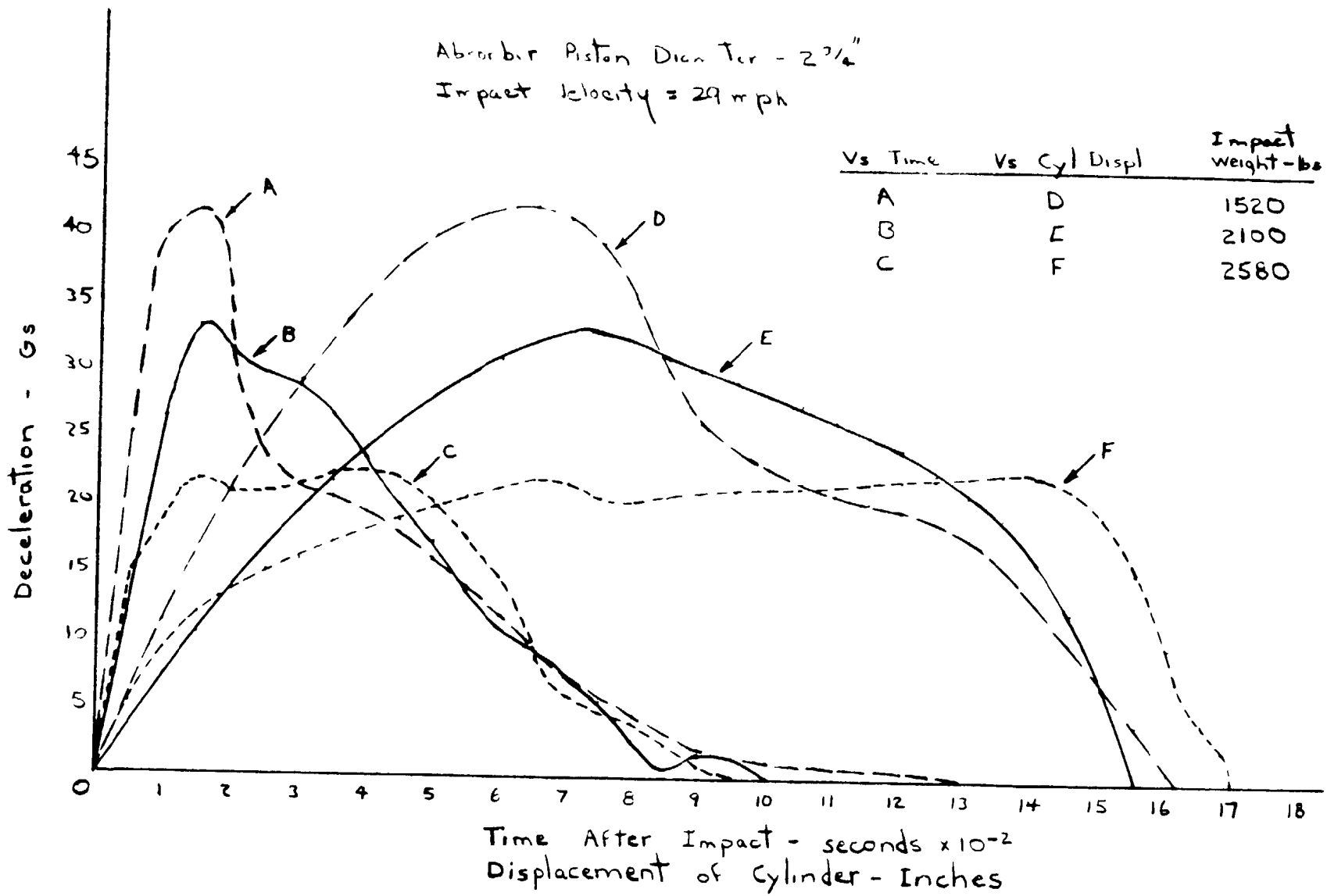

Figure A 28 VARIABLE ORIFICE HYDRAULIC SHOCK ABSORBER PERFORMANCE FOR VARIOUS IMPACTING MASSES

relatively lightweight structure designed to withstand the relatively low forces produced in normal operations, such as during collisions with loading docks, but which would yield and dissipate energy under the forces developed in a high velocity impact by another vehicle. Directional sensitivity is also relatively low and energy dissipation density is high for such devices.

Of the uni-directional metal working energy absorbers, the Tor-Shok and the friction tube are probably the most suitable since they can be designed to provide bending strength and therefore contribute to the lateral support of the guard. Although some of the other devices, by themselves, have much higher values of specific energy absorption, their high directional sensitivity would require considerable structure to provide a workable system for oblique impacts. As a result, the specific energy dissipation capacity based on the complete underride guard system would probably be comparable to the other methods.

Crushable materials offer the advantages of low directional sensitivity and high specific energy absorption. However, in most instances a backup structure to support the crushable material would be necessary which would reduce the weight advantage of such a system. Another problem of using lightweight crushable materials is the ability to accommodate the large volume of material that would be needed without interfering with the functioning of other components essential to the operation of the vehicle.

A characteristic that would appear to be more desirable for application to automobile bumper systems, as opposed to underride guards, is a cycling or automatic reset capability that can be provided by hydraulic or viscoelastic solid media shock absorbers. These devices can dissipate energy (stroke) without damage to components and would be particularly beneficial for absorbing the energy of low velocity "parking lot" type collisions that are quite frequently encountered by automobiles. However, such devices are disadvantageous in terms of relative cost and probable need for more frequent maintenance.

APPENDIX A REFERENCES

A-1. McGehee, John R., "Experimental Investigation of Parameters and Materials for Fragmenting-Tube Energy-Absorption Process", NASA TN D-3268, February, 1966.

A-2. McGehee, John R., "A Preliminary Experimental Investigation of an Energy-Absorption Process Employing Frangible Metal Tubing", NASA TN D-1477, October, 1962.

A-3. Guist, Leroy R. and Marble, Donald P., "Prediction of the Inversion Load of a Circular Tube", NASA TN D-3622, September, 1966.

A-4. Warner, Robert W. and Kaskey, Arthus G., "An Impact Energy-Absorbing Strut Employing Tube Cutting", NASA TN D-4941, December, 1968.

A-5. Anonymous, "Basic Research in Vehicle Crashworthiness", Thirteenth Progress Report", 1 July to 31 July, 1969, Cornell Aeronautical Laboratory, Inc., pages 2-1 to 2-3.

A-6. Sarrailhe, S. R., "An Energy Absorber for Crash Protective Restraint Systems", Aeronautical Research Laboratories (Australia) S & M Note 324, April, 1968.

A-7. Platus, D. R., "MRI Rolling Ring Prototype Strut No. 1 - Test Summary", Mechanics Research Incorportated TR-103-1, September 24, 1968.

A-8. Platus, D. R., "Cyclic Deformation Crew Attenuator Struts for the Apollo Command Module", Mechanics Research Incorporated, Paper for Presentation at the 38th Shock and Vibration Symposium, St. Louis, Missouri, May 1-2, 1968.

A-9. Extracts from Menasco Auto Bumper Test Report RD198B500.

A-10. "A Proposal for Research on Bumper and Heavy Vehicle Underride Guards", CAL Proposal No. 1441-69, May, 1969, pages 25-30.

A-11. "Experimental Safety Vehicle Program, Technical Elements", Volume II of V, Digitek Corporation, 15 December 1968, pages 2-27 to 2-28.

A-12. Anonymous, "Energy Absorbing Characteristics of Crushable Aluminum Structures in a Space Environment", Final Engineering Report, Advance Structures Group, Bendix Corporation Report SPP-65-107, July 24, 1965.

A-13 Daigle, D. L. and Lonborg, J. O., "Evaluation of Certain Crushable Materials", Technical Report No. 32-120 (Contract No. NASw-6), Jet Propulsion Laboratory, C.I.T., January 13, 1961.

A-14. Lipson, S., "Cellular Aluminum for Use in Energy Dissipation Systems", NASA CR-93, 1964.

A-15. Brooks, G. W. and Carden, Huey D., "A Versatile Drop Test Procedure for the Simulation of Impact Environments", Noise Control Shock and Vibration, Volume 7, No. 5, September-October, 1961, pages 4-8.

A-16. Knoell, A. C., "Environmental and Physical Effects on the Response of Balsa Wood as an Energy Dissipator", CIT Technical Report No. 32-944, June 15, 1966.

A-17. Shield, Richard and Corington, Clarke, "High-Velocity Impact Cushioning, Part VI - 108C and 100C Foamed Plastics", Texas University, Structural Mechanics Research Laboratory [AD250550], September 1960.

A-18. "Experimental Safety Car Study", Final Report, Phase I, Americar Machine & Foundry Report No. ASL-E-168-5, August, 1968.

A-19. Ryan, James J., "Reduction in Crash Forces", Fifth Stapp Automotive Research Crash Conference, September, 1961.

APPENDIX B

COMPONENT TESTS OF FRICTION TUBE ENERGY ABSORBING DEVICES

Upon selection of the friction tube, developed at CAL, as the energy dissipating device for the yielding guard design, dynamic tests were performed to determine that the devices would perform satisfactorily in a test rig simulating the basic geometry on the contemplated guard design. The data obtained from three drop tower tests are presented herein.

The tests were performed using the test fixture shown in Figure B-1. The impacting mass was a 1,783 pound weight dropped from a height of 17 feet, resulting in an impact velocity of 22.6 MPH. Instrumentation consisted of two single axis accelerometers attached to the impacting weight and positioned to monitor accelerations of the weight in the free-fall direction. Two accelerometers were used to provide a redundant measurement as a safeguard against equipment failure. High speed motion pictures were also taken for each test.

Details of the friction tube configuration tested are shown in Figure B-2. The first test used a friction tube having a constant slot width of 0.5 inch because the static tests of this configuration produced approximately the force level needed to absorb the energy of the falling weight within the available stroke of the test fixture. The data from the first test are shown in Figure B-3. The deceleration data are obtained directly from the accelerometers and the velocity and displacement data are obtained by integrating the acceleration data.

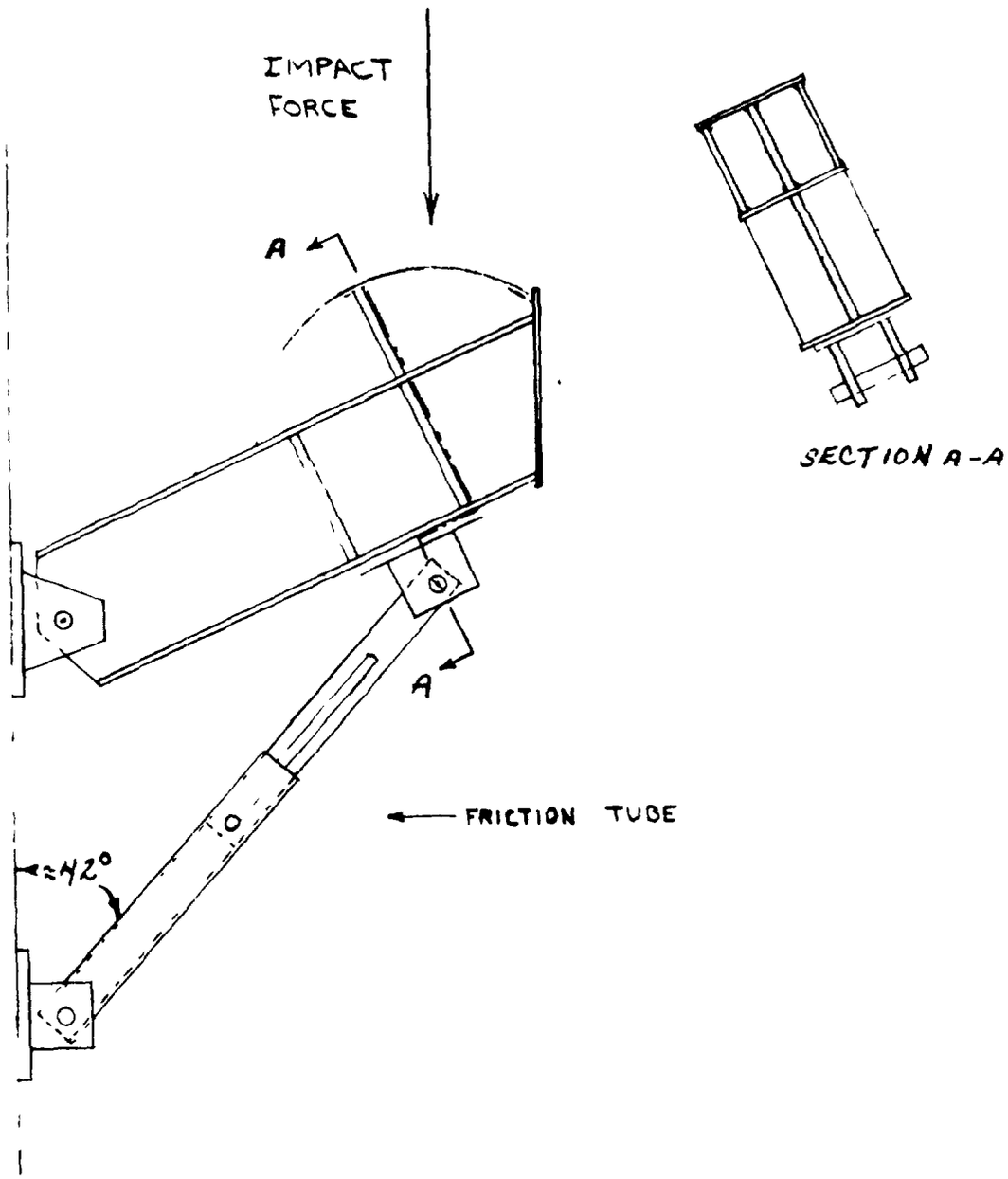

Figure B-1 DROP TEST FIXTURE

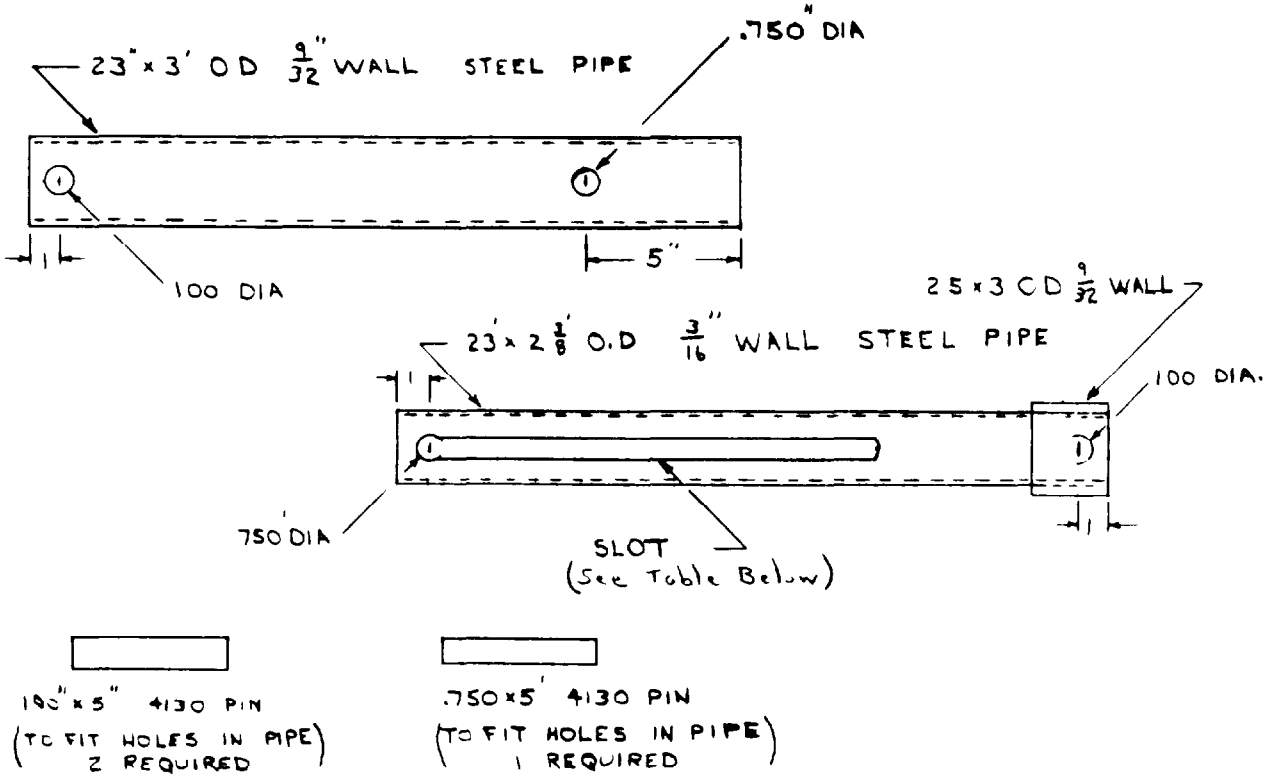

SLOT CONFIGURATIONS

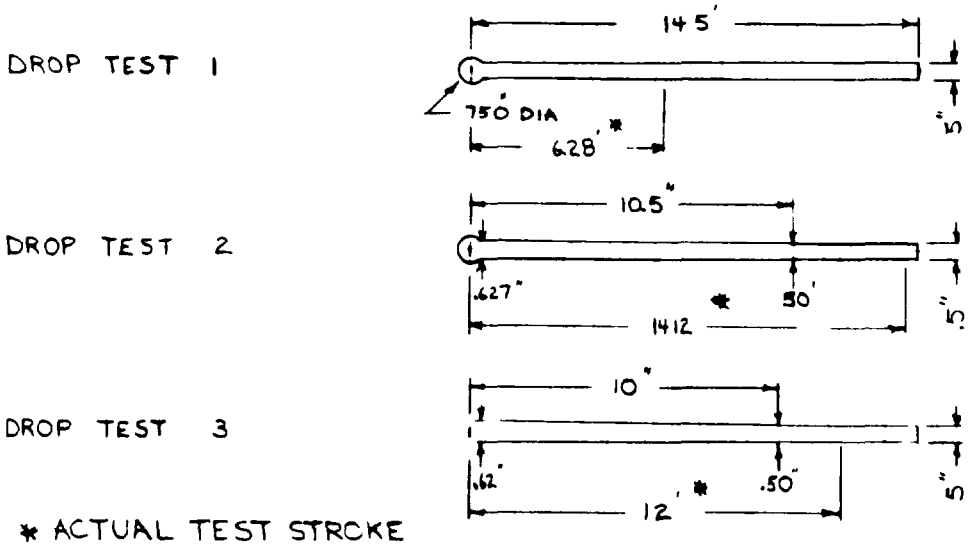

Figure B-2 FRICTION TUBE CONFIGURATIONS TESTED

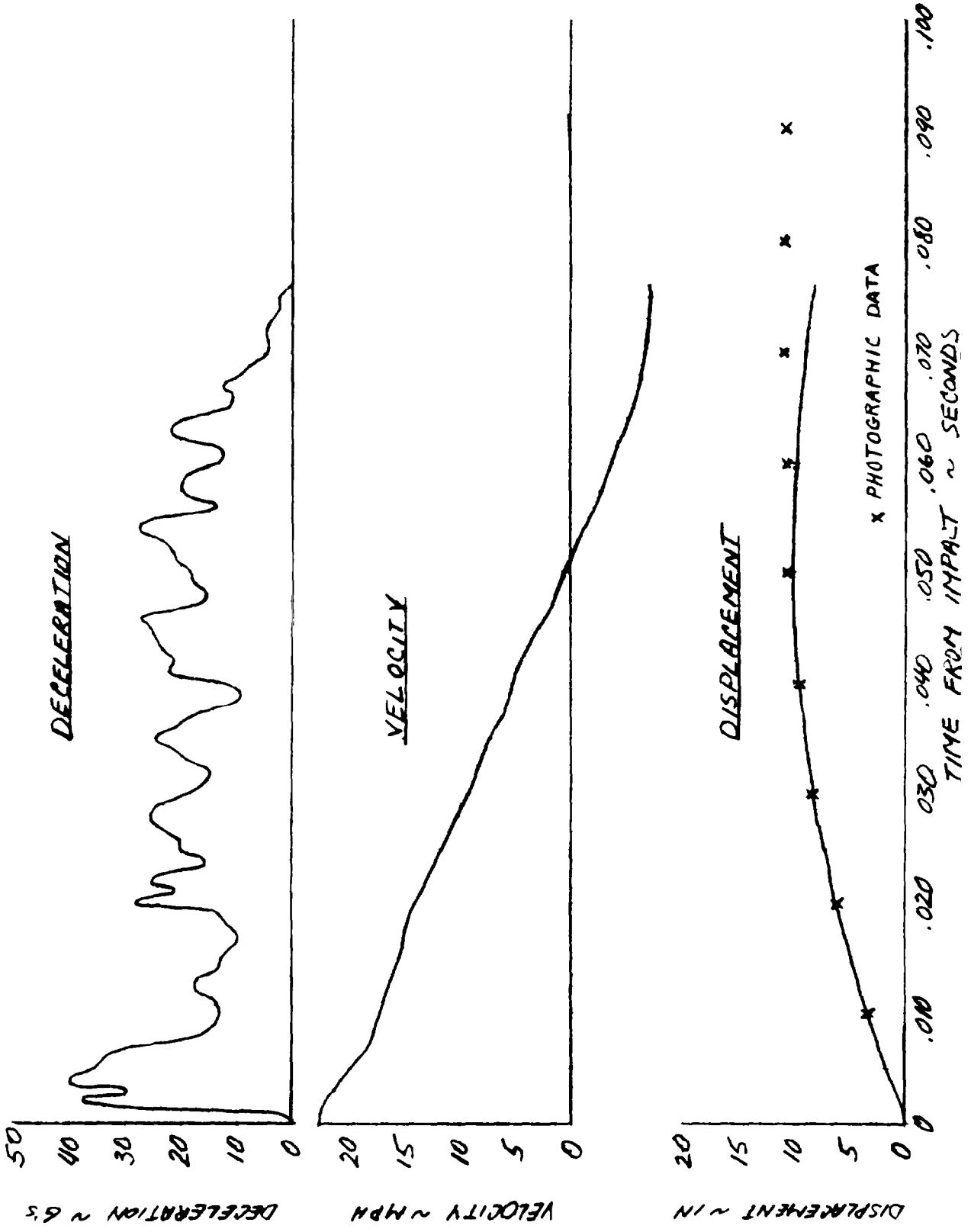

Figure B-3 FRICTION TUBE RESPONSE – DYNAMIC TEST NO. 1

Examination of the d celeration data of Figure B-3 shows an initially high deceleration followed by a fluctuating response about a mean value of approximately 20 G deceleration. The initial peak is a result of the inertia of the rather massive test rig which was accelerated to the velocity of the impacting body in a distance of the order of two inches. (A block of wood was attached to the lower surface of the falling weight to cushion the initial impact.) The oscillating deceleration is a result of the mode of collapse of the friction tube. Wall clearance between the two tubes comprising the friction tube allows some buckling of the two tubes when they are subjected to a compressive load. This buckling periodically increases the resistive force of the friction tube through a binding action between the inner and outer tubes.

The results of the first test indicated a higher resistive force (58,000 lb. average force) than was expected based on the static tests, hence, the slot width was increased (as shown in Figure B-2) for the second test in order to decrease the average deceleration while increasing the total displacement. The slot geometry selected for the second test would normally produce a force having an increasing ramp characteristic over the initial portion of the stroke followed by a constant force for the remainder of the stroke. Unfortunately, a fabrication oversight resulted in a sharp corner at the transition from the working pin hole to the slot. The sharp corner gouged the pin which resulted in a greatly decreased force level over the entire stroke of the device as can be seen from the deceleration data in Figure B-4. The average deceleration is quite low over the major portion of the displacement with a rapid increase to a large deceleration at the end of the stroke as a result of the bottoming of the test rig against a wooden stop provided for this purpose.

The high initial deceleration resulting from the test rig inertia is greater for test 2 than for test 1 because a thinner block of wood was used as the cushion on the impact face of the falling weight for test 2. The wood cushion was approximately 3 inches thick for test 1 and only about 1 inch thick for test 2.

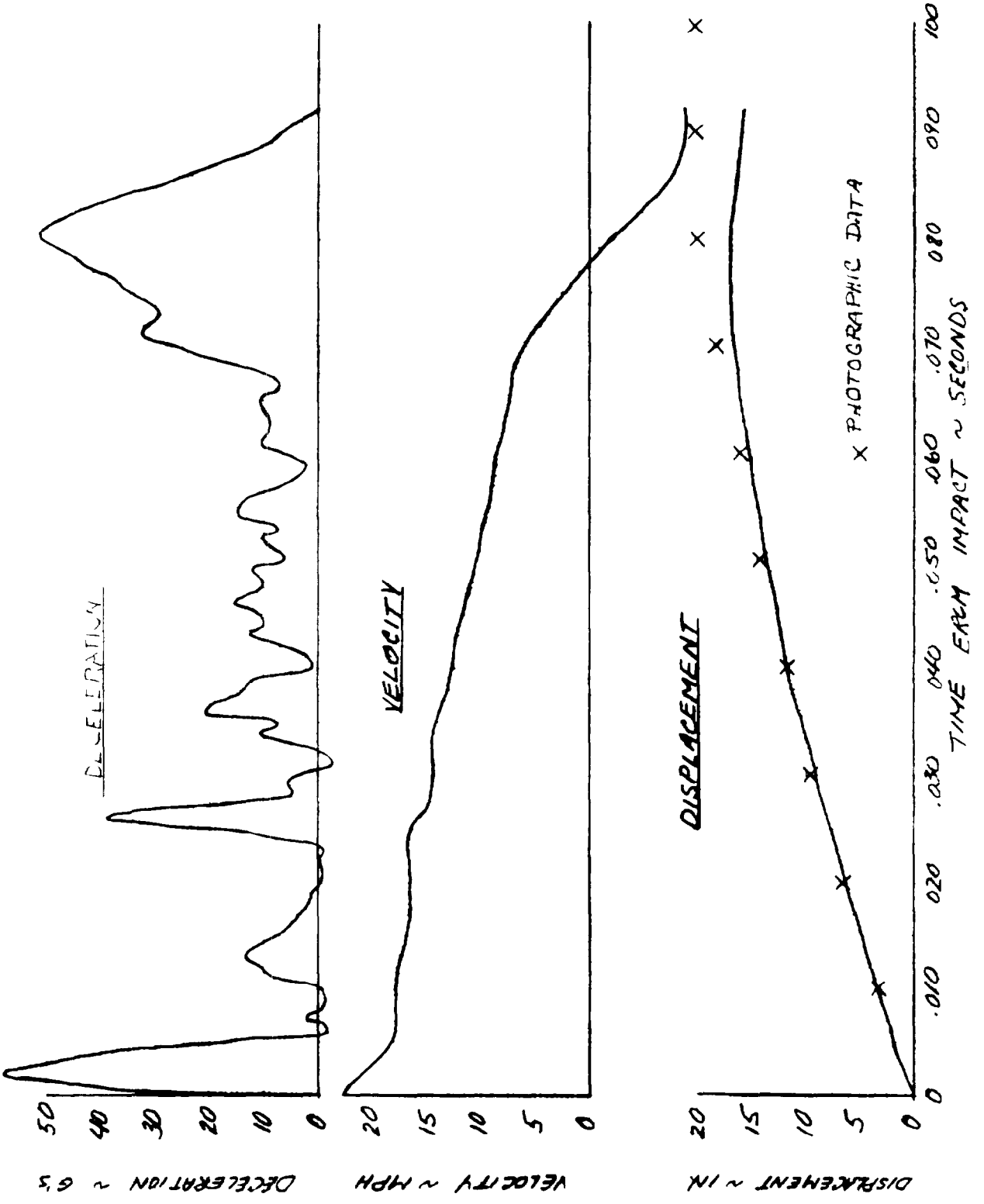

Figure B-4 FRICTION TUBE RESPONSE – DYNAMIC TEST NO. 2

Test 3 was a repeat of test 2 with the slot fabrication error corrected. The results, presented in Figure B-5, are as expected in that the average deceleration increases in a roughly linear fashion over most of the displacement. The initially high inertia effect was most severe for test 3 because the same block of wood was used on the impact face of the falling weight as was used in test 2 and hence the wood had little cushioning ability remaining for the second impact. The average resistive force produced by the device in this test as calculated from the absorbed energy and actual stroke was approximately 30,000 lbs.

Figures B-3 through B-5 also show displacement data obtained from the motion pictures for tests 1-3, respectively. The agreement between the doubly integrated accelerometer data and the motion picture data is generally good, however, the photographic data tend to give higher maximum displacements.

The following conclusions were drawn from these tests:

1. An underride guard utilizing the basic configuration represented by the test rig should perform satisfactorily.

2. For friction tubes with pinned end mountings, the clearance between the inner and outer tubes should be minimized to reduce the fluctuations of the resistive force caused by binding.

3. Friction tubes perform satisfactorily dynamically. The results of test 1, which used the same friction tube slot configuration as a prior static test, indicated an increase in the average force of approximately 50 to 60% over the static case. It is not possible to determine the extent to which this

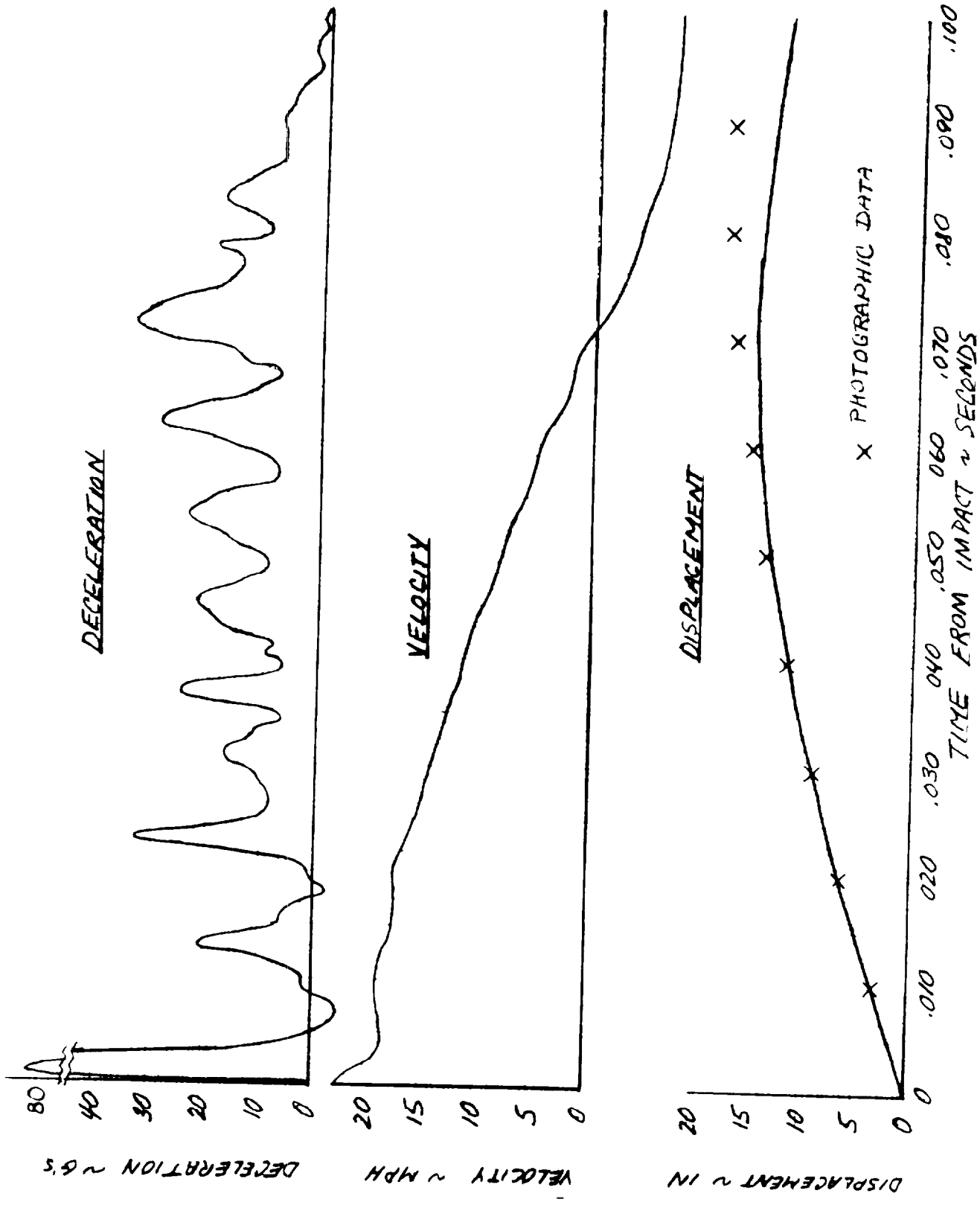

Figure B-5 FRICTION TUBE RESPONSE – DYNAMIC TEST NO. 3

increase may be the result of dynamic effects (strain hardening) and/or of the binding between the inner and outer tubes.

APPENDIX C

MATHEMATICAL MODEL OF AUTOMOBILE-TRUCK UNDERRIDE COLLISION

Concurrent with the experimental testing of underride guards was an effort to mathematically simulate the underride collision to explore the effects of various guard load-deflection properties on vehicle impact response. The underride guard collision model is illustrated in Figure C-1. The automobile is treated as a one-dimensional, two-degree-of-freedom system consisting of two masses connected by springs The masses represent the mass of the engine and the passenger compartment and the springs simulate the nonlinear crush characteristics of various parts of the automobile structure.

It may be shown that for this model, the barrier force, F, is given by

$$F = m_c a_c + m_e a_e$$

where m_c, m_e, a_c, and a_e represent the compartment and engine, masses and decelerations. Shown in Figure C-2 is a comparison between the measured longitudinal force on the rigid barrier and the load calculated from the measured engine and compartment decelerations for the first two simulated rigid underride guard tests (1966 Ford, 18 inch and 24 inch barrier height). Because these curves generally agree in each case, the simplified model was expected to provide a reasonable estimate of vehicle performance.

Experimental data from Tests 1 and 2 and from Reference C-1 were used to determine load-deflection properties for the springs that would result in a good match between the simulated and experimentally

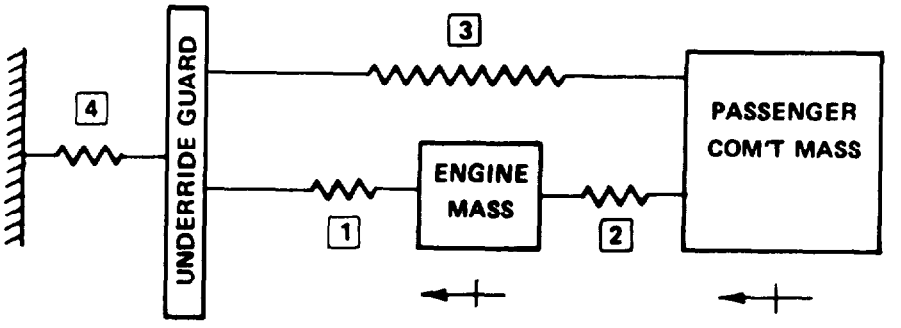

Figure C-1 UNDERRIDE GUARD COLLISION MODEL

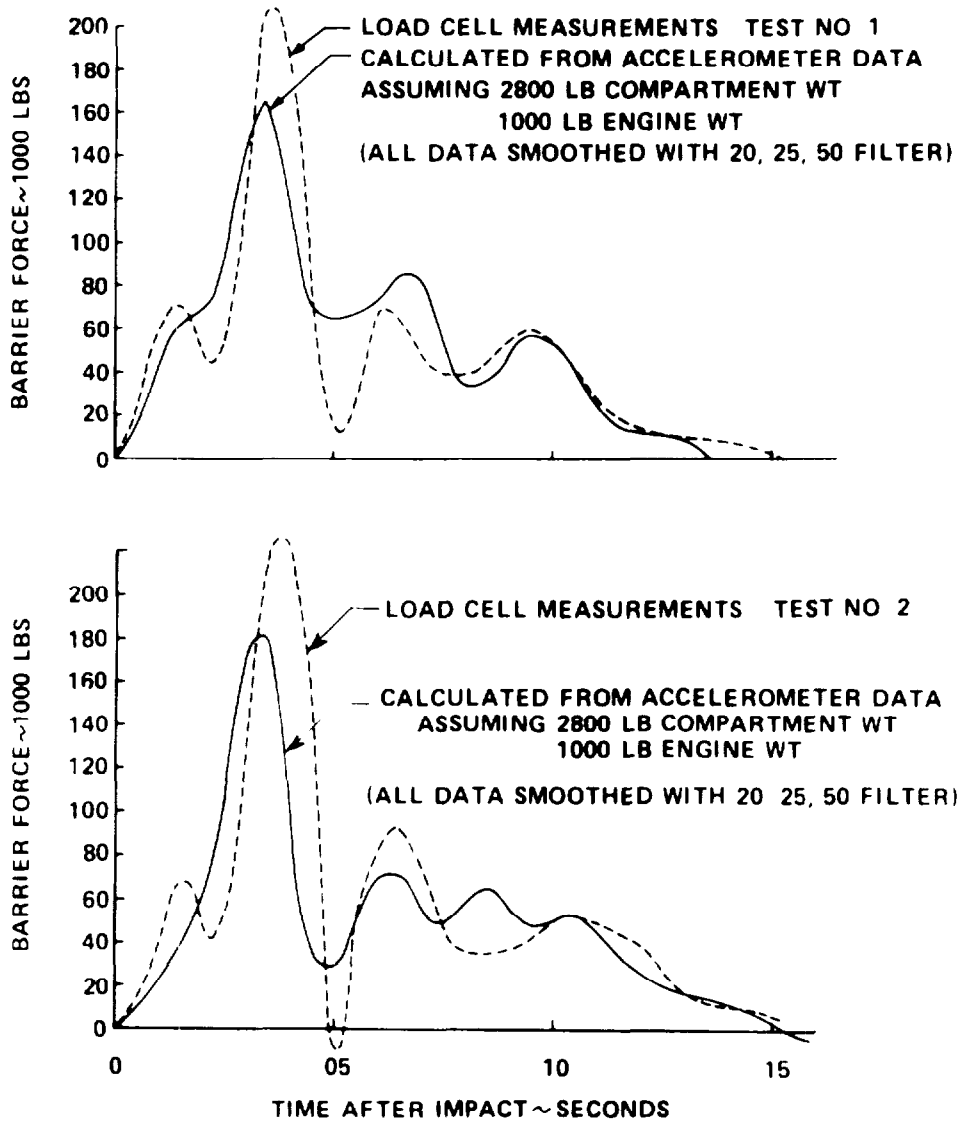

Figure C-2 NORMAL BARRIER FORCE MEASURED AND CALCULATED FROM ACCELEROMETER DATA

measured vehicle responses. It should be noted that in a certain sense the approach is phenomenological since no attempt was made to determine the relationship between the actual vehicle structure and its collapse properties. The adequacy of curve fittings to the experimental data from which the various spring characteristics were obtained is indicated by the small differences between the simulation and test results shown in Figure C-3. It is to be noted, however, that the responses beyond that time at which any of the springs begin to unload, could be subject to significant error because the unloading characteristics of the springs for vehicle crush distances other than those experienced in the tests are unknown. The approximate times at which unloading occurs are indicated by the arrows on the plots showing times of maximum vehicle crush.

Assuming that the structural properties of the vehicle are not velocity sensitive, the model may be exercised at lower velocities, or similarly, at higher velocities if impact is into a yielding structure. A limitation on the application of the model is that the total deflection of the vehicle cannot exceed that measured in the rigid barrier test. Despite this limitation, the model was deemed useful for indicating trends.

Some results from the model applied to exploring the effects of various underride guard force-deflection characteristics (spring 4 in Figure C-1) are displayed in Figures C-4, C-5, C-6, and C-7. Results are also shown for a hypothetical car modified to exhibit different force-deformation properties in the region ahead of the engine represented by spring No. 1 in Figure C-1. Impact speeds for the simulated collisions with the 18 in. and 24 in. high underride guards were the same as those measured in tests 1 and 2 respectively.

In general, the results show greater vehicle crush distances for the case of the higher underride guard which would be expected in view of the lesser engagement of the vehicle and the slightly higher speed. For both underride guard heights, yielding barriers do not

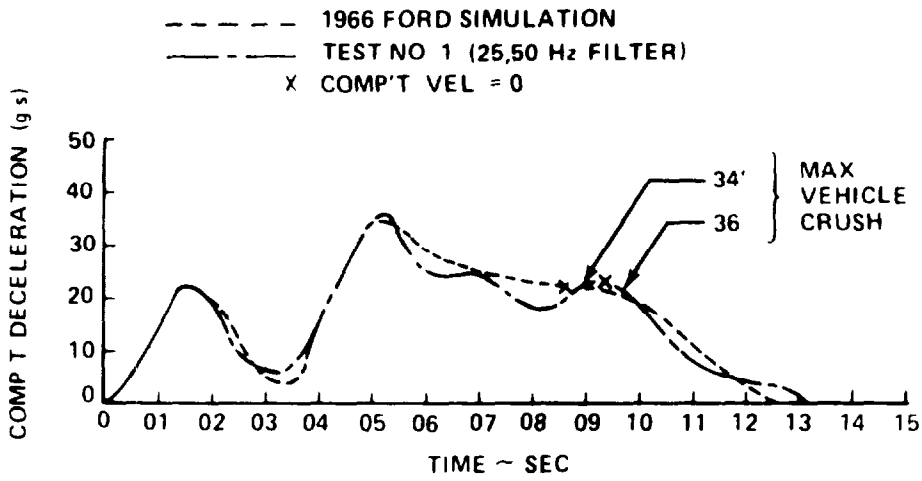

Figure C-3 COMPARTMENT DECELERATION -- 18" RIGID UNDERRIDE GUARD

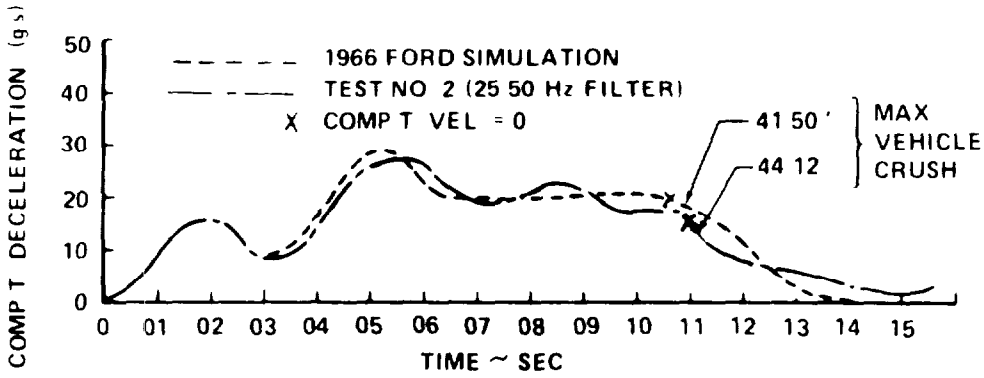

Figure C-3 COMPARTMENT DECELERATION -- 24" RIGID UNDERRIDE GUARD

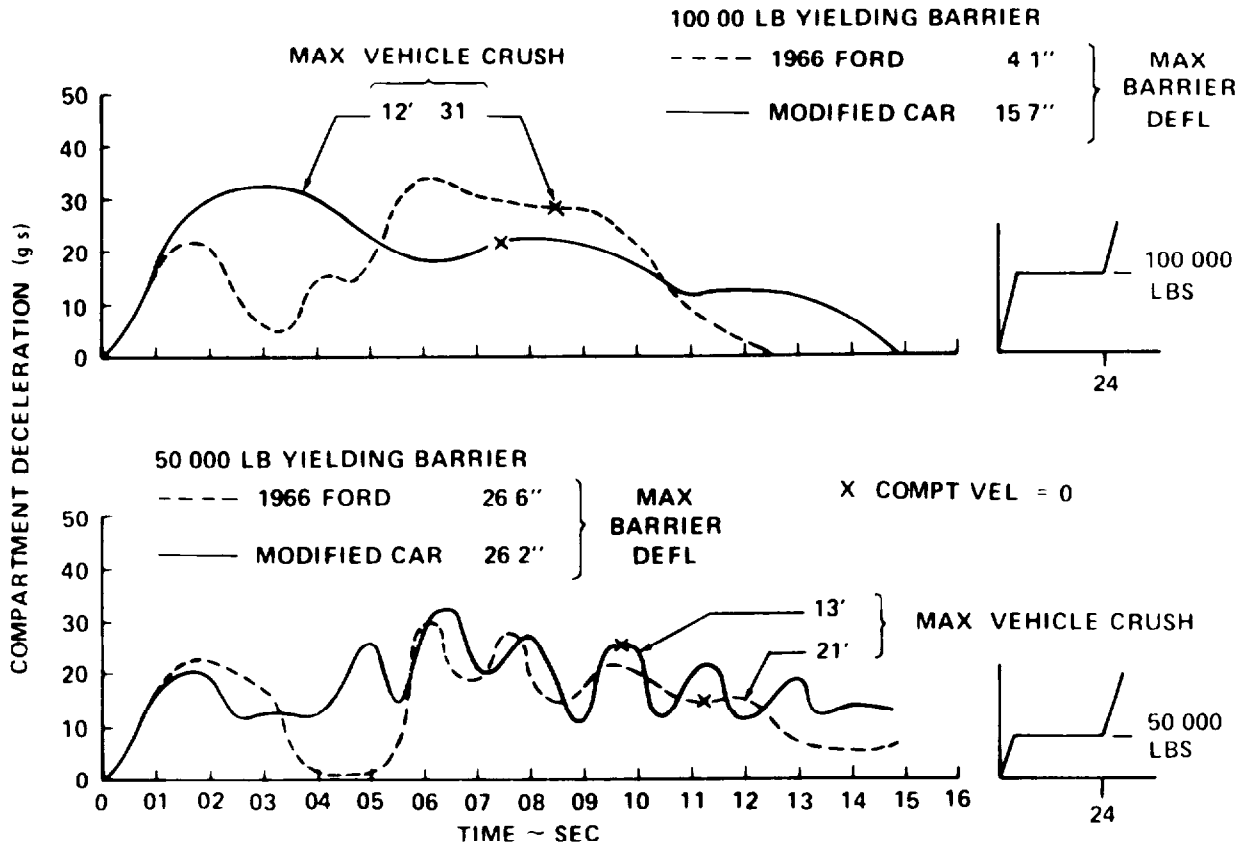

Figure C-4 COMPARTMENT DECELERATION -- 18" YIELDING UNDERRIDE GUARD WITH CONSTANT FORCE CHARACTERISTICS, 2 FOOT STROKE

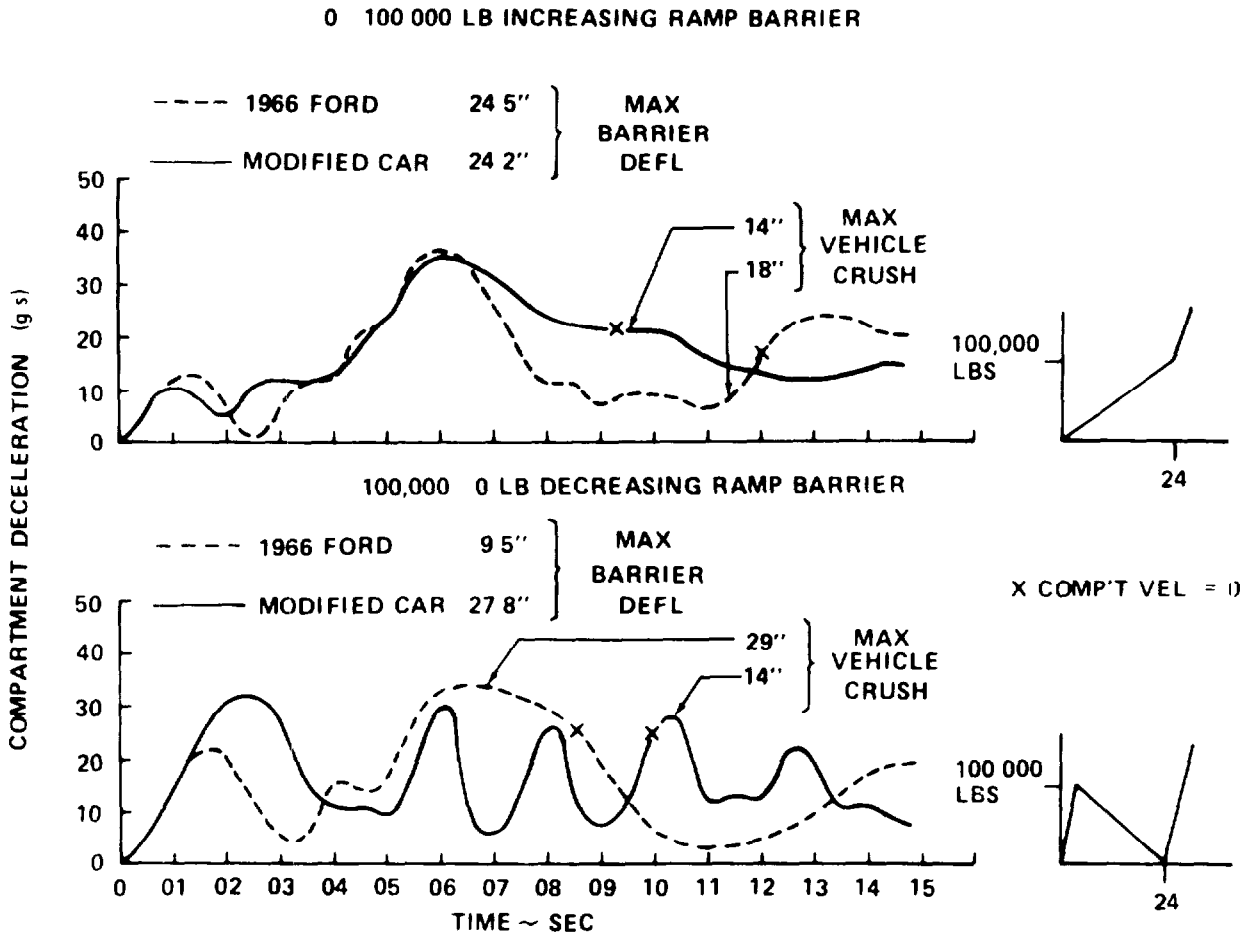

Figure C-5 COMPARTMENT DECELERATION -- 18" YIELDING UNDERRIDE GUARD WITH VARIABLE FORCE CHARACTERISTICS, 2 FOOT STROKE

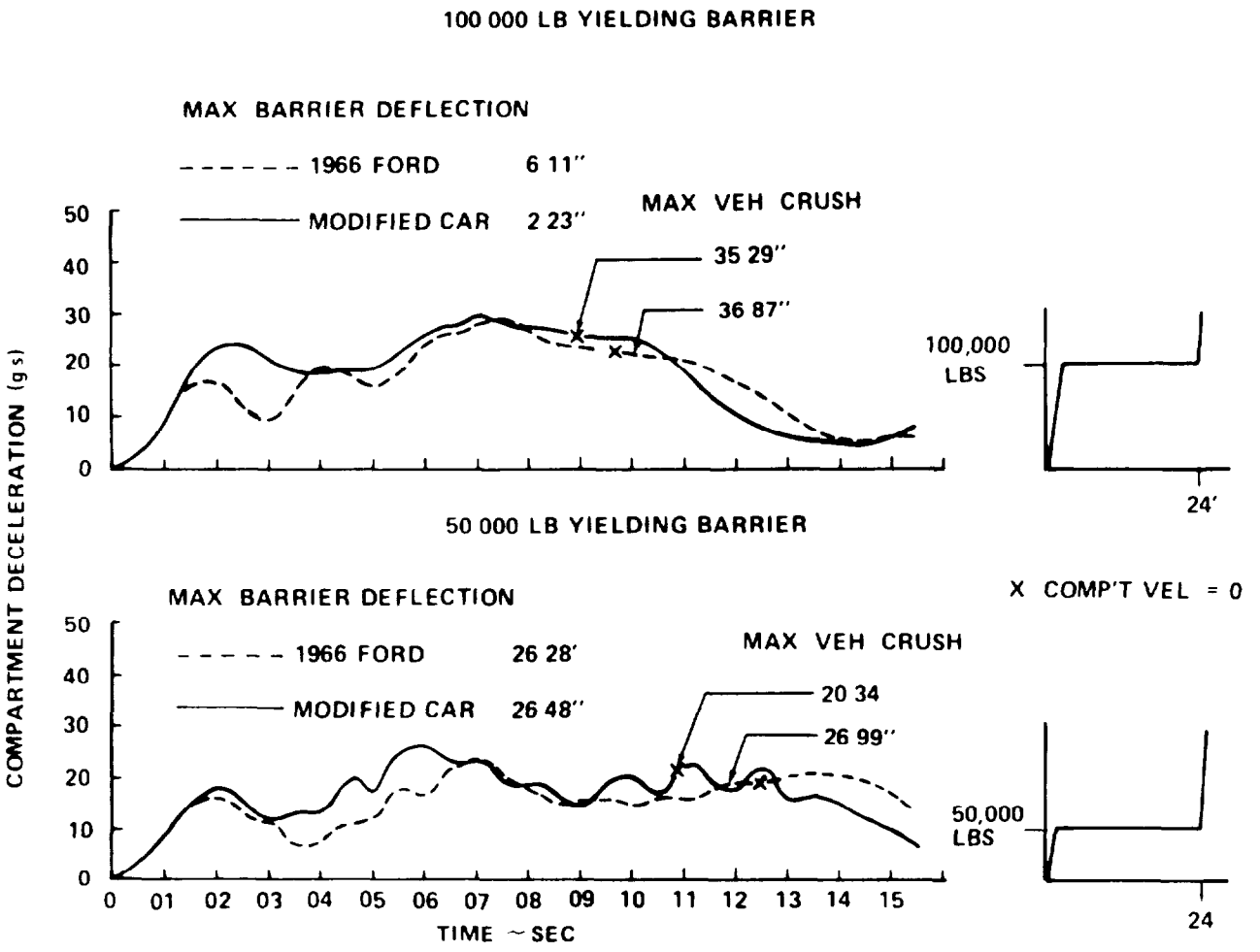

Figure C-6 COMPARTMENT DECELERATION -- 24" YIELDING UNDERRIDE GUARD WITH CONSTANT FORCE CHARACTERISTICS, 2 FOOT STROKE

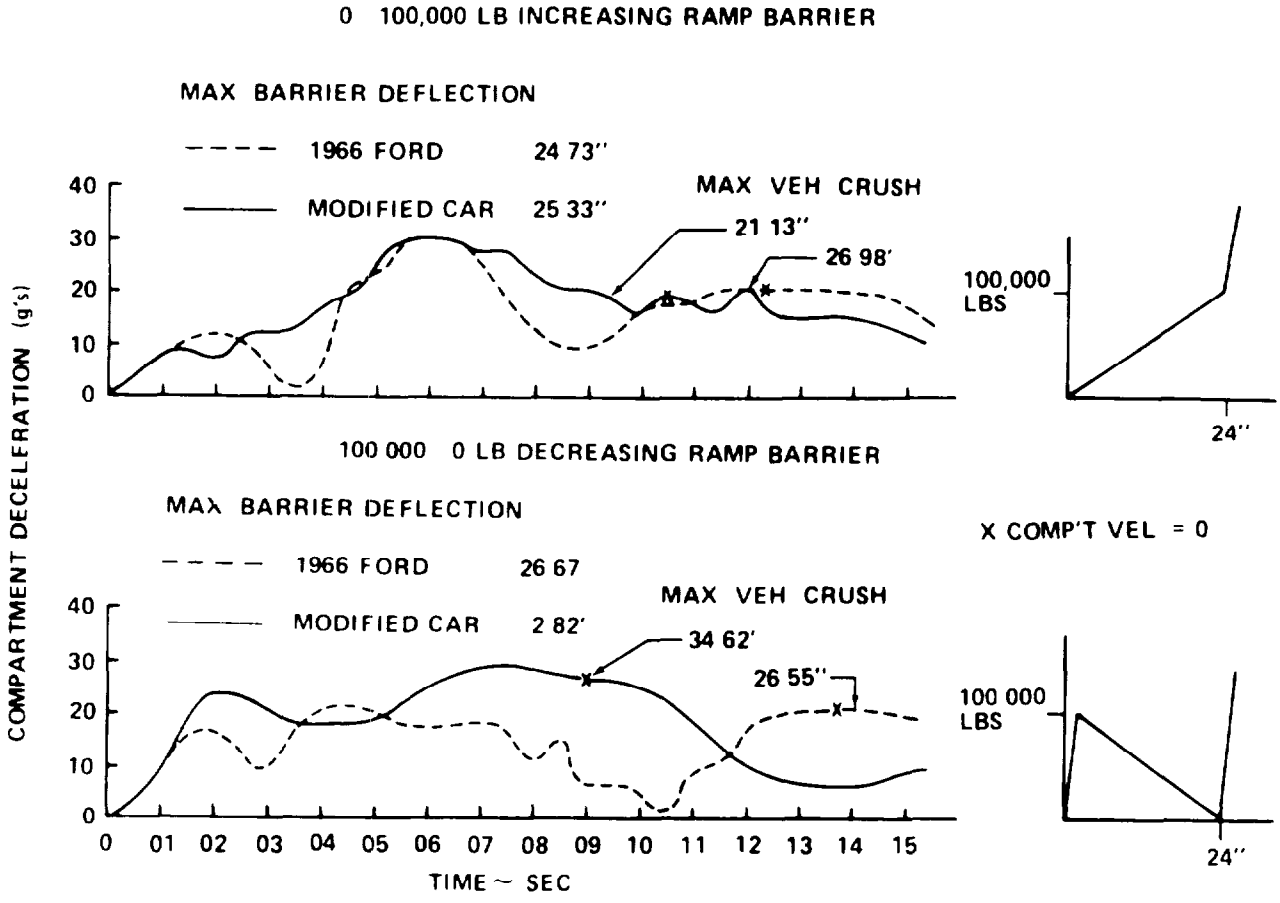

Figure C-7 COMPARTMENT DECELERATION -- 24" YIELDING UNDERRIDE GUARD WITH VARIABLE FORCE CHARACTERISTICS, 2 FOOT STROKE

appear to have a large effect on the peak "g" level of the passenger compartment. Rather, the most notable difference is a decrease in the amount of vehicle crush. It may be noted that the 50,000 lb. constant force yielding guard reaches the full 24 inch stroke early in the impact and that the 100,000 lb. barrier has only relatively small deflections. This indicates that, for maximum energy absorption by the underride guard device, the force level should be between these values for an assumed underride guard stroking distance of two feet. The two foot stroke was arbitrarily selected as being approximately representative of the maximum stroke allowable if penetration of the compartment of the impacting vehicle by fixed structure of the truck is to be avoided. The energy absorbed by the 50,000 lb. underride guard with a two foot stroke represents approximately 60 percent of the initial kinetic energy of the vehicle in the cited simulations.

Of the three waveforms investigated for the yielding underride guard, (constant force, increasing ramp and decreasing ramp) the constant force characteristic indicated as good or better results than either of the other two, and an attempt was then made to define the optimum constant force level. Computer simulations for 18" high underride guards yielding at force levels of 60,000, 70,000, 80,000 and 90,000 lbs. were run. The results are shown in Figure C-8 and indicate that minimum compartment deceleration levels and structural crush of the impacting vehicle would be obtained with a yielding guard force of approximately 60,000 to 70,000 lbs. This force level range was selected as the design target value for the 18" yielding underride guard used in Tests 8 and 9.

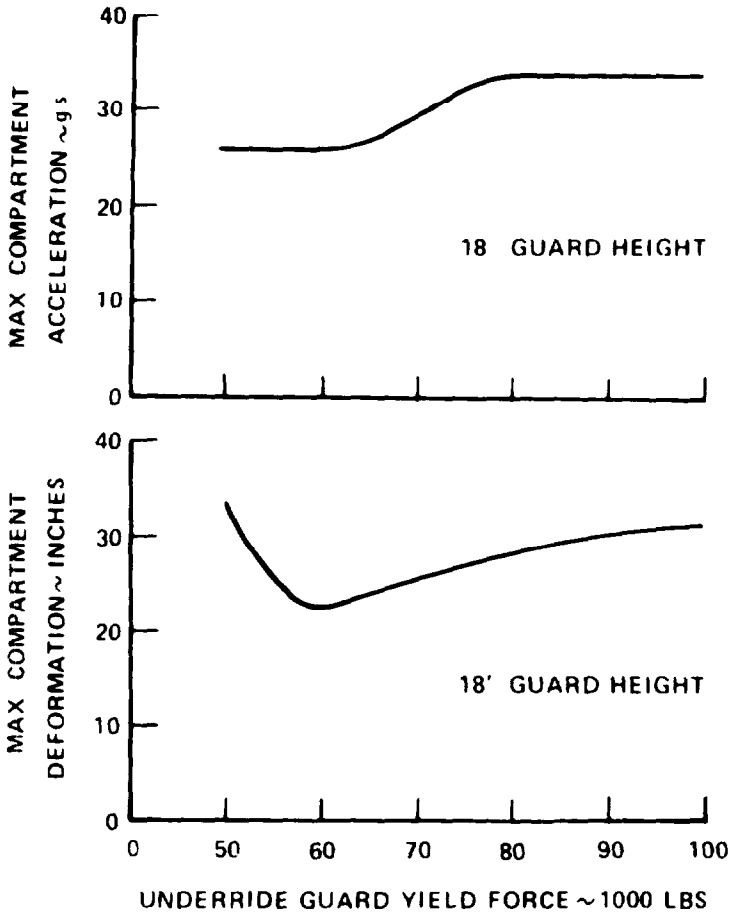

Figure C-8 **COMPUTER SIMULATION RESULTS FOR MAXIMUM COMPARTMENT DECELERATION AND DEFORMATION**

APPENDIX C REFERENCES

C-1. Miller, Patrick M. and Mayor, Richard P., "Basic Research in Automobile Crashworthiness - Summary Report", Final Technical Summary Report, Cornell Aeronautical Laboratory, Inc., Report No. YB-2684-V-6, October, 1969.

APPENDIX D

STRESS ANALYSIS OF TEST TRAILERS AND RIGID UNDERRIDE GUARD DESIGNS

Approximate analyses of the structure of the flatbed and van trailers used in the test program were performed to ascertain the magnitude of underride guard loads that might be sustained without failure of the trailer structure. In addition, two of the rigid underride guard designs tested were analyzed to determine their approximate load carrying capabilities. The method of analysis and results of these various calculations are given in the following paragraphs.

Flatbed Trailer Strength

The primary loading of the the truck structure by a car impacting the underride guard produces a compression load and a bending moment in the target vehicle structure. The flatbed trailer in cross-section is approximately as shown in Figure D-1.

A horizontal load P applied to the underride guard at a distance L below the neutral axis C-C can be represented as a compressive load P at the centroid of the trailer cross-sectional area and a bending moment PL. The maximum load is determined by one of the following expressions for maximum fiber stress for elastic bending:

Top extreme fiber (tensile stress in side rail)

$$S_T = \frac{MC_1}{I_{cc}} - \frac{P}{A_T}$$

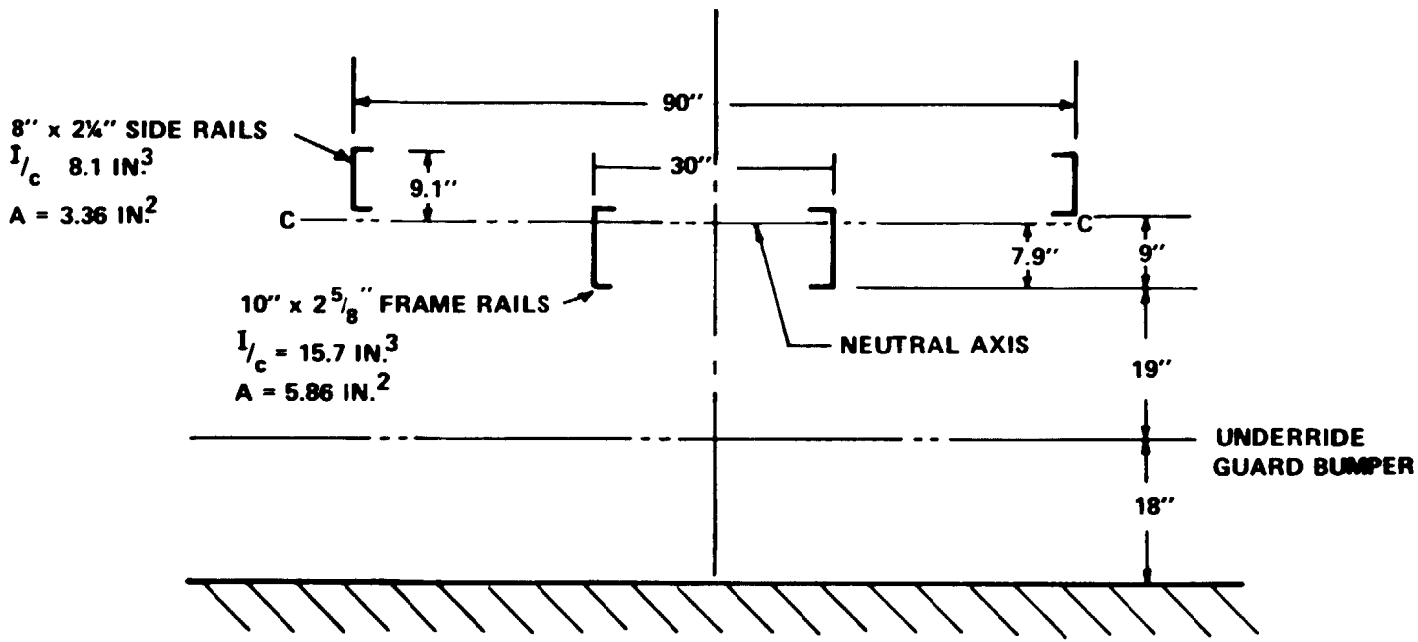

Figure D-1 FLATBED TRAILER CROSS-SECTION

Bottom extreme fiber (compressive stress in frame rail)

$$S_B = \frac{MC_2}{I_{cc}} + \frac{P}{A_T}$$

where:

M = bending moment PL = 26.9 P in-lb

C_1 = distance from neutral axis to top extreme fiber = 9.1 in.

C_2 = distance from neutral axis to bottom extreme fiber = 7.9 in.

I_{cc} = moment of inertia of the cross-sectional area about neutral axis = 495 in.^{4}

A_T = total cross-sectional area of members.

Substitution of the appropriate values for the terms in each of the above equations and solving for P gives a maximum load of 74,000 lbs. based on a compressive yield stress of 36,000 psi in the bottom extreme fiber of the main frame rails.

This simple calculation indicates the minimum force capability of the trailer because it assumes an elastic limit. In actual practice the maximum load capacity will be higher due to redistribution of the stress as the structure begins to yield plastically. Calculation of the trailer strength for plastic yielding, assuming a constant stress distribution of 60,000 psi across the trailer cross-section, gives a maximum underride guard force capability of 141,000 lbs. In the most severe test (Test 7) using this trailer, the average force level was 70,000 lbs. with a shorter deviation peak load of 168,000 lbs. Observation of films of the test and post-crash inspection of the trailer structure indicated that the

ultimate load capacity was probably closely approached as there was evidence of plastic yielding that resulted in a slight amount of permanent set (bending) of the rails.

Van Trailer Strength

The van trailer strength was calculated assuming the trailer to be a column loaded eccentrically by the force applied to the underride guard. Measurements were taken of the trailer to determine the cross-section properties of the various parts of the structure and for calculation of the moment of inertia. The moment of inertia was calculated to be 38,500 in.^{4}. Assuming a yield stress of 30,000 psi, a maximum allowable horizontal force of approximately 170,000 lbs. applied by an underride guard with 24 inch ground clearance was calculated. This calculated strength of the trailer indicated that if the local attachments of the guard could be made sufficiently strong the gross trailer strength would probably be adequate to provide an essentially rigid structure.

The details of the guard design and its attachment to the trailer structure are indicated in Figure 7 of Section 3.0. For this guard design, the existing trailer frame in the vicinity of the axles was extended to the rear of the trailer using 3" x 2" x 3/16" wall structural tubing. In this manner the underride guard longitudinal loads were distributed over many cross-members of the trailer floor structure and was also taken directly into the existing trailer frame.

18" Rigid Underride Guard Used on Flatbed Trailer

This analysis was performed assuming a uniformly distributed load (W $\sim$ lb/in) acting upon the guard bumper in a horizontal direction. Using the theorem of Three Moments from continuous beam theory, the bumper reaction forces and bending moment distribution were

found for the uniformly distributed load. This underride guard, shown in Figure 2 of Section 3.0, was idealized for analysis as shown in the sketch below

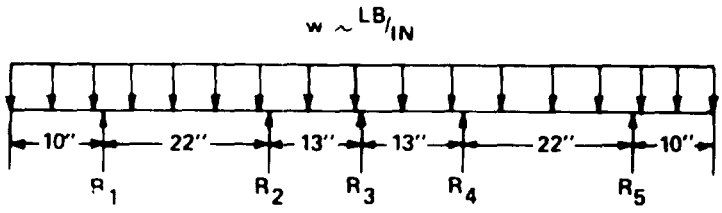

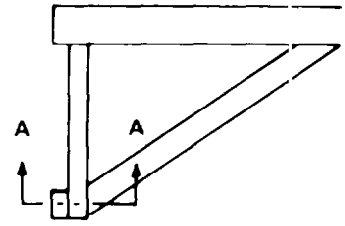

SECTION A A

The forces depicted are all in a horizontal plane which passes through the guard bumper member. The five horizontal reaction forces have been calculated using the compression yield strengths of the diagonal compression struts and the plastic bending strength of the vertical members The maximum allowable loads for the five reactions are

$$R_1 = R_5 = 78,000 \text{ lb.}$$

$$R_2 = R_4 = 45,000 \text{ lb.}$$

$$R_3 = 81,000 \text{ lb.}$$

The results of the application of the theorem of Three Moments from continuous beam theory gives the following results for the general solution in terms of the distributed load w.

Bending Moments				Reactions			
M_1	=	M_5	= -50w	R_1	=	R_5	21.96w
M_2	=	M_4	= -28 9w	R_2	=	R_4	18.25w
M_3	=		-6.675w	R_3	=		9.6w

These results indicate that R_2 and R_4 are the critical reactions that limit the distributed load, w, to a value of 2,470 lb/in. The total uniformly distributed load is therefore 222,000 lbs. for a guard 90 inches wide.

It is interesting to note that if the short diagonal I-beam strut, whose horizontal component is essentially R_2, is replaced by another standard 3" x 2 5/8" I-beam having approximately twice the web thickness as that which was used, only about 10 lbs. would be added to the guard weight but $R_{2\,max}$ would then be approximately 58,000 lbs. With this stronger I-beam the maximum distributed load would then be 3,180 lb/in giving a total load capacity of approximately 290,000 lbs.

Note that the ultimate load capability of the underride guard is approximately 330,000 lbs. which is the sum of the reaction loads R_1 through R_5. To fully utilize this load capacity would obviously require a non-uniformly distributed load.

It should be remembered that the above analysis is for the guard strength alone and not the guard-trailer system. The test results and the calculations of the trailer strength both indicate that the guard is stronger than the trailer structure.

24" Rigid Underride Guard Used on Van Trailer

This analysis was performed using the same procedure as was used for the flatbed rigid guard analysis. The guard, shown in Figure 7 of Section 3.0, is represented as shown below for analysis purposes where

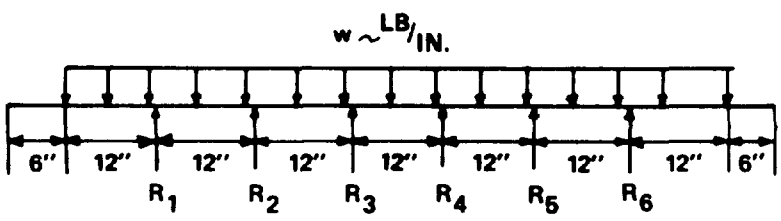

the forces are the horizontal components in the plane of the bumper. The six reaction forces have been calculated based on the maximum static load capabilities of the diagonal compression struts. The maximum loads for the six reactions are:

$$R_1 = R_6 = 61,000 \text{ lb.}$$
$$R_2 = R_5 = 80,000 \text{ lb.}$$
$$R_3 = R_4 = 53,000 \text{ lb.}$$

The results of analyzing this guard using continuous beam theory are as follows.

Bending Moments	Reactions
$M_1 = M_6 = -72w$	$R_1 = R_6 = 24.32w$
$M_2 = M_5 = 3.79w$	$R_2 = R_5 = 4.1w$
$M_3 = M_4 = -15.16w$	$R_3 = R_4 = 13.58w$

These results indicate that R_2 and R_5 are the critical loads which limits the distributed load, w, to 1,950 lb/in. The total uniformly distributed load capacity of the guard is therefore 164,000 lbs. Note that the uniform load selected for this analysis is applied only to within six inches of such end of the guard. If the guard is loaded with a uniformly distributed load over the entire width, the bending moments M_1 and M_6 become quite large and the distributed unit load to about 1,000 lb/in resulting in a low total load for the guard.

The ultimate load for this guard is about 244,000 lbs. for a non-uniformly distributed load which takes advantage of the maximum possible guard reaction loads.

In conclusion, it should b remembered that calculations such as those presented here usually tend to be conservative and that the actual static load capabilities of the various structures are probably greater than indicated. In addition, the load capacity for the various structures may be different for dynamic loading than for static loading. There is some indication from the work reported herein that the structures did exhibit greater strengths than the calculations indicate. However, it cannot be determined from the efforts of the present study whether this apparent increase in load carrying capability is a reflection of a difference between static and dynamic loading or an inaccurate knowledge of the static load limits.

GPO 928-217